Dielectric Resonator Antennas (DRA) for satellite and body area network applications

Muhammad Faiz Alam

UNIVERSITE PARIS-EST
Ecole Doctorale MSTIC

THESIS
Submitted for the partial requirement of
Doctor of Philosophy

Specialization: Electronics, Optronics and Systems

Presented by
Alam Muhammad Faiz

Dielectric Resonator Antennas (DRA) for Satellite and Body Area Network Applications

Etude et réalisation d'antennes diélectriques pour les applications satellitaires et corps (BAN).

Thesis directed by Jean-Marc Laheurte

Reviewers:

Ala SHARAIHA	Professor of Université de RennesI
Olivier PASCAL	Professor of Université ToulouseIII

Examiners:

Odile Picon	Professor of Université Paris Est (UPEMLV)
Jean-Marc Laheurte	Professor of Université Paris Est (UPEMLV)
Christophe Roblin	Assistant Professor of TELECOM Paris Tech
Benoit Pousssot	Assistant Professor of Université Paris Est (UPEMLV)

Dedicated to:

Taha & Saira

Acknowledgements

I wish to express my sincere gratitude to my thesis director Jean Marc Laheurte, whose highly professional suggestions and rigorous guidance helped me a lot to succeed in my research work. Whenever I got stuck up in the complexities, far sighted and result oriented proposals always encouraged me to go deep into the issues to seek rationally all possible options before concluding the results. My estranged results and oddity based analysis were immediately corrected while core issues were directed to focus upon. This strategy and resourcefulness boosted my potential to perceive, evaluate and overcome timely the imminent errors encapsulated within every stage of research.

I am really grateful to Madame Odile Picon, directress of Esycom for her support to smoothly go through all procedural and administrative tasks and to provide me a peaceful, friendly and competitive research environment.

I am deeply indebted to Benoit Poussot and Thierry Alves for their ever readiness to suggest me novel and invaluable practicable tips so as to evaluate multi-faceted problems in simplest ways. It helped me to refine and optimize the final results. Their active and extensive involvement in patronizing me to handle sophisticated electronic instruments to be employed in antenna measurements and to test their capabilities in real application environment kept me abreast of the innovating technical knowledge. Obviously that will remain an asset for me throughout my professional carrier. Equally important is the contribution made by professors Marjorie Grzeskowiak, Elodie Richalot and Laurent Cirio to whom I have sought on and off their expert opinions related to my project. I deeply acknowledge their candid approach to pinpoint flaws and deficiencies in my work and to propose me how to opt different strategies to obtain the desired results. Their encouragement and sharing of ideas made me learn some additional tools to analyze and verify the final results.

My senior colleagues and friends in Esycom such as Hakim Takhedmit, Ottara Berenger , Muhamad Nasserddin, Mame Diarra, Fatiha Elhatmi, Walid Haboubi and Rafael Quiroz significantly contributed in boosting my moral and keeping me always at high spirit. Research team at Esycom is incomplete without the mention of device fabrication experts Stephane PROTAT and David DELCROIX whose esteemed opinion made me to anticipate the possible constraints meted out to design structures and to devise an alternative strategy to avoid the wastage of time and manufacturing cost. I really appreciate their precious efforts to keep laboratory environment up-to-date both in terms of equipments and measurement facilities.

I am thankful in advance to my reviewers and examiners for their valuable evaluation of the work and future guide line in the field of research.

Finally I deeply appreciate the collaboration between Government of Pakistan (HEC) and Government of France to financially support the students to pursuit their PhD studies in this highly competitive and learning environment.

Alam Muhammad Faiz
July 2, 2012.

Abstract

Technologies such as direct broad cast satellite system (DBSS), Geosynchronous Earth Orbit (GEO) and Low Earth Orbit (LEO) satellite communications , global positioning system (GPS), high accuracy airborne navigation system and a large variety of radar systems demand for high level of antenna performance. Similar is the requirement for upcoming land based wireless systems such as cellular and indoor communication systems that is needed some more specific and additional features added to the antenna to compensate for the deficiencies encountered in system's performance. Though metallic antennas are capable enough to fulfil all the operational requirements, however at very high frequencies and under hostile temperature conditions they are constrained to face certain limitations. To avoid these constraints the performance of Dielectric Resonator Antennas (DRAs) is evaluated and their new applications are proposed. In the thesis, two types of antenna applications are sought:

- First is for tracking and satellite applications that needs a larger aperture coverage in elevation plane. This coverage is realized with a good CP purity by proposing two ports dual linearly polarized DRA working at X-band. The DRA is excited by two orthogonal H-shaped aperture slots yielding two orthogonal polarizations in the broadside direction. A common impedance bandwidth of 5.9% and input port isolation of -35 dB are obtained. The broadside radiation patterns are found to be highly symmetric and stable with cross polarization levels -15dB or better over the entire matching frequency band. The maximum measured gain is found to be 2.5dBi at 8.4 GHz.
- The 2nd type of antenna is a dual pattern diversity antenna to be used in the Body Area Network (BAN) context. This antenna combines a slot loop and DRA yielding broadside and end-fire radiation patterns respectively. Based upon the feeding techniques, the DG antenna is further divided into two categories one with planar feeds and the other with non-planar feeds (slot loop excited by planar CPW but DRA excited by vertical monopole) .Both types are successfully designed and measured upon body when configured into different propagation scenarios. The non-planar feeds antenna allows wider common impedance bandwidths than the planar feeds (4.95% vs 1.5%) . In both cases, a maximum value of DG=9.5dB was achieved when diversity performance tests were carried out in rich fading environments. This value is close to the one (10 dB) theoretically reached in a pure Rayleigh environment and was obtained with efficiencies of 70% and 85% for the slot loop and the DRA respectively. Therefore, we conclude that these antennas could be used on the shoulders or the chest of professional clothes (firemen, policemen, soldier) where full planar integration is not a key issue but where the communication must be efficient in harsh environments and for various gestures, positions and scenarios.

Key Words: DRA, H-shaped aperture slots, Symmetric radiation patterns, Slot loop, Diversity Gain (DG), Body Area Network (BAN).

Résumé

Que l’on considère les domaines des télécommunications, de la navigation ou de la localisation, un niveau élevé de performances de l'antenne permet de relâcher l’effort sur les niveaux de sensibilité des récepteurs ou les performances en linéarité et en gain des émetteurs. Il est donc utile de poursuivre des recherches sur de nouveaux types d’antennes en particulier pour les applications émergentes.
Aux fréquences élevées et dans des conditions de température hostiles, les antennes à résonateur diélectrique (DRA) sont par exemple plus adaptées que les antennes métalliques. .
Les antennes DRA, de par leur nature volumique, ont également la capacité de s’intégrer à des antennes métalliques 2D avec un couplage réduit.
Dans la thèse, deux types d'applications de l’antenne DRA correspondant à ces 2 propriétés sont recherchés

- la réalisation d’un élément rayonnant pour un réseau phasé embarqué sur un véhicule terrestre ou un avion. Cet élément de base requiert une couverture en élévation supérieure à celle des éléments imprimés pour permettre une poursuite typique de ±70°. Cette couverture dans un cône large est assurée avec une bonne pureté de polarisation circulaire en utilisant deux ouvertures à fente en H orthogonales parfaitement découplées en bande X. La bande passante commune en impédance pour les 2 ports est de 5.9% avec une isolation de -35 dB. Les diagrammes de type “broadside” sont très symétriques avec des niveaux de polarisation croisée inférieurs à -15dB sur toute la bande. Le niveau maximum de gain est 2.5dBi à 8.4 GHz.
- La deuxième structure est destinée à la diversité d’antennes dans le contexte des réseaux corporels ou Body Area Network. L’antenne à diversité combine une antenne fente en boucle avec un DRA ce qui permet dans un espace compact de réaliser des diagrammes de type “broadside” et “endfire” respectivement. Les alimentations considérées sont de 2 types; Soit purement planaire (microruban et coplanaire) soit mixte en combinant une alimentation coaxiale et une alimentation coplanaire. Les antennes réalisées sont testées avec succès sur le corps pour différents types de scenarii. Lorsque les alimentations mélangent une alimentation coaxiale et une alimentation coplanaire, on obtient une bande passante en impédance commune supérieure au cas où les 2 ports sont planaires (4.95% vs 1.5%). Dans les deux cas, un gain en diversité de 9.5 dB est mesuré pour un milieu riche en multi-trajets. Cette valeur est proche du maximum théorique (10 dB) obtenu dans un canal de Rayleigh. On conclut donc que ces antennes compactes et peu sensibles à la présence du corps peuvent trouver leur place dans des vêtements professionnels (type pompier, pêcheur, etc…) où l’intégration n’est pas un élément clé mais où l’influence du milieu et la variété des mouvements et scénarii ne doivent pas empêcher un bon fonctionnement de l’antenne.

Mots clés: DRA, ouverture en H, diagrammes de rayonnement symétriques, boucle fente, gain de diversité (DG), Body Area Network (BAN).

Table of Contents

Chapter 1

Introduction

Contents

1.1 Problem statement:

This thesis is based on two distinct contractual projects ruled by the ESYCOM Laboratory. The common link between them is the use of DRAs as the heart of the antenna system.

1/ Project 1: Antenna element for digital beamforming arrays in the Ka-band.

The first project was an industrial one supported by AXESS EUROPE aiming the development of smart antenna arrays using digital beamforming (DBF) at Ka-band frequencies [1-2].
This project is related to the increasing demand for mobile access to fast data services in future broadband satellite systems. In-flight data exchange between aircrafts and satellites for real-time internet access is a prominent example with extensions to trains or trucks also anticipated.

Connexion by Boeing [3] was the first in-flight online Internet connectivity service allowing travelers to access a high-speed Internet connection while on board a plane in flight through a wired Ethernet or a wireless 802.11 Wi-Fi connection. The infrastructure used a phased array antenna Ku band antenna manufactured by either Boeing or Mitsubishi Electric Corporation

on the aircraft, leased satellite transponders, and ground stations (Fig. 1.1). The service provided downlink speeds of up to 20Mbit/s and uplink speeds up to 2 Mbit/s. Connexion by Boeing turned out to be a commercial failure in 2006 but a partnership between Honeywell et Inmarsat should provide a new service by 2015 in the Ka band (downlink 50Mbit/s at 20 GHz and uplink 5 Mbit/s at 30 MHz).

On the other hand, DBF provides a high degree of system flexibility, e.g. adaptive interferer cancellation and multiple-beam generation. These antennas are key subsystems for the next generation of communication platforms for mobile users. They have been the heart of the project called SANTANA (**S**mart **Ant**enn**a** Termi**na**l) initialised in 2001 and funded by the German government [4]. Within the SANTANA project, highly integrated transmit / receive modules are developed to demonstrate the technology of Ka-band multimedia terminals emploing digital beamforming. A complete medium size DBF system has been realised (64 antenna elements each for the transmiting / receiving terminal). This system has been successfully demonstrated by establishing communication links between the DBF terminal and moving platforms (car or plane).

In the future, this advanced technology is intended to complement or even replace existing airborne communications systems, which operate mostly in the Ku-band.

The scope of our project was to design appropriate radiating elements for an antenna array associated to a Ka-band receiver.

This radiating element must be designed with the triple constraint of polarization purity, impedance bandwidth and angular coverage. The efficiency of this radiating element is also mandatory as the total array size must be kept as small as possible.

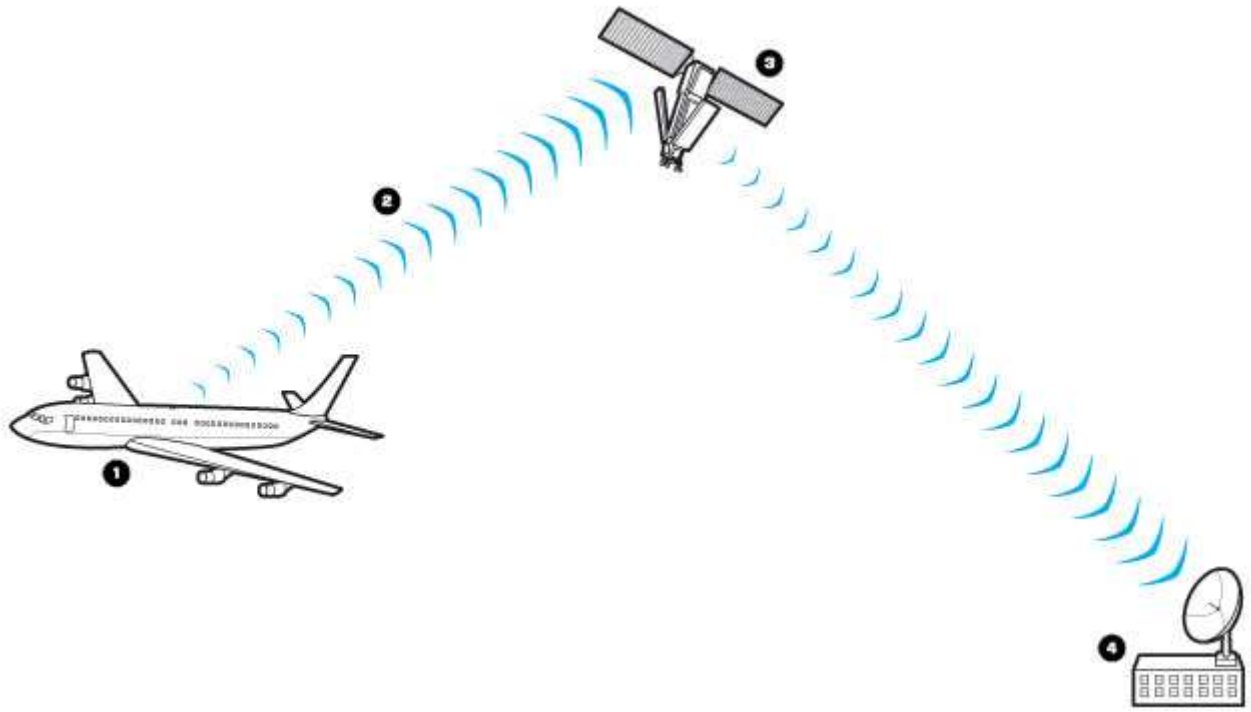

Figure1.1: Concept of Satellite systems for on-board multimedia and Internet traffic

Orthogonal linear polarizations can be used to improve isolation between receive and transmit paths in the RF front end, or to re-use a frequency for separate channels. Also, to avoid polarization mismatches in satellite communication systems, a dual linearly polarized or a circularly polarized antenna is considered to be the best solution. A circularly polarized antenna can be obtained with a single port but the phase quadrature combination of two orthogonal linearly polarized ports is usually preferred if wider 3dB AR bandwidths are required. High decoupling between these 2 ports is any case of major importance to respect the regulations.

In reported dual linearly polarized antennas, the impedance bandwidth and radiation patterns symmetry are often limited. One such type of situation is presented in Figure1.2 where the asymmetric radiation patterns limit the circular polarization purity [5].

For tracking applications, the need for large aperture coverage (say greater than ±70° in elevation) is also a key. When this coverage must be realized with a good CP purity and in bandwidths greater than few percents, common printed topologies are rapidly limited.

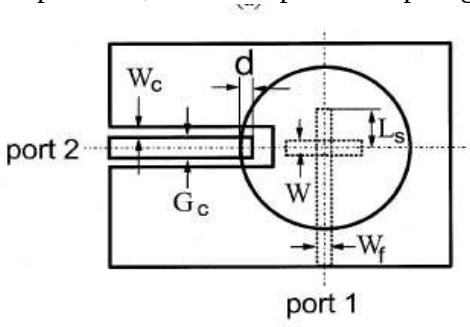

(a)

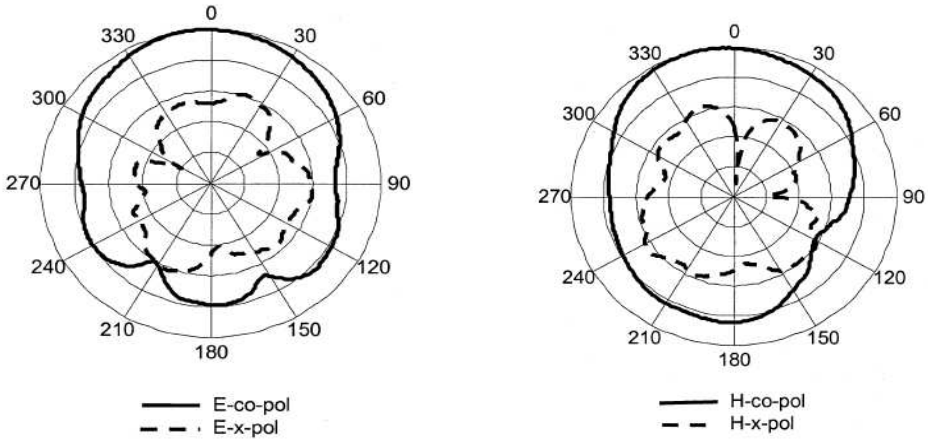

(b)

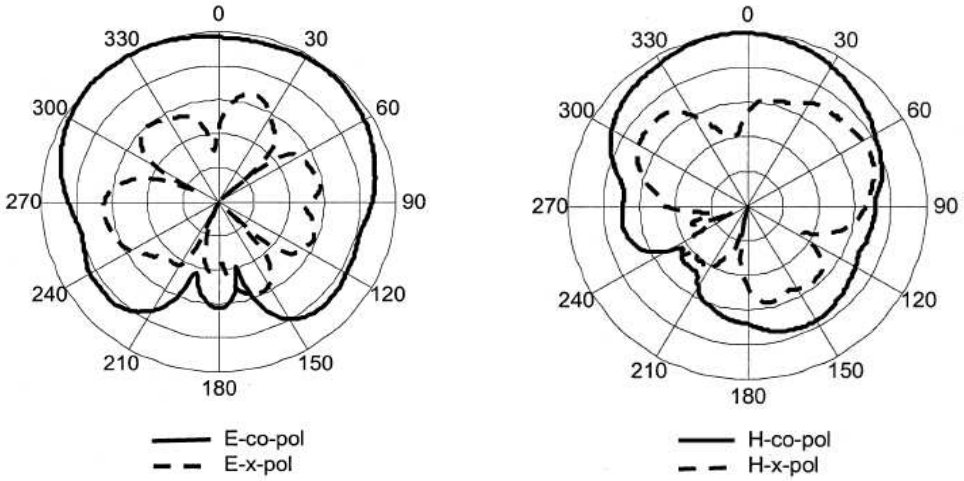

(c)

Figure:1.2 (a) picture of the antenna structure (b) port1:E&H co-polarization in broadside direction (c) port2: E&H co-polarization in broadside direction [5]

2/ Diversity antennas for Body-worn applications

In the frame of the ANR project BANET launched in 2007, the laboratory was involved in the development of antennas specifically dedicated to the BAN environment [6] and in the theoretical and experimental modelling of the BAN channel (Fig 1.3). The first objective of BANET was to provide a framework, models and technologies to design optimised wireless communication systems targeting the widest range of body area network based applications, in the consumer electronics, medical and sport domains

In indoor environments, two or more antenna structures working at the same resonance frequency but yielding different radiation patterns are often required to obtain the diversity features fighting the multi-path fading. To maintain compactness, these antennas must be integrated to each other while providing diversity features at the same time, i.e., distinct patterns/polarizations with high port decoupling. A two-port dual-pattern antenna yielding broadside and end-fire type radiation patterns normally offer an excellent Diversity Gain (DG) performance but owing to integration constraints it is often difficult to observe pure pattern forms rather they get de-shaped due to the effects of ports coupling. One such case is presented in Figure1.4 where it can be observed that in a dual-pattern ISM band antenna, high coupling levels have excessively de-shaped the expected radiation patterns which in turn increases the pattern correlation and reduces the DG.

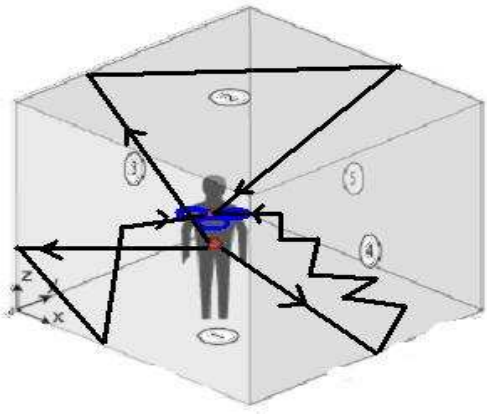

Figure1.3: A person walking in chamber is depicting a scenario in which signals from the transmitting antenna planted at belly (red) get reflected from the walls and other objects are received by the diversity antenna attached to the chest (blue).

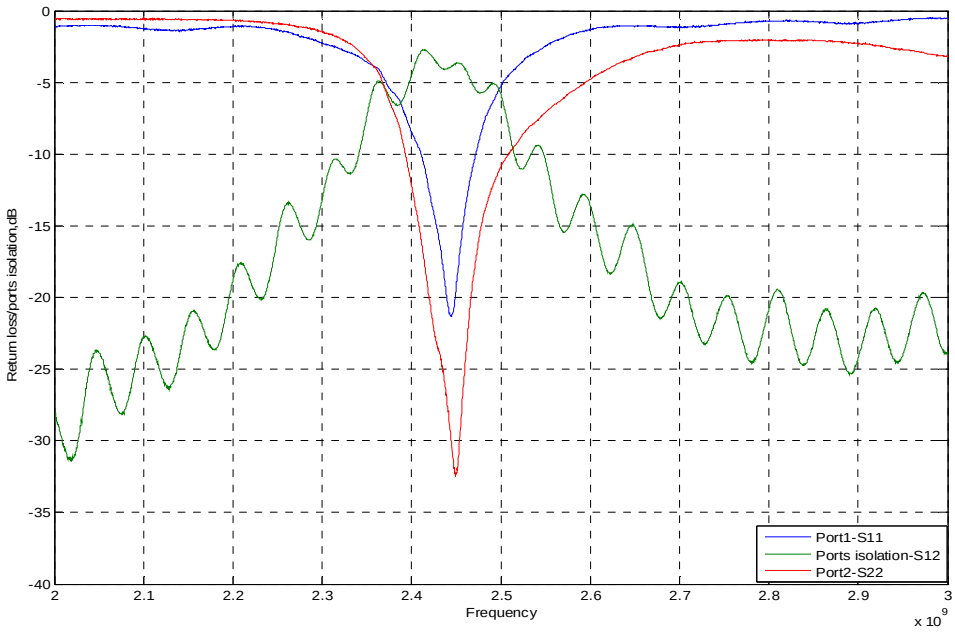

(a)

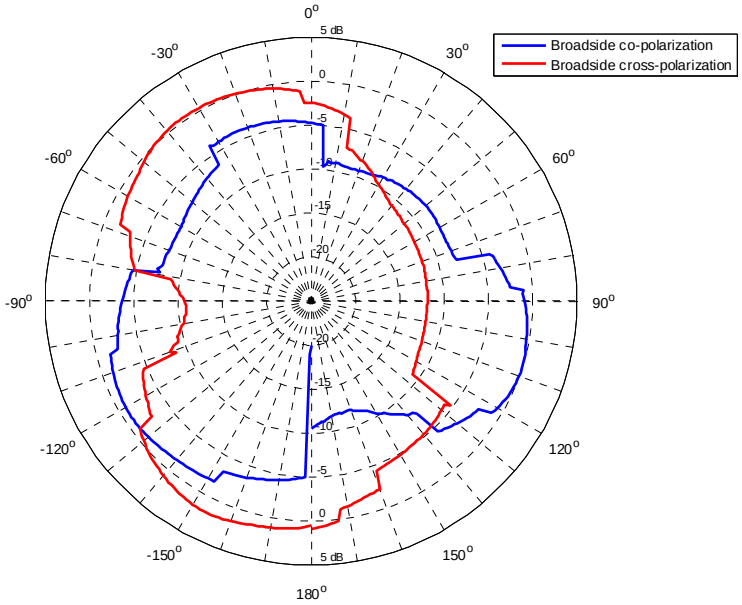

(b)

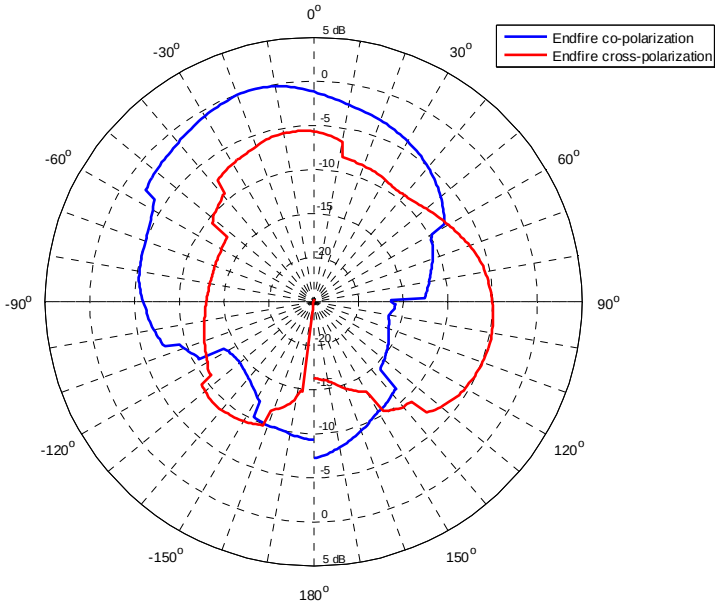

(c)

Figure1.4: (a) ISM band dual radiation pattern antenna depicting high level of ports coupling (-3dB) (b) De-shaped broadside radiation patterns (c) De-shaped end-fire type radiation patterns

In both projects, the need for compact dual-polarized antennas showing high polarization purity in large beamwidth and bandwidth is a great challenge with metallic antennas. The main expectation of this thesis is that Dielectric Resonator Antennas (DRAs) are good

candidates for the projects depicted above. This will culminate in the design and fabrication of two prototypes

1/ A dual linearly polarized X-band (8-12) GHz DRA yielding wide impedance bandwidth and symmetric radiation patterns to be used for radar and satellite applications. The prototype was developed at frequencies below the targeted Ka band to release the effort on the antenna fabrication, the main goal being the validation of the feeding strategies to reach the antenna performance.

2/ A diversity antenna showing a dual pattern and based on a slot-loop and DRA for Body Area Network (BAN) applications at 2.4GHz.

The main motivations for the choice of DRA are described below

1.2 Scope of Dielectric Resonator Antennas:

Dielectric materials are non conducting materials just like ordinary insulators but have peculiar characteristics to handle the effect of alternating electric fields which when applied, disturb its dipole orientations. Its behaviour then depends upon the situational property which defines how it reacts to the applied electric field and the induced dipole moment produced in it.
There is a long list of such materials either naturally available or synthetically fabricated by doping the mixture of different ceramic materials
The dielectric material's behaviour is recognized by a term "relative permittivity" or "dielectric constant" that is commonly expressed as $\varepsilon r = \varepsilon/\varepsilon_0$ where ε_0 is called permittivity of free space, i.e., the dielectric constant values are referenced with respect to the air ($\varepsilon r=1$).
The dielectric constant represents the ability of a material to carry an alternating current to the ability of vacuum to carry alternating current thus introducing certain capacitance in that material. Alternatively, when a potential is applied, it concentrates the electrostatic lines and correspondingly stores certain amount of energy, relative to the permittivity of the vacuum. Apart from efficient radiating elements in the form of antennas, the dielectric materials are used either in capacitors to increase their capacitance or in microwave circuits as resonators to increase the Q-factor of oscillators and filters.

The trendy next generation communication systems are shifting to higher and higher frequencies limiting metallic antennas performance. Apart from severe metallic losses or poor radiation efficiencies, they offer narrower impedance bandwidths such as in microstrip patch antennas. Under these circumstances, the performance of Dielectric Resonator Antenna (DRA) offers best results compared to other antennas families. Some of its characteristics are enumerated below that truly speak of their viability and applicability.

- ***Design & shape flexibility***: A broad variety of DRA shapes ranging from triangular to hemispherical and elliptical to split forms can effectively be employed. Some typical shapes among them are shrewdly manipulated to lower the resonance frequencies which cater to specific application needs where integration of large volume is a problem. For instance, for a given radius and dielectric constant the TE01 mode of the split cylinder DRA yields nearly 30% lower resonance frequency that its HEM11 mode yet both introduce same type of broadside radiation patterns [7]. The split cylinder DRA working in its TE01mode is presented in Figure1.5.

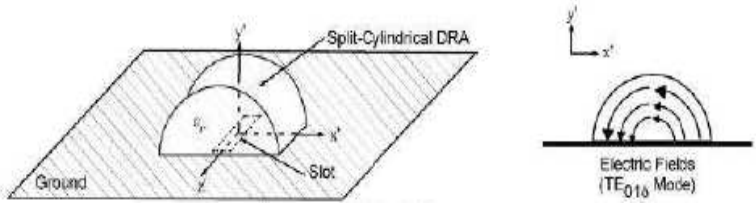

Figure:1.5 A DRA radiating it its TE01 mode[7]

- ***Wider impedance bandwidth***: In terms of performance, generally DRAs are compared with microstrip patch antennas however the former yields much wider impedance bandwidth than the latter. One such situation is depicted in Figure1.6 where at resonance frequency of 35GHz, the -10dB impedance bandwidth of the DRA (dielectric constant=10) is found to be 15.6% while for microstrip patch antenna it is just 2.6% [7].

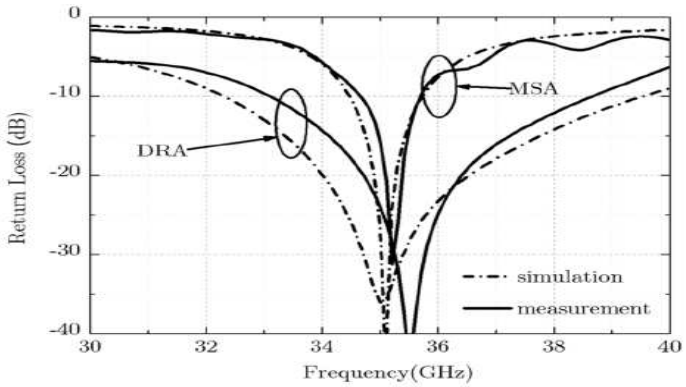

Figure1.6: Impedance bandwidths comparison between a DRA and microstrip patch antenna (MSA) [7]

- ***Ease of integration with other antennas***: DRA can be easily integrated to other types of antennas and in many cases it is just loaded upon them and as an additional advantage it lowers the resonance frequency and enhances the impedance bandwidth. One such set up is shown in Figure 1.7 where loading of the DRA upon patch antennas has reported an increase in their bandwidth from mere 2% to 10% [7].

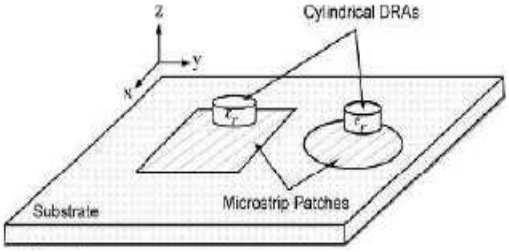

Figure1.7: DRA loaded upon square and circular microstrip patches [7].

- ***Negligible dielectric losses***: As no metallic losses are associated with DRAs and also dielectric losses are negligible so it offers an overall better efficiency particularly working at high frequency when compared to patch antenna. This comparison is illustrated in Figure1.8

where at 35.5GHz frequency the radiation efficiency of DRA is found to be 95% while for patch antenna it is 86% [8].

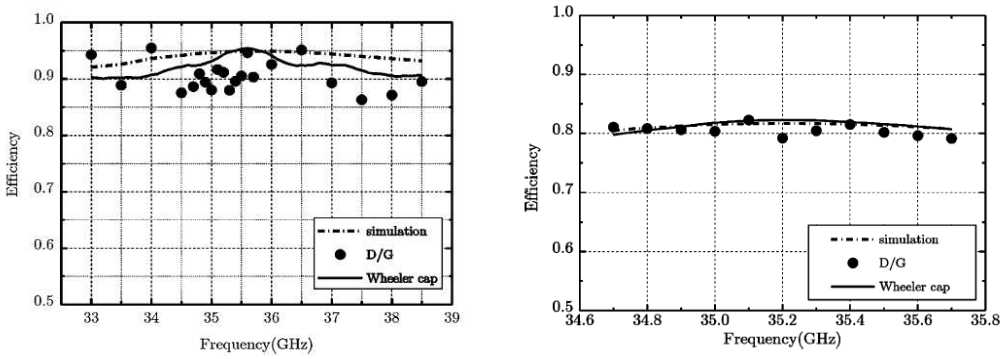

Figure1.8: Radiation efficiencies of (a) DRA as 95% (b) patch antenna as 86% [8].

- ***High temperature tolerance***: Excessive metallic losses at high temperatures disturb antenna frequency but due to negligible such losses in dielectric materials, DRAs are supposed to remain stable especially in adverse circumstances such as fire or war conditions [4].

- ***Versatile and flexible excitation techniques***. Normally patch antenna design require two substrates, one for supporting the patch while other is used to etch the feed structure thus restricting an access to other type feeds available to DRAs. Many innovative but simple feed excitations described in section2.2 can easily be employed to get DRA's improved performance [4]-[6].

1.3 Outline of the thesis:

The thesis is composed of five chapters of which the first chapter introduces general information, the problem statement, contribution of the thesis and the proposed solutions. The other chapters are more specific and target how the core issues are to be resolved.

Chapter2: Until the fundamental characteristics of the DRAs are thoroughly known, it is difficult to fully exploit their most significant aspects to design efficient and highly capable antennas. Chapter2 briefs the details of their possible geometry shapes, radiating modes yielding typical resonant frequencies and radiation patterns, choices of feed mechanism, and ways and means to optimise the expected results to fit to desired applications. Finally it elaborates the fabrication issues and also suggests some remedial measures.

Chapter3: In this chapter starting from the theoretical information, first of all fabrication issues would be resolved that mainly include DRAs mounting and gluing with the ground planes and the associated feed structures. These are evaluated in terms of changes in the resonance frequencies, bandwidths and radiation patterns. Based upon these conclusions, certain sensitivities and tolerances would be marked and be given due attention while finally designing a two ports dual linearly polarised DRA with high ports isolation and symmetric radiation patterns to be used at X band for radar and satellite applications.

Chapter4: This chapter includes rigorous simulation techniques to design a dual radiation patterns diversity antenna @2.4GHz to be used for Body Area Network (BAN) applications. In first part slot loop antenna that is to yield broadside radiation patterns is fed by coplanar waveguide line while DRA that is to yield end-fire type radiation patterns is fed by non-planar vertically embedded monopole from below the ground plane. In second part both feeds are made planar that is slot loop and DRA are excited by microstrip lines etched on the opposite side of the ground plane. Hence two compact antenna structures are realized that offer different types of advantages, one with larger common impedance bandwidth while the other facilitating its integration upon the body surface. Before the fabrication takes place, both are subject to on the body tests to observe if any change in their performance.

Chapter5: It is assigned to the actual measurements of the antennas and to evaluate their Diversity Gain (DG) performance in the BAN context. Both antennas, one with non-planar and other with planar feeds are measured in the free space and then planted at different body positions in receiving mode. A top-loaded monopole in transmitting modes is worn at belly position thus forming several communication links. The multi-path effects and time delayed replica of signals received at the diversity antenna are statistically assembled. Finally, suitable models are applied to observe their Diversity Gain (DG) performance.

Chapter6: This is dedicated to the overall conclusion and future prospects of the dual linear polarized and diversity gain antennas in the frame of DRAs.

References of the introduction

[1] F. Gargione, T. Iida, F. Valdoni, F. Vatalaro, “Services, technologies, and systems at Ka band and beyond-a survey”, *IEEE Jour. Sel. Areas Communicat.*, vol. 17, iss. 2, Feb 1999.
[2] P. Chitre, R. Gupta, “Satellite systems for multimedia and Internet traffic”, *IEEE MTT-S, Microwave Symposium Digest*, USA, vol. 2, pp. 1129- 1132, 2001.
[3] W.H. Jones, M. de La Chapelle, “Connexion by Boeing – broadband satellite communication system for mobile platforms”, *IEEE MILCOM*, vol. 2, pp. 755-758, 2001.
[4] A. F. Jacob and Al, “Active antenna arrays at Ka-band: Status and outlook of the SANTANA project," 2010 Proceedings of the 4th European conference on Antennas and Propagation, (Eucap)
[5] Yong-Xin Guo and Kwai-Man Luk “Dual-Polarized Dielectric Resonator Antennas” IEEE TRANSACTIONS ON ANTENNA AND PROPAGATION.VOL.51, No.5,May 2003 pp1120-1123.
[6] Christophe Roblin, Jean-Marc Laheurte, Raffaele D’Errico, Azeddine Gati and David Lautru, et al. “Antenna design and channel modeling in the BAN context—part II: channel, Annals of Telecommunications“, Vol. 66, No 3-4, March-April 2011
[7] Aldo Petosa, “DIELECTRIC RESONATOR ANTENNA HANDBOOK” ARTECH HOUSE, INC 685 Canton Street Norwood,MA 02062.
[8] Qinghu Lai, Georgios Almpanis, Cristophe Fumeaux, Hansruedi Benedickter and Ruediger Vahldieck “Comparison of the Radiation Efficiency for the Dielectric Resonator Antenna and the Microstrip Antenna at ka Band” IEEE TRANSACTIONS ON ANTENNA AND PROPAGATION, VOL.56, No.11,November 2008 pp3589-3592.

Chapter 2

A General Survey of DRAs

Contents

Apart from efficient radiating elements, Dielectric Resonator Antennas (DRAs) are very flexible in offering different shapes so any one can be chosen that is cylindrical, rectangular, hemispherical conformal or high profile that suits to particular needs, however operating in their fundamental modes they all radiate like horizontal magnetic dipoles, independent of their shapes.

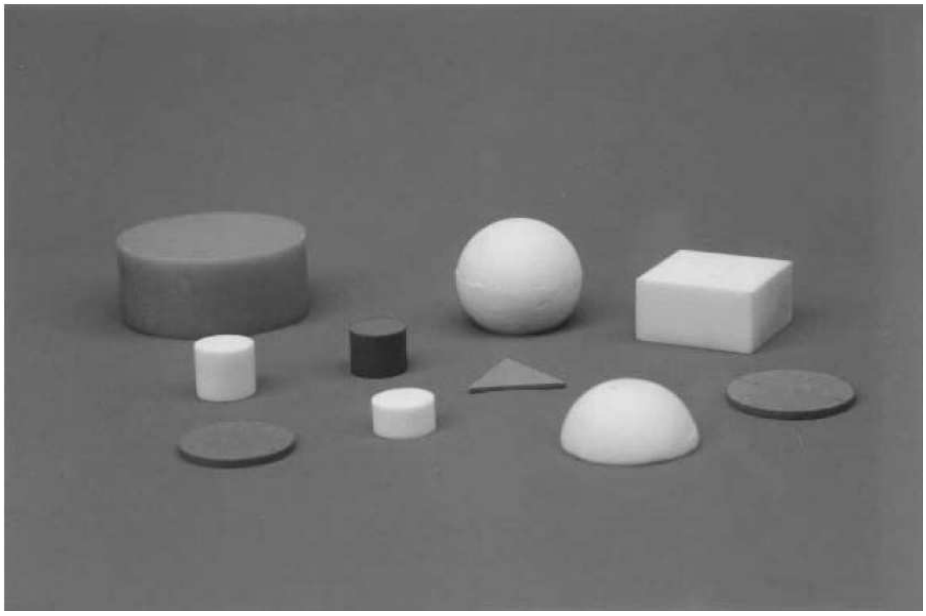

Figure2.1: Different shapes of DRAs .The picture shows cylindrical rectangular hemispherical low profile circular-disk, low profile triangular and spherical-cap DRAs. [1]

Special design shapes placed on the ground plane are presented in Figures 2.2, 2.3, 2.4, 2.5 and 2.6:

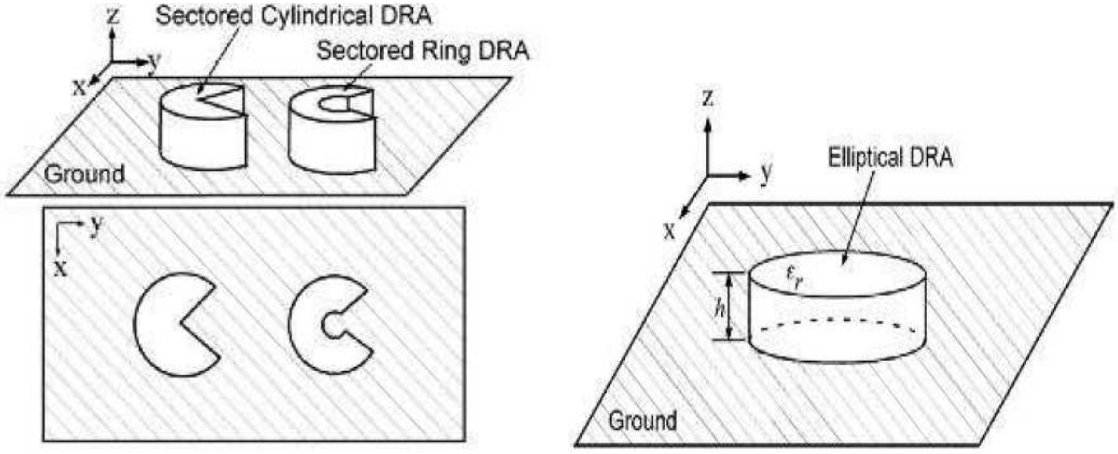

Fig2.2: Sectored and elliptical shaped DRAs to fulfil specific shape requirements [2]

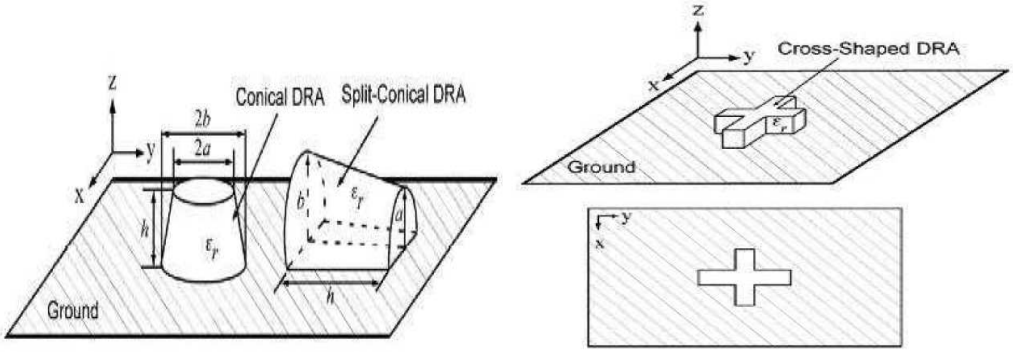

Fig2.3: Conical for large bandwidth and cross-shaped for dual polarization purposes [2]

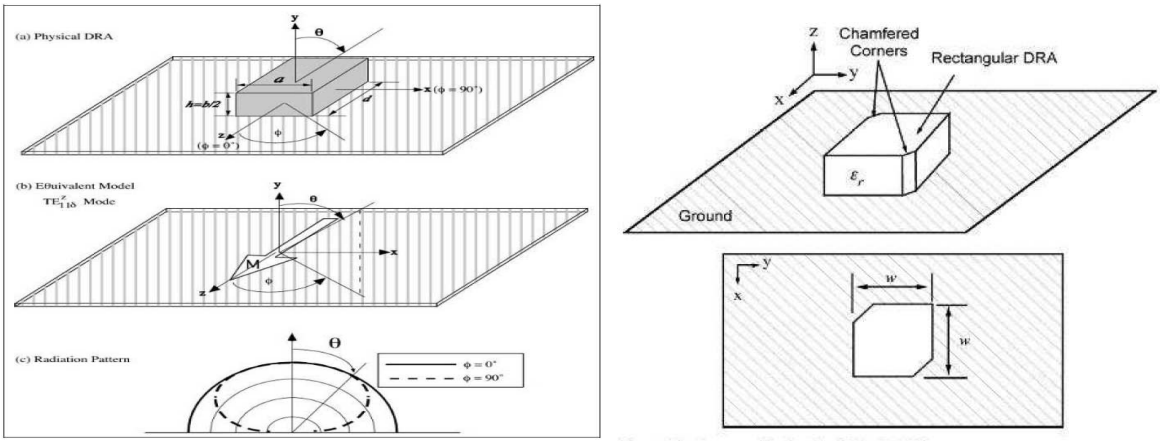

Fig2.4: Rectangular to yield broadside radiation patterns and Chamfered-shaped for circular polarization [2]

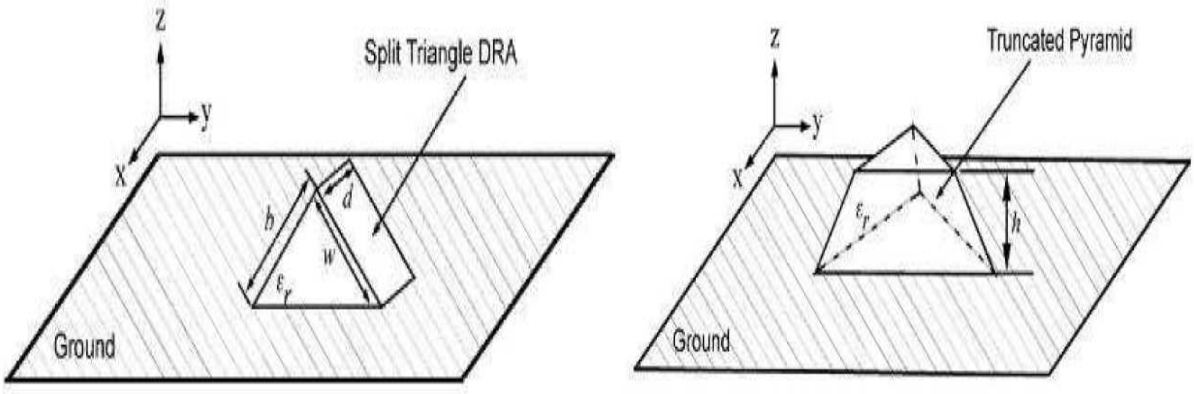

Fig2.5: Triangle and Truncated-shaped for more specific integration needs [2]

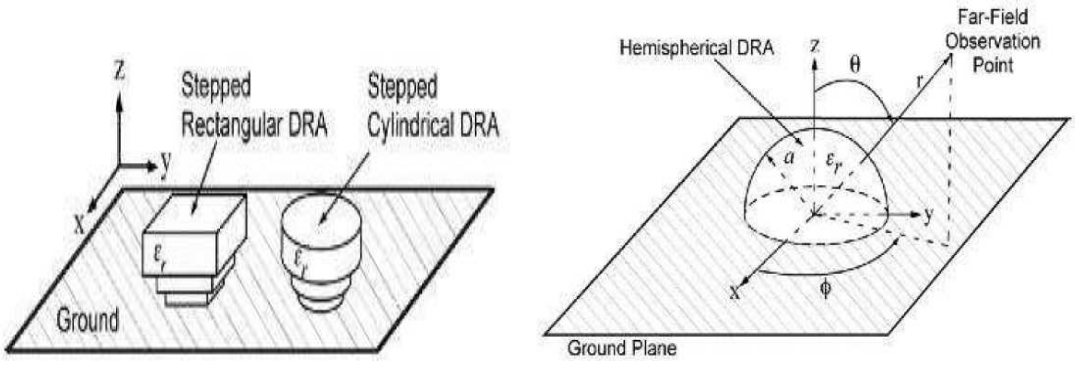

Fig2.6: Stepped for larger bandwidth and Hemisphere shaped for analysis purpose [2]

2.1 Cylindrical DRA Characteristics:

A DRA can be analysed in terms of its shape and modes of excitation. The electromagnetic near fields inside the resonating body are the prime sources of interpreting the far field radiation patterns and thus help to understand the overall characteristics of the antenna. Though many design shapes are available as shown in Figure 2.1, however the best one is that which is either readily available or that is simple to cut, grind and mould. It is for this reason that a circular cylindrical shape has been chosen for the proposed designs.

2.1.1 Resonant Modes:

Whatever may be the geometry shape of the DRA that is cylindrical, rectangular and hemispherical, ultimately it is analysed in terms of its resonant modes, near-field distribution inside the resonator, far-field radiation into the space, resonant frequency and impedance bandwidth. The resonant modes are generally classified into two categories such as *Transverse Electric (TE) and Transverse Magnetic(TM).* Both TE & TM must refer to a coordinate axis. For instance if TE is considered, it represents that in the direction of propagation the Electric field component vanishes while it becomes Transverse (perpendicular) to it [5]-[6]. For cylindrical DRA, it is suggested to make a mode analysis on the basis of cavity resonant model in which outer surfaces of the cavity are approximated by perfect magnetic walls so that eigen function expansion for the fields can be utilised. Then, on the same footings, same analytical approach can be extended to the mode analysis of rectangular or hemispherical shaped DRAs.

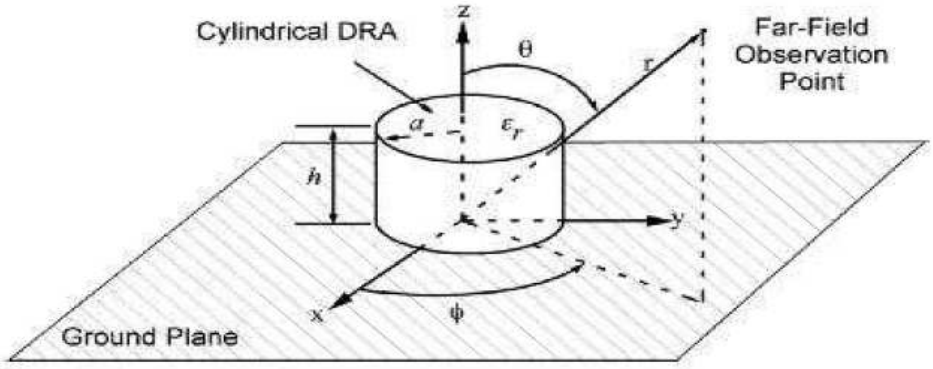

Fig2.7: Cylindrical DRA placed on the ground plane [2]

An isolated cylindrical DRA with radius "a" and height "h" on a large ground plane supports three distinct modes that is TE (to z), TM (to z) and hybrid. TE (Ez=0) and TM (Hz=0) are axially symmetric and have no φ variation while hybrid modes do have. At higher frequencies, pure transverse electric or pure transverse magnetic fields behaviour does not exist distinctively. So they are termed as hybrid electromagnetic fields and are represented by HEM, the lowest of them is HEM_{11} [6] .These fields are φ dependent and can be categorised into further two groups HE (if E_z component is dominant) and EH (if H_z component is dominant). However, for practical purposes only TE, TM and HEM_{11} are mostly considered. To identify the field variations along azimuth (φ), radial (r) and axial (z) usually three indices that is npm are used such as TE_{npm} or $TM_{npm..}$ The 1st index represents the no. of full period field variations in azimuthal direction, the 2nd index indicates the no. of radial variations while 3rd index specifies that the dielectric resonator is shorter than half wave length which is rarely used and hence for most of the cases it is omitted. The field description then depends upon just first two indexes n & p. When 1st index is zero, the electromagnetic field is circularly symmetric and seems in the form of concentric circles when viewed form the cross section side.

For cylindrical DRA of radius 'a' and height 'h or d', the field distribution can be described in terms of Bessel functions as:

$$TE: \quad H_z^{npm} = Jn\left\langle \left(X_{np}^{TE} r\right) \middle| a \right\rangle \begin{Bmatrix} \sin(n\phi) \\ \cos(n\phi) \end{Bmatrix} \sin\left[(2m+1)\pi z / 2h\right] \tag{2.1}$$

$$TM: \quad E_z^{npm} = Jn\left\langle \left(X_{np}^{TM} r\right) \middle| a \right\rangle \begin{Bmatrix} \sin(n\phi) \\ \cos(n\phi) \end{Bmatrix} \cos\left[(2m+1)\pi z / 2h\right] \tag{2.2}$$

n=1,2,3….. p=1,2,3…… m=0,1,2……

where Jn is the nth order Bessel function of the first kind while $\left(X_{np}^{TE}\right)$ and $\left(X_{np}^{TM}\right)$ are the roots that satisfy the corresponding characteristics equations:

$$J_n\left(X_{np}^{TE}\right) = 0 \quad \text{and} \quad J_n\left(X_{np}^{TM}\right) = 0$$

The simplified mathematical expression for the resonant mode frequencies is given by equation (2.3):

$$f_{npm} = \frac{C}{2\pi a\sqrt{\varepsilon_r}} \sqrt{\begin{Bmatrix} X_{np}^{TE^2} \\ X_{np}^{TM^2} \end{Bmatrix} + \left[\frac{\pi a}{2d}(2m+1)\right]^2} \tag{2.3}$$

Employing the corresponding mode, for instance TM110 mode the expression (2.3) reduces to:

$$f_{TM110} = \frac{C}{2\pi a\sqrt{\varepsilon_r}} \sqrt{\left\{X_{np}^{TM^2}\right\} + \left[\frac{\pi a}{2d}\right]^2} \qquad \text{in which} \quad \left(X_{np}^{TM^2}\right) = (1.841)^2$$

Practically Important Modes:

From application point of view, some typical modes are categorised as;

In open space dielectric resonator acts as a radiator either radiating broadside radiation patterns employing $TE_{01\delta}$ mode or HEM_{11} mode while monopole like radiation patterns (end-fire) using TM_{01} mode. As per need of a typical radiation pattern, any of the modes can be excited using a suitable feeding mechanism.

$TE_{01\delta}$ mode:

Usually this mode is excited in split-cylindrical shape for which the design formula is given in equations (2.4) and (2.5)

$$fr_{TE01}(GHz) = \frac{30(k_0 a)}{2\pi a(cm)} \tag{2.4}$$

$$k_0 a = \frac{2.327}{\sqrt{\varepsilon_r + 1}} \left\{ 1 + 0.212 \frac{a}{h} - 0.008 \left(\frac{a}{h} \right)^2 \right\} \tag{2.5}$$

TM_{110} (HEM_{11}) mode:

Its simplified design formula is given by the equation (2.6) as:

$$fr_{TM110} = \frac{c}{2\pi a \sqrt{\varepsilon_r}} \sqrt{(1.841)^2 + \left(\frac{\pi a}{2d} \right)} \tag{2.6}$$

TM_{01} mode:

Its simplified design formula is narrated by equations (2.7) & (2.8) such as:

$$fr_{TM01}(GHz) = \frac{30(k_0 a)}{2\pi a(cm)} \tag{2.7}$$

$$k_0 a = \frac{\sqrt{(3.83)^2 + \left(\frac{\pi a}{2d} \right)^2}}{\sqrt{\varepsilon_r + 2}} \tag{2.8}$$

The resonant frequency associated to each mode is briefed in the example of Table2.1

Table2.1: For ε_r=38, if a=0.6415cm and h=0.281cm

No.	Modes	Frequency
1	TE_{01}	3.98 GHz
2	$TM_{110}(HEM_{11})$	5.26 GHz
3	TM_{01}	6.12 GHz

2.1.2 Typical Mode Excitation

Depending upon the resonant frequency and the required type of radiation pattern such as broadside or end-fire a particular mode is excited. To accomplish it effectively, proper excitation methods are chosen which are mainly driven by:

- Type of the excitation feed.
- Position of the excitation feed.

Take for instance the case of a coaxial probe excite the TM_{110} (HEM_{11}) mode. It is to be placed close to the peripheral boundary of the cylindrical DRA whether embedded inside or poled equidistant outside it to yield corresponding broadside radiation pattern. Now, if the same probe is shifted gradually towards the centre of the DRA, the TM_{110} mode diminishes while $TM_{01\delta}$ emerges to dominate so instead of exhibiting broadside, it presents the end-fire type radiation pattern. On the other hand, if aperture slot is to be employed, it is to be placed at the centre, for generating a broadside radiation pattern while to seek end-fire pattern it is supposed to be shifted to the DRA boundary.

It is important to note that a crucially important factor is the aspect ratio (a/h). It describes that a taller DRA with smaller diameter can yield the same resonance frequency as that of very short in height but very large in diameter however, both structures posses different Q values. According to different permittivity values, there is a limit of (a/h) and beyond it further control of shape may not be possible. The aspect ratio(a/h) also plays a significant role in determining as if to merge two closely resonating modes to generate *wider -10dB bandwidth or not.*

To make the concept clearer, we consider the near field distributions inside the cylindrical DRAs and their corresponding far field radiation patterns in terms of TE_{01}, TM_{01} and TM_{110} (HEM_{11}) resonant modes [7-9].

ModeTE_{01}:

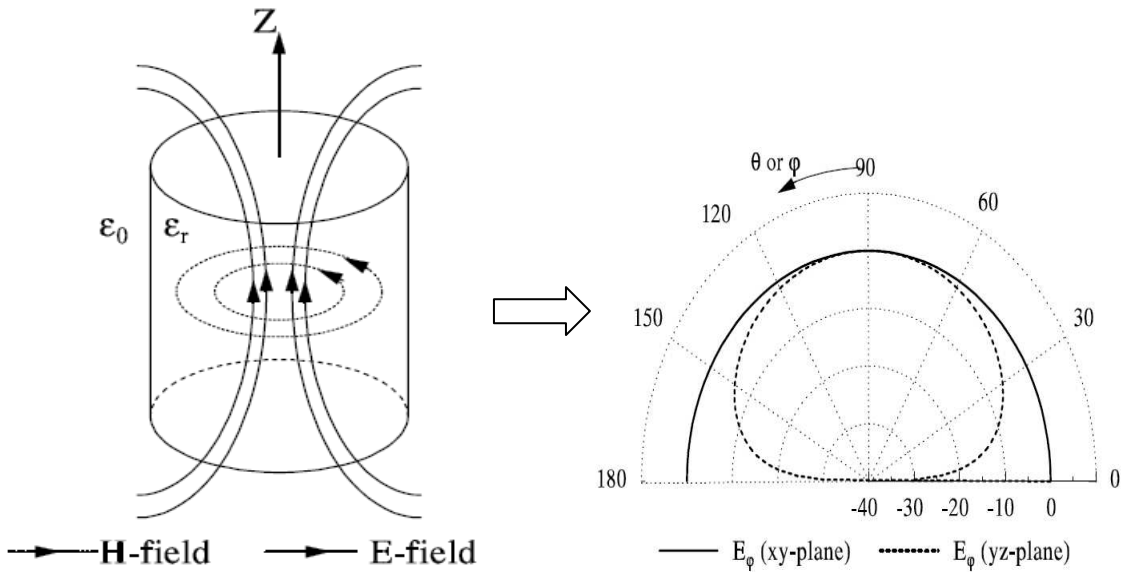

Fig2.8: ModeTE_{01} and its broadside far field radiation pattern [1].

Mode TM_{01}:

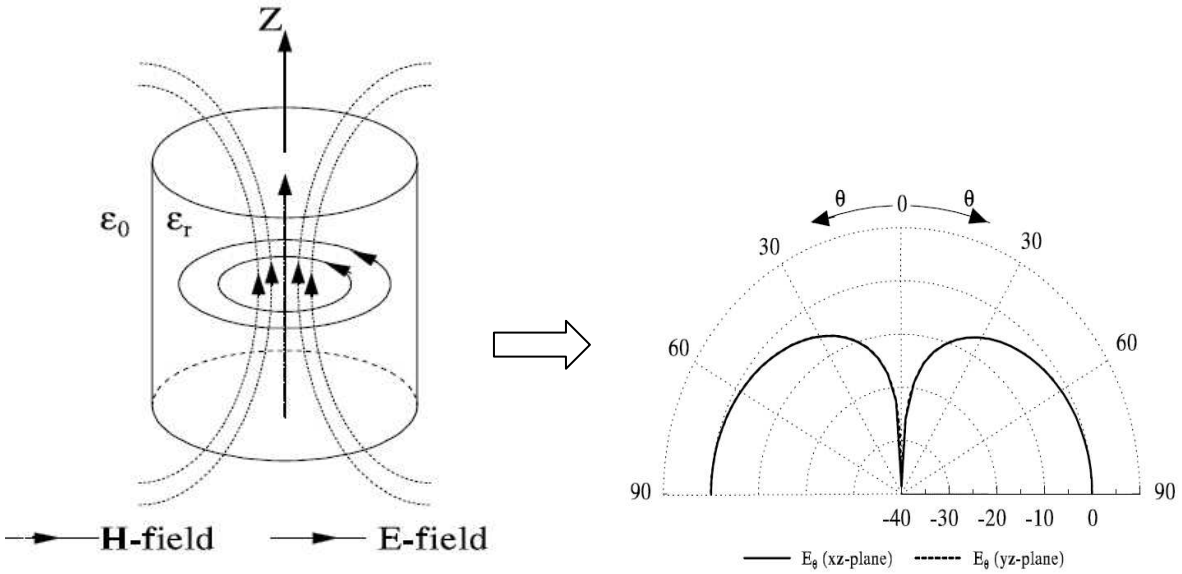

Fig2.9: ModeTM_{01} and its monopole like far field radiation pattern [1].

Mode TM_{110} (HEM_{11}):

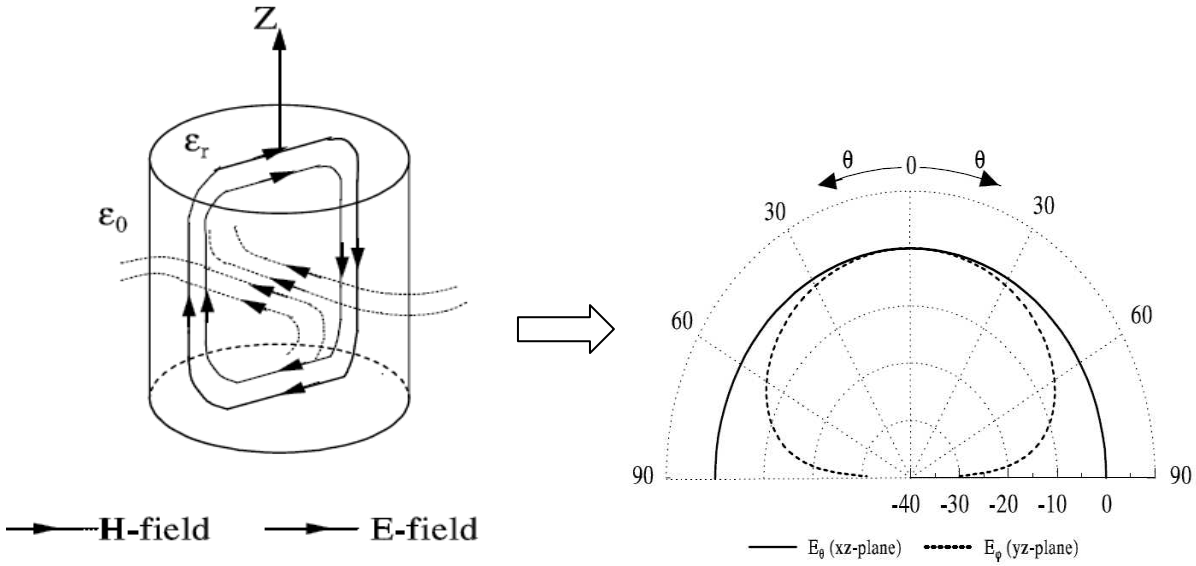

Fig2.10: Mode TM_{110} (HEM_{11}) and its broadside far field radiation pattern [1].

In practice, the excitation source may resonate several modes simultaneously [10]. The field strength for a typical mode depends upon the exactness of the feed location and its operating frequency.

These far field radiation patterns have clear resemblance to other renowned antenna types. The TE_{01} seems like radiation pattern of half wavelength narrow slot on the ground plane and directed to the axis of resonator. The radiation pattern from TM_{01} seems like a quarter

wavelength monopole above the ground plane [10]. The HEM_{11} resembles to that of half wavelength narrow slot on the ground plane.
A graphical representation of patterns has been given in Fig2.11 that explains how a gradual transformation in pattern shape takes place at par with the changing locations by an aperture slot under the DRA.

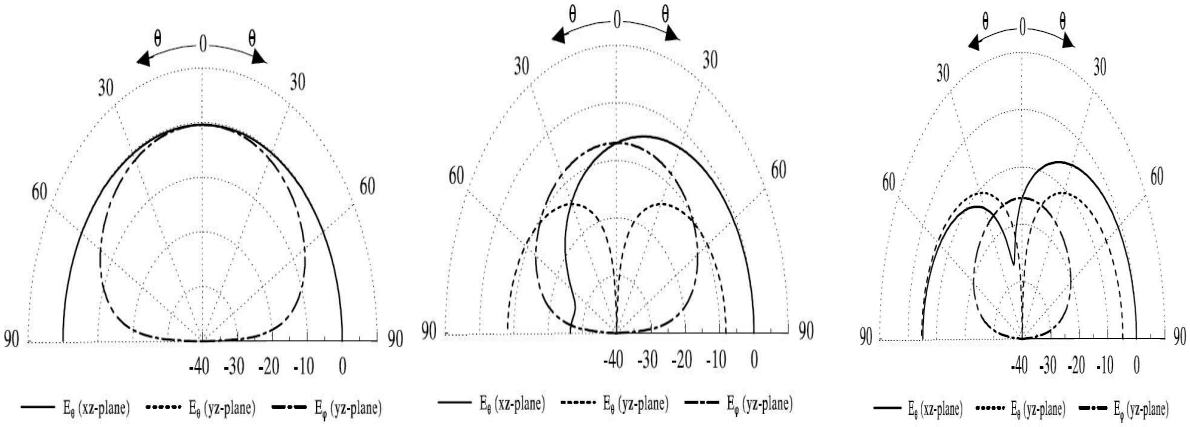

(Centre) (Mid way to Boundary) (Close to Boundary)

Fig2.11: Changing radiation patterns corresponding to different slot positions under DRA [1]

It is interesting to observe that when slot is exactly located at the centre the pattern generated is perfectly symmetric with no cross polarisation, However, when slot shifts from centre to boundary, the cross polarization grows and ultimately transforms to totally different pattern .

2.2 Survey of Excitation Techniques

There are some general rules which simplify the feeding mechanism, applicable to any DRA type and that can further be refined by using numerical methods[11]-[12].
While coupling to the DRA, typically one source (Electric or Magnetic) is considered that in turn defines the amount of energy being coupled. Using this principal, a resonance can be sought and tuned over a specific range while slightly displacing the feed position with respect to the DRA. As a normal practice it should be located with in the stronger field influence whether Electric or Magnetic .Let if J1 is the source electric current and E2 is the Electric field inside the DRA then the amount of coupling from electric source is given by:

$$K \infty \int_V (E_2 . J_1) dV \tag{2.9}$$

Similarly if M1 is the source magnetic current and H2 is the magnetic field inside the DRA then the amount of coupling from magnetic source is given by;

$$K \infty \int_V (H_2 . M_1) dV \tag{2.10}$$

The coupling mechanism not only transfers energy to the DRA but also generates loading effect which directly controls DRA's Q factor .Both external Q- factor and loaded Q-factor are expressed mathematically as ;

$$Q_{ext} = \frac{Q}{K} \tag{2.11}$$

$$Q_L = \frac{Q}{1+K} \tag{2.12}$$

This phenomenon suggest that maximum power is transferred from the coupling port to the DRA when k =1 so in view of it a particular excitation method is selected.

2.2.1 Aperture Slot

It is a renowned coupling technique with the advantage of having the feed network located below the ground plane to avoid unwanted radiations that cause distortion and degrade the pattern shape. For HEM_{11} or TM_{110} being the dominant resonant mode, the aperture at the DRA centre behaves like magnetic current flowing parallel to its length and as a result excites the magnetic fields in the DRA body causing broadside radiation pattern in the far field [13-15]. It is depicted in Figure 2.12. The slot is fed by microstrip line because it is easy to etch on the substrate and to seek impedance matching. This technique is particularly recommended for high frequency designs requiring highest level of precision and etching accuracy.

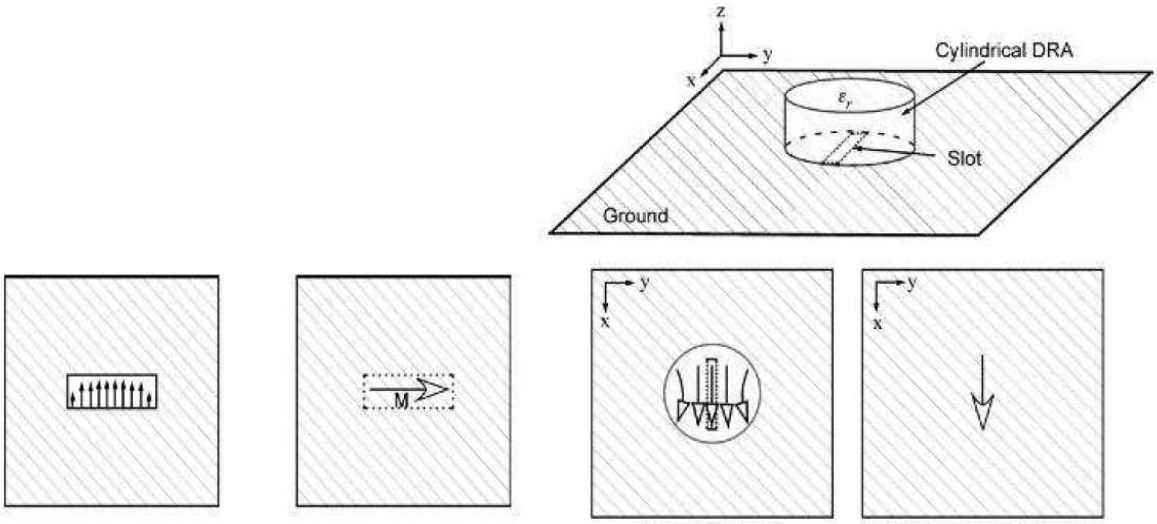

Fig2.12: Electric and Magnetic field distributions in slots [2]

The slot's resonance is avoided to reduce backward radiation. So the slot's dimensions are kept small enough to avoid its resonance merge with that of the DRA and large enough to couple sufficient amount of energy. Although the exact size of the slot is determined by the numerical method, however one can estimate its length (l_s) and width (w_s) to start with as:

$$l_s = \frac{0.4\lambda_0}{\sqrt{\varepsilon_e}} \tag{2.13}$$

Where

$$\varepsilon_e = \frac{\varepsilon_r + \varepsilon_s}{2} \tag{2.14}$$

ε_r and ε_s are dielectric constants of DRA and substrate respectively.

$$w_s = 0.2\, l_s \tag{2.15}$$

A quarter wavelength stub length can significantly improve the coupling to the DRA as its reactance cancels out to that of the slot. It is given as

$$s = \frac{\lambda_g}{4} \tag{2.16}$$

Where λ_g is the guided wavelength in the substrate thus used.

2.2.2 Coaxial Probe

The probe can be considered as a vertical electric current that is positioned to achieve strong coupling to the DRA. The level of coupling is optimized while adjusting the height and diameter of the probe. Depending upon the shape of DRA and probe location, different modes can be excited that is when it is fed axially only TM modes are excited. To be more precise that if TM_{01} mode is to be excited, the feed probe is expected to be located at the centre thus yielding quarter wavelength monopole like far field radiation patterns. On the other side when HEM_{11} (TM_{110}) mode is required, the feed probe is supposed to be located close to the peripheral boundary so as to yield broadside radiation patterns. The location of probe at two different positions and associated electric and magnetic fields are presented in the Fig 2.13. This is a simple mechanism as in this case one can directly couple to 50Ω without going for matching network [16-19].This technique is particularly recommended at lower frequencies to cope with the fabrication issues, however it is equally efficient and result oriented at higher frequencies. For instance compared to slot feed's approximate position in the peripheral area of the cylindrical DRA, it is simple to locate the probe at its centre when to excite TM01 mode .

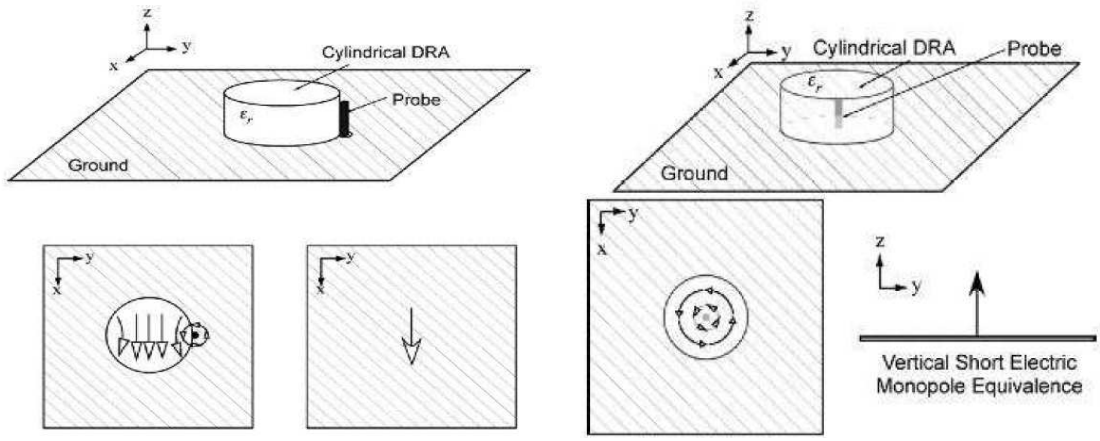

Fig2.13: To excite DRA Electric and Magnetic current distributions in monopole [2]

2.2.3 Microstrip Line

Direct and Proximity couplings are amongst the simplest methods. It excites the magnetic fields in the DRA to produce the short horizontal magnetic dipole [20]. The amount of coupling can be improved by controlling a parameter *s* or by increasing the dielectric constant (permittivity) value of the material used. It is a common conclusion that for low value of dielectric constant, minimum energy is coupled. However, with increase in its value other limitations are encountered particularly at higher frequencies further reduction in size can cause fabrication process too sensitive and that may introduce faulty results. Similarly the

consequence reduction in impedance bandwidth can limit its wideband applications. The behaviour of the coupling fields can be observed from the Fig2.14.

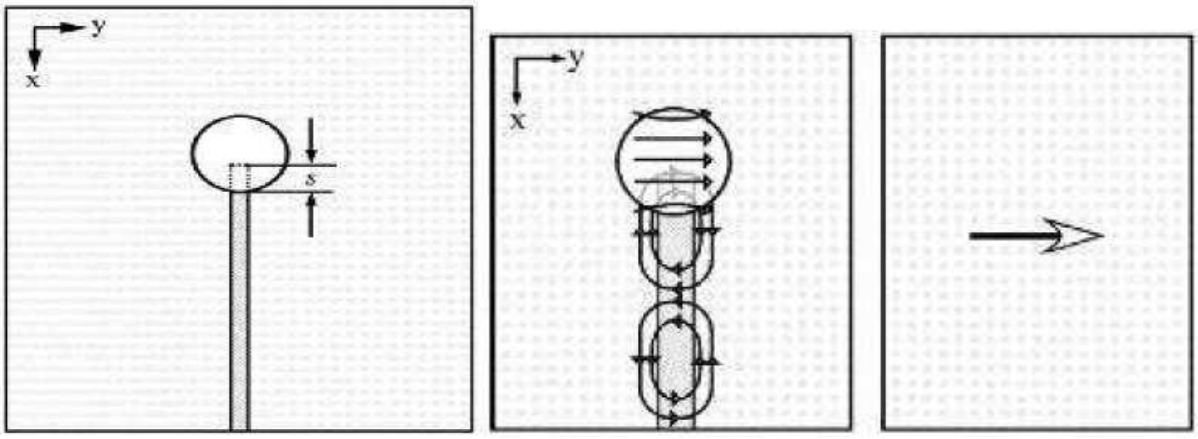

Fig2.14: Electric and Magnetic field distributions in proximity coupling [2]

2.2.4 Coplanar Feeds

The coplanar loop efficiently couples energy to the DRA. The coupling level and desired mode excitation can be obtained by gradually sliding the DR element over the loop [21-24]. By shifting the loop from the edge to the centre one can yield required resonance frequency and radiation patterns. One such arrangement with field distribution is shown in Fig2.15.

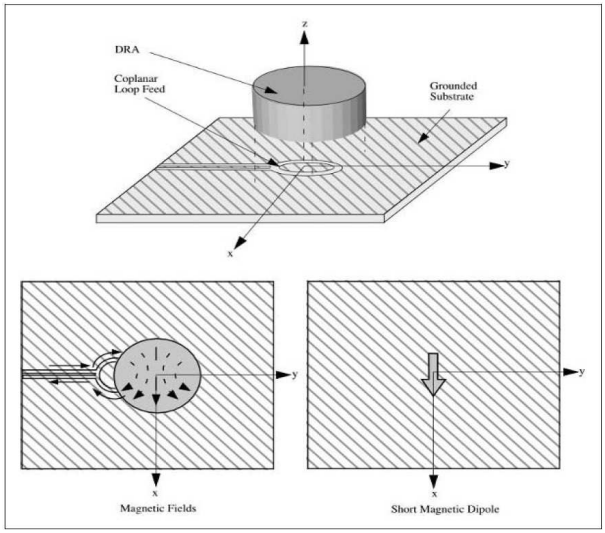

Fig2.15: Magnetic fields distributions in coplanar feed coupling to DRA [1]

2.2.5 Dielectric Image Guide

At millimetre-wave, if microstrip feed lines are used, the conductor losses become significant. To avoid this problem the use of dielectric image guide is the best solution .The dielectric image guide couples the energy to the DRA that is located in its proximity. Again, considering associated limitations, a higher permittivity value can be chosen to enhance the coupling level. This method also offers an added advantage that it can be utilised as series

feed to linear array designs [25]. Fig2.16 speaks of the magnetic fields distribution in the image guide and their coupling behaviour to the resonator.

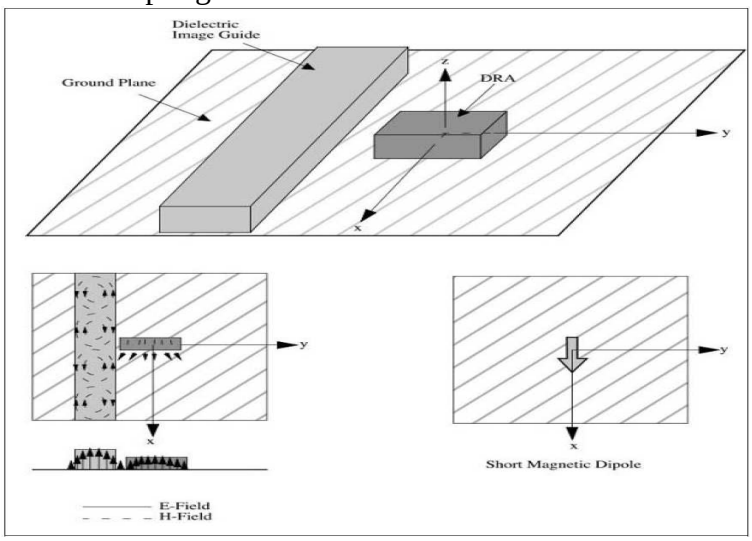

Fig2.16: Magnetic fields distributions in dielectric image guide and its coupling to DRA [1]

2.3 Dual Port Excitations

For circular polarization purposes dual ports excitation is preferred over single port so as to yield a wider 3dB Axial Ratio (AR) bandwidth. For both circular and linear polarizations, highly decoupled ports are usually required. Different feed combinations can be chosen to suite particular requirements that is *similar feeds* or *hybrid feeds* .These can be viewed in terms of ports isolation, coupling level, radiation pattern symmetry and ease of fabrication [26]. Consider for instance, the following cases:

2.3.1 Hybrid combination of coaxial probe and aperture slot

Though better port isolation is obtained but at the same time two other problems arise such as:

- Fabrication constraints, while drilling and embedding the probe into the DRA body needs a lot of accuracy. It also introduces additional air gap which at higher frequencies greatly shifts the results.
- Probe yields asymmetrical radiation patterns that are not acceptable to obtain circularly polarized waves.

2.3.2 Hybrid combination of aperture slot and coplanar waveguide

Again good level of port isolation is obtained, yet it is constrained due to:

- Fabrication of waveguides particularly in thin substrates is a cumbersome task that requires high level of precision and accuracy.
- It restricts its usage to a number of applications.

2.3.3 Similar combination of two aperture slots

Though comparing with hybrid combinations it introduces comparatively poor ports isolation, however, it adds other important advantages such as;

- A simple fabrication process that eliminates the possibility of variation in results.
- The feeding network is below the ground plane so spurious radiation interferences are avoided and the integration of the DRA with printed feed structures is facilitated.
    - Whatever may be the choice of combinations, alike or hybrid it is recommended to set priorities in terms of design feasibilities.

2.4 Bandwidth Enhancement Techniques

The use of the broadband devices in the modern communication systems is on the rise so a practical purposes antenna is supposed to have wider bandwidth [31-33]. The bandwidth limitation of antennas is usually linked to their input impedance because it is the quantity which changes with frequency so improvement in impedance response can help us to enhance its bandwidth.
This approach can be implemented into four broad categories:

i. Simple structures; controlling permittivity (ε_r) & aspect ratios(a/h).
ii. Q-factors reduction; introduction of air gap.
iii. Usage of matching networks.
iv. Employment of multiple resonators.

2.4.1 Simple Structures

Among numerous choices, it is the most simple and result oriented approach. After selecting the resonant mode, it is the resonator's dielectric constant value and its aspect ratio (a/h) that define the obtainable bandwidth. In simple geometric shapes such as cylindrical DRAs the smallest possible ε_r value makes Q-factor low which as a consequence results in wider bandwidth [34].

$$BW = \frac{S-1}{Q\sqrt{S}}.100\% \qquad (2.17)$$

Where S= desired VSWR at the input of DRA port.
However, there are some limitations which are always associated with every type of design, for example in this case though the Q-factor can be decreased accordingly by lowing the value of dielectric constant but if lowered drastically, it fails to capture enough amount of electromagnetic energy and to act as an efficient resonator.
The other choice is to seek proper aspect ratio value (For cylindrical DRA a/h=0.329) that generates two closely merged resonances such that a wider (-10dB) impedance bandwidth is obtained. Being simple in fabrication, it is preferred over other techniques. One such device is shown in Fig2.17.

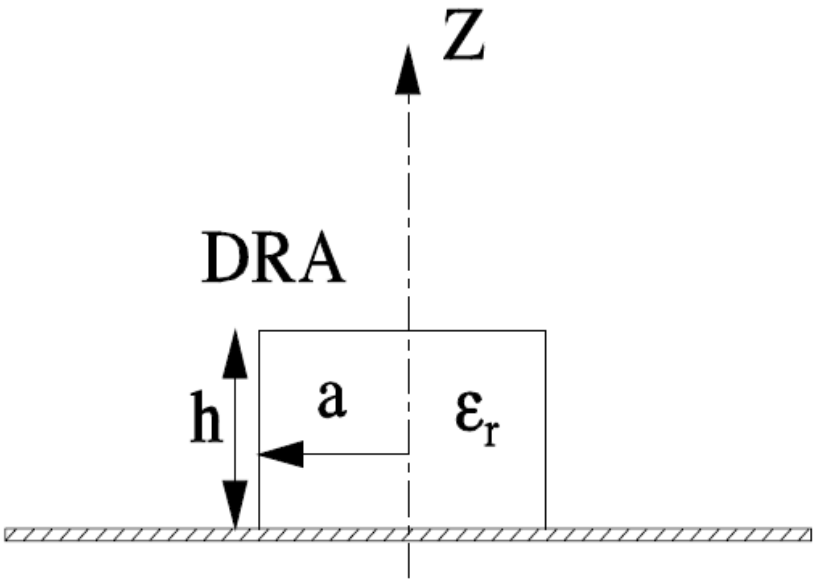

Fig2.17: A single piece DRA structure with radius a and height h [1]

2.4.2 Q-factors reduction

By the introduction of air gap surrounding the monopole and enclosed by the DRA body helps in lowering the effective dielectric constant of the DRA [27] which as a result lowers the Q-factor and thus increases the bandwidth while pushing the resonant frequency upwards. Comparatively wider bandwidths are achieved at the cost of higher complexity of the fabrication process. One such model is presented in the Fig2.18. A very slight displacement of DRA with respect to the centrally located monopole can shift the resonance frequency from desired position. A very careful and highly precise cutting and grinding of DRA piece is required otherwise undesired air gap size may drastically influence the results.

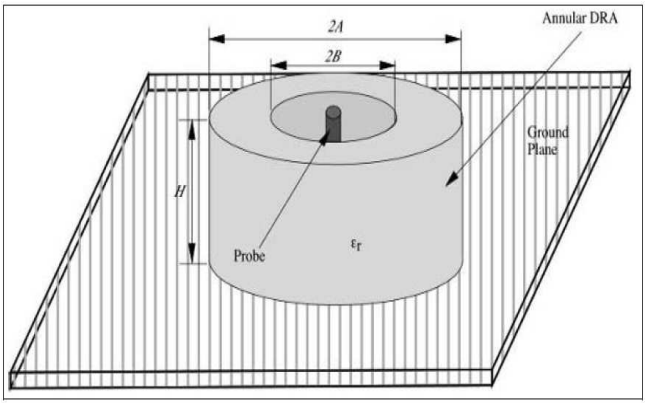

Fig2.18: Air gap enclosed structure to enhance bandwidth [2].

2.4.3 Impedance matching

The bandwidth can also be enhanced by manoeuvring impedance matching by using different types of material before matching to desired DRA. For instance flat matching inserts, loaded notches and multi-segment DRAs are common techniques. A high permittivity inserts between the feed and resonating body element is fitted to couple the energy efficiently. A rectangular shaped DRA with under laid high permittivity insert is shown in Fig2.19. Back radiation is common problem with aperture slot feeds, however if a carefully selected insert is used not only coupling is improved but back radiation is also controlled.

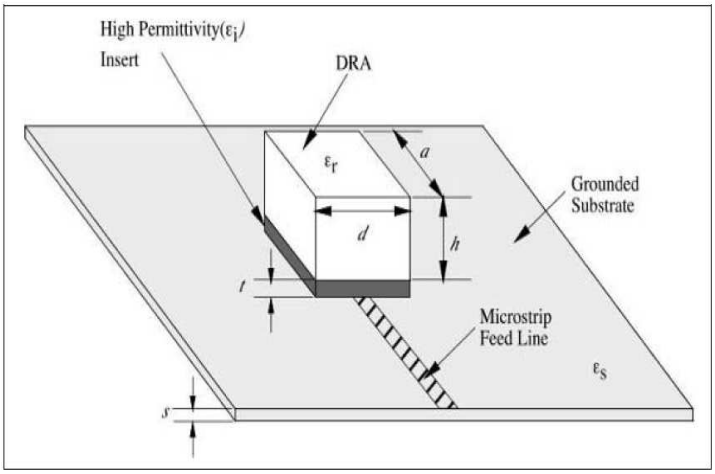

Fig2.19: DRA with high permittivity insert in its structure to enhance bandwidth [1]

2.4.4 Multiple Resonators

Considering individual design sizes, multiple elements are made to resonate at slightly apart frequencies which are shrewdly tuned either to merge to offer wider bandwidth or to separate to yield multi- bands [28-29]. Such types of stacked DRAs excited by a probe, are depicted in Fig2.20. The major disadvantage in this scheme is that it is difficult to accurately position and paste the upper element. So a better solution to this problem can be found in using proper aspect ratio factor for which there is no need to cut the pieces into different dimensions.

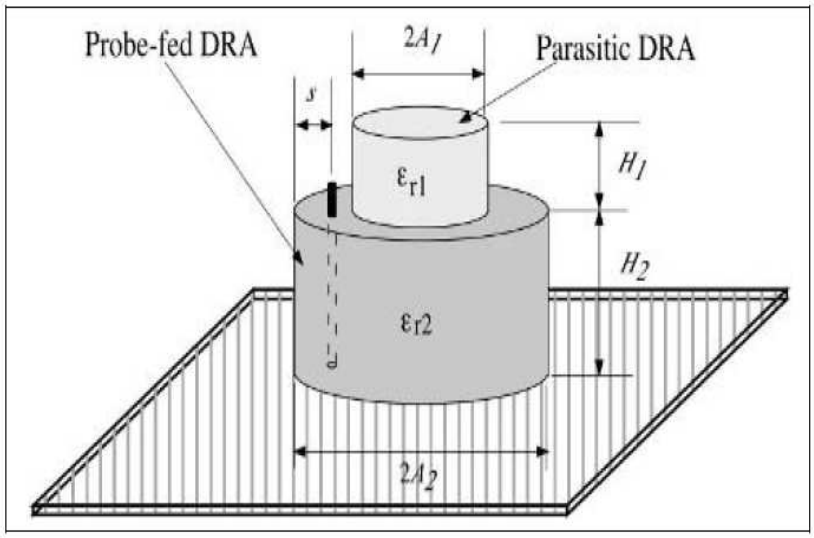

Fig2.20: Stacked DRAs to merge two close resonant frequencies to enhance bandwidth [2]

2.5 Ground Plane Effects

Normally, during the calculations an infinite size ground plane is used but from practical point of view it is always finite with well defined dimensions. Because of scattering from the edges of the ground plane, this factor directly influences the radiation pattern emanating from the antenna. In order to evaluate the effect of edge on radiation patterns, generally two methods are employed one is the numerical method such as Method of Moment (MoM) for smaller radiating structures and other is Geometrical Theory of Diffraction (GTD) that is for larger radiating structures [30-32]. The GTD is basically is an extension of Geometric Optics(GO) that is a ray tracing technique in which direct and reflected rays are superimposed to get overall field influence as is shown in Figure2.21.

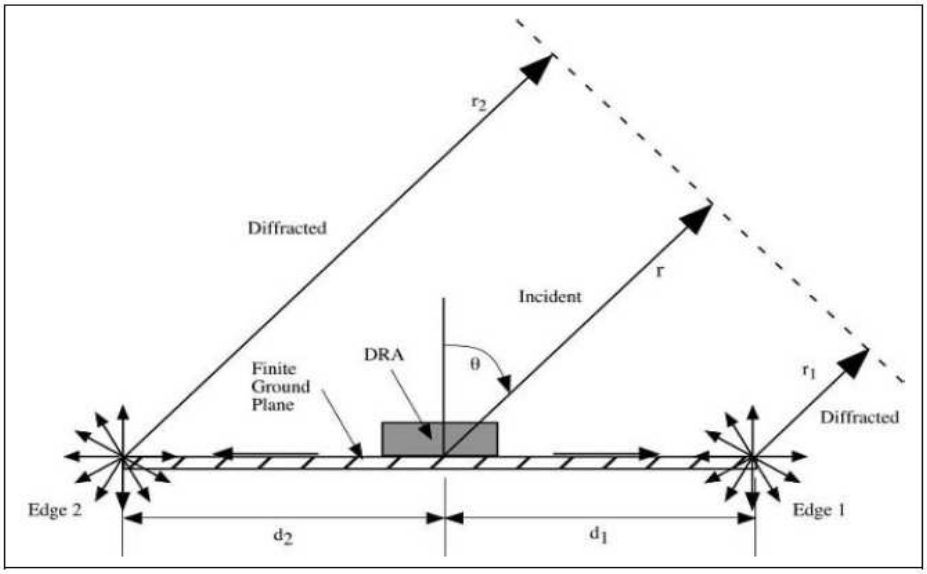

Fig2.21: Diffracting fields bending from a finite ground plane edges [1]

The total radiated field E can be expressed in terms of vector sum of GO fields (E_{go}) and diffracted fields (E_d), such as;

$$E = E_{go} + E_{d1} + E_{d2} \tag{2.18}$$

The diffracted fields from the edges can be found from the following relation;

$$E_d = 0.5E_{go}(\theta = \pm 90°)D(d_i, \psi_i, n).\frac{e^{-jkd_i(1\pm\sin\theta)}}{\sqrt{d_i}}.e^{-jkr} \tag{2.19}$$

Where

i = 1,2(Represent two edges)

$D(d_i, \psi_i, n)$; Diffraction Coefficient

n=2 for plane wedge

It has been observed by numerical methods that finite ground plane introduces ripples in the front and back radiation patterns which are not present in the infinite ground plane. It indicates that after reflection from the edges the recombination of radiations undergo some constructive or destructive patterns. The size of the ground plane can be varied to see if any, impact upon the radiation patterns. It is estimated that front to back ratio can be improved to certain extent by enlarging the size of the ground plane and that can be attributed to the possible reduction in edge slipped back radiations.

2.6 Circularly Polarised DRAs

Considering wide choices of feed structures available to DRAs some are particularly proposed to generate CP waves. These include:

Simple designs employing single feed:

- Truncation of two opposite corners of a rectangular DRA.
- Exploitation of crossed shaped slot or slot inclined at 45° with respect to DRA.

A bit more complex dual ports design:

- Employment of quadrature feeds.

Complex fabrication designs:

- Utilisation of single and pair parasitic patches.
- Use of perturbed annular slot.

Basic principal of single port technique is to excite two nearly degenerate orthogonal modes to generate a CP wave which usually offers a few percent 3dB (AR) bandwidth and obviously in some applications it is not sufficient. On the other hand a quadrature fed DRA yields two spatially orthogonal E-fields to yield a CP wave that can significantly enhance 3dB(AR) bandwidth even though at the cost of its design complexity.

2.7 DRA Arrays

A single element DRA's gain could be about 5 dBi which can be increased by an array arrangement. The overall performance of an array can be evaluated in terms of the following parameters;

i. Geometry and dimensions of DRA elements.
ii. The spacing among elements.
iii. The number of elements used.
iv. The feed mechanism.

Depending upon a particular need any of the aforementioned techniques can be employed, some of such mechanisms are depicted in the diagram 2.22[36].

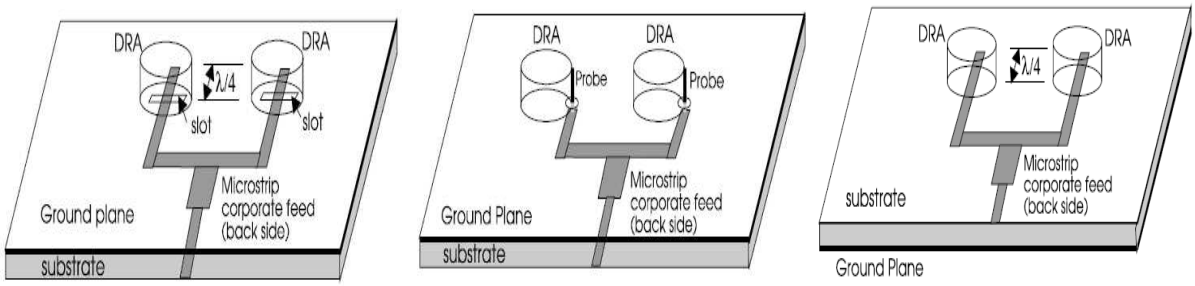

Fig2.22: Possibility of different feeds structure to construct arrays [2]

Array Types

To understand the working of an array, certain general rules are taken into consideration.
Like for other antenna arrays, the overall radiation pattern of DRA depends upon the radiation pattern of single element multiplied by the array factor that is:

$$E = n \times E_0 \times AF \qquad (2.20)$$

Where:
E= Overall radiated electric field.
E_0 = Electric field at same point produced by single DRA at the centre of array.
AF= Array factor that depends upon the geometrical structure (Linear or Planar), the phase difference of current among elements and the operation frequency. AF corresponds to the following mathematical relations:

Linear E-plane array (along x- axis direction);

$$AF = \frac{1}{n}\frac{\sin[n(k_0 s\sin\theta\cos\phi)/2}{\sin[(k_0 s\sin\theta\cos\phi)/2} \tag{2.21}$$

Linear H-plane array (along y- axis direction);

$$AF = \frac{1}{n}\frac{\sin[n(k_0 s\sin\theta\sin\phi)/2}{\sin[(k_0 s\sin\theta\sin\phi)/2} \tag{2.22}$$

Where: ko=2π/λo (wave number)

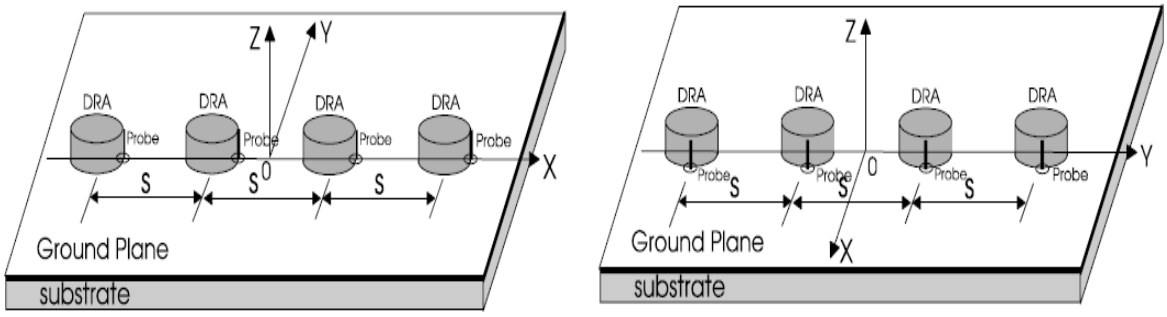

Fig2.23: E-plane and H-plane arrays arranged along x-axis and y-axis [2]

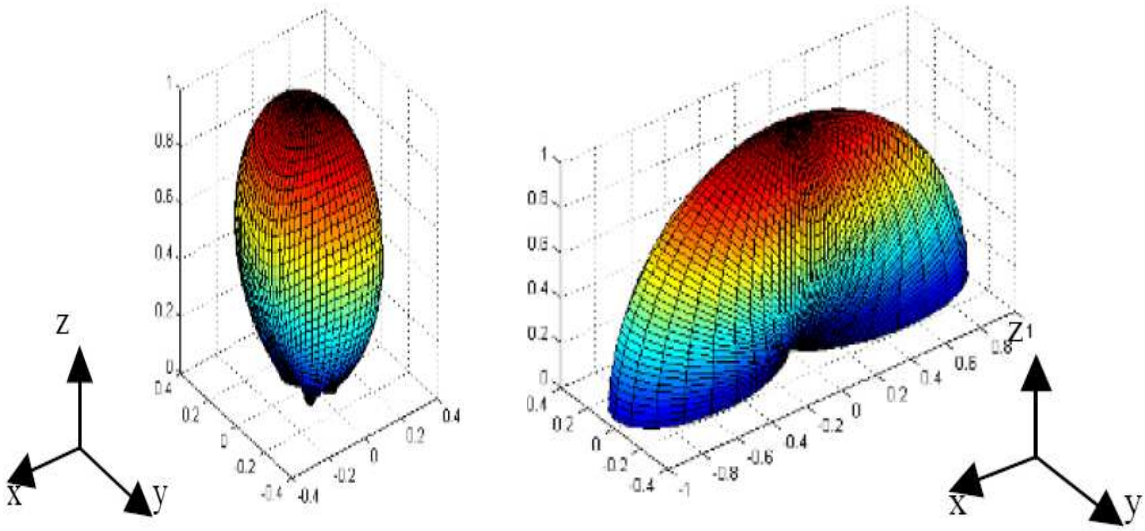

Fig2.24: E-plane & H-plane linear arrays radiation patterns [2]

DRAs operating at fundamental mode with broadside radiation, the E-plane array with spacing s= λ/2 has higher directivity than H-plane, while the number of DRA elements in the array make the beam width narrow [37]. These are illustrated in the Figs2.23&2.24.

Planar array;

$$AF = \frac{1}{mn}\frac{\sin[m(k_0 s_x \sin\theta\cos\phi)/2]}{\sin[(k_0 s_x \sin\theta\cos\phi)/2]}\frac{\sin[n(k_0 s_y \sin\theta\sin\phi)/2]}{\sin[k_0 s_y \sin\theta\sin\phi)/2]} \tag{2.23}$$

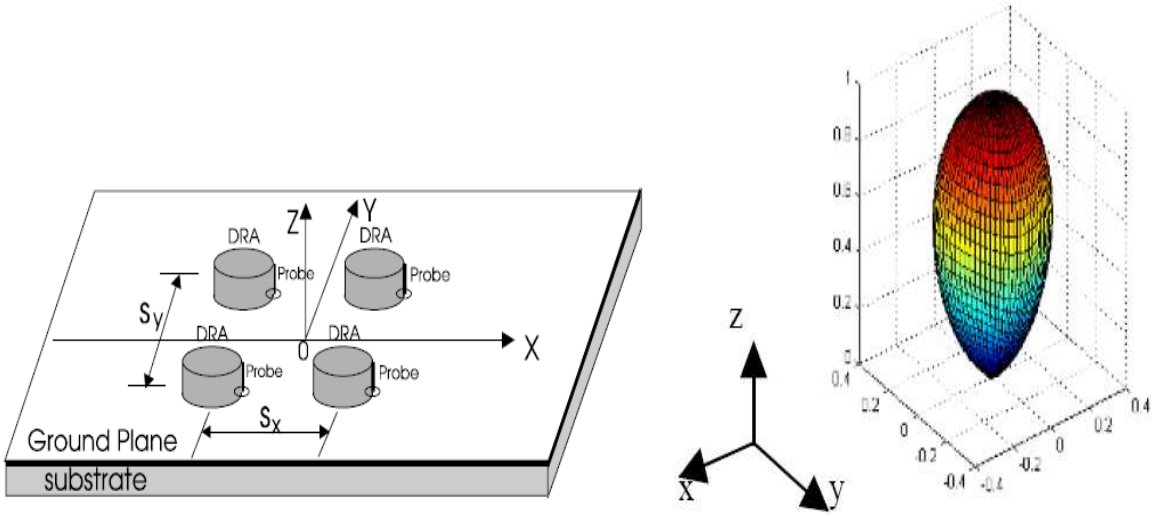

Fig2.25: 2× 2 elements planar array and its more focussed radiation pattern in the broadside direction [2].

CP array:

The arrays can also be constructed while using (CP) DRA elements. One such array consists of 2×2 elements configuration and is presented in the Fig2.26. The arrangement is coupled by single unequal crossed slots that are fed by sequentially rotated microstrip lines. However, if dual port coupling is to be used some viable mechanism is to be devised to employ quadrature feed so that the array can generate (CP) wave [38-39]

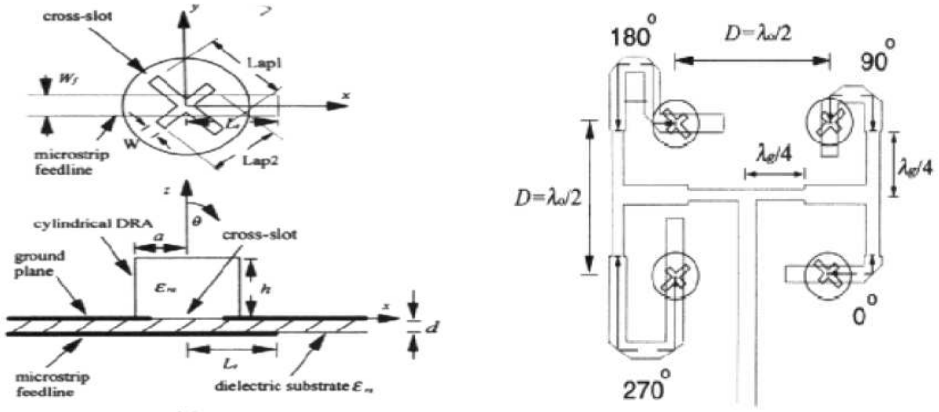

(a) (b)

Fig2.26 (a) Cross-slot coupling of unequal slot lengths (b) 4 elements sequentially rotated microstrip fed circularly polarised array [1].

Mutual coupling:

An array require that elements be arranged into closer packing, however at the same time leaving some space margin to introduce some isolation among radiating elements is also important. The coupling level or electromagnetic interaction not only depends upon proximity of array elements but also on structure's orientation, values of the dielectric constant, the heights of DRAs and the thickness of the substrate used. Corresponding to the degree of severity of these factors, nearly all important radiation characteristics are influenced such as radiation pattern, directivity, operation frequency and bandwidth. Various tests have reported that a spacing of $\lambda/2$, generally offers better isolation both in E-plane and H-plane configurations.

2.8 DRA Fabrication Issues

One of the inherited advantages of DRA is its use at millimetre wave frequencies and until a very sophisticated process aided by micromachining is available a poor fabrication process is involved. Though newer methodologies such as Low Temperature Co-fired Ceramic (LTCC) technology have already matured enough to handle such delicacies and has yielded wonderful results but for very few experimental prototypes it is either unavailable or too expensive to manufacture. So one is constrained to rely upon some alternative methods though at the cost of little bit variations in the expected results.
When evaluating the performance issues, the DRA may suffer from the following factors:

- Fabrication tolerance of DRA structure & feed network.
- DRA cutting and mounting accuracies.
- Possible variation in permittivity values.
- Adhesive materials to glue DRA bodies to the ground planes.
- Un-wanted air gaps.

The degree of influence of these factors upon fabricated designs can be verified by comparing repeatedly the theoretical results to those with the measured ones.

2.9 Conclusion

The basic characteristic and performance issues of the DRAs have been thoroughly analysed. It has been estimated that they can fulfil our needs in the best possible way. So setting the priorities, crucial points are marked and practicable strategies are ready to materialise the design. These designs are thought to be simple enough to avoid any fabrication complexity and efficient enough to offer outstanding performance even in adverse circumstances.

References:

[1] Kwai- Man Luk and Kwok-Wa Leung; *Dielectric Resonator Antennas* Research Studies Press LTD,England.

[2] Aldo Petosa ; DRA Hand book

[3] R.K Mongia,A.Ittipiboon, "Theoratical and Experimental Investigations on Rectangular Dielectric Resonator Antennas", *IEEE Transactions on Antennas and Propagation*,Vol.45, No.9,Sept.1997,pp.1348-1356.

[4] S.C Gao,L.W. Li,M.S. Leong and T.S.Yeo, "Dual-polarized slot-coupled planar antenna with wide bandwidth", *IEEE Trans.Antenna and propagate*.,Vol.51,No.3 ,pp.441-448,March 2003.

[5] S.A Long, M.W.McAllister, and L.C .Shen, " The resonant cylindrical dielectric cavity antenna," *IEEE Trans.Antennas Propag*.,Vol.AP-31,no.5,pp.406-412,May 1983.

[6] Darko Kajfez and A.A.Kishk, "Dielectric Resonator Antenna-Possible Candidate for Adaptive Antenna Arrays", University of Mississippi,USA.

[7] Y.KOBASHI and S.TANAKA, "Resonant Modes of a Dielectric Rod Resonator Short Circuited at Both Ends by Parallel Conducting Plates",*IEEE Tras.Microwave Theory & Tch.*,1980,VolMTT-28 no,10 pp.1077-1085.

[8] D.Kajfez and P.Guillon, Dielectric resonators, Vector Fields, Oxford, Mississippi,1990.

[9] K.F.Lee.K.M.Luk and P.Y. Tam, " Crosspolarisation characteristics of circular patch antennas", *Electron.Lett*., Vol.28.pp.587-589,1992.

[10] K.W.Leung..K.M. Luk.K. Y. A.Lai and D.Lin, " Theory and experiment of a coaxial probe fed dielectric resonator antenna", *IEEE Trans. Antennas Propagat*., Vol.41.pp.1390-1398,Oct,1993.

[11] David M .Pozar, " Microwave Engineering" by Jhon Wiley & Sons,Inc.

[12] R.E Collin ,Foundation for Microwave Engineering,Mc Graw-Hill,1966.

[13] A.Ittipiboon,R.K.Mongia,Y.M.M.Antar,P.Bhartia,M.Cuhaci, " Aperture Fed Rectangular and Triangular Dielectric Resonators for Use as Magnetic Dipole Antennas", *IEE Electronic Letters*,Vol. 29,No,3, 1993, pp.2001-2002.

[14] A.A.Kishk, A.Ittipiboon, Y.M.M Antar, M. Cuhaci, " Dielectric Resonator Antenna Fed by a Slot in the Ground Plane of a Microstrip Line", Proc.Eight Int .Conf.on Antennas and Propagation, ICAP'93,Apr, Part 1,pp. 540-543.

[15] K.W .Leung , K.Y.A Lai, K.M. Luk, D.Lin, " Input Impedance of Aperture Coupled Hemispherical Dielectric Resonator Antenna", *IEE Electronics Letters*, Vol.29, 1993,pp.1165-1167

[16] G.Zhou, A.A. Kishk, A.W. Glisson, " Input Impedance of a Hemispherical Dielectric Resonator Antenna Excited by a Coaxial Probe", *IEEE Antennas and Propagation Symposium*,Ann Arbour Michigan ,June 1993,pp, 1038-1041.

[17] G.P Junker,A.A Kishk,A.W Glisson,D.Kajfez, " Effect of an Air Gap Around the Coaxial Probe Exciting a Cylindrical Dielectric Resonator Antenna", *IEE Electron Letters*, Vol.30, No.3,Feb. 1994, pp.177-178.

[18] G.P.Junker, A.A Kishk, and A.W.Glisson," Input Impedance of Dielectric Resonator Antennas Excited by a Coaxial Probe", *IEEE Trans. Antennas and Propagation*,Vol.42.No.7,July 1994,pp.960-966.

[19] M Cooper, A,Petosa, A.Ittipiboon,J.S.Wight, " Investigation of Dielectric Resonator Antennas for L-Band communication", Antenna Technology and Applied Electromagnetics Symp ANTEM ' 96, Ottawa, Canada, Aug.1996.

[20] R.A .Kranenburg, S.A. Long, " Microstrip Transmission Line Excitation of Dielectric Resonator Antennas", *IEE Electronics Letters*, Vol.24,Sept,1998,pp.1156-1157.

[21] R.Kranenberg, S.A Long, J.T.Williams, "Coplanar Waveguide Excitation of Dielectric Resonator Antennas", *IEEE Transactions on Antennas and Propagation*, Vol.39,Jan.1991.pp.119-122.
[22] C Curry, " Novel Size- Reduced Circularly Polarized Antennas", Master's Thesis, Royal Military College,Kingston, Canada,July 2000.
[23] M.S Al Salameh, Y.M.M. Antar, G.Seguin, A. Petosa, " Analysis and Measurement of Compact-Size DRA With CPW Feed", USNC/URSI National Radio Science Meeting,Boston, MA ,July 2001,pp,221.
[24] J.P.S.McKenzie, "Dielectric Resonator Antennas Fed by Coplanar Waveguide at Extremely High Frequecy", Master's Thesis,Royal Military College,Kingston.
[25] M.T .Birand, R.V. Gelsthorpe, " Experimental Millimetric Array Using Dielectric Radiators Fed by Means of Dielectric Waveguide" *IEE Electron Letters*, Vol.17.No.18,Sept.1981,pp.633-635.
[26] Y.X Guo, K.M. Luk, "Dual polarized dielectric resonator antennas", *IEEE Trans.Antennas and Propagat*.,Vol.51 no.5,pp.1120-1123.
[27] S.M. Shum and K.M. Luk, "Stacked Annular Ring Dielectric Resonator Antenna Excited by Axi-Symmetric Coaxial Probe", *IEEE Transactions on Antennas and Propagation*, Vol.43, No.8,Aug.1995,pp.889-892.
[28] A.A.Kishk, A.W.Glisson and J.P.Junker, " Study of Broadband Dielectric Resonators",Proceedings of the 1999 Antenna Applicatios Symposium, Allerton Park, Monticello, Illinois,Sept,1999,pp,45-68.
[29] A.A.Kishk, B.Ahn and D.Kajfez, "Broadband Stacked Dielectric Resonator Antennas", *IEE Electronics Letters*, Vol.25,No18,Aug.1989, pp.1232-1233.
[30] J.B. Keller, " Geometric Theory of Diffraction," J.Opt.Soc. of America, Vol.52, No.2, Feb,1962, pp. 1160-130.
[31] R.G .Kouyoumjian, P.H Pathak, " A Uniform Geometric Theory of Diffraction for an Edge in a Perfectly Conducting Surface" ,*proc,IEEE*, Vol.62,Nov.1974,pp.1448-1461.
[32] C.A .Balanis, Antenna Theory: Analysis and Design, Harper and Row,1982.
[33] Cushcraft Corporation, "Antenna Polarization Considerations in Wireless Communications Systems", 48 Perimeter road Manchester,NH 03103.
[34] G.DROSSOS,Z.WU and L.E.DAVIS, "Circular polarised cylindrical dielectric resonator antenna" , *Electronics Lett*.,1996,vol.32,no.4,pp.281-283.
[35] M.B .OLIVER,Y,M,M. ANTAR,R.K.MONGIA and A.ITTIPIBOON. "Circularly Polarised Rectangular Dielectric Resonator Antenna" , *Electronics Lett*.,1995,vol.31,no.6,pp.418-419.
[36] A.Petosa, R.K.Mongia, A.Ittipiboon and J.S.Wight, "Experimental investigation on feed structures for linear arrays of dielectric resonator antennas", Proceedings of IEEE AP-S Conference, California, USA,pp,1982-1985,1995.
[37] A.Petosa, R.K .Mongia, A. Ittipiboon and J.S.Wight, "Investigation on a Microstrip Fed Series Array of Dielectric Resonator Antennas", *IEE Electronics Letters*,Vol.31.No.16,Aug.1995,pp.1306-1307.
[38] K.K.Pang, H.Y.Lo, K.W.Leung, K.M.Luk and E.K.N.Yung, "Circularly polarised dielectric resonator antenna Subarrays", *Microwave and Optical Technology Letters*, Vol.27,No.6,pp.377-379,2000.
[39] M.Haneishi and H.Takazawa, "Broadband circularly polarised planar array composec of a pair or dielectric resonator antennas", *Electronics Letters*, Vol.21,No.10,pp.437-438,1985.

Chapter 3

DRA with dual Linear Polarization & Symmetric Radiation Patterns Performance at X-band (8-12) GHz

Contents

It is realised that with a dual linearly polarised DRA structure, a wider 3dB Axial Ratio (AR) bandwidth is obtained and that can either be utilized to generate dual polarized waves for radars or a circularly polarized wave for satellites working in X-band (8-12) GHz [1]. In view of such applications, large impedance bandwidth and purely symmetric radiation patterns are crucially required. As per requirement of the project, we are to be confined to the dual linear polarization design of the DRA.

To design and test antenna with such capabilities the preliminary investigations start with rigorous simulation techniques. The investigation process is made to evolve from around 7 GHz frequencies and progressed to the lower end of X-band (8 GHz) because of possible upward frequency shift when considering and compensating for the critical factor of low permittivity adhesive material used to glue DRA body on the feeding substrate. Before taking into account the exact nature and role of such material, it is imperative to evaluate it in terms of its permittivity and quantity of usage in the fabrication process.

For dual linear polarization purposes, the DRA in its $TM_{110}(HEM_{11})$ mode to yield broadside radiation patterns that is detailed in section 2.1.2, is excited by two orthogonal ports via microstrip feed lines that couple electromagnetic energy through aperture slots etched on the ground plane. The excitation of this mode strictly requires that these aperture slots be confined to the central area of the cylindrical shaped DRA and at the same time to offer a good level of de-coupling between the ports to avoid resonance frequency shift and radiation pattern degradation. To resolve this issue the rectangular-shaped aperture slots are moulded to H-shaped aperture slots that are reported to be more efficient to couple the energy [2]. This strategy makes the slots to not only remain confined to the smaller central region of the DRA but also supports to manipulate stubs lengths and feed line positions in order to improve ports isolation. For each port starting from rectangular slots, the H-shaped aperture slots are analysed independently and then their performance is optimised while adjusting both of them under the available DRA bottom space.

3.1 Design of an aperture-coupled cylindrical DRA

Considering the symmetry of the DRA body with reference to the slot position, port2 is first set to analysis. Following the design formula given in equation 2.4, the cylindrical DRA resonant frequency is 7.3 GHz respectively with a height of 4.7mm (H), a diameter of 10mm (D) and a dielectric constant material εr equal to 6. The DRA is placed above a substrate of 0.508mm thickness with a permittivity εr=3.38. A microstrip feed line is etched on the bottom side. The width of the feeding line is set to 1 mm to match 50Ω characteristic impedance. A rectangular slot is etched on the topside ground plane to enable inductive coupling energy transfer. Ground plane dimensions are fixed to 40mm*40mm.
The basic design structure is depicted in Fig 3.1 where a rectangular shaped aperture slot is located exactly at the DRA centre.

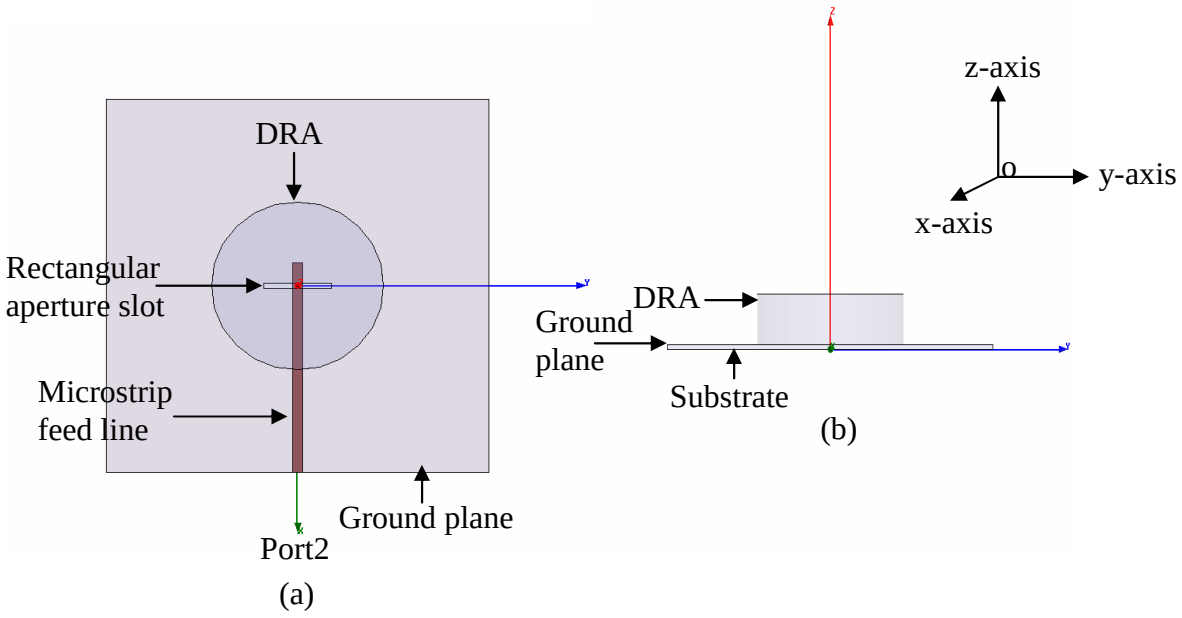

Figure 3.1 Rectangular shaped aperture slot located at the DRA centre (a) Top view (b) Side view

3.1.1 Estimation of aperture slot length:

To estimate aperture slot's length keeping its approximate width to 0.6mm and stub length to 2mm, a parametric study analysis is made by a simulation process for which the impedance curves are presented in Figure 3.2. All impedance curves are calculated with de-embedding process and are referenced at the slot level.

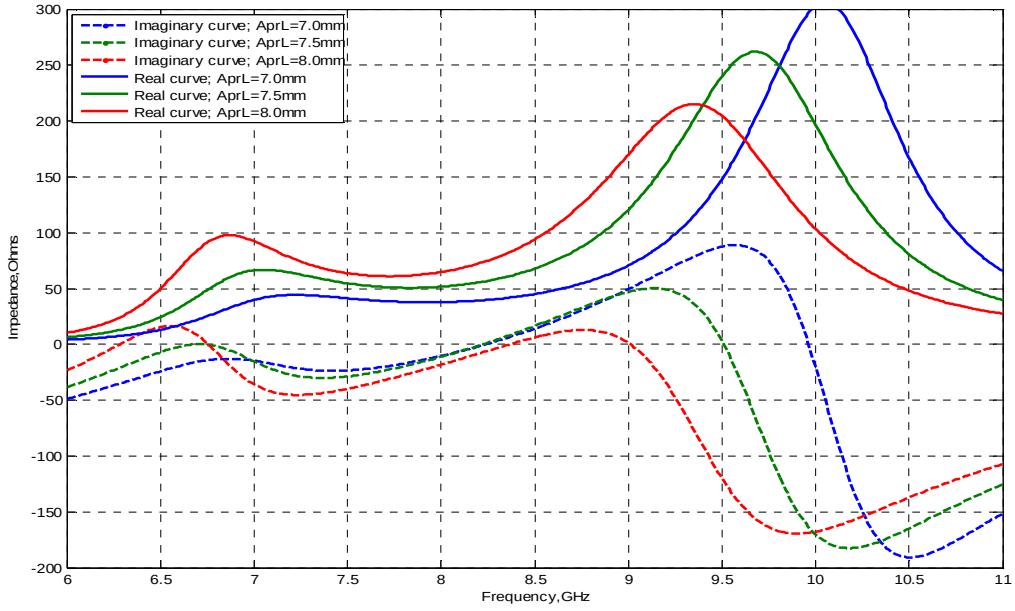

Figure 3.2: Family of impedance curves representing different slot lengths

The results available from Figure3.2 suggest two possible resonances, one is taking place around 7 GHz and the other beyond the 9 GHz. For 7mm aperture length around 7 GHz the imaginary part correspond to nearly 50 Ohms of the real part. So this length is suitable to make DRA resonate. On the other hand, beyond 9 GHz frequency with the increase of slot lengths there is a tendency of downward shifting of resonances that is from around 10GHz down to 9 GHz. This responsiveness to the slot sizes confirms the slot resonances. These are observed to be parted away from the desired DRA resonance. So considering the constraint of limited availability of space, aperture length of 7mm is assumed to be suitable for further analysis. Because that is neither too narrow to limit proper coupling to the DRA nor too large to itself resonate in proximity to it.

3.1.2 Width effect of aperture slot:

Until now the width of the aperture was kept as 0.6mm however to be more precise there is a dire need to ascertain its exact value. For this purpose corresponding to slot widths, various parametric impedance curves are obtained which are presented in Figure 3.3.

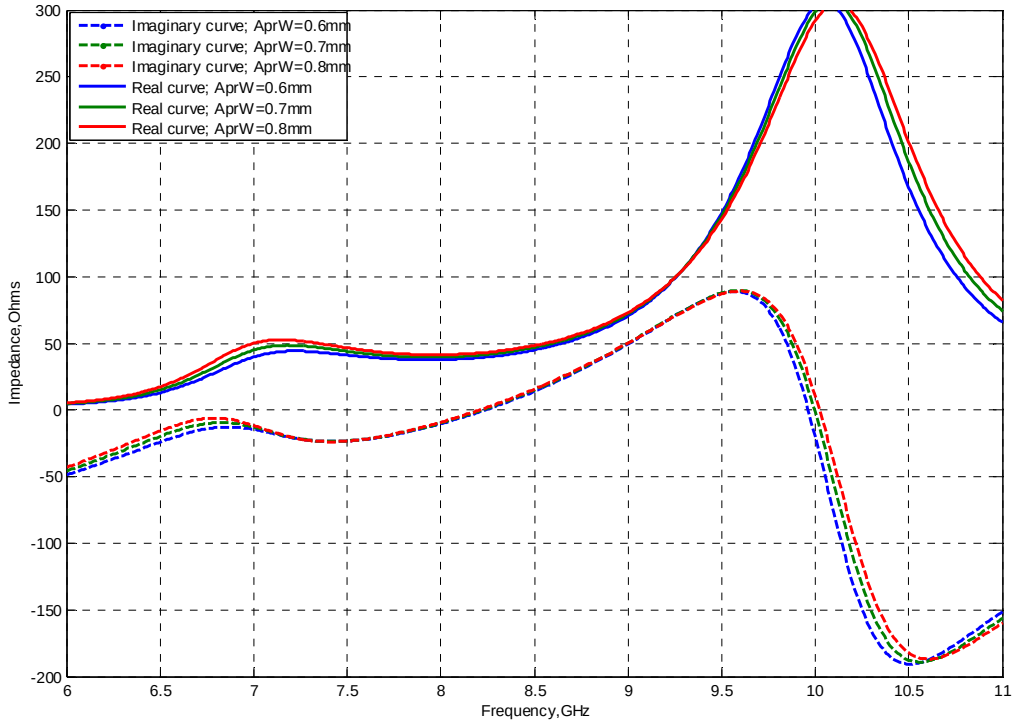

Figure 3.3: Set of impedance curves representing different slot widths

It can be observed from Figure3.3 that real parts of the impedance curves remain nearly same at 50 Ohms around 7.3GHz for all slot widths of 0.6mm, 0.7mm and 0.8mm while corresponding imaginary parts too are un-affected. It means slot widths do not greatly influence the DRA resonance. Nearly similar response is observed around 10GHz that is the basically the slot resonance. Both DRA and slot resonances are found to be widely apart. So among available choices a suitable width is to be chosen. It is supposed to be neither too narrow to etch on the ground plane nor too large to cause smaller space adjustment problem. Considering these constraints, 0.6mm width seems to be more convincing and practicable and is thus selected for further design analysis.

3.1.3 Parametric analysis of stub lengths:

An extended quarter wave length stub ($\lambda_g/4$) plays a significant role in improving the coupling mechanism when its reactance cancels to the reactance of the aperture slot. So choosing the slot's length as 7mm and width as 0.6mm, a set of impedance parametric is evaluated that corresponds to different stub lengths. It is to be observed that at what length of stub, the imaginary part of the impedance becomes purely zero. The family of curves thus obtained is presented in Figure3.4.

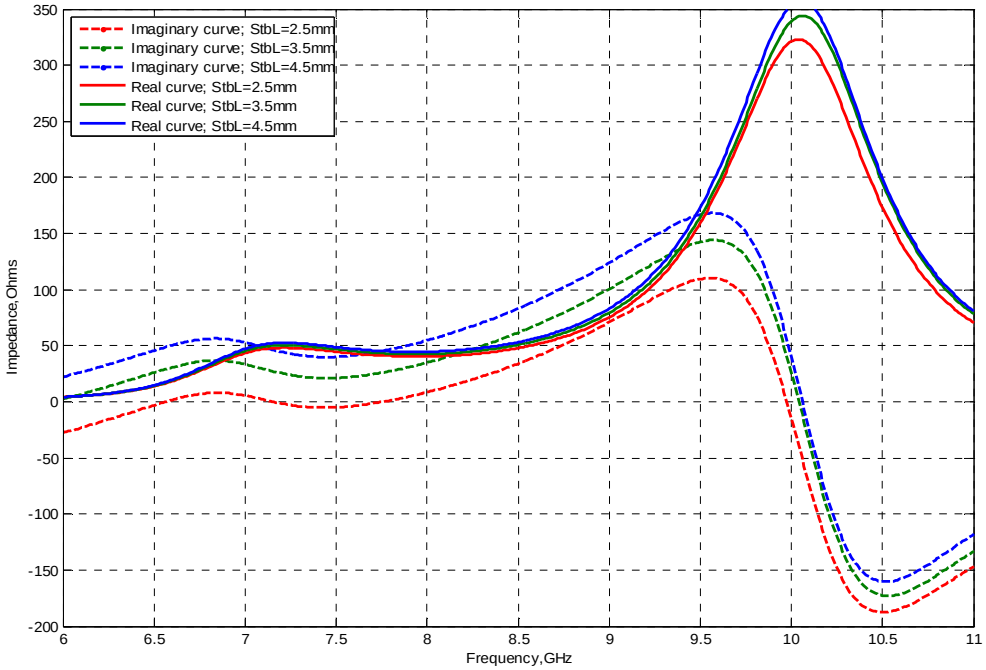

Figure 3.4: Set of impedance curves representing different stub lengths

It can be noted from the Figure3.4 that stub length of 2.5mm absolutely nullifies the reactance parts of the impedance thus improving the coupling to the DRA at 7.3 GHz. As expected there is no change in the real parts of the impedance and for all stub lengths of 2.5mm, 3.5mm and 4.5mm the imaginary parts vary. Similarly, at around 10GHz frequency a slight change in imaginary curves is observed but real parts are again found to be nearly un-affected. Hence to proceed further to the design, a stub length of 2.5mm seems more appropriate and is thus employed.

For the rectangular shaped aperture slot located at DRA centre a length of 7mm and a width of 0.6mm is finally chosen. Using these dimension and employing a stub length of 2.5mm the design is analyzed. The simulated -10dB return loss (6.75GHz-8.5GHz) result is depicted in Figure3.5 which offers an impedance bandwidth of 22%.

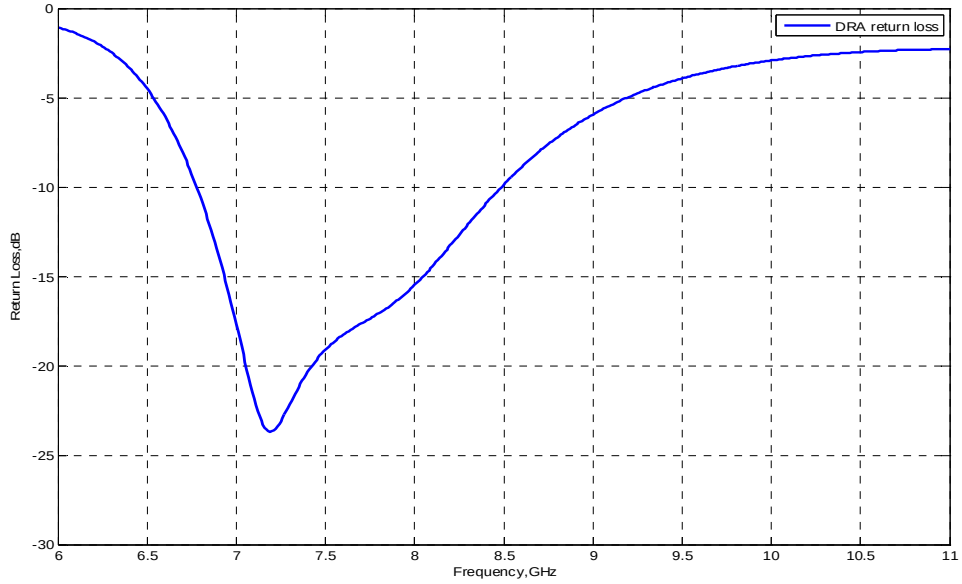

Figure 3.5: Port2 return loss curve corresponding to optimum values of rectangular shaped aperture slot located at DRA centre

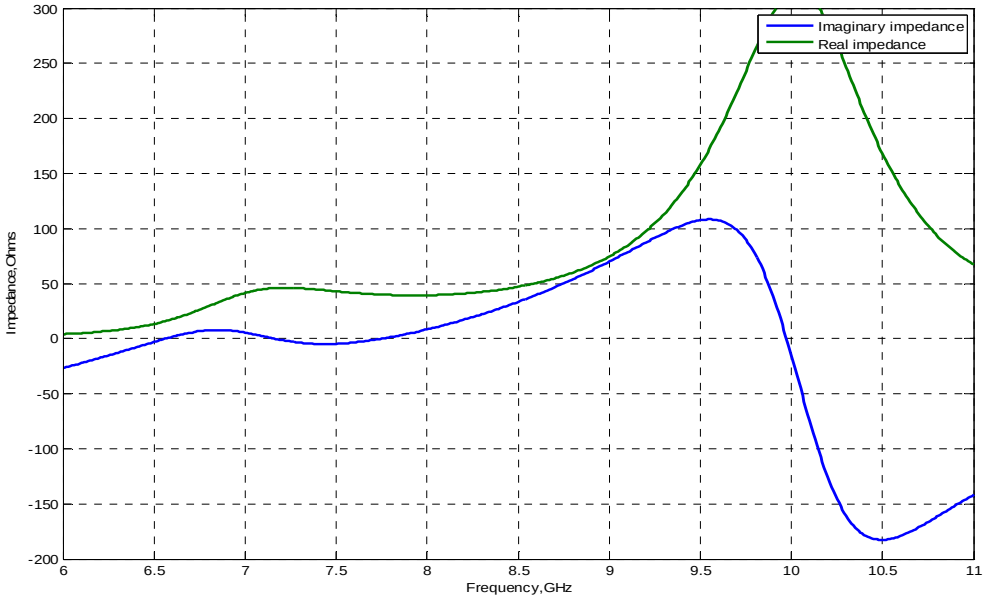

Figure 3.6: The impedance curves representing resonance at 7.3 GHz.

Figure3.5 and Figure 3.6 show that DRA resonance takes place at around 7.3GHz where imaginary part of the impedance is zero while real part is around 50 Ohms.

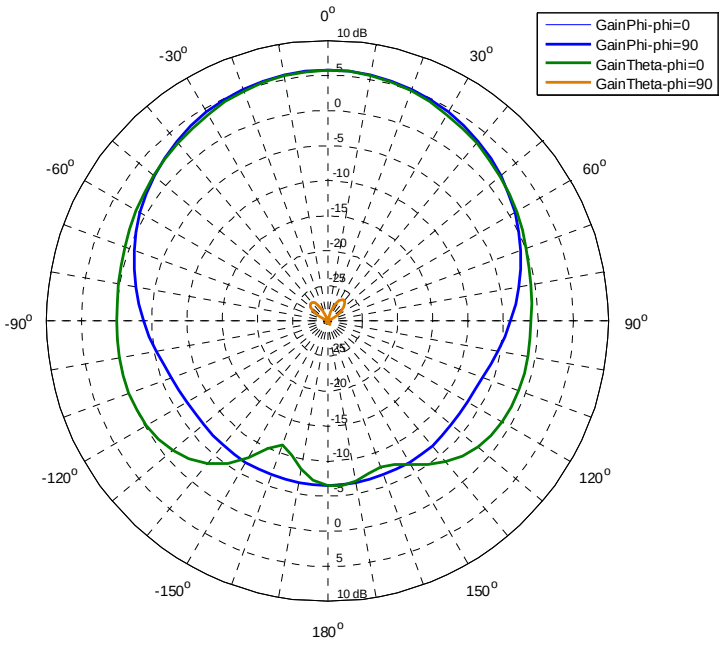

Figure 3.7: Broadside radiation patterns in the xoz(E) and yoz(H) planes.

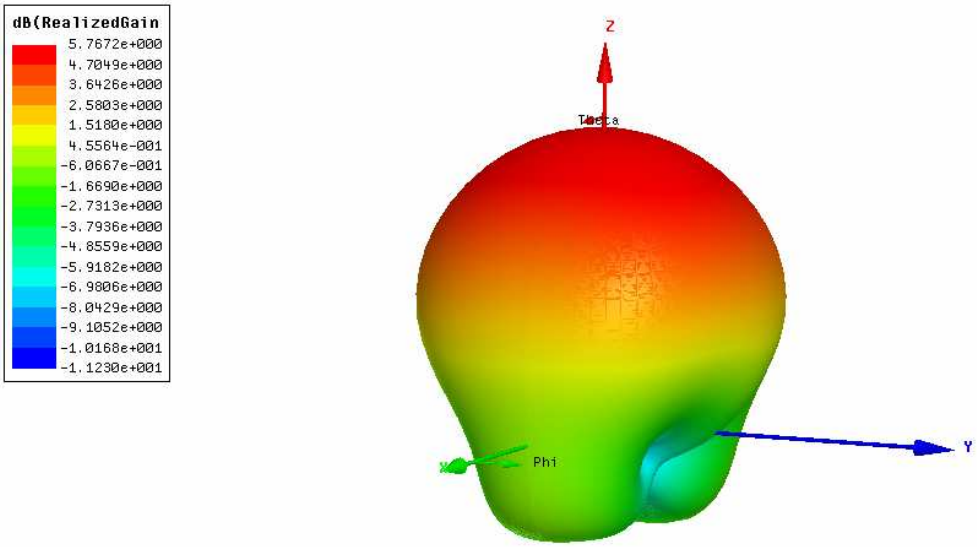

Figure 3.8: 3D polar plot representing broadside radiation

The broadside radiation patterns in the xoz(E) plane and yoz(H) plane at 7.3GHz are depicted in Figures 3.7 and 3.8 . The co-polarization level in both planes is found to be nearly 30dB higher than the cross-polarization in the broad direction. A gain of 5.7 dBi, which is expected from a single DRA element with radiation efficiency of 98% is obtained. Both plane patterns are exactly symmetric with 3dB Half Power Beam Width (HPBW) of 90° however, E plane pattern is found to be slightly wider towards horizon. The front to back ratio (F/B) in both planes is estimated to be 12dB. The radiation patterns are found to be stable with nearly same pattern shapes ranging from 7GHz to 8GHz, however shape degradation is observed when shifting either to lower or to upper sides of this frequency range.

3.2 Modification to H-shaped aperture slot:

As two aperture slots are to be adjusted simultaneously at the centre of cylindrical DRA to excite its TM_{110} (HEM_{11}) modes so as to yield broadside radiation patterns, hence rectangular shape is modified to H-shaped slot. This shape structure introduces better space utilisation that facilitates the exact DRA positioning upon the slots thus always remained confined to the desired resonating mode. The rectangular shaped slots geometry on the other hand is expected to cross the DRA central zone and occupy some of its peripheral boundary thus interfering with TM01 mode excitation that is not desirous owing to its different resonance frequency and radiation patterns. The H-shaped slot also assures good level of energy coupling to the DRA owing to its magnetic polarisability and smooth field variation due to the presence of side legs [2]. An equivalent size H-shaped aperture slot is employed at the centre with central length of 4.2mm and two leg lengths each of 2mm however, the width is kept same as of 0.6mm.The structure illustrated in Figure3.9 is analyzed for different stub lengths ranging from 2mm to 4.5mm for which impedance and return loss curves are given in Figures 3.10 and 3.11 respectively.

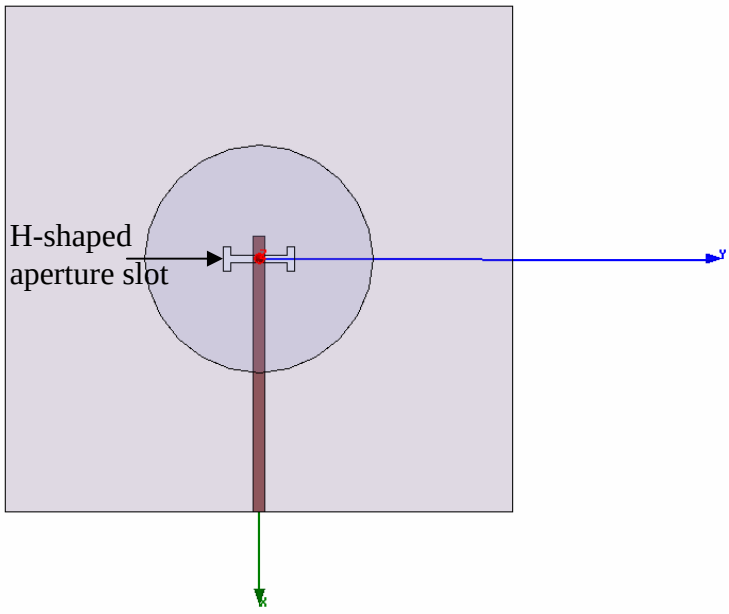

Figure 3.9: Design geometry when H-shaped aperture slot is located at the DRA centre

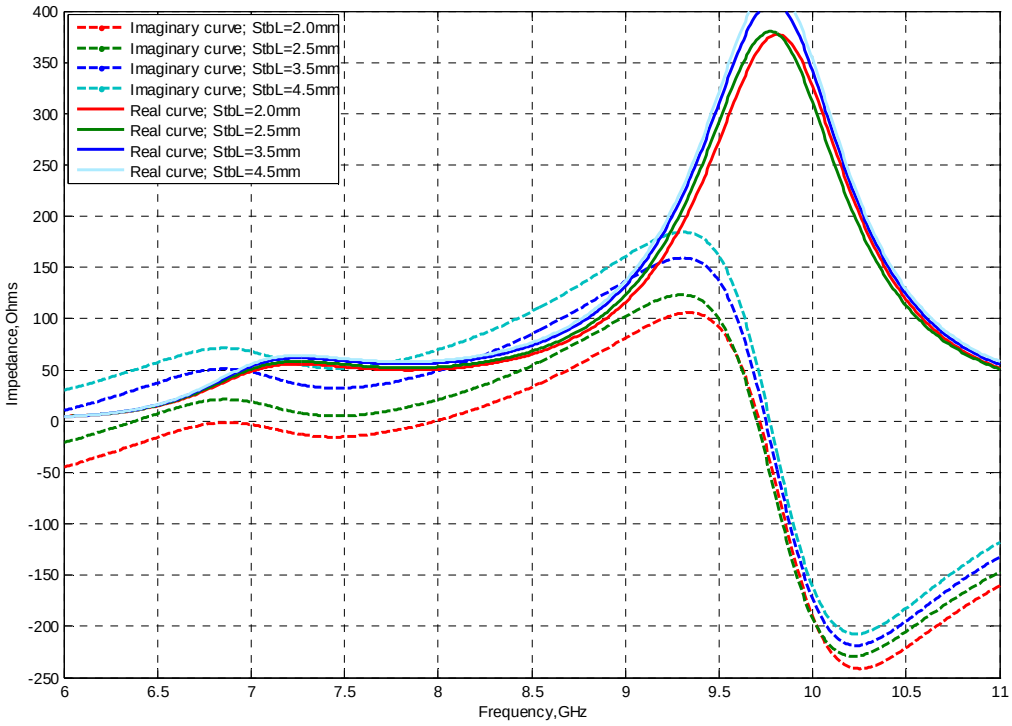

Figure 3.10: Impedance response curve when H-shaped slot is located at DRA centre

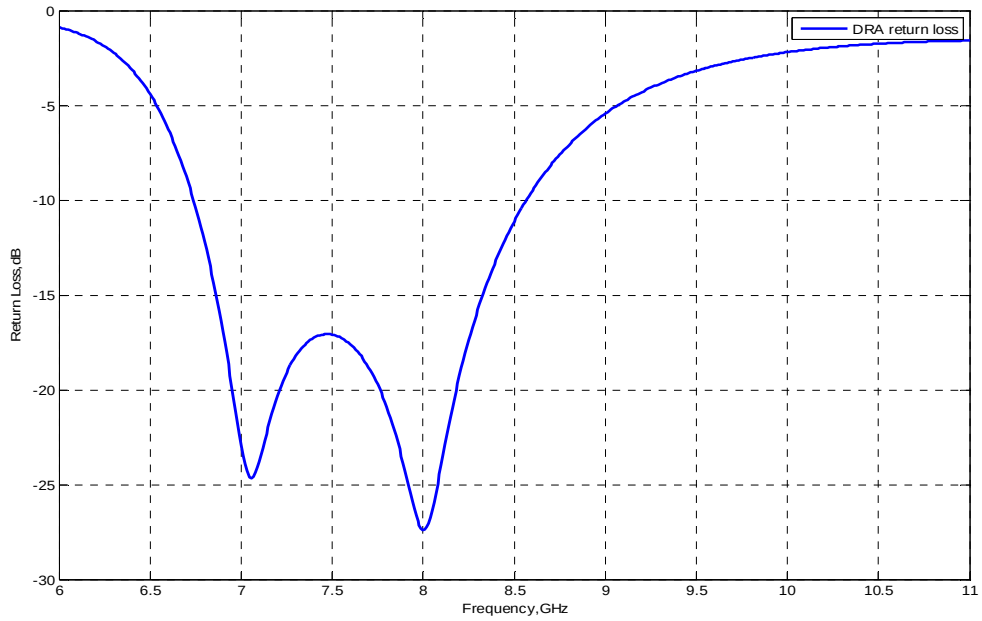

Figure 3.11: Return loss curve for H-shaped slot located at centre

It is interesting to observe that 2mm stub length employed to the H-shaped slot nullifies the imaginary part of the impedance while same result is obtained when 2.5mm stub length is

employed to the rectangular shaped slot. The -10dB return loss ranges from 6.75GHz to 8.5GHz that offers impedance bandwidth of 23%

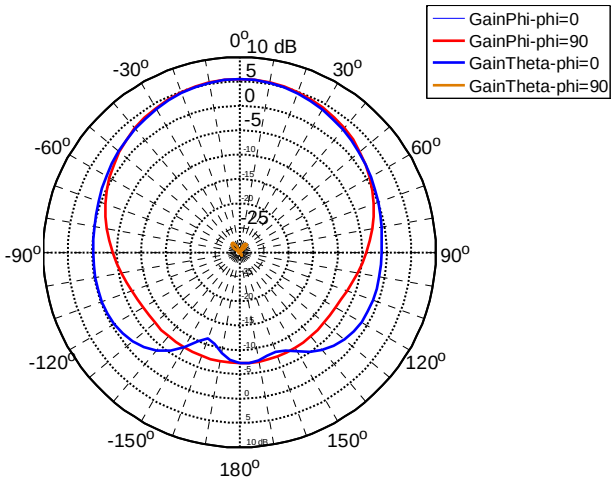

(a)

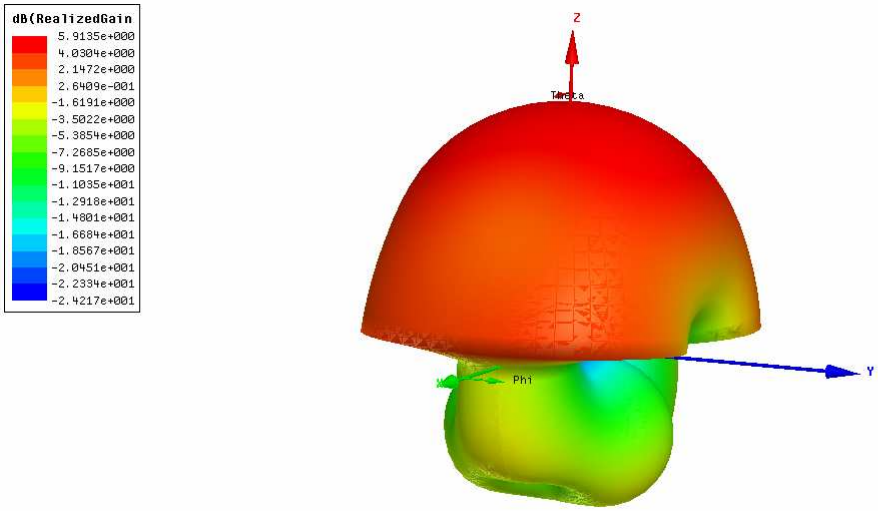

(b)

Figure 3.12: Broadside radiation patterns in the xoz(E) and yoz(H) planes at 7.3GHz
(a) 2D radiation pattern (b) 3D polar plot with infinite ground plane

The broadside radiation patterns in the xoz(E) and yoz(H) planes are depicted in Figures 3.12(a) and (b). Nearly same results are observed as in the case of rectangular slot located at centre that is the co-polarization levels in both planes are nearly 30dB better than the cross-polarization in the broadside direction. It yields a gain of 5.7 dBi with radiation efficiency of

98%. Both plane patterns are purely symmetric with 3dB Half Power Beam Width (HPBW) of 90° however, E plane pattern is found to be slightly wider towards the horizon. The front to back ratio (F/B) is found to be around 11dB. The patterns are found to be stable with in the band from 6.75GHz to 8.5GHz frequency, however shifting either to lower or higher frequency range, degradation in the pattern shapes is observed.

3.3 H-shaped aperture slot offset position:

To generate some space to adjust simultaneously two similar H-shaped slots it is imperative to shift them from the DRA centre. The new position is expected to confine to the desired resonant mode. This situation is elaborated in Figure3.13

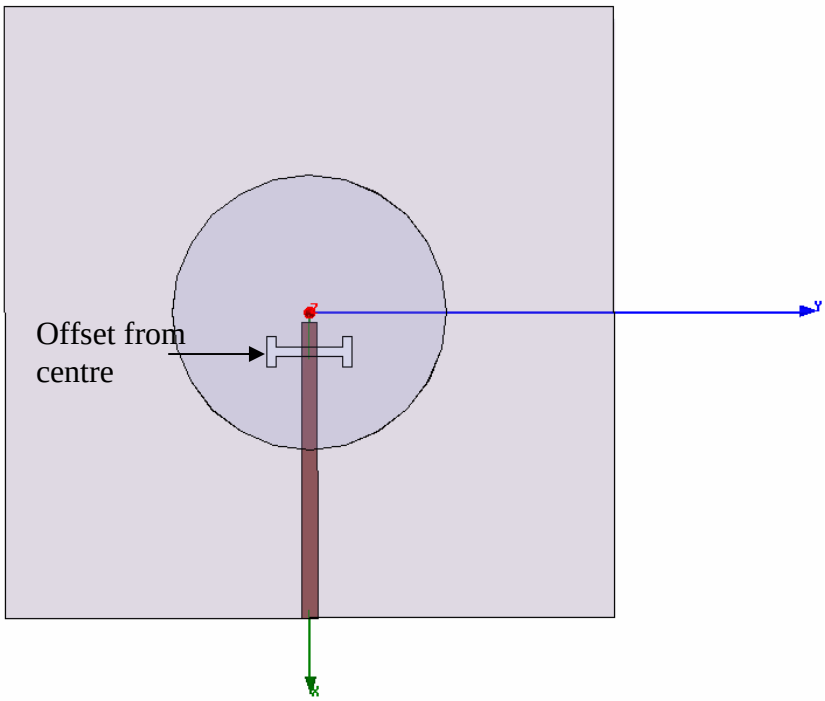

Figure 3.13: Design geometry when H-shaped slot is offset from the DRA centre

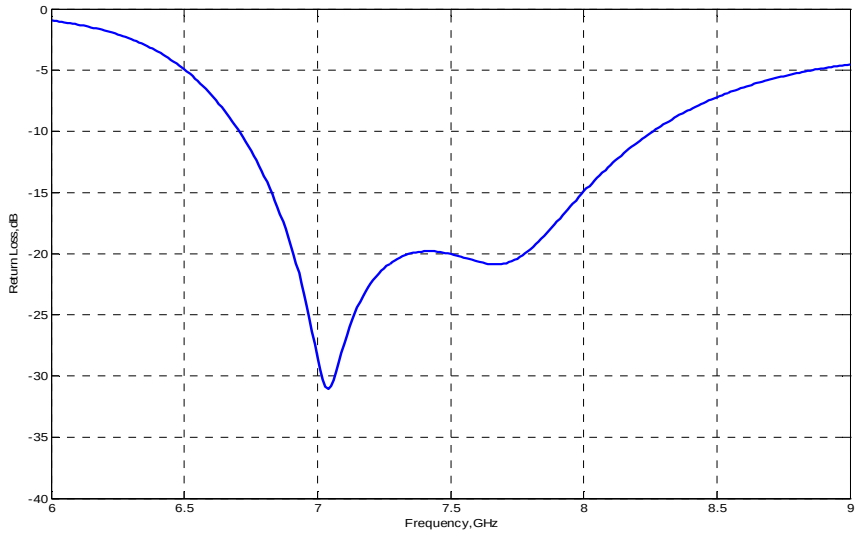

Figure 3.14: Return loss curve for H-shaped slot shifted from centre

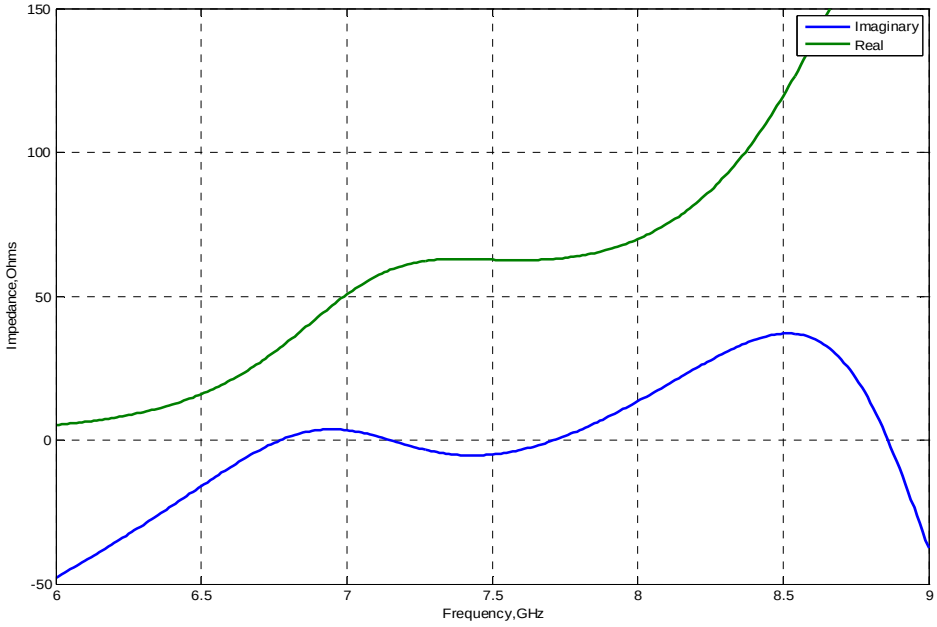

Figure 3.15: Impedance curve when H-shaped slot is offset from DRA centre

A slight adjustment was made in the size of H shaped slot with central length of 4.4mm and side leg lengths each of 2mm. The stub lengths is kept at 1.9mm and slot is offset at 2.6 mm from the DRA centre. The resulting return loss and impedance curves are presented in Figures 3.14 and 3.15 respectively. The DRA resonance is observed at around 7.3GHz while impedance bandwidth is found to be 22%.

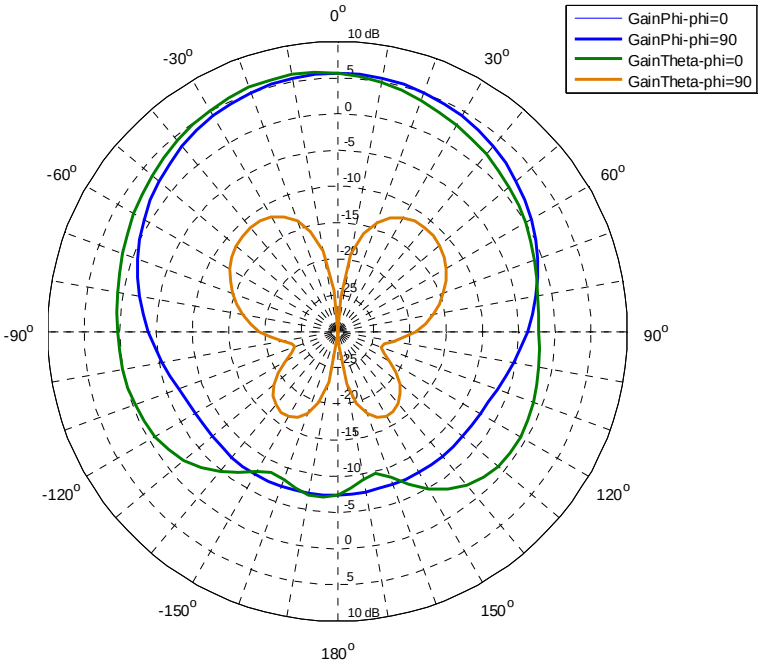
GainPhi-phi=0
GainPhi-phi=90
GainTheta-phi=0
GainTheta-phi=90
0°
30°
60°
90°
120°
150°
180°
-30°
-60°
-90°
-120°
-150°
10 dB
5
0
-5
-10
-15
-20
-25

(a)

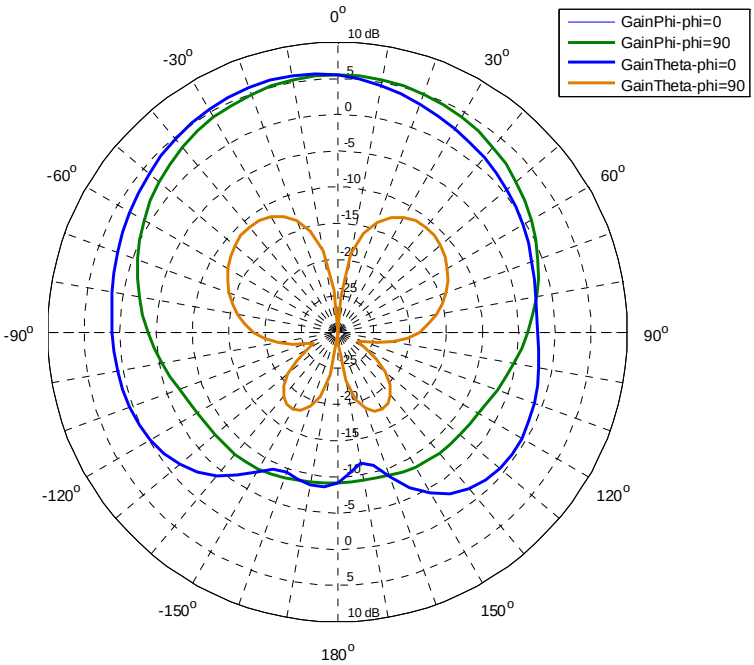
GainPhi-phi=0
GainPhi-phi=90
GainTheta-phi=0
GainTheta-phi=90
0°
30°
60°
90°
120°
150°
180°
-30°
-60°
-90°
-120°
-150°
10 dB
5
0
-5
-10
-15
-20
-25

(b)

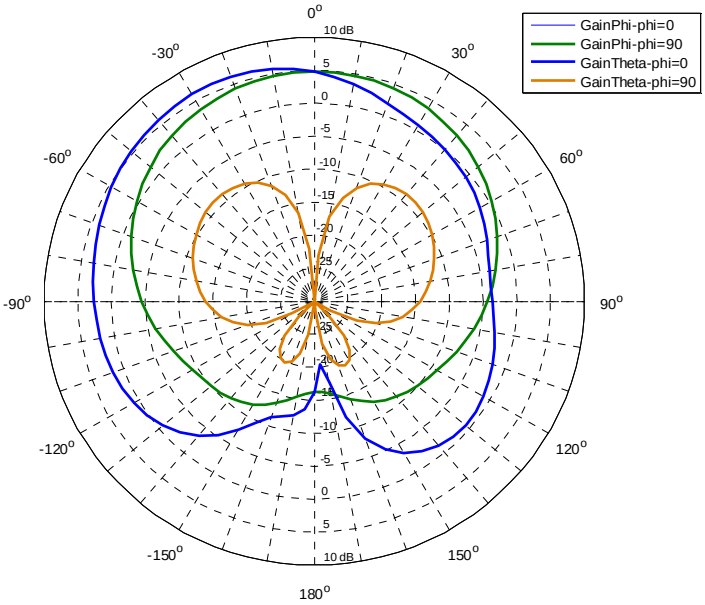
GainPhi-phi=0
GainPhi-phi=90
GainTheta-phi=0
GainTheta-phi=90
0°
30°
60°
90°
120°
150°
180°
-30°
-60°
-90°
-120°
-150°
10 dB
5
0
-5
-10
-15
-20
-25
-30
-35
-40
-15
-10
-5
0
-5
10 dB

(c)

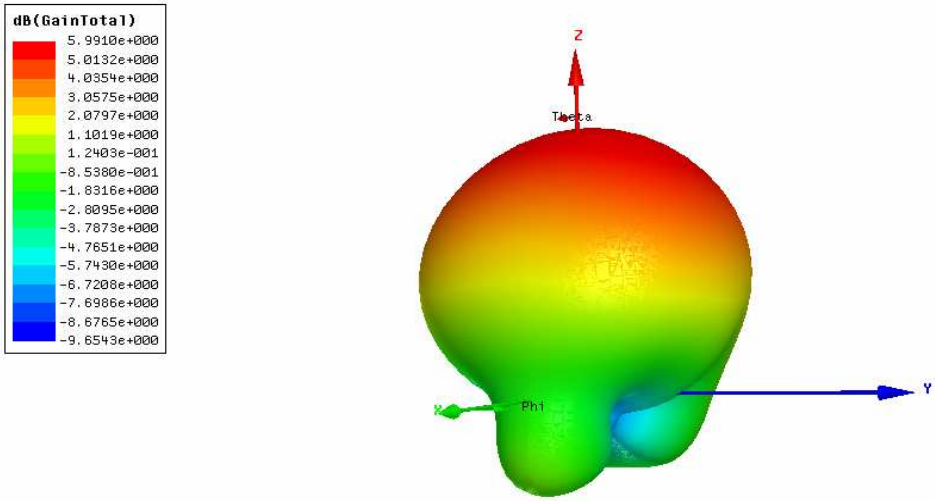
dB(GainTotal)
5.9910e+000
5.0132e+000
4.0354e+000
3.0575e+000
2.0797e+000
1.1019e+000
1.2403e-001
-8.5380e-001
-1.8316e+000
-2.8095e+000
-3.7873e+000
-4.7651e+000
-5.7430e+000
-6.7208e+000
-7.6986e+000
-8.6765e+000
-9.6543e+000
Z
Theta
Phi
X
Y

(b)

Figure 3.16: Broadside radiation patterns in the xoz(E) and yoz(H) planes at (a) 7.3GHz (b)7.5GHz (c)8GHz (d) 3D polar plots at7.3GHz

The xoz(E) and yoz(H) plane radiation patterns at 7.3GHz, 7.5GHz and 8GHz are depicted in Figures 3.16(a), (b) and (c) respectively. The E and H-plane radiation patterns are found to be symmetric at 7.3GHz frequency, however E-plane pattern becomes slightly asymmetric when shifted to 8GHz. -3dB Half Power Beam Width (HPBW) for both planes is estimated to be around 90° . The co-polarization levels in both planes are still 30dB or better than the cross-polarization in the broadside direction. It shows a gain of 5.6 dBi with radiation efficiency of 98% like that when the slot is located at DRA centre. However, the cross-polarization levels except in the broadside direction have slightly increased and it is expected phenomenon that anticipates the slot's shifting from the centre. The front to back ratio (F/B) at 7.3GHz is found to be 13dB, at 7.5GHz it is around 14dB and at 8GHz it scales to 7dB.

3.4 Single port (Port1) performance analysis:

As port2 has yielded desired results so assuming its presence (loaded with 50Ω) port1 is set to excite the other orthogonally located H-shaped slot as shown in Figure3.17.The central height is 4.4mm and two legs each of 2mm long give it exactly the same dimension as for port2 slot, similar is the open stub's length of 1.9mm.The lower leg of the vertically oriented H-slot is positioned at the origin that generates a gap of 0.7mm from the stub of the port2 feed. This gap is sufficient enough to maintain a good level of ports de-coupling.

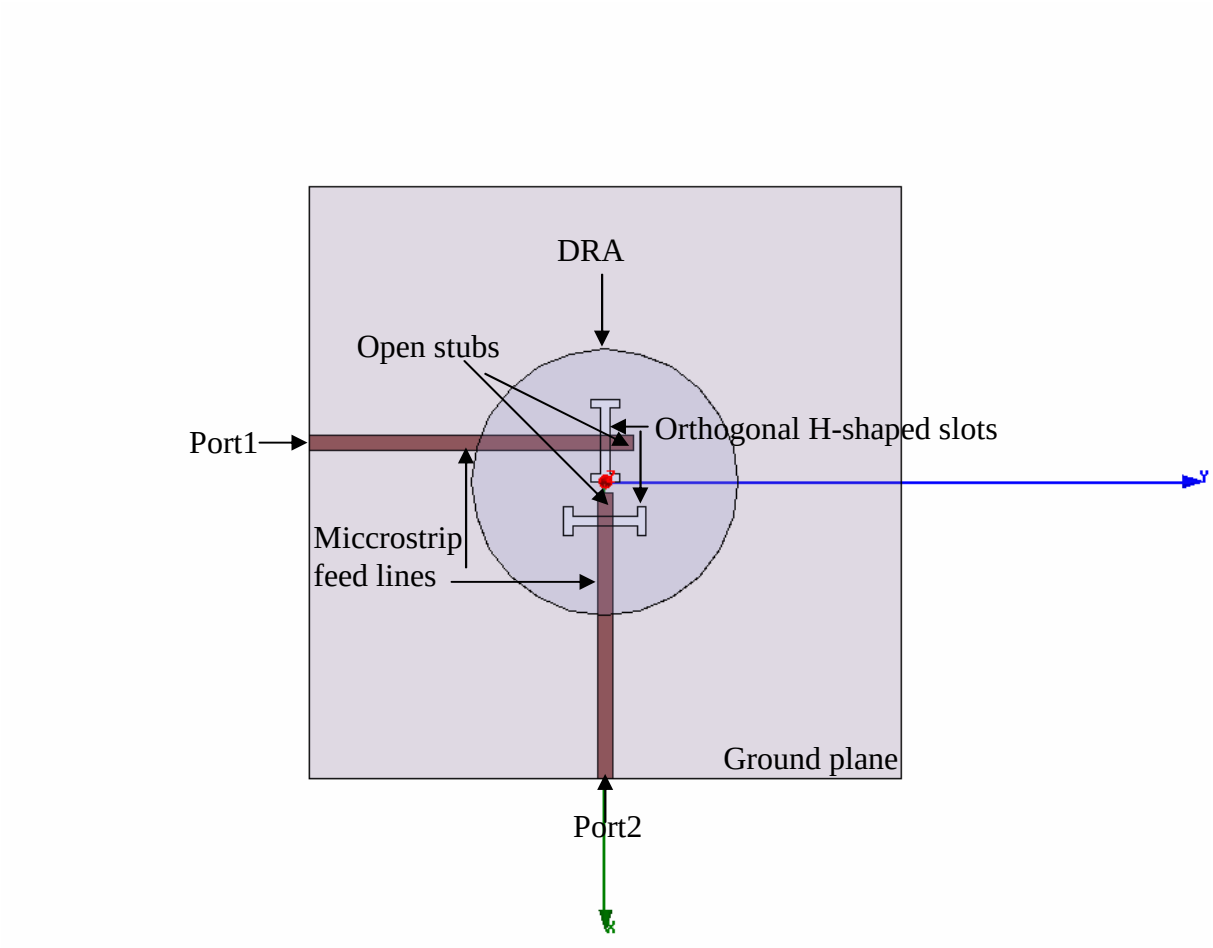

Figure 3.17: Port1's slot design geometry in the presence of port2.

Though with reference to slot2, slot1 is not symmetrical located under the DRA position, yet it is capable of exciting the exact desired mode thus introducing negligible cross polarization in its radiation patterns and supporting to yield better ports isolation.

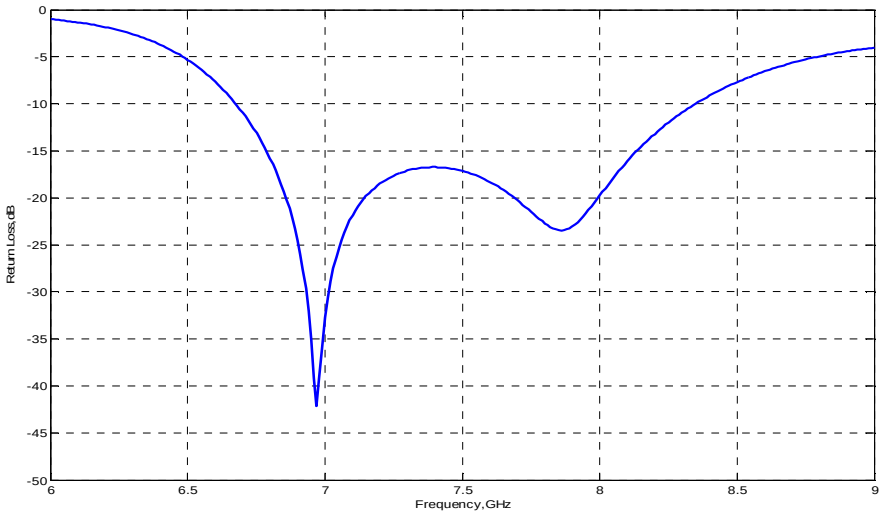

Figure 3.18: Return loss curve for port1 feeding to orthogonally located H-shaped aperture slot

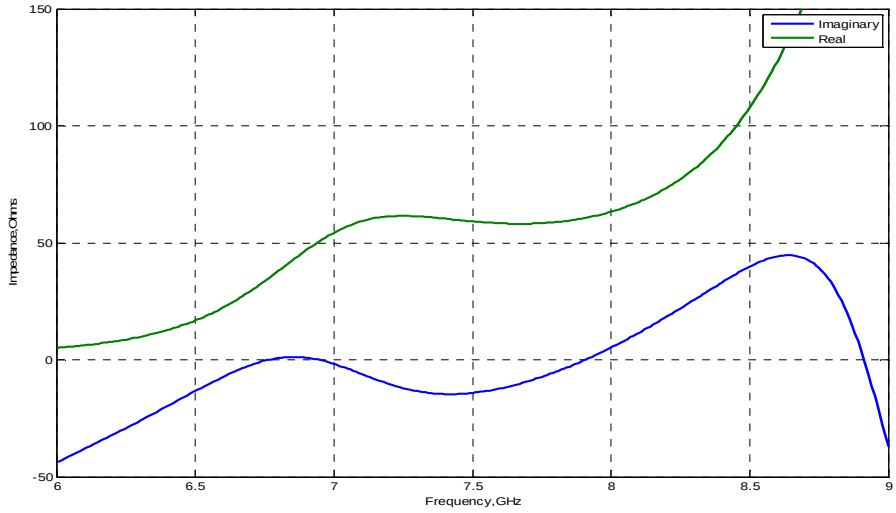

Figure 3.19: Impedance curves

For port1 Figures 3.18 and 3.19 depict the return loss and impedance curves respectively. It is evident from the curves that resonance is taking place at around 7.3 GHz and that is the expected resonance of the DRA. -10dB return loss from 6.7GHz to 8.3GHz yields a bandwidth of 22%

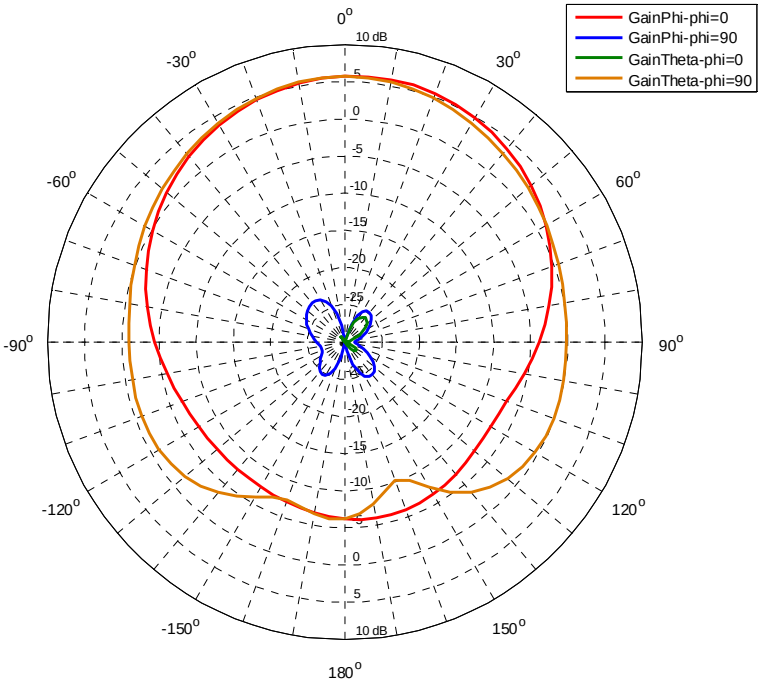
GainPhi-phi=0
GainPhi-phi=90
GainTheta-phi=0
GainTheta-phi=90
0°
30°
60°
90°
120°
150°
180°
-150°
-120°
-90°
-60°
-30°
10 dB
5
0
-5
-10
-15
-20
-25

(a)

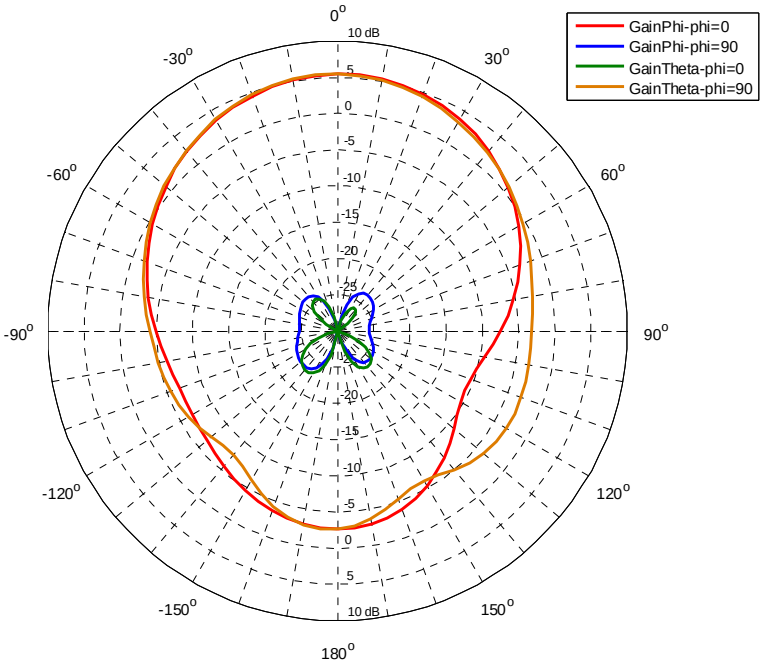
GainPhi-phi=0
GainPhi-phi=90
GainTheta-phi=0
GainTheta-phi=90
0°
30°
60°
90°
120°
150°
180°
-150°
-120°
-90°
-60°
-30°
10 dB
5
0
-5
-10
-15
-20
-25

(b)

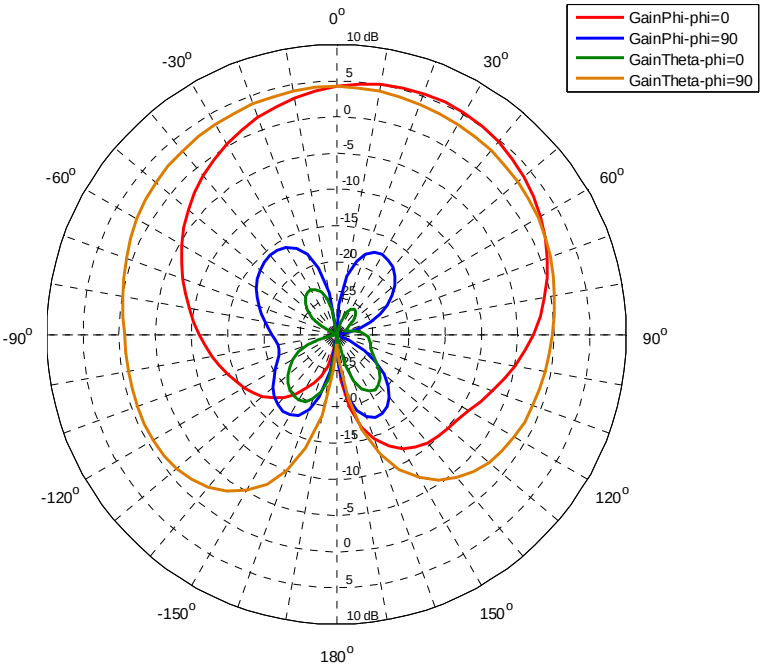

(c)

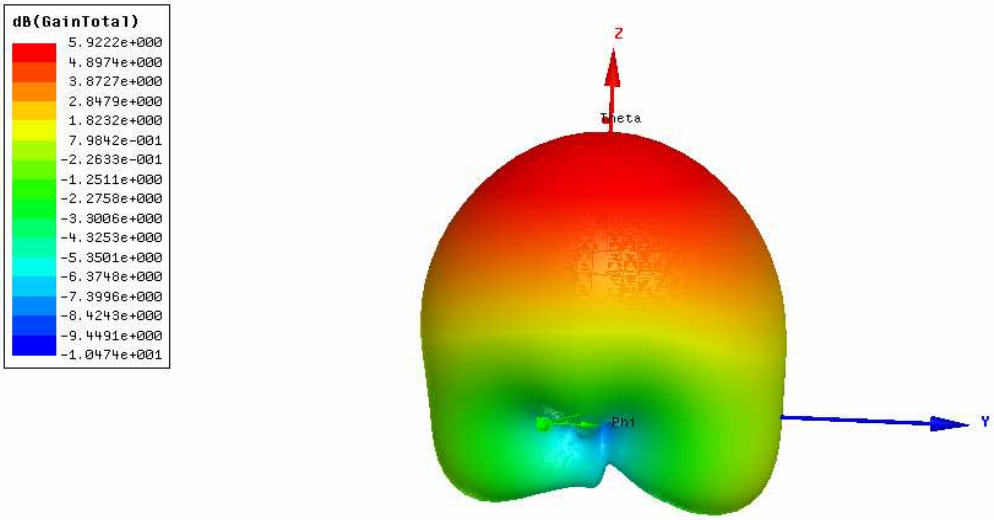

(d)

Figure 3.20: Broadside radiation patterns in the yoz(E) and xoz(H) planes at (a) 7.3GHz (b) 6.6GHz (c) 8.4GHz (d) 3D polar plot at 7.3GHz

The broadside radiation patterns in the yoz(E) and xoz(H) planes are depicted in Figures 3.20(a) at 7.3GHz (b) at 6.6GHz (c) at 8.4GHz and (d) 3D polar plot at 7.3GHz .
With reference to case (a) at 7.3GHz frequency both planes exhibit purely symmetric radiation patterns. The co-polarization levels are 30dB better than the cross-polarization in the broadside direction. The gain is found to be of 5.7 dBi and radiation efficiency of 98%. The 3dB Half Power Beam Width (HPBW) is of 90° however, E plane pattern like in port1 case, is found to be slightly wider towards the horizon. The patterns are observed to be stable with in the range of 6.7GHz to 8 GHz, however shifting to lower or higher than this range, slightly changes the patterns shape. One such situation is depicted in case (c) at 8.4GHz where a minor level asymmetry is observed between the E and H plane radiation patterns. The front to back ratio (F/B) in case (a) at 7.3GHz is around 11.8dB, in case (b) at 6.6GHz is about 7.9dB and in case (c) at 8.4 GHz it is observed to be 10dB.

3.5 Dual ports (Port1 & Port2) combined performance:

So far both ports have yielded expected results at 7.3GHz .The two ports design is finalized with the design parameters summarized in Table1.The specific notation subscripts associated with the abbreviation letters can be viewed from the diagram given in Figure3.42.

Table1: Port1 and Port fed aperture slots design values

DRAfeeding Ports	Aperture slots size Length(L)&Width(W)	Feed lengths (L_f)	Stub lengths(L_s) (From slot's centre)
Port1	L_1=4.4mm,L_{1L}& L_{1H} =2mm W_1=0.6mm	L_{f1} =21.9mm	L_{s1} =1.9mm
Port2	L_2=4.4mm,L_{2R} & L_{2L} =2mm W_2 =0.6mm	L_{f2} =19.3mm	L_{s2}=1.9mm

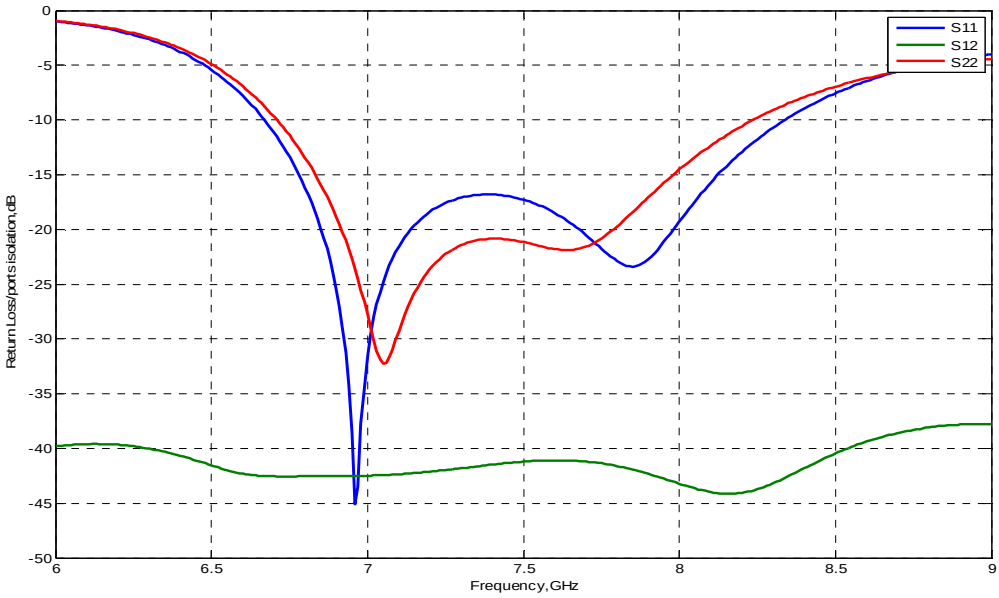

Figure 3.21: Port1 and Port2 return loss curves with an isolation of -42dB.

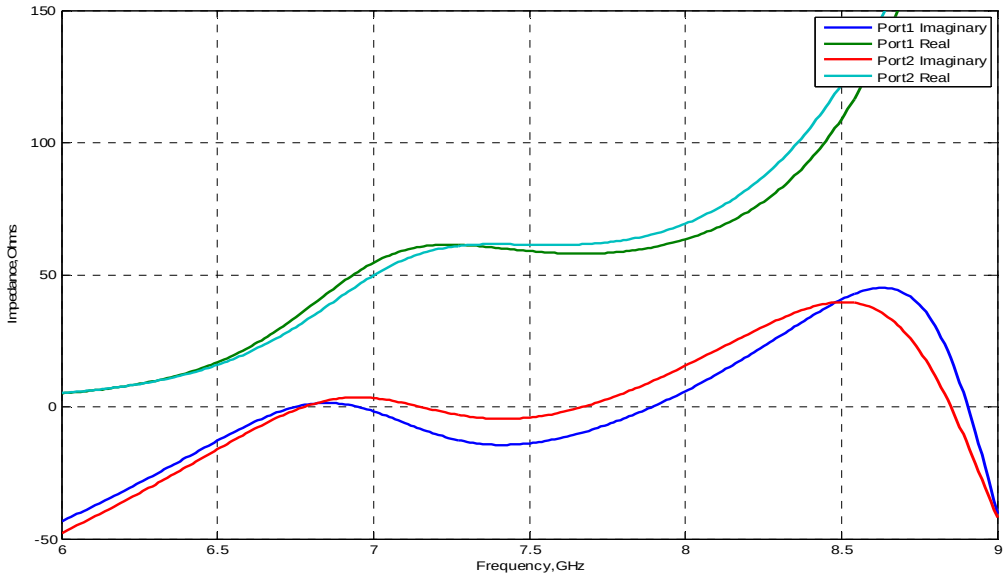

Figure 3.22: Impedance plot curves corresponding to two ports.

The return loss and impedance curve results for port1 and port2 are presented in Figure3.21 and 3.22 respectively. -10dB impedance bandwidth for port1 is found to be 22% (6.7GHz to 8.3GHz) while for port2 it is estimated to be 20% (6.75GHz to 8.25GHz) .The worst isolation between the ports is observed to be -42dB.

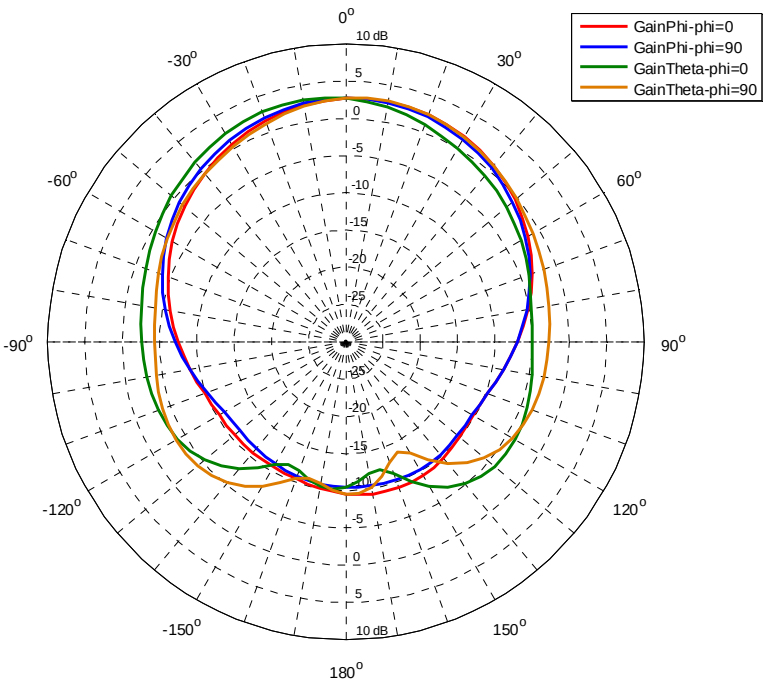

(a)

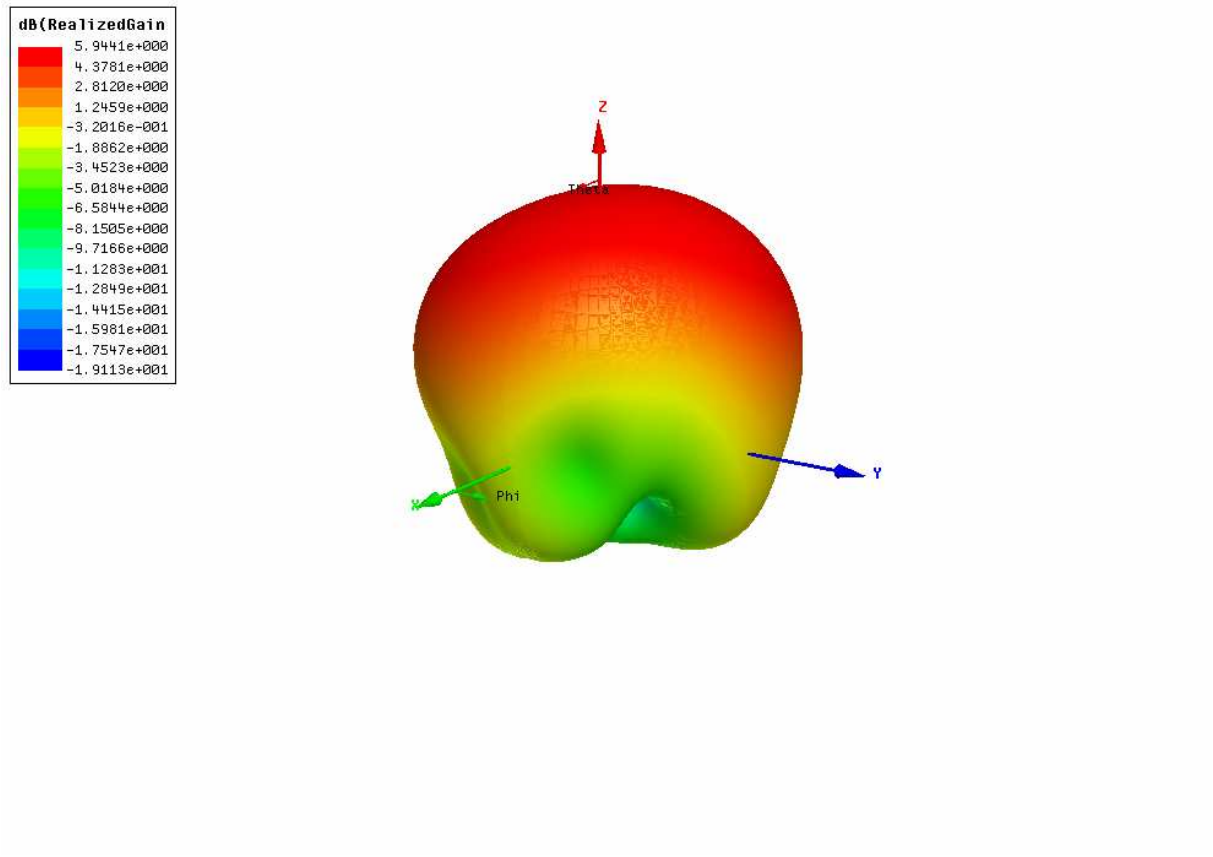

(b)

Figure 3.23: (a) Port1 and Port2 broadside radiation patterns (b) 3D polar plot.

The port1 and port2 radiation patterns are depicted in Figures 3.23(a) and (b). It is evident from the figure that patterns are nearly symmetric in xoz and yoz planes. The total gain being the magnitude of theta gain and phi gain is equal to the gains obtained in single excitation cases that is 5.7dBi. The average value of 3dB HPBW is around 95° while radiation efficiency still stands to 98%. The front to back ratio (F/B) is estimated to be 12dB.

3.6 Adhesive material's analysis:

A DRA bonded to the ground plane and the associated feeding network is expected to go under certain changes in its performance. Actually, it is not possible exactly to determine the permittivity and the thickness of the adhesive material with which the DRA body is glued to the ground plane. Generally, if the permittivity value of the adhesive material is lower than that of the DRA, as is assumed in the present case, the resonance frequency shifts to upper side [3]. Equally important is the applied thickness that is with very thin layer, less is the upward shift and with more thickness, more is the shift. These parameters can be estimated to certain extent by performing parametric simulations however, the exact effects are realized and confirmed by measuring the results.

3.6.1 Single port (Port1) parametric analysis:

Port1's impedance parametric results are depicted in Figure3.24. Comprising of different thicknesses, the ordinarily available adhesive material was used with supposed permittivity of

3. As expected there is an upward shift in resonance frequency corresponding to the layer's thicknesses. For example, with layers of 1.0mm, 0.15mm and 0.2mm an upward shift from 7.3GHz to around 7.5GHz is observed.

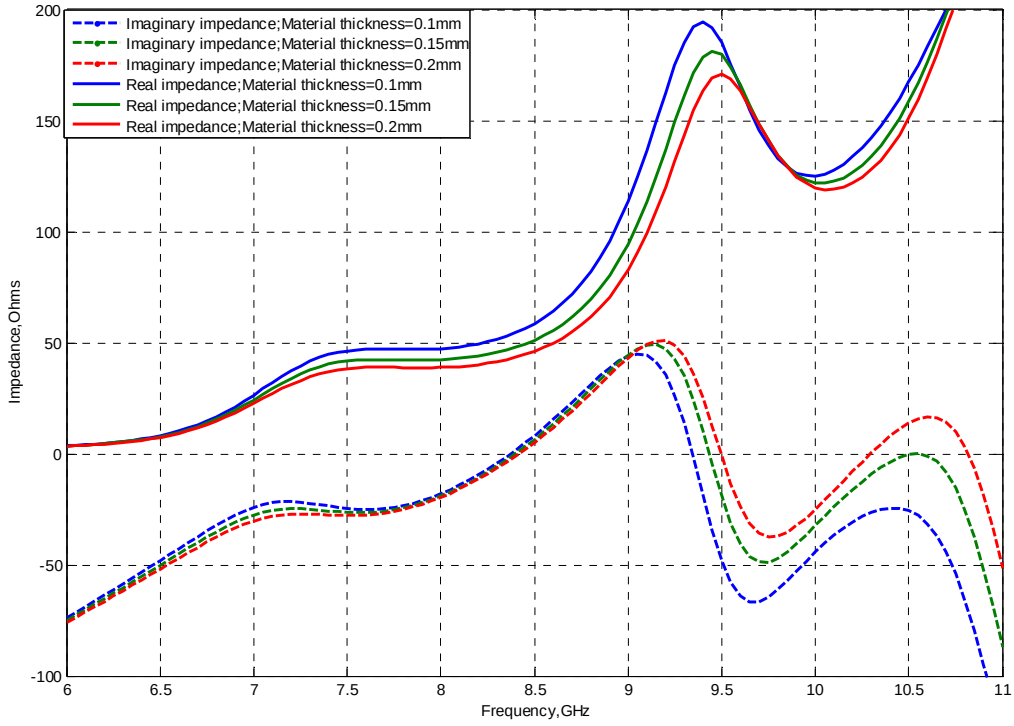

Figure 3.24: Port1 parametric impedance curves for different layers of adhesive material

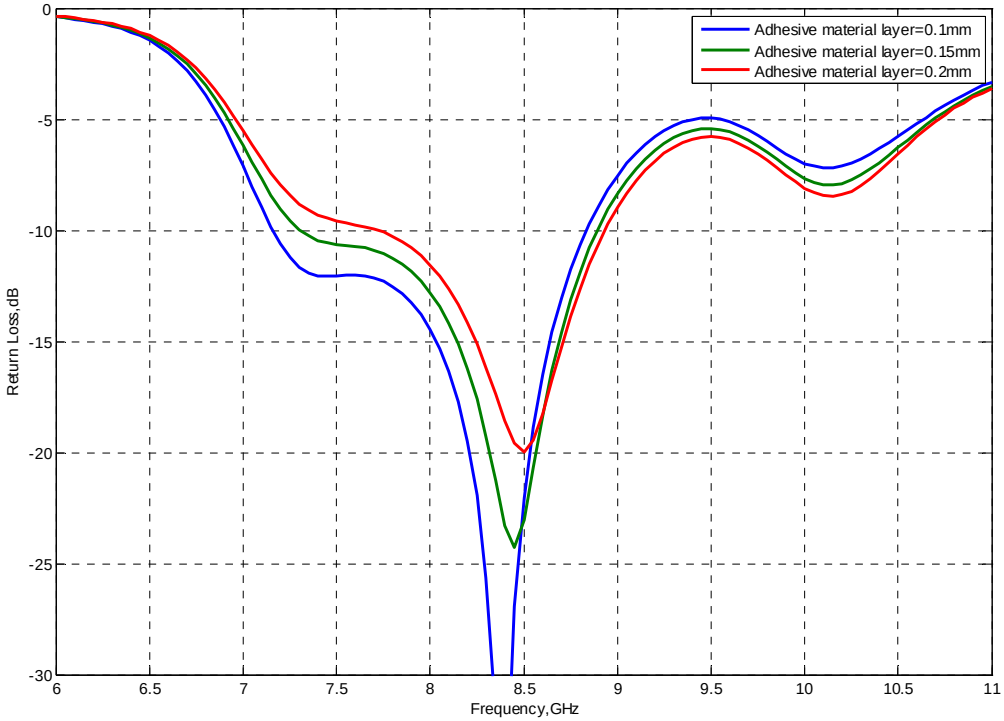

Figure 3.25: Port1 return loss curves for different layers of adhesive material

As is evident from the Figure 3.25 that adhesive material has affected the level of coupling to the DRA. So it needs to be improved by slightly adjusting the slots and stubs sizes. The result after these adjustments are made, are presented in Figure3.26.

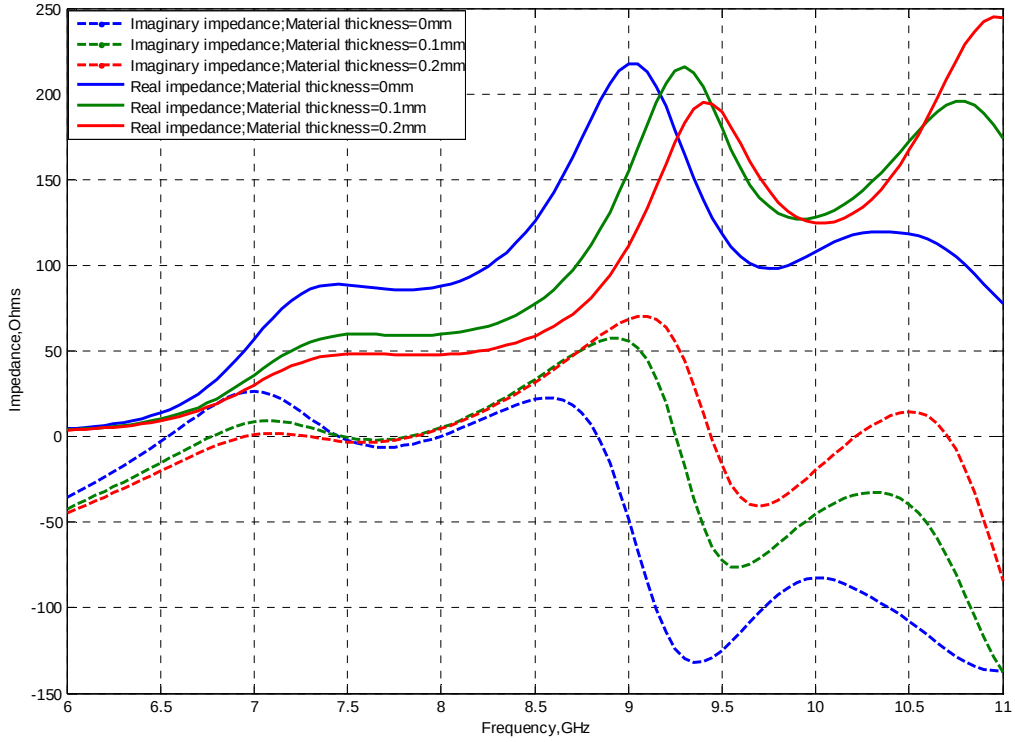

Figure 3.26: Port1 impedance curves after slight increase in slot and stub lengths.

As 0.2mm thickness is expected to be more robust in shifting the resonance frequency so it is taken into account for further design analysis.

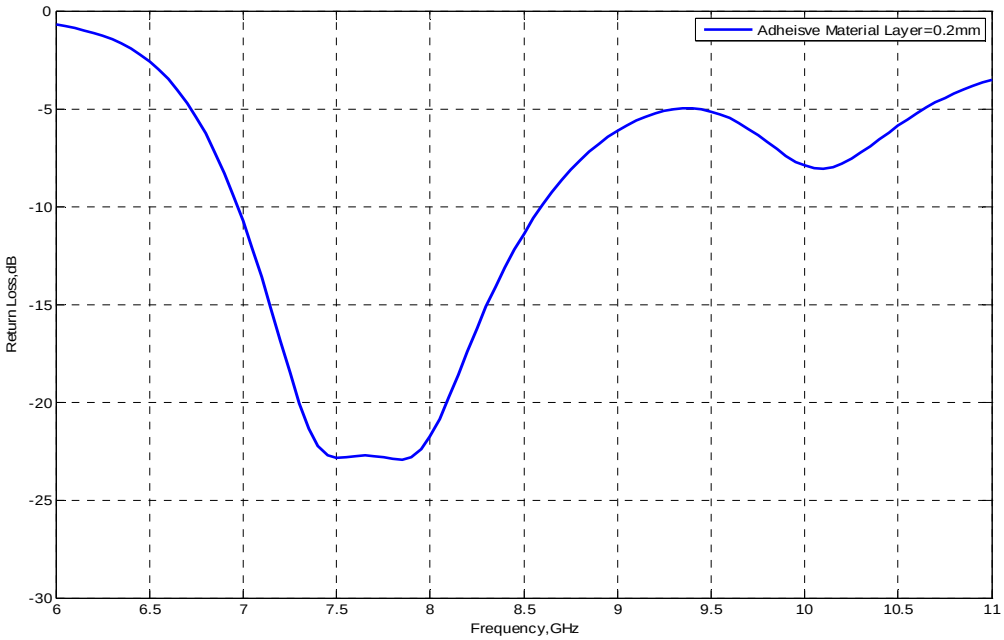

Figure 3.27: Return loss curve with adhesive material thickness (0.2mm)

The return loss curve in the presence of adhesive material layer of 0.2mm thickness is presented in Figure3.27. There is an upward shift in frequency from 7.3GHz to around 7.5GHz. The -10dB impedance bandwidth (7GHz to 8.6GHz) is found to be 20%. The other resonances around 9.5GHz are the slot resonances that are dependent upon corresponding slot sizes.

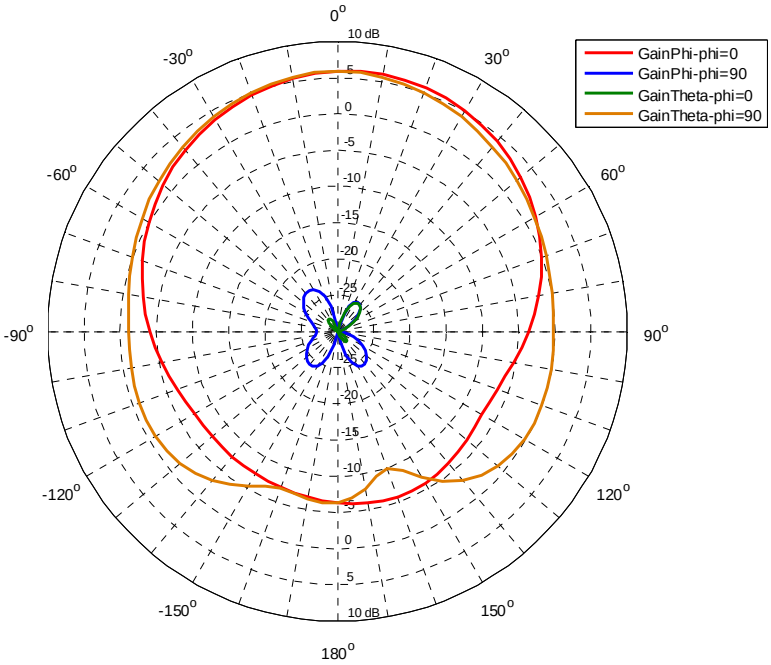

Figure 3.28: Broadside radiation patterns at 7.5GHz in yoz & xoz planes

For port1 the broadside radiation patterns are depicted in Figure3.28. The co-polarization level is 30dB higher than the cross-polarization level in the broadside direction. The yoz(E) and xoz(H) plane radiation pattern are purely symmetric with -3dB HPBW around 130°. The gain is estimated to be 5.7dBi while radiation efficiency of 98%. The (F/B) is observed to be around 10dB.

3.6.2 Single Port (Port2) parametric analysis:

Port2's parametric impedance results are depicted in Figure3.29. Again in compliance with port1 case, different adhesive material's layers comprising of permittivity of 3, are taken into consideration. This presents that for three such layers of 0.1mm, 0.15mm and 0.2mm in thickness the simulated results depict slight up-ward shift of DRA resonance frequency. Similarly the level of coupling to the DRA is found to be reduced as is presented in Figure3.30.

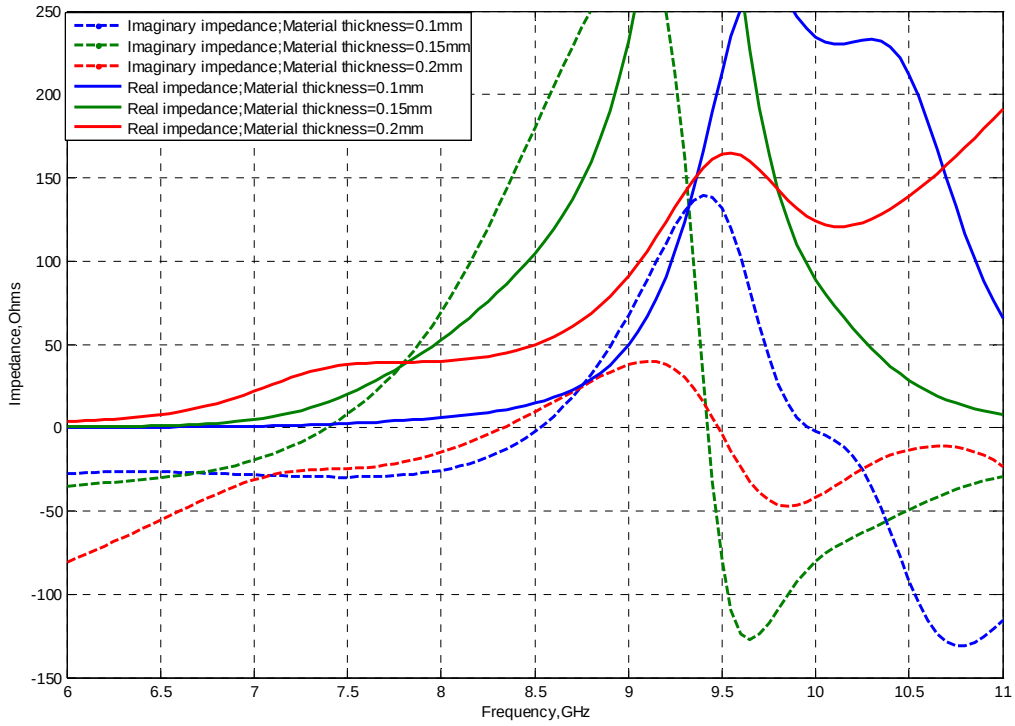

Figure 3.29: Port2 parametric impedance curves for different layers of adhesive material

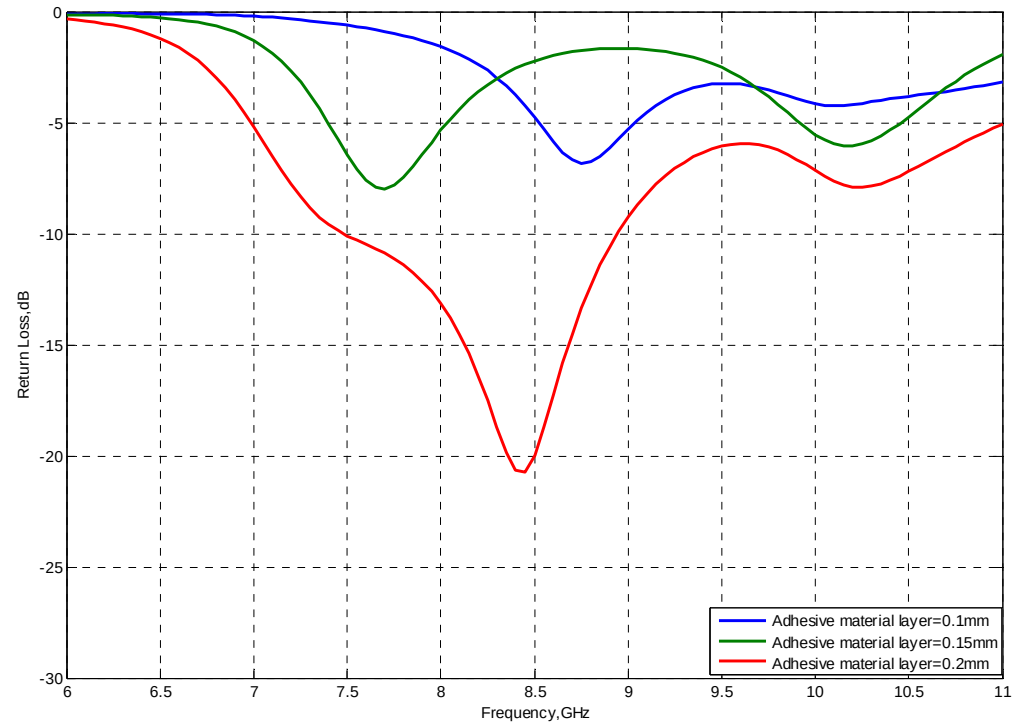

Figure 3.30: Return loss curves with different adhesive material layers

In accordance with port1 and its slot, port2 and its slot are also slightly adjusted to properly couple to the DRA. The simulation results for different adhesive material layers are depicted in Figure3.31.

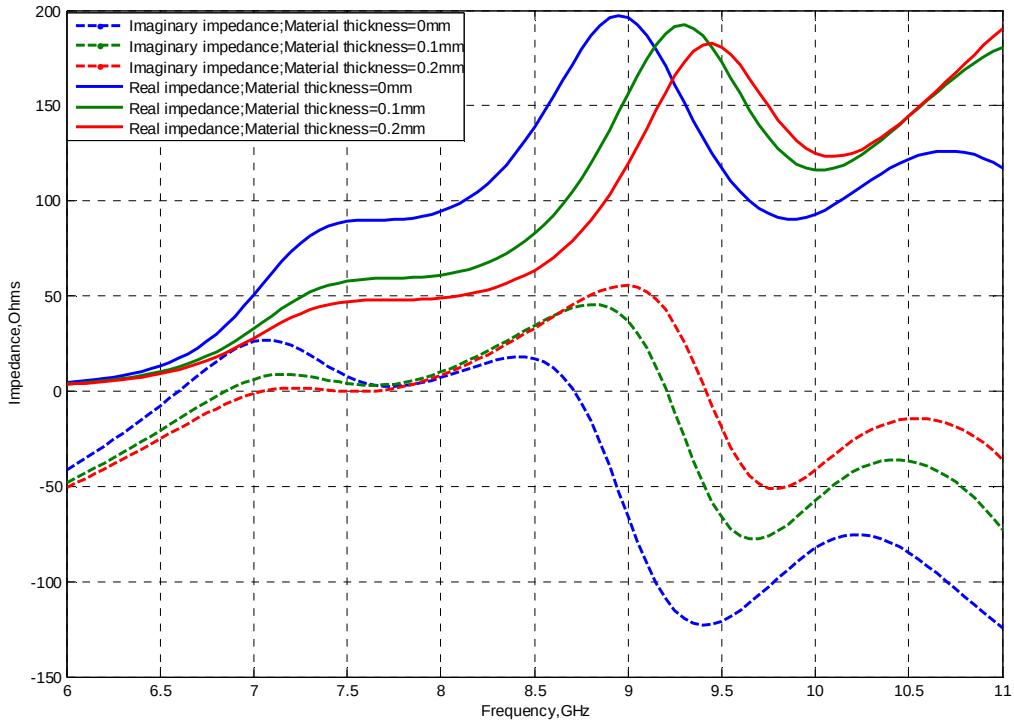

Figure 3.31: Port2 impedance curves after slight increase in slot and stub lengths.

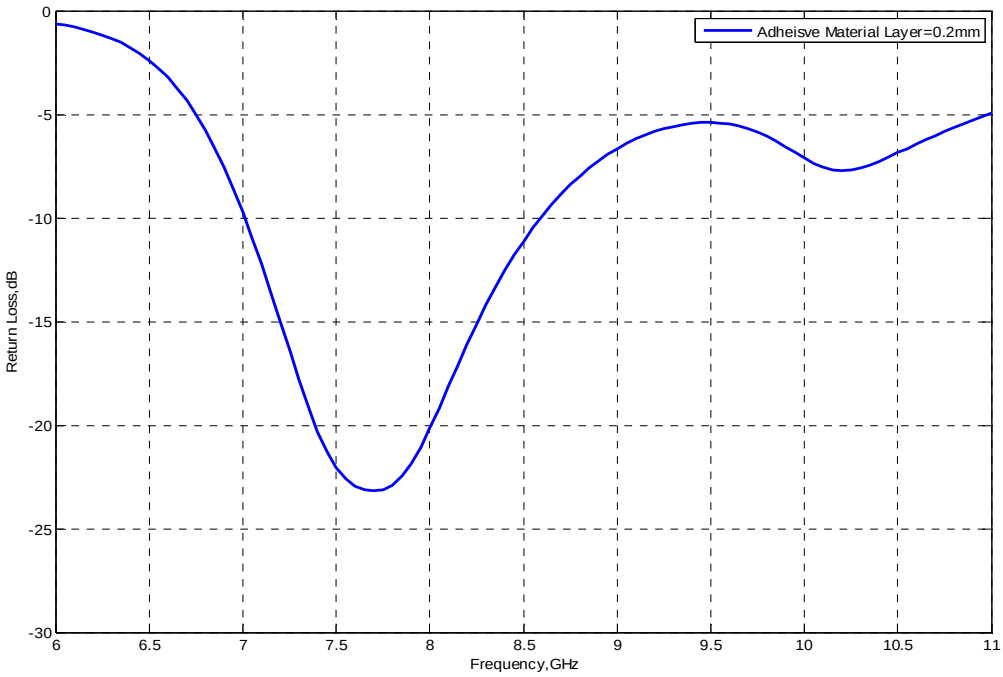

Figure 3.32: Return loss curve with adhesive material thickness (0.2mm)

The return loss curve in the presence of adhesive material layer of 0.2mm thickness is presented in Figure3.32. Like in port1, there is an upward shift in frequency from 7.3GHz to around 7.5GHz. The -10dB impedance bandwidth (7GHz to 8.6GHz) is found to be 20%. The other resonances around 9.5GHz are the expected slot resonances.

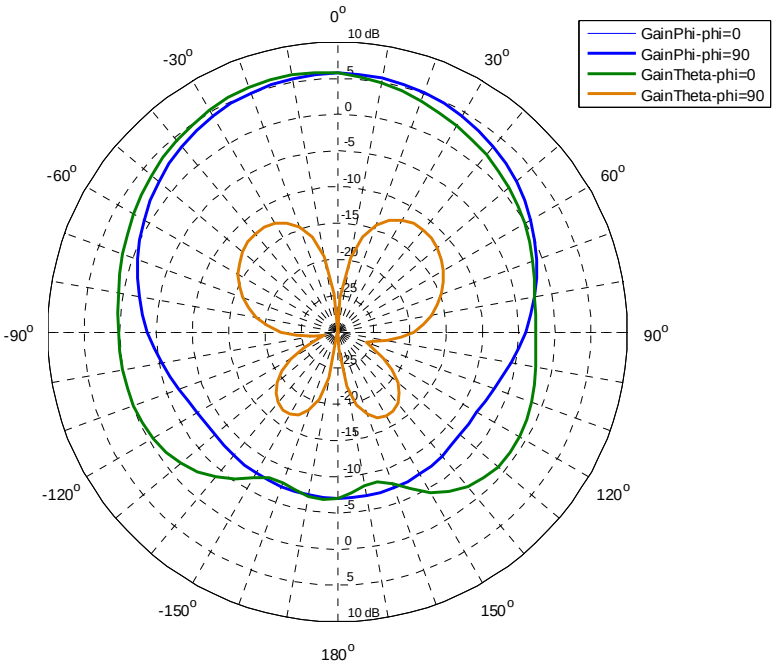

Figure 3.33: Broadside radiation patterns at 7.5GHz in xoz & yoz planes

For port2 the broadside radiation patterns are depicted in Figure3.33. For both planes the co-polarization level is 30dB higher than the cross-polarization level in the broadside direction. Both plane patterns xoz(E) and yoz(H) are found to be symmetric however with -3dB HPBW of 120°. The gain is estimated to be 5.7dBi with radiation efficiency of 98%. The (F/B) is estimated to be around 12dB.

3.7 Port1&Port2 combined performance with adhesive material:

Both ports working independently are found to undergo similar up-ward shift in resonance frequency due to the adhesive material's effect. To evaluate simultaneous performance of the ports that under went slight increase in their stub and slot lengths due to the influence of adhesive material, the design values are given in Table2. The symbols used in the Table can be traced to schematic diagram given in Figure3.37. Based upon these values and employing adhesive material layer of 0.2mm, the two ports impedance and return loss curves are given in Figures3.34 and 3.35 respectively.

Table2:Port1 and Port2 adjusted slots and stubs design values

DRA feed Ports	Aperture slots Size Length(L)&Width(W)	Feed Lengths (L_f)	Stub lengths(L_s) (From slot's centre)
Port1	L_1=4.6mm,L_{1L}& L_{1H} =2mm W_1=0.5mm	L_{f1} =22.05mm	L_{s1} =2.1mm
Port2	L_2=4.6mm,L_{2R}& L_{2L} =2mm W_2 =0.5mm	L_{f2} =19.5mm	L_{s2}=2mm

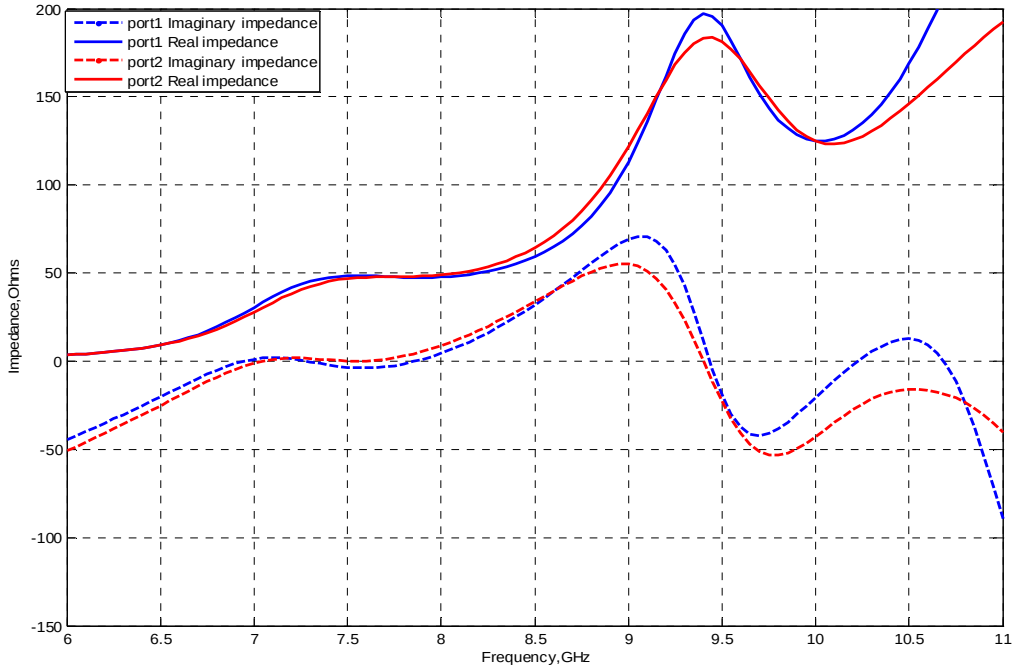

Figure 3.34: Two ports impedance curves representing DRA resonance around 7.5GHz

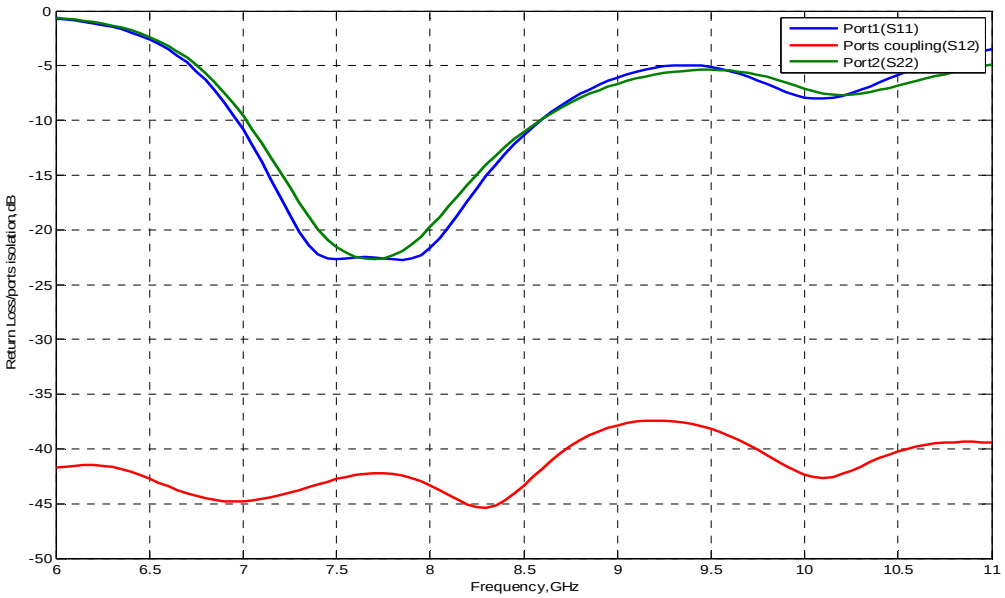

Figure 3.35: Port1 and Port2 return loss curves with an isolation of -40dB.

As is evident from Figure3.35 that -10dB impedance bandwidth for both ports (7GHz to 8.6GHz) are found to be 20% and that is exactly in individual port cases. Thus the common impedance bandwidth is also 20% while worst ports isolation stands to -42dB.

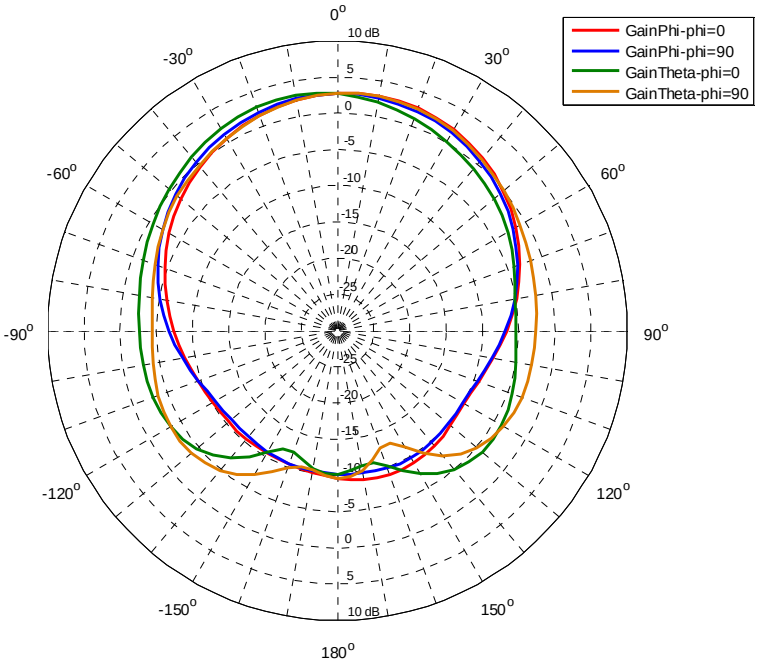

(a)

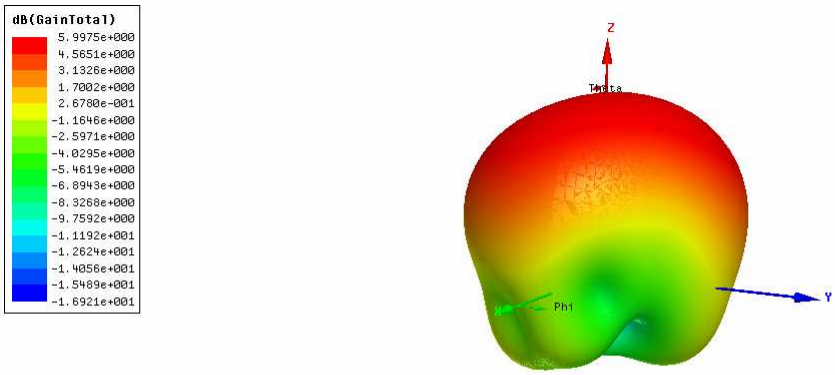

(b)

Figure 3.36: Port1 and Port2 broadside radiation patterns in xoz & yoz plane at 7.5GHz
(a) 2D pattern (b) 3D polar plot

Two ports broadside radiation patterns are depicted in Figure3.36. There is a pure symmetry in xoz and yoz plane radiation patterns with -3dB HPBW for both plane patterns to be 70°. The total gain that is constituent of gain theta and gain phi is found around 5.7dBi with radiation efficiency of 98% while (F/B) stands to 12dB.
The radiation patterns are found to be stable in the matching frequency band.

- After thoroughly analysing the main constraints that may influence the performance of the DRA, its prototype is finalized.

3.8 X band DRA Fabrication & Measurements:

It is clear from rigorous simulations and the analysis that there is a definite upward shift in resonance frequency, the range of which is not sure.

3.8.1 Antenna design parameters:

A cylindrical shaped DRA with diameter (D)= 18mm and height (H)=5mm is composed of dielectric material of relative permittivity εr=6. A substrate of permittivity of εr=3.38 and thickness(t)=0.508mm is used to support a ground plane of 4cm×4cm size upon which two H-shaped aperture slots are etched to feed the DRA. Opposite to the ground plane two orthogonal microstrip lines each of width *w*=1mm and characteristic impedance of 50Ω are etched to feed the DRA. Using the design parameters given in Table2, the design structure is fabricated that is depicted in Figure 3.37(a) Figure 3.37(b).
The H-slot fed through microstrip feed line 1 is displaced 2.2mm (along –ve x-axis) while H-slot fed through microstrip feed line 2 is displaced 2.3mm (along +ve x-axis) from the DRA centre. This generates a space of 3.1 mm between the microstrip feed lines and 2.4 mm between the slots that assures a proper isolation.
An ordinary glue that is commercially available is used to bond the DRA with the ground plane.

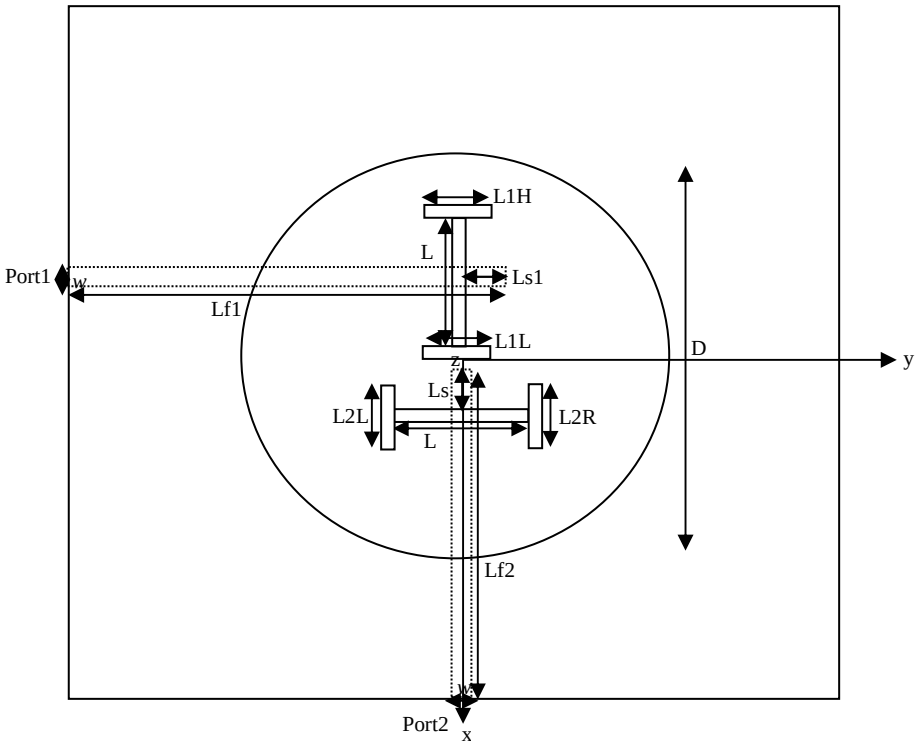

(a)

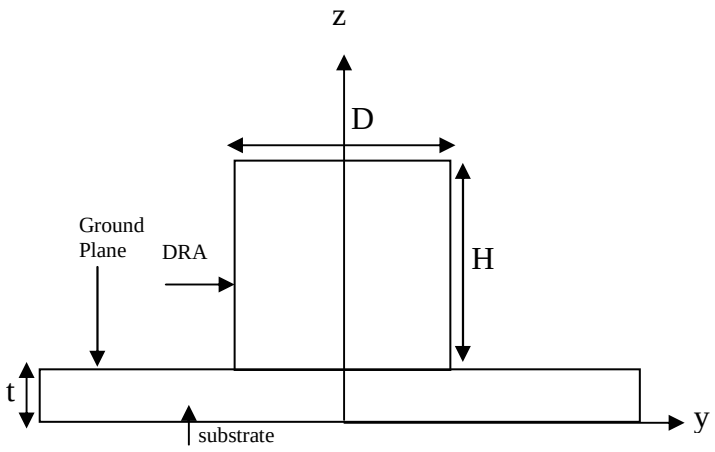

(b)

Figure 3.37: X band DRA design geometry fed by two orthogonal H-shaped aperture slots (a) Top view (b) Side view

3.8.2 Measured results:

The fabricated design is pictured in Figure 3.38(a) & (b). Figure 3.39 shows the measured return loss and isolation curves. The -10dB return loss at (8.1GHz-8.6GHz) yields a common bandwidth of 5.9% while the ports exhibit an input isolation of -35dB. The impedance response can be visualised from the smith chart plots presented in Figure3.40.

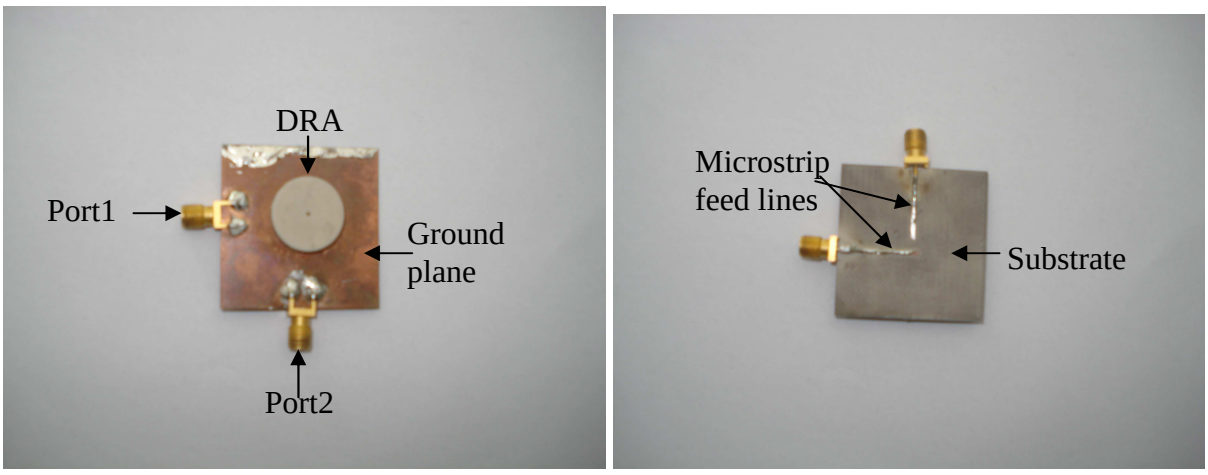

(a) (b)

Figure3.38: X band DRA fabricated design (a) top view (b) bottom view

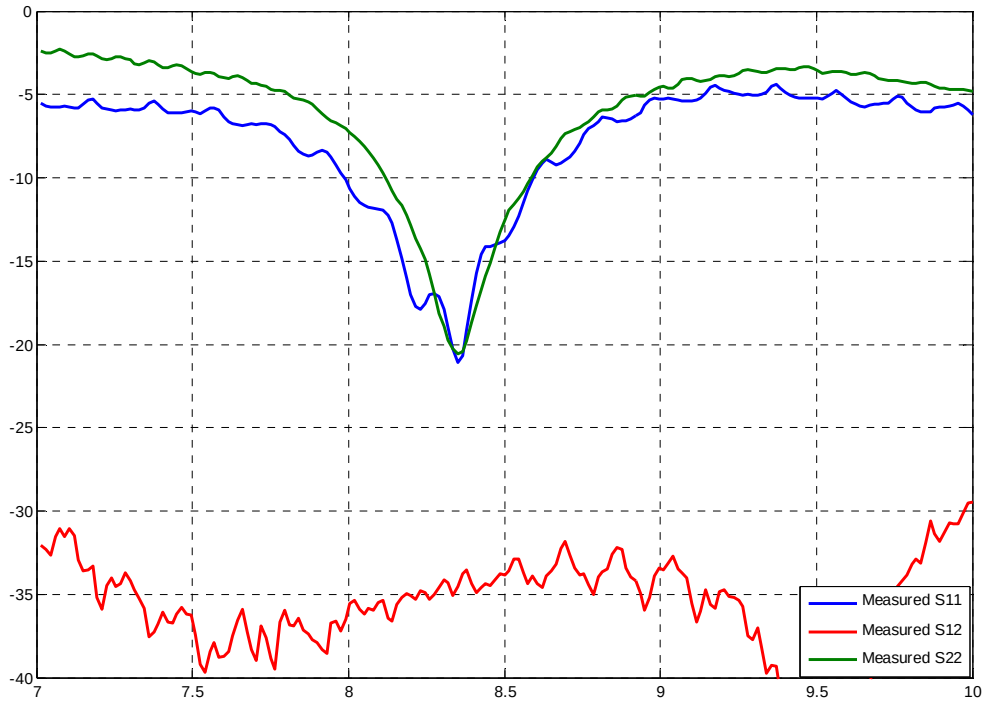

Fig3.39: X band DRA measured return loss and ports isolation curves

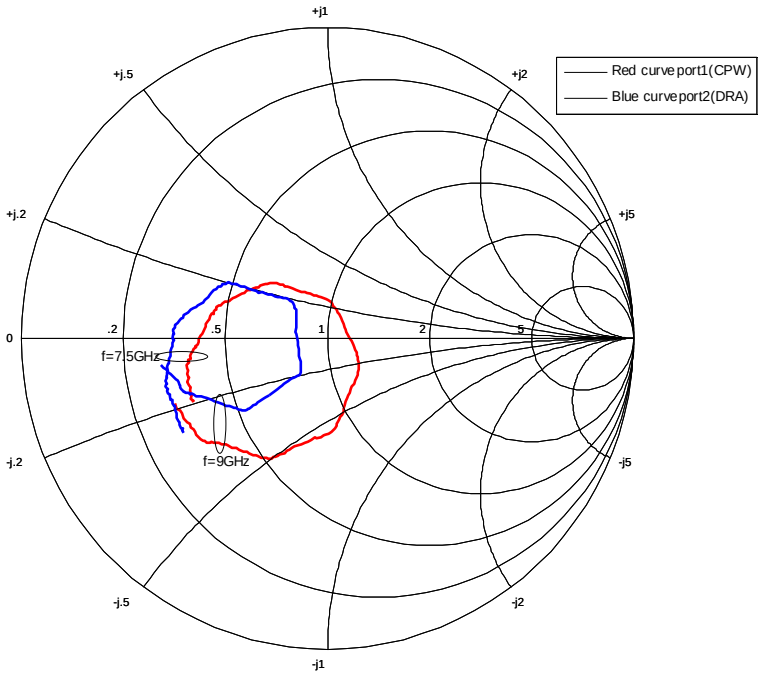

Fig3.40: X band DRA Port1 and Port2 Smith chart curves

The port1's radiation patterns in the yoz-(E) plane and xoz-(H)plane are shown in Figure3.41(a) and (b) respectively.

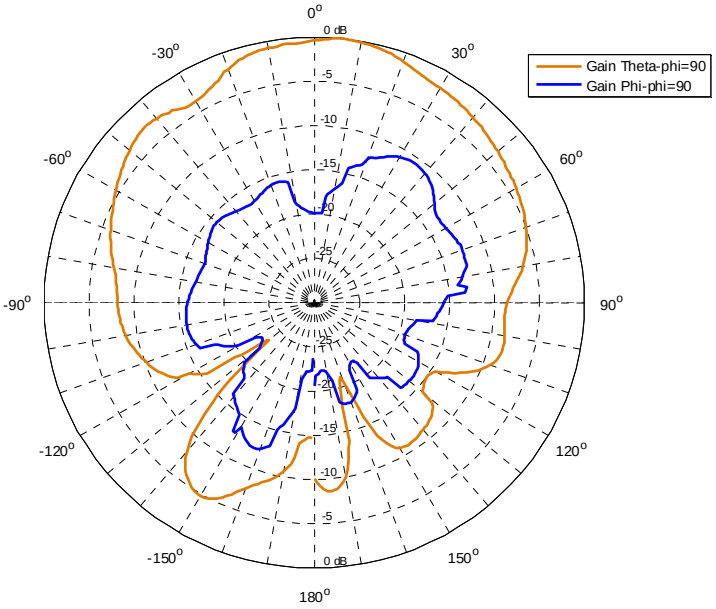

(a)

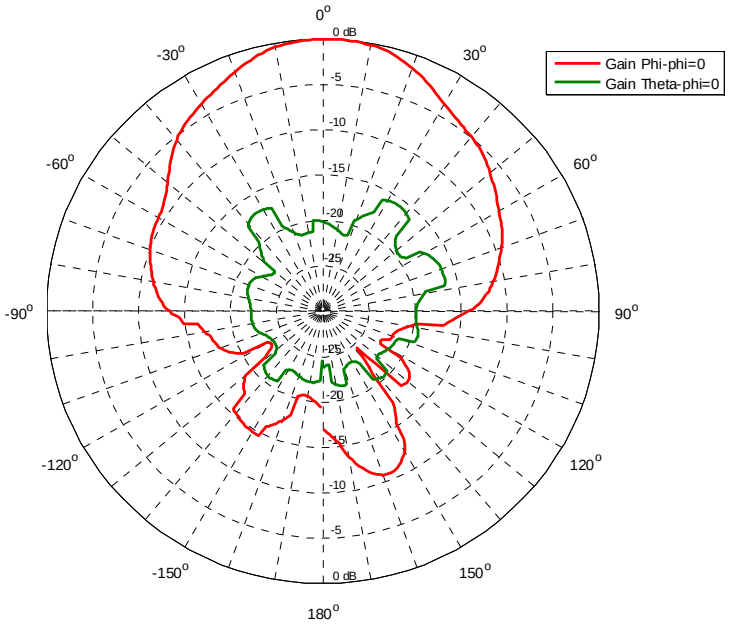

(b)

Fig3.41: Port1 broadside radiation patterns @8.35GHz (a) yoz(E) plane (b) xoz(H) plane

The Port2's radiation patterns in the xoz-(E) plane and yoz-(H) plane are shown in Fig.3.42(a) and (b) respectively.

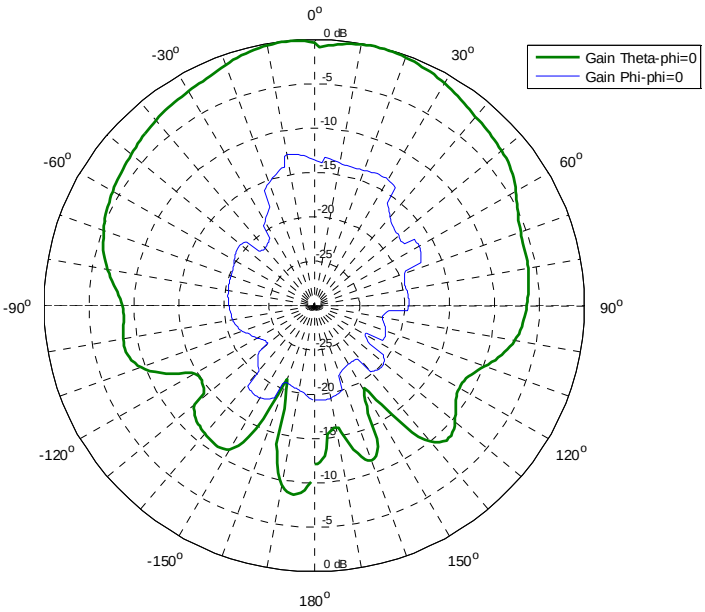

(a)

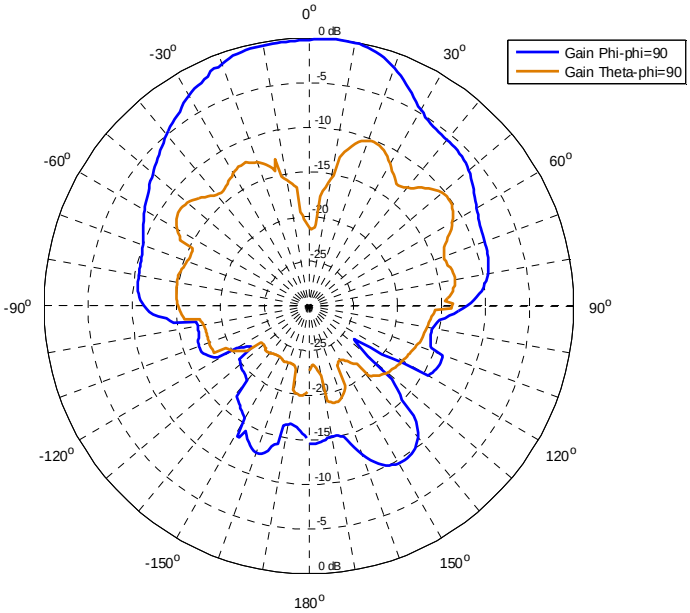

(b)

Fig3.42: Port2 broadside radiation patterns @8.35GHz (a) xoz(E) plane (b) yoz(H) plane

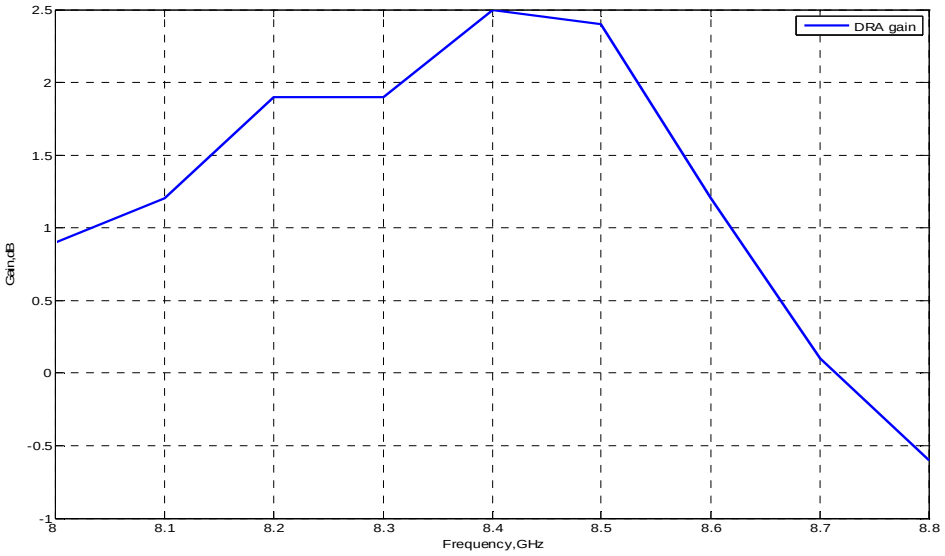

Figure3.43: DRA single element gain

3.8.3 Performance analysis:

A DRA @ (8.1GHz-8.6GHz) excited by dual H-shaped slots has been measured to obtain two orthogonally polarized fields in the broadside direction. Figure3.39 presents a more robust shift in frequency to the upper side of the matching band. -10dB impedance bandwidth for port1 ranges from 8GHz to 8.6GHz while for port2 it is from 8.15GHz to 8.6GHz. This generates a common impedance bandwidth of 5.9% that is narrower than the expected value. This change could be attributed to the adhesive material's real impact, uneven layer distribution between the DRA bottom and the ground plane and obviously fabrication imperfection. The input ports isolation of -35 dB is ideally suited to seek better performance at X-band. The maximum measured gain depicted in Figure3.43 is found to be 2.5dBi at 8.4 GHz.

In both port radiation patterns a cross-polarization of -20dB is observed in the broadside direction. However, the cross- polarization in port2 xoz(E)plane increases to -15dB. The radiation patterns are found to be purely symmetric with maximum directivity towards the broadside direction that can be observed from Figures3.41 and 3.42. As expected the E-plane patterns are found to be wider than that of H-plane patterns. A little backward radiation is attributed to the small ground plane size and can be further reduced if a larger ground plane is used.

It was observed during the measurement that connectors if not properly shielded, play a role in disturbing the radiation patterns, especially port2 xoz(E) was found to be very sensitive to change the patterns. So a very thick absorbing material be assured to cover the connectors to suppress their role.

3.9 Conclusion:

Though common impedance bandwidth still needs to be improved, yet two ports dual linearly polarized X-band DRA with improved performance in terms of better ports isolation and symmetric radiation patterns has been successfully designed. It seeks promising applications in the satellite and radar communication systems, typically it is applicable to uplink frequency band (7.9 GHz-8.4 GHz) that has been assigned to military communications satellites.

References

1 ALDO PETOSA “Dielectric Resonator Antenna Handbook” 2007 ARTECH HOUSE,INC.685 Canton Street Norwood, MA

2 D. M. POZAR and S.D TARGONSKI “Improved Coupling for Aperture Coupled Microstrip Antennas” ELECTRONICS LETTERS 20th June 1991, Vol.27, No.13

3 L.Dussopt,Y.Toutain,J.P.Coupez and J.M.Laheurte “Circularly polarized microstrip arrays built on polymethacrylate imide foam” ELECTRONICS LETTERS 12th October 2000 Vol,36 No.21

4 G.P.Junker ,A.A Kishk ,A.W. Glisson and D.Kajfez “Effect of air gap on cylindrical dielectric resonator antenna operating in TM01 mode” ELECTRONICS LETTERS 20th January 1994 Vol.30 No.2. pp 97-98

5 R.Chair, A.A. Kishk & K. F.Lee “Wideband Simple Cylindrical Dielectric Resonator Antennas” IEEE MICROWAVE AND WIRELESS COMPONENTS LETTERS, VOL.15, N°4, APRIL 2005

6 Yong-Xin Guo and Kwai-Man Luk “Dual Polarized Dielectric Resonator Antennas” IEEE TRANSACTIONS ON ANTENNAS AND PROPAGATION, VOL.51, N°5, May 2003.

7 Chair,R.;Kishk,A.A.;Lee,K.F “Wide band dual polarized dielectric resonator antennas at x-band” Antenna and Propagation Society international symposium, 2005 IEEE page(s); 214-217 vol.4B

Chapter 4

Dual Pattern Antenna combining a Slot Loop and a DRA

Contents

A two ports dual pattern diversity antenna is assumed to be best suited to seek Diversity Gain (DG) performance in the context of Body Area Network (BAN) applications [1]-[2]-[3]-[4]. This diversity antenna design is supposed to integrate two different types of antennas, one yielding broadside while the other end-fire types of radiation patterns however,

maintaining same resonance frequency and yielding common impedance bandwidth around 2.4GHz(ISM band). The unified structure is to be fed by two independent ports thus exciting the respective antenna branches. To start with initial design, Coplanar Waveguide (CPW) fed slot loop is employed to yield broadside while vertical monopole fed DRA to yield end-fire types of radiation patterns. The design structure of the slot loop is analysed first independently and then under the influence of the DRA which is to be bonded to it. The performance of this structure is evaluated in free space and upon the phantom model characterizing the human body. Similarly the design structure of the DRA is evaluated and its performance in the context of free space and upon the phantom model is analyzed. After the individual performances of slot loop and DRA are optimised, the unified structure is subject to analysis to observe corresponding -10dB common bandwidth and level of mutual coupling. This compact structure is too subject to free space and phantom model analysis to observe if any change in its performance. Finally this compact diversity antenna is cleared for fabrication.
One main disadvantage in the initial design is the non-planar feed to the DRA and that is expected to restrict its on-body applications. So other design is envisaged in which both slot loop and DRA are fed by planar microstrip feed lines, etched on the opposite side of the ground plane that contains the slot loop and the DRA. Initially the slot loop design is analyzed and optimized and is subject to free space and phantom model tests. Then same is repeated for the DRA branch. After individual antennas exhibit satisfactory performance, the compact structure is evaluated to observe its common impedance bandwidth and mutual coupling. Following the free space and phantom model tests, this more compact diversity antenna is finalized.

4.1 CPW fed slot loop initial design:

The coplanar waveguide (CPW) line with characteristics impedance of 50 Ω and fed by port1 is used to excite the slot loop antenna. The slot is etched in a square shaped ground plane of small dimensions supported by equivalent sized substrate of 5cm×5cm with dielectric constant of(εr=3.38) and of height h=0.508mm.The schematic diagram of the design is depicted in 4.1.

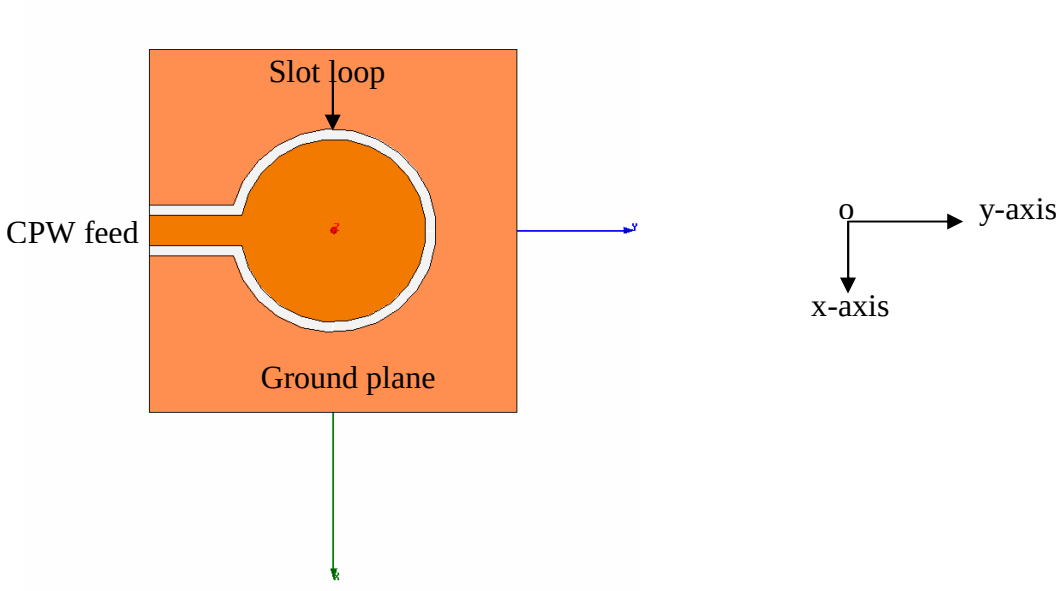

4.1: slot loop antenna fed by coplanar waveguide (CPW) line

The guided wavelength (**λg)** that is to be used in terms of Slot Length (SL) is calculated from the equations 4.1 and 4.2 [5]:

$$\lambda_g = \frac{\lambda}{\sqrt{\varepsilon_{eff}}} \quad \text{.....(4.1)}$$

$$\varepsilon_{eff} = (\varepsilon_r + 1)/2 \quad \text{.....(4.2)}$$

So using εr =3.38 the guided wavelength is estimated to be $\lambda_g = 96mm$ (by HFSS simulation).

As initial analysis keeping Slot Width (SW = 1mm), the Slot Length SL is determined to suit to 2.4GHz resonance frequency. The parametric results are presented in Figure 4.2 which are explicitly summarized in Table4.1.

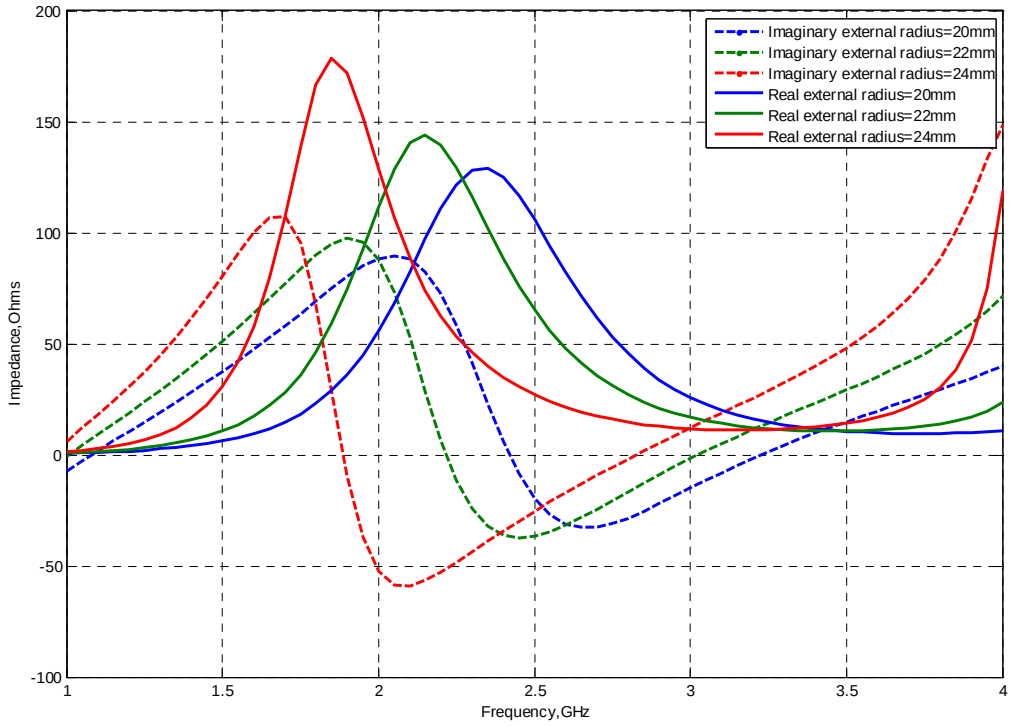

(a)

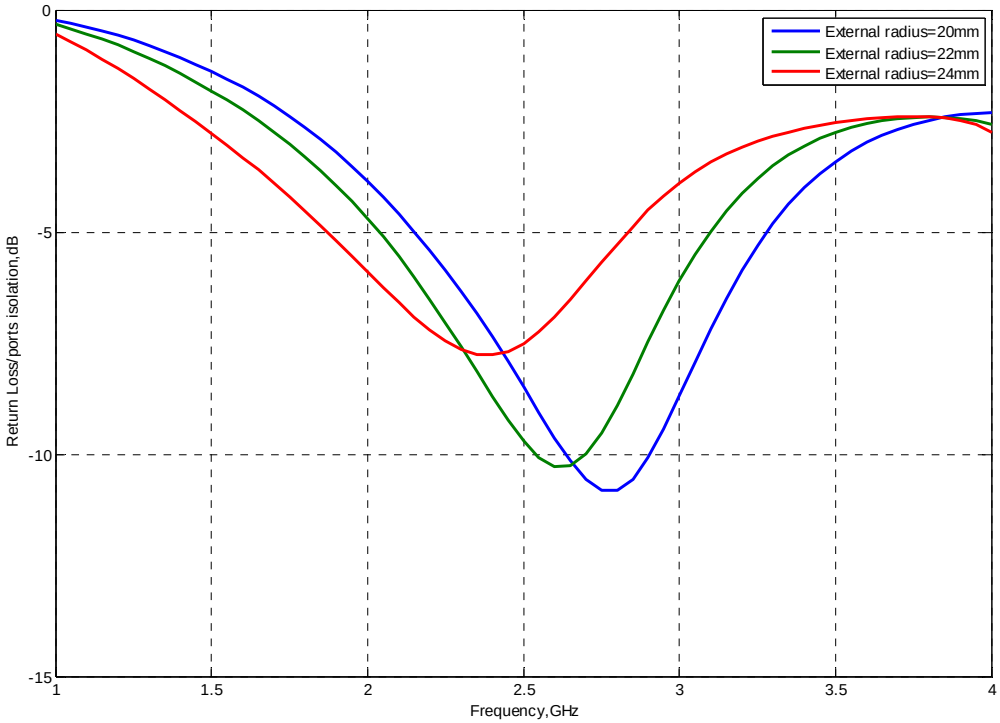

(b)

4.2: Parametric analysis for (a) impedance and (b) return loss curves in terms of different slot lengths

Table4.1: Parametric analysis of slot length when width=1mm & guided wavelength (λ_g=96mm)

Slot External Radius R(mm)	Slot Length (SL)mm	Slot Length (λ_g)	Resonance Frequency (f_r)GHz
20 mm	108 mm	1.1 λ_g	2.4 GHz
22 mm	121 mm	1.2 λ_g	2.25 GHz
24 mm	133 mm	1.4 λ_g	1.8 GHz

As can be observed from the results presented in Figure 4.2 and in Table 4.1, a slot's external radius of 20 mm (1.1 λ_g) yields a resonance around 2.4 GHz but the real part of the impedance stands to 125 ohms and that needs to be corrected to 50 ohms. Before refining these results, it is suitable here to observe the effect of slot widths. A parametric simulation is performed for slot with external radius of 20mm. The results are presented in Figure 4.3 while their summarized description is given in Table 4.2.

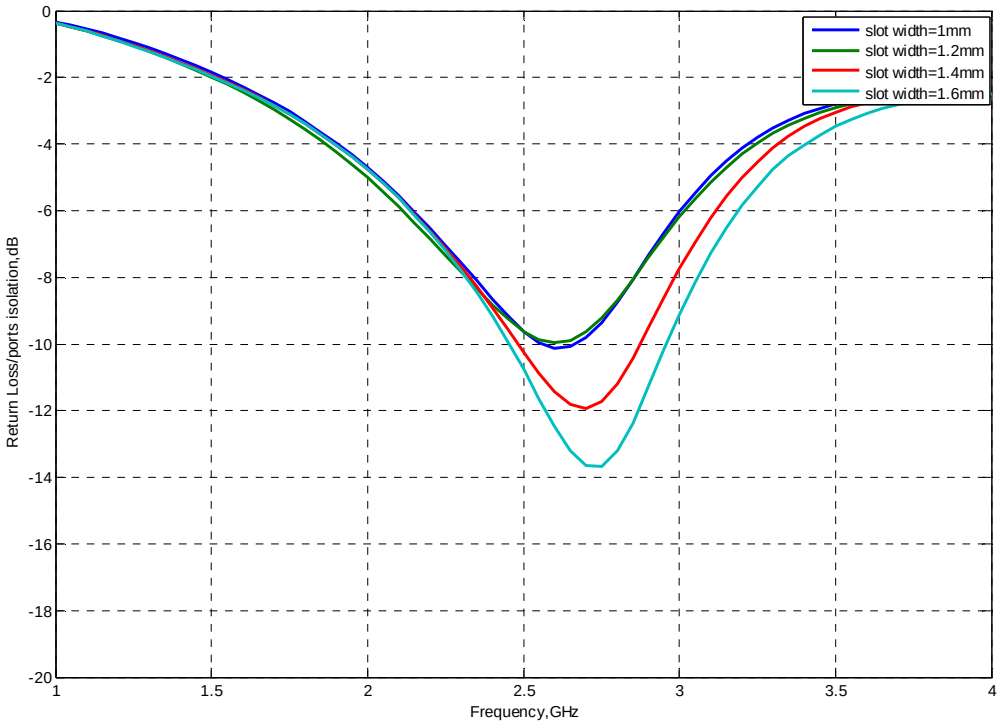

4.3: Parametric analysis for return loss values in terms of slot widths

Table4.2: Parametric analysis of slot widths when slot external radius is 20mm

Slot width (SW)mm	Return loss value (dB)	Impedance bandwidth (%)
1.0mm	-8dB	18%
1.2mm	-8dB	18%
1.4mm	-10dB	14%
1.6mm	-10dB	18%

It is apparent from Fig.4.3 and Table 4.2 that the increase in the slot width (SW) improves the coupling and hence yields wider bandwidths. This signifies that any suitable value of SW can be chosen that fits to the specific bandwidth requirements.
Now we come to ascertain that slot should precisely exhibit either parallel or series resonance around 2.4GHz, with real impedance peak standing to 50 ohms and imaginary to 0 ohm. It was tried to seek parallel resonance with real impedance at 50ohms but it did not work. Then series resonance was found to yield real impedance at 50ohms with slot's average radius of 28.5mm and width of 3.6mm.The results are presented in Figure 4.4(a)

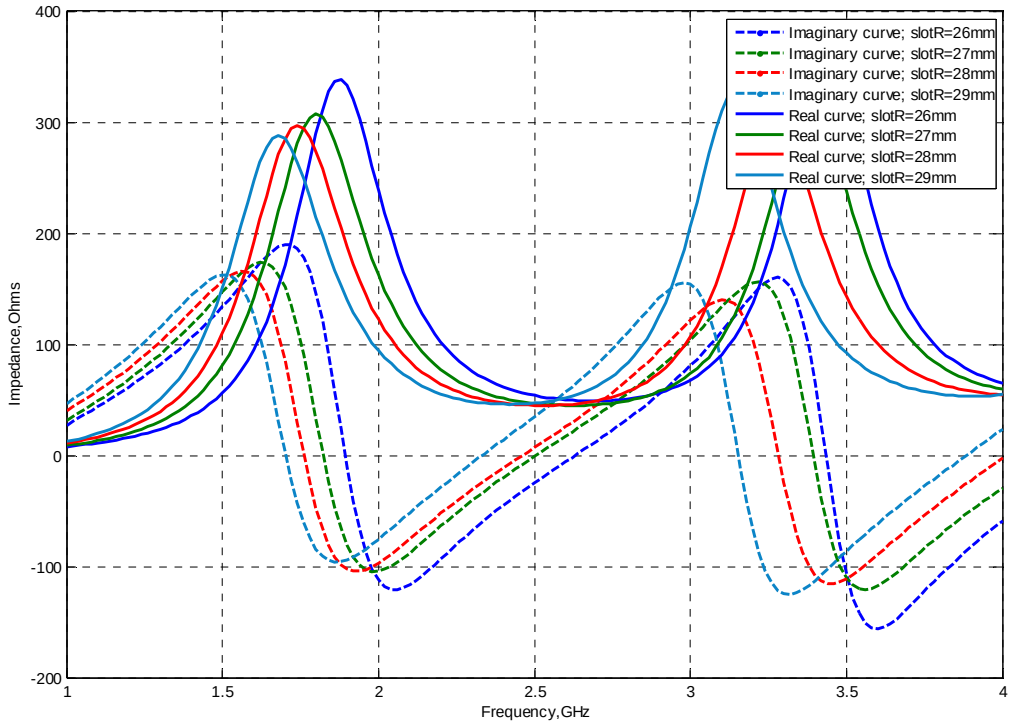

Figure 4.4(a): port1 slot loop radii impedance curves to seek series resonance

Though desired results are sought but DRA placement inside the slot loop is found to change this resonance and also the antenna size gets larger. So a mid way is sought to not only slot tolerate the effect of DRA presence but also remain compact in size.
For this purpose slot with external radius of 23mm and width of 1.4mm is analysed. The basic antenna design values are tabulated in Table 4.3.

Table4.3: Slot loop antenna; basic design values.

Structure elements	Specific parameters	Numerical value
CPW line	S-W-S	1.4mm-7mm-1.4mm
Slot loop	External radius(R1)	23mm
Slot loop	Internal radius(R2)	21.6mm
Slot loop	width	1.4mm
Slot loop	Circumference length	146mm

Based upon the estimated design values enlisted in Table4.3, the simulated results are presented in Figure 4.4 through 4.7 in terms of impedance matching , return loss and radiation patterns.

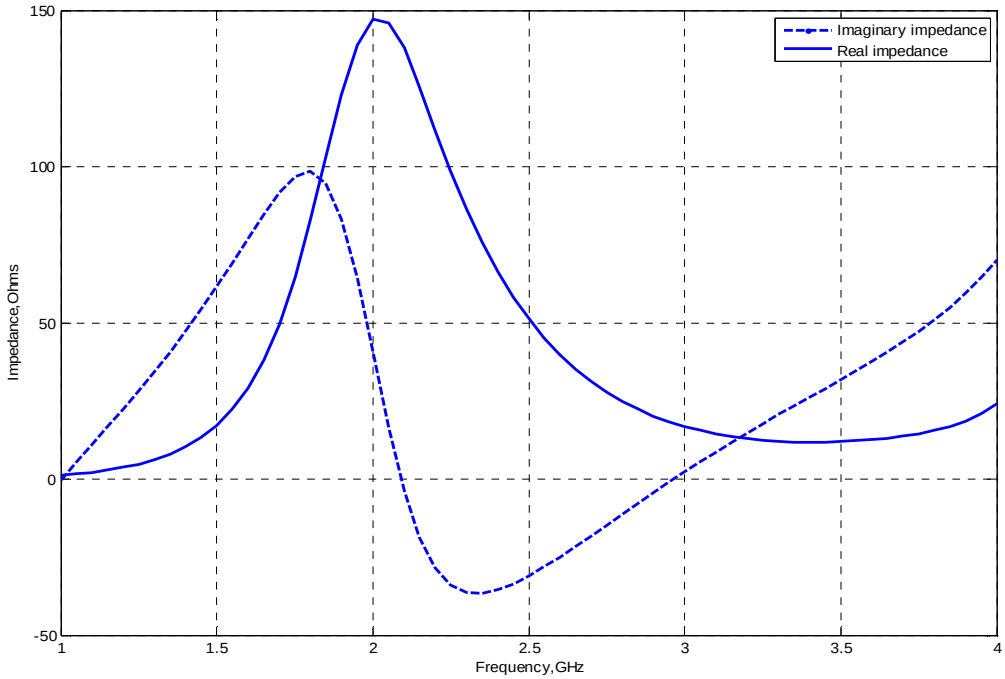

Figure 4.4(b): Port1 slot loop impedance curves.

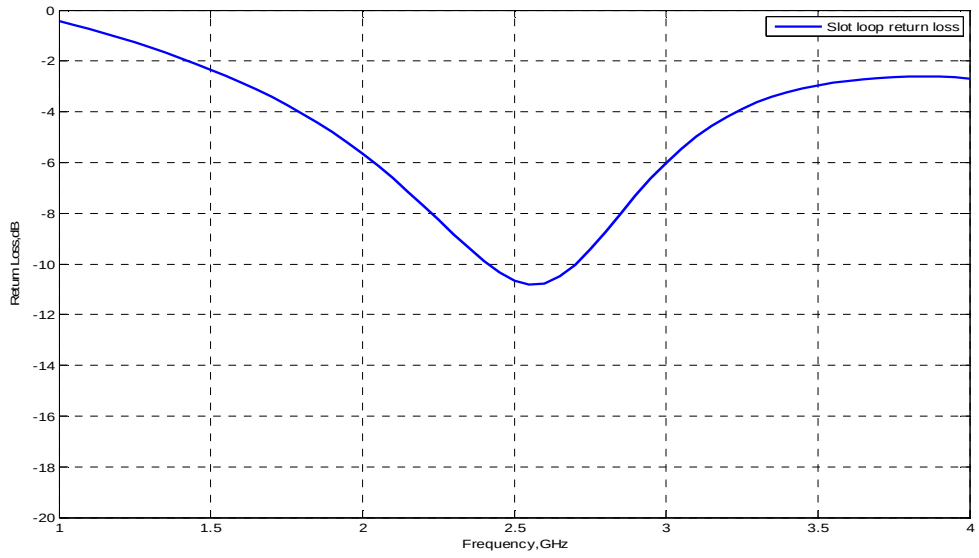

Figure 4.5: Port1 slot loop return loss curve.

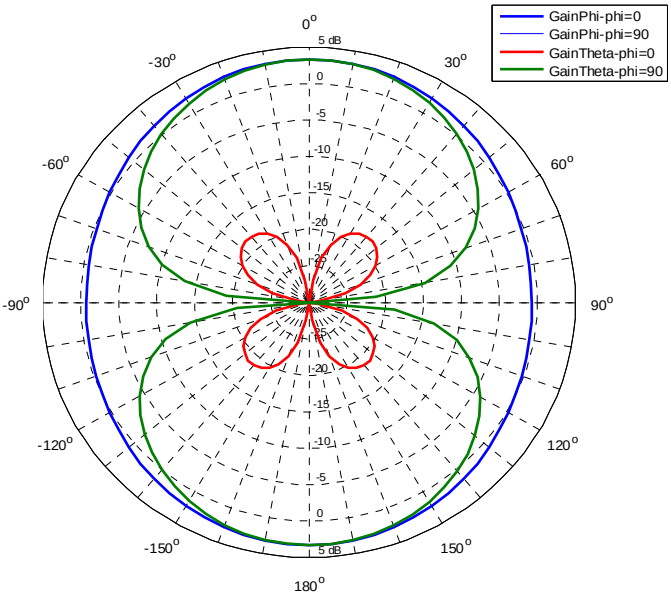

(a)

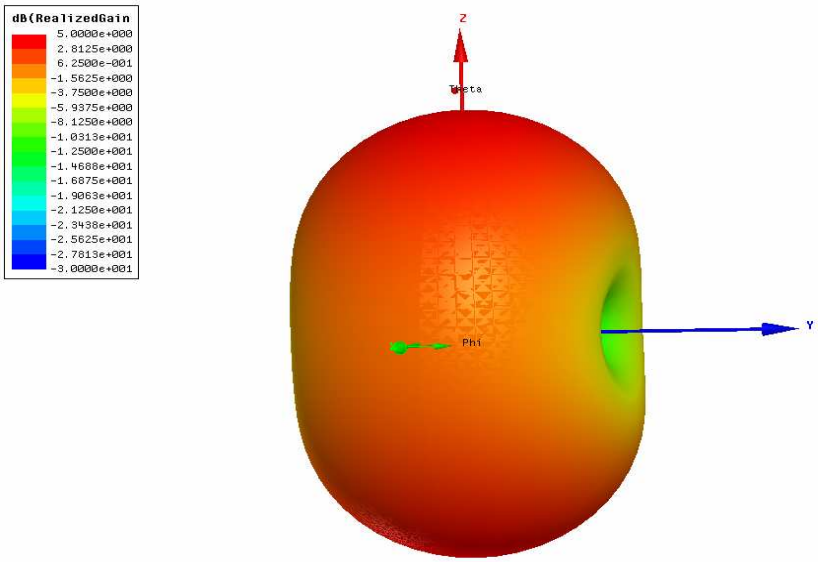

(b)

Figure 4.6: (a) Elevation plane (yoz & xoz) radiation patterns (b) 3D polar plot

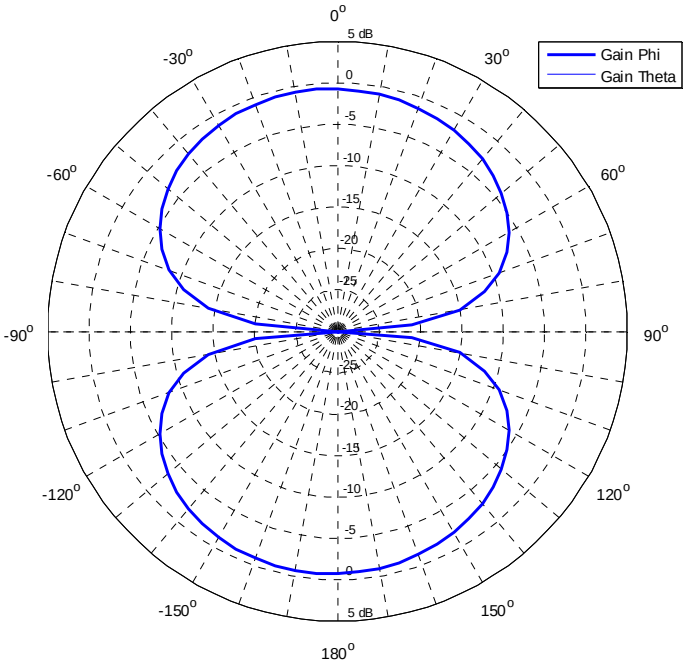

Figure 4.7: Azimuthal plane (xoy) radiation pattern.

4.1.1 Basic performance analysis:

The impedance and return loss curves depicted in Figure 4.4 and Figure 4.5 show that slot loop's required matching at 2.4GHz is mid way between parallel and series resonances. As DRA positioning inside the slot loop is expected to influence the slot's matching so will be finalized. The elevation plane (yoz & xoz) radiation patterns are presented in Figure 4.6(a) and (b). Both the E-plane (yoz) and H-plane (xoz) fields exhibit pure symmetry in their broadside shapes however, xoz plane pattern is observed to be narrower as compared to the yoz plane. The -3dB Half Power Beam Width (HPBW) for yoz plane is found to be 80° while for xoz plane it is increased to 120°. The cross-polarizations in the broadside direction are noted to be -30dB or better. The antenna gain is observed to be 3.3dBi with radiation efficiency of 100%. A similar shaped pattern is also observed in the backward direction and that could be attributed to the absence of any back patch. Along with the observation of elevation plane radiation patterns, the behaviour of azimuthal plane radiation pattern is also considered. Figure 4.7 presents the radiation pattern in azimuthal plane that reveals larger value of Gain phi as compare to the Gain theta.

4.1.2 DRA loading effect:

As slot loop antenna is supposed to include within its circumference area, a Dielectric Resonator Antenna (DRA) to yield end-fire type radiation pattern [6] so it is pertinent here to analyse this effect. To accomplish it a cylindrical shaped DRA composed of dielectric constant (εr=30) bearing radius of 15mm and height of 12mm and thus resonating at the same 2.4GHz frequency is loaded at the centre of the slot loop. Due to this loading effect the slot

loop antenna is expected to undergo certain changes which are presented in Figure 4.9 through Figure 4.12.

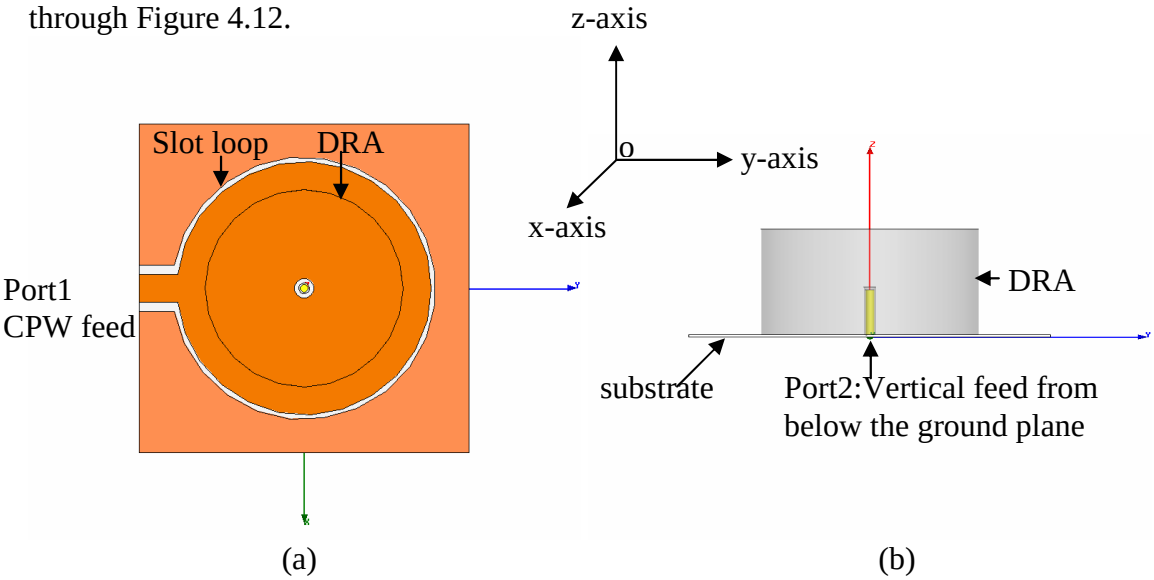

Figure 4.8: slot loop antenna encircling DRA (a) top view (b) side view

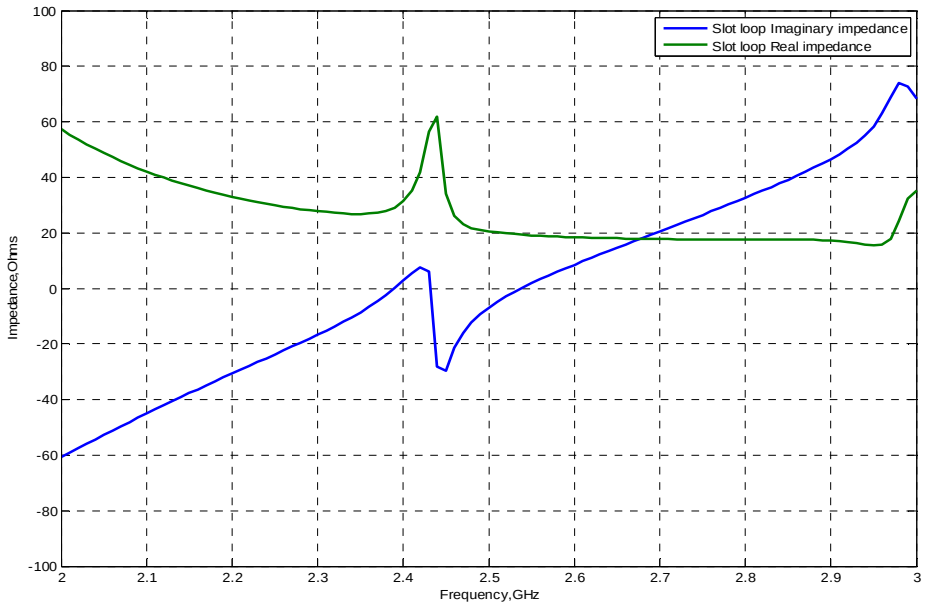

Figure 4.9: slot loop impedance curve showing a parallel resonance around 2.42GHz.

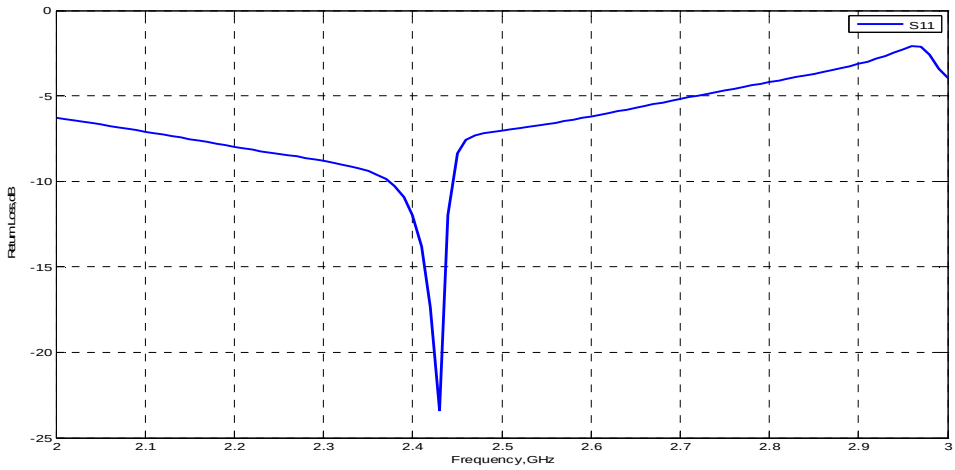

Figure 4.10: slot loop return loss with slight downward shift in resonance frequency.

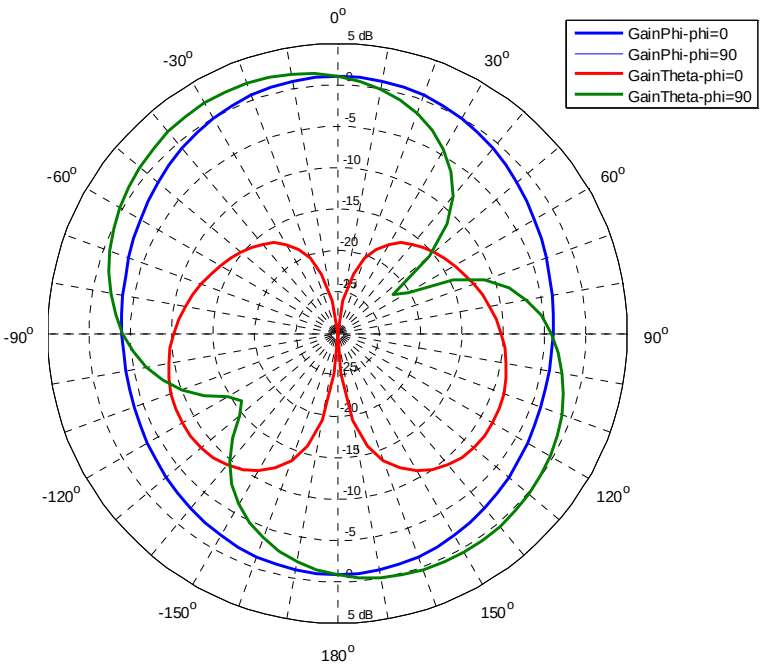

(a)

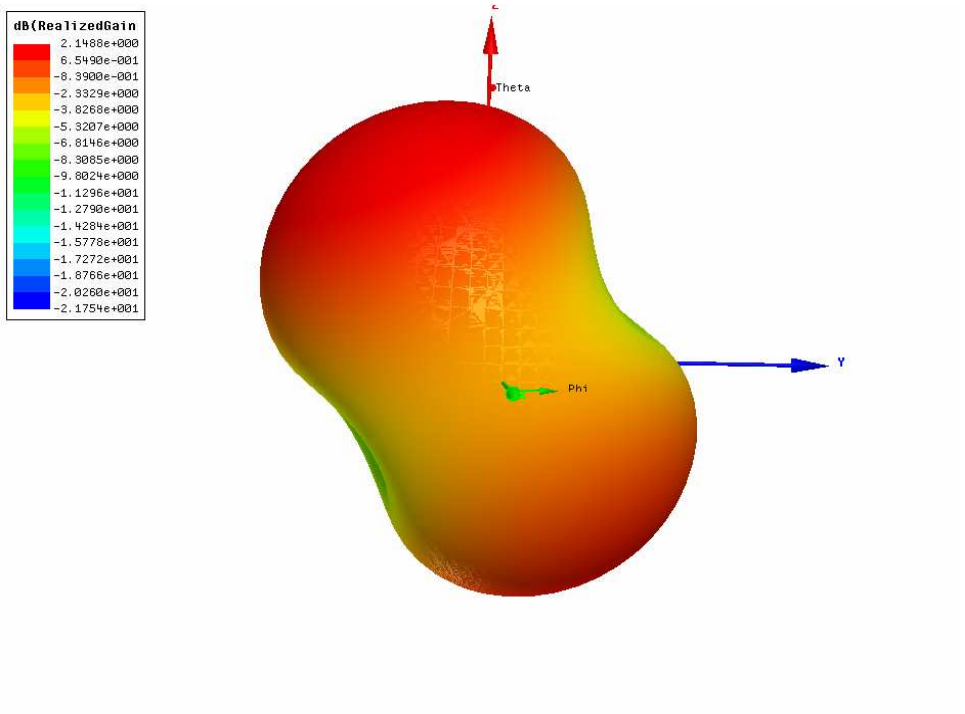

(b)

Figure 4.11: (a) Radiation patterns; tilt in yoz plane but symmetry in (xoz) plane (b) 3D polar plot

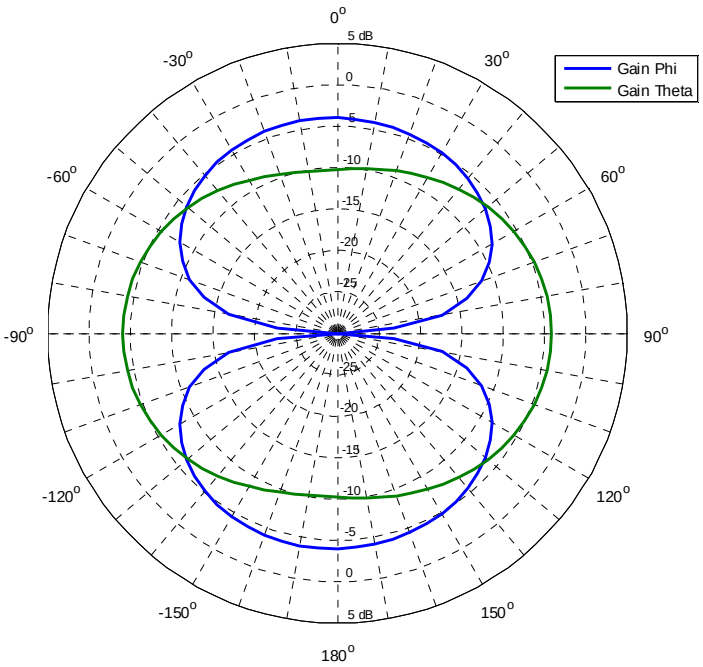

Figure 4.12: Azimuthal plane radiation patterns representing nearly equal Gain phi and Gain theta.

DRA loaded slot loop's impedance and return loss curves are given in Figures 4.9 and 4.10 respectively and that speak of slight change in its resonance frequency from 2.1GHz to 2.42GHz with -10dB RL bandwidth of just 1.2% however, -8dB RL bandwidth seems to be widened. From the study of the impedance curves, it appears that the DRA loading results in its resonance too that appears to be very close to the slot's resonance and resultantly introduces sharp parallel resonance around 2.42 GHz.
The (yoz) and (xoz) plane radiation patterns are depicted in Figure 4.11(a) and (b) and it can be observed that yoz plane pattern is tilted towards 30 angle theta with reference to the broadside direction while xoz is found to be un-effected and still shows pure symmetry in its shape. These pattern shapes introduce a gain of 1dBi towards the broadside direction. Again yoz plane pattern is observed to be narrower as compared to the xoz plane and -3dB Half Power Beam Width (HPBW) are seen to be nearly same as in slot loop radiating with out the DRA. The radiation pattern in both planes tend to exhibit symmetry when shifted to lower or upper sides of the band that is at 2.35GHz and at 2.45GHz however gain is found to be reduced to 1.8dBi and .8dBi respectively. The cross-polarizations in the broadside direction are still noted to be -30dB or better. The radiation efficiency of the antenna drops from100% to 95%. Nearly same radiation pattern behaviour is observed in the backward direction. The azimuthal plane radiation patterns are given in Figure 4.12 which shows that due to increase in its level, the Gain theta is now comparable to that of Gain phi.
It can be concluded from the preceding analysis that slot loop antenna performs well in the presence of DRA however the design parameters needs to be re-adjusted.

4.2 CPW fed slot loop final design:

As it has been observed that the DRA loading introduces a bit change in the slot loop behaviour, so there is a need to slightly re-adjust its design values so that optimised result can be achieved. A rigorous simulation process used the design values enlisted in Table4.4 to observe improvement in -10dB impedance bandwidth and radiation pattern shapes. The important point here is to note the reduction of slot width to just 0.7mm and obviously that is needed not only to maintain compactness to the antenna structure but also to reduce coupling to the DRA to suppress its influence in the slot loop resonance.

Table4.4: Compact structure slot loop design parameters with corresponding values.

Structure Elements	Specific Parameters	Numerical value
CPW Line	S-W-S	1.4mm-7mm-1.4mm
Slot Loop	external radius	20mm
Slot Loop	Internal radius	19.3mm
Slot Loop	width	0.7mm
Slot Loop	Circumference Length	122mm
Guided Wavelength	$1.2\lambda_g$	-

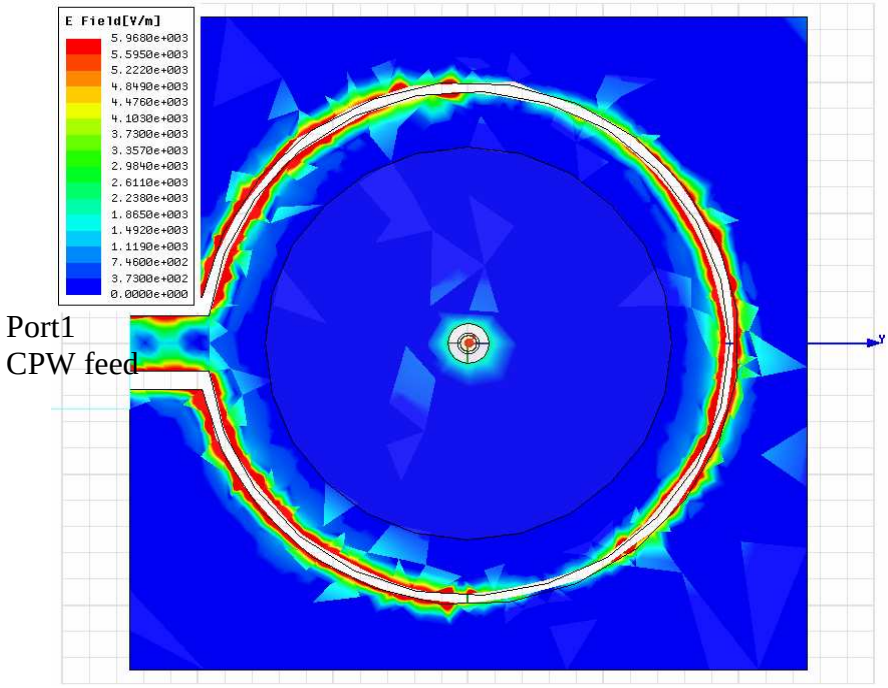

Figure 4.13: Slot loop representing E-field configuration in its structure.

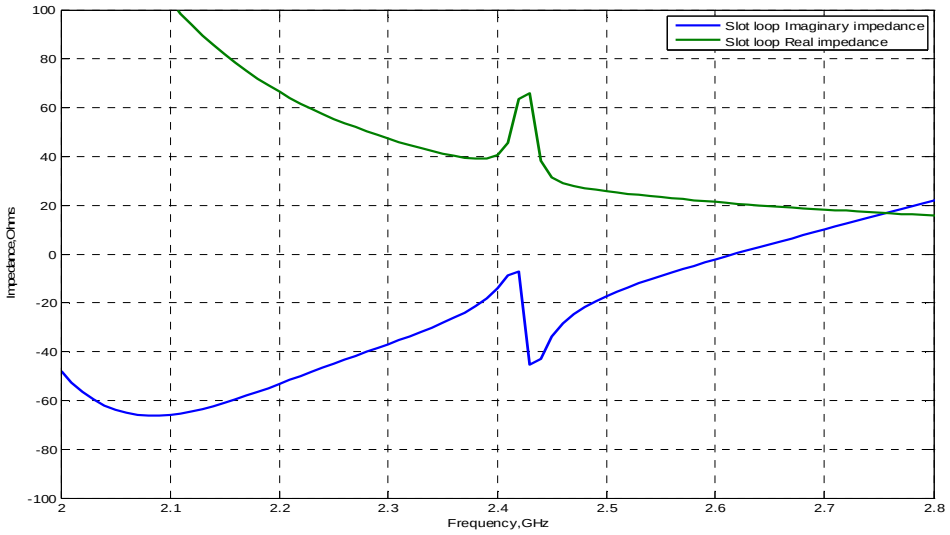

Figure 4.14: Slot loop impedance curve showing resonance around 2.42GHz

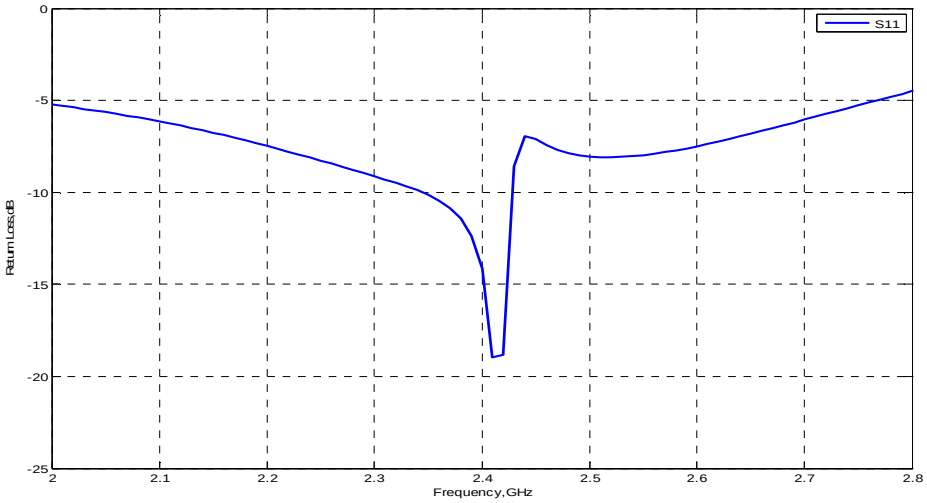

Figure 4.15: Slot loop representing return loss with impedance bandwidth of 2.4%.

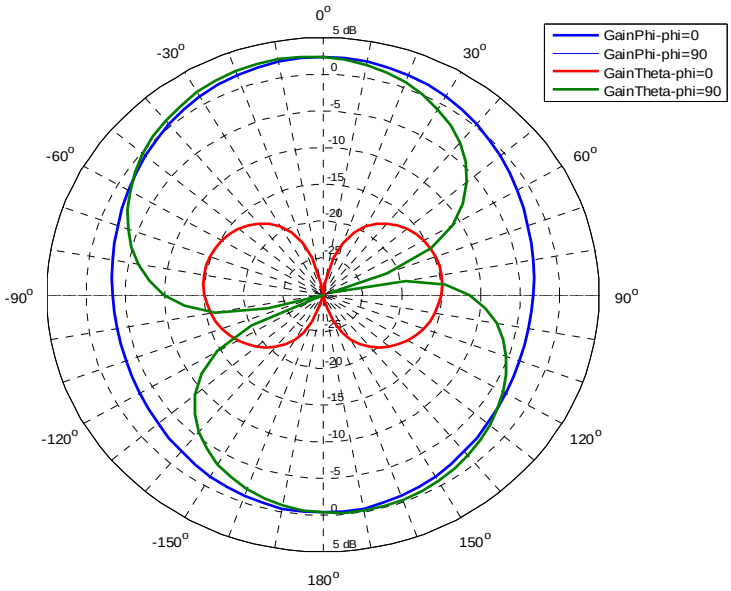

(a)

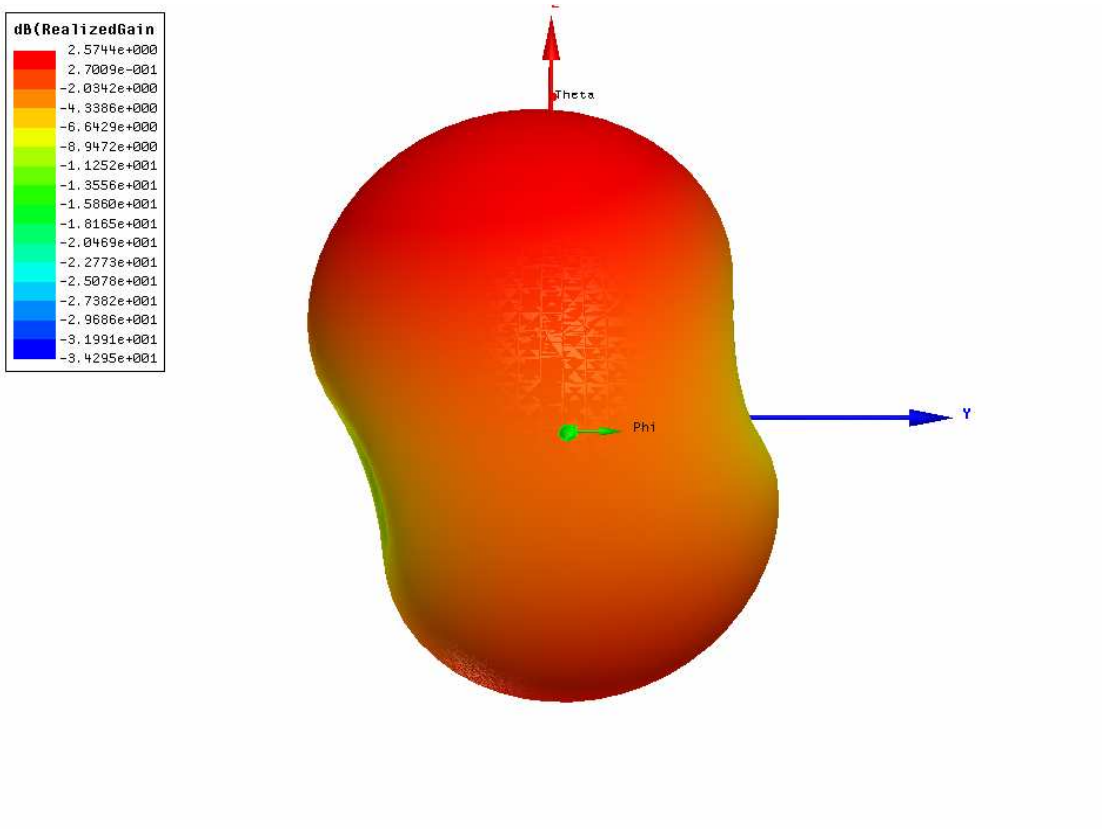

(b)

Figure 4.16: (a) Slot loop radiation; tilt in yoz plane pattern has reduced (b) 3D polar plot

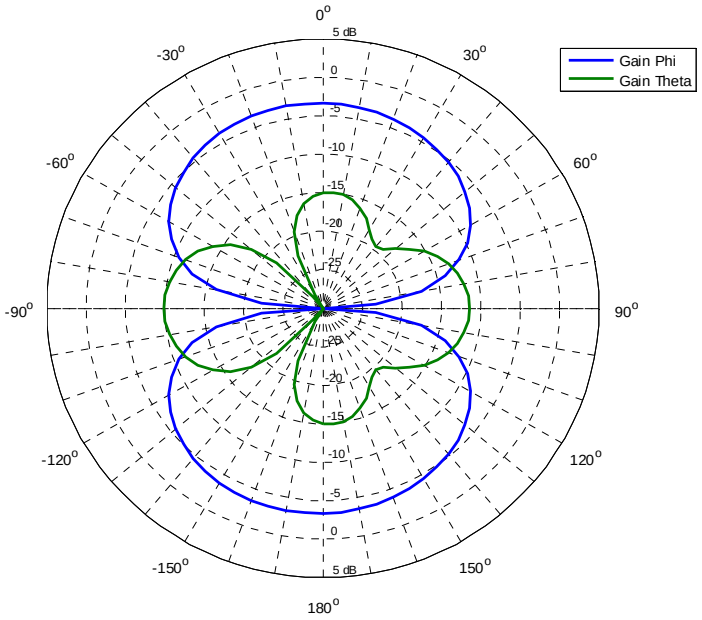

Figure 4.17: Radiation pattern presenting larger value of Gain phi as compare to Gain theta.

4.2.1 Final design analysis:

The impedance and return loss curves are given in Figure 4.14 and Figure 4.15 respectively which show an improvement in the results. The -10dB impedance bandwidth is around 2.4% while antenna resonance takes place around 2.42 GHz. Again at around -7dB level, a wider impedance bandwidth is possible.
The yoz plane and xoz plane radiation patterns are depicted in Figure 4.16(a) and (b) and as is evident from the results that the tilt in yoz plane radiation pattern has reduced while xoz plane pattern is found to be symmetric. As observed in section (4.1.2) the yoz plane pattern is still narrow as compared to the xoz plane while -3dB Half Power Beam Width (HPBW) is seen to be un-changed. The radiation patterns are found to be stable with in the frequency band from 2.35GHz to 2.42GHz. The gain is estimated to be 2.3dBi with radiation efficiency of 98%.The cross-polarizations in the broadside direction are as usual -30dB or better. The azimuthal plane radiation patterns that are presented in Figure 4.17 speak of higher Gain phi value than that of Gain theta.

One significant issue is the obligation of the utilisation of small ground planes to keep the antenna size as small as possible. Corresponding to different ground plane sizes, some important results are enlisted in Table 4.5. It is observed that slightly larger ground planes (60mmx60m) could provide larger BW (8% here).

Table4.5: The effect of ground plane size upon Bandwidth, Gain, F/B, -3dB (HPBW) beam width and antenna efficiency.

Ground Plane Size (mm)	Impedance Bandwidth	Broadside Gain(dBi)	F/B (dB)	Elevation Plane -3dB(HPBW) yoz/xoz (Plane)	Antenna Efficiency
50×50	2.4%	2.3dBi	2.3/-1.3	75°/100°	95%
60×60	8 %	5.5dBi	5.5/1.9	70°/90°	98%
70×70	9.5%	5.7 dBi	5.7/2.1	70°/85°	97%

4.2.2 On-body performance:

As the proposed antenna is to be employed for the Body Area Network (BAN) applications, body surface tests are crucial to evaluate its real performance. It is estimated that lossy nature of the skin characterized by dielectric constant of (εr=53) and loss tangent of .002 will change the performance parameters of the slot antenna. The simulations tests are performed while placing the antenna at a height of 15mm above the cylindrical shaped phantom representing real human body' trunk with radius of 20cm and height of 40cm. The change in the size of the phantom trunk is observed not to significantly change the results. However, antenna height upon the phantom is found to be sensitive and slot loop's proximity to the body offers wider change in results. But as this antenna is intended to be worn on specially fabricated professional cloths, hence due height is maintained that is at 15mm.

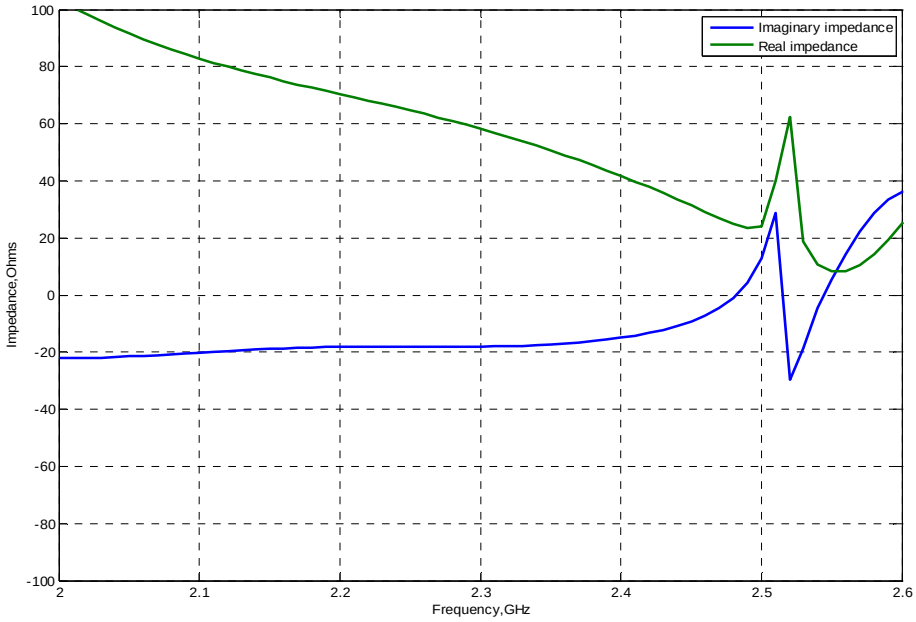

4.18: Impedance curves when slot loop planted on the body surface

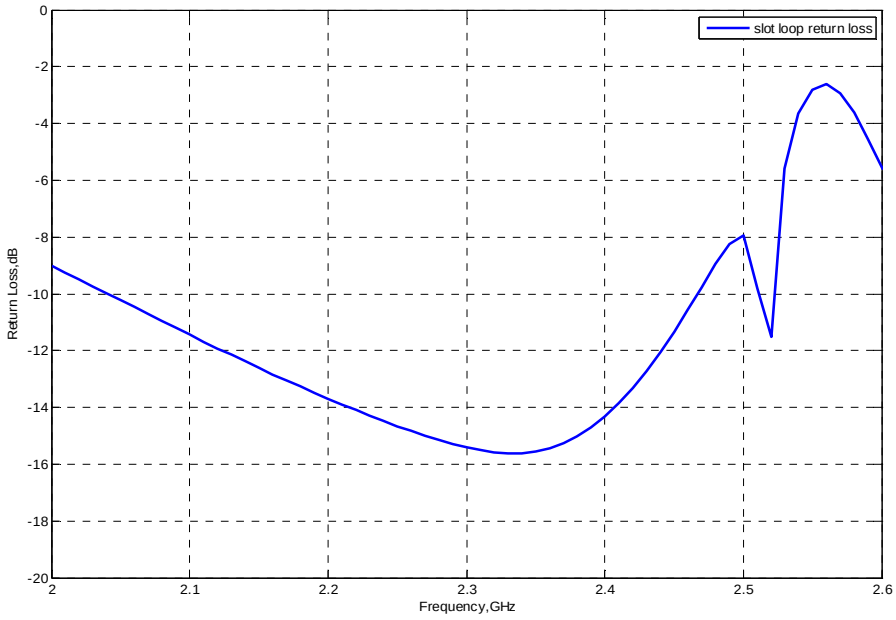

Figure 4.19: Return loss curve with slot loop planted on the body surface

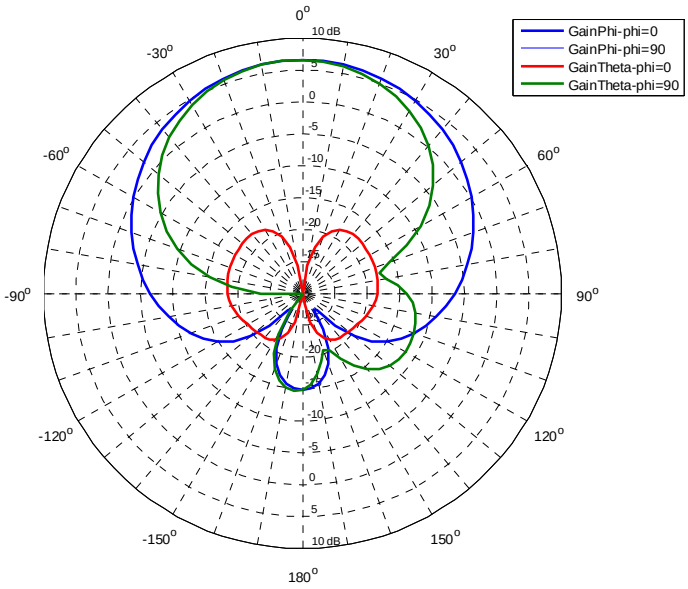

(a)

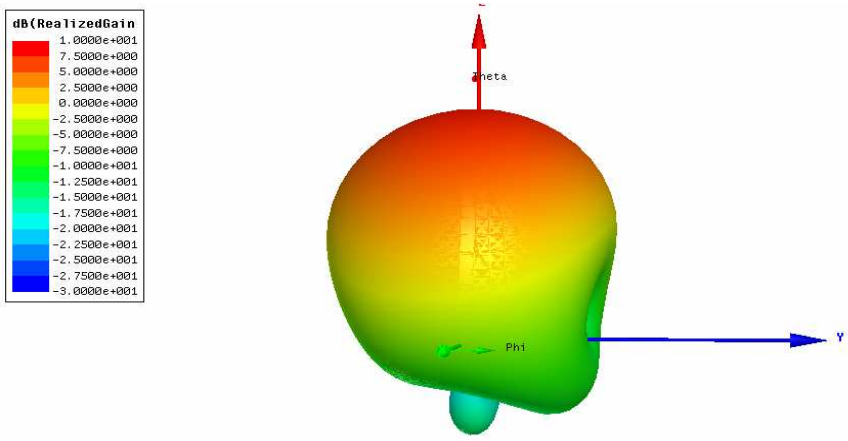

(b)

4.20: Radiation patterns on body surface (a) yoz & xoz planes (b) 3D polar plot

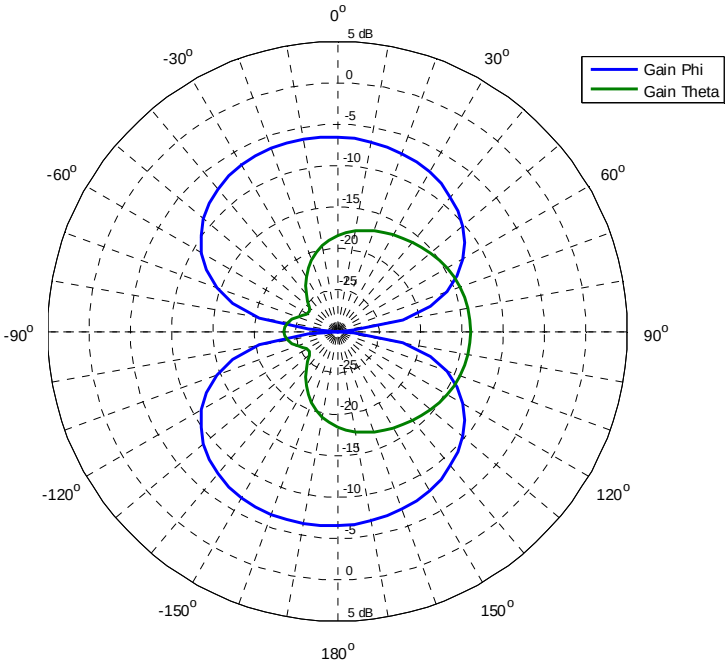

4.21: Azimuthal plane radiation pattern presenting larger value of Gain phi as compare to Gain theta.

The results of on the body tests are depicted in Figure 4.18 through 4.21. The impedance and return loss curves presented in 4.18 and 4.19 respectively show upward shift in resonance frequency around 2.51GHz and widening of the -10dB impedance bandwidth to 18%. The yoz plane and xoz plane radiation patterns are depicted in Figure 4.20(a) and (b) and as expected these are found to be more directional in the broadside direction owing to the presence of lossy material in the backward direction where radiations are prone to high absorption. The yoz plane pattern is still narrow as compared to the xoz plane. The gain is estimated to be 6.5dBi while radiation efficiency has dropped from 98% to 70%.The cross-polarizations in the broadside direction are as usual -30dB or better. The azimuthal plane radiation patterns that are presented in Figure 4.21 speak of higher value of Gain phi as compare to Gain theta, however both have been found reduced as compared to body free case.

4.3 Vertical monopole fed DRA initial design:

The TM01 mode of the DRA is excited to yield end-fire type radiation pattern. The excitation of this mode is accomplished by feeding the DRA with coaxial probe located at its centre. The probe is inserted into the DRA vertically from below the substrate. It is the same slot antenna structure within which the DRA is to be located. The resonance frequency of the cylindrical shaped DRA is calculated while considering the permittivity of the material with which it is made up of and by calculating its radius and height values. The mathematical equations (4.3) and (4.4) can be employed to seek a desired design of the DRA [6].

$$k_0 a = \frac{\sqrt{(3.83)^2 + \left(\frac{\pi a}{2h}\right)^2}}{\sqrt{\varepsilon_r + 2}} \quad \text{.....4.3}$$

$$fr_{TM01}(GHz) = \frac{30(k_0 a)}{2\pi a(cm)} \quad \text{.....4.4}$$

Where:
a=radius of the DRA
h=height of the DRA
Permittivity (εr) =30
The resonance frequency calculations are given in Table4.6

Table4.6: monopole fed DRA design values

Structure element	Radius / Height	Location
DRA	15mm / 12mm	Centre of slot loop
Embedded monopole	0.5mm /7mm	Centre of DRA

Generally the feed embedded inside the DRA is not considered at the time of resonance frequency calculation. The resonance frequency is determined precisely by the simulation process that also takes into account the sensitive issues if any associate to the feed structure, the real value of dielectric constant along with loss tangents etc. By rigorously repeated processes, the results are refined and optimised while taking into consideration the possible constraints of the fabrication. One such constraint is the effect of adhesive material with which the DRA body is glued to the ground plane and that has been detailed in Chapter 3. So it is important to keep the DRA height a bit higher so as to compensate for obtaining the exactly desired resonance frequency. However if no large change in results is observed, the additional size can easily be removed at the time of measurements to always remain confined to the desired results.

As DRA resonance mostly depends upon its dimensions and value of the dielectric constant used, equally important is the probe height inside it. To excite TM01 mode a suitable probe in the form of monopole is embedded at the centre of the DRA. The height and thickness of this probe is estimated by the simulation process, the results for which are given in 4.22.

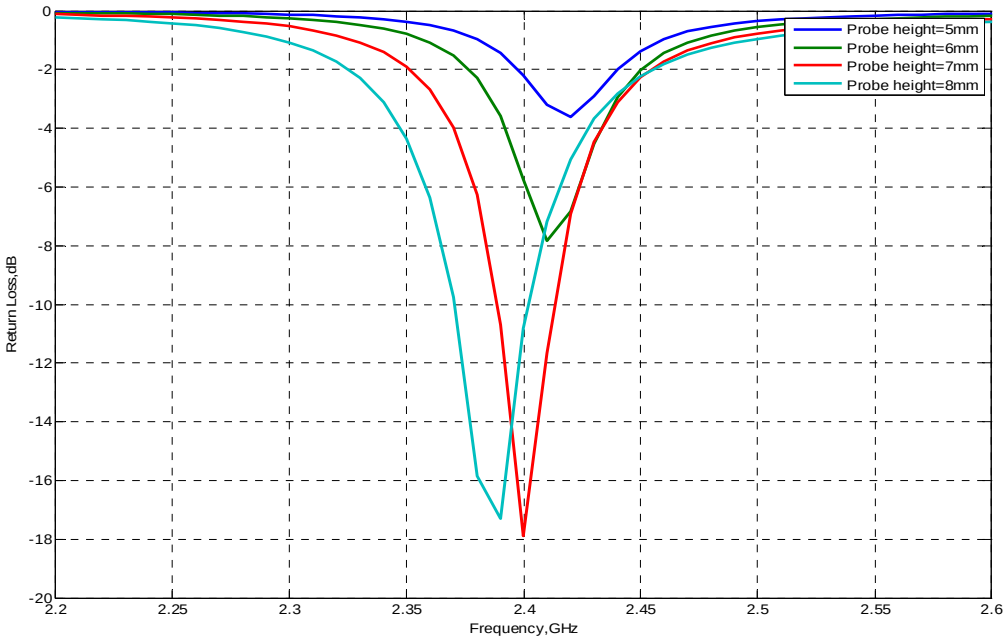

4.22: Parametric return loss curves representing different probe heights.

As can be observed from the family of parametric results presented in the Fig.4.22 that -10dB return loss level is reached when monopole's height inside the DRA is found to be 7mm or 8mm. Both of these heights yield nearly the same result so this introduces an enhancement in the fabrication tolerance. It justifies that while inserted into DRA, the monopole's height is not so sensitive and can assume slightly different value thus nullifying errors attributed to it. On the other hand the thickness of the probe is clearly insensitive to couple electromagnetic energy to the DRA so any suitable or readily available piece of copper wire can be utilized for this purpose. However, for further design analysis 7mm height is considered and its result is presented in 4.23.

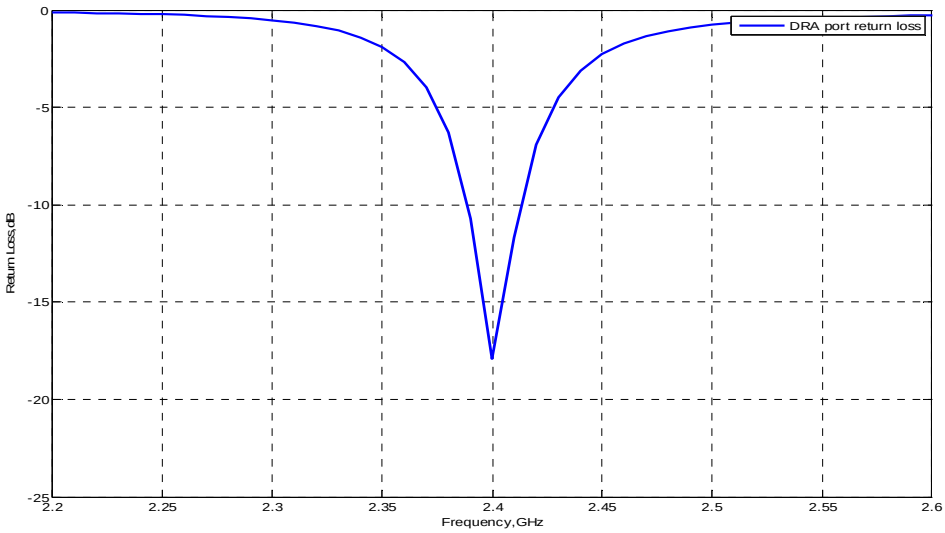

Figure 4.23: DRA return loss depicting resonance at 2.4GHz frequency.

It is crucial to evaluate the role of the adhesive material that is generally expected to shift the resonance frequency upward. It has been evaluated in that the dielectric constant of the bonding material is around (εr=2) and actual layer of 0.2mm thickness gets employed. One such detailed analysis is depicted in Appendix A. Considering these effects, a parametric analysis is made for which the results are presented in Figure 4.24.

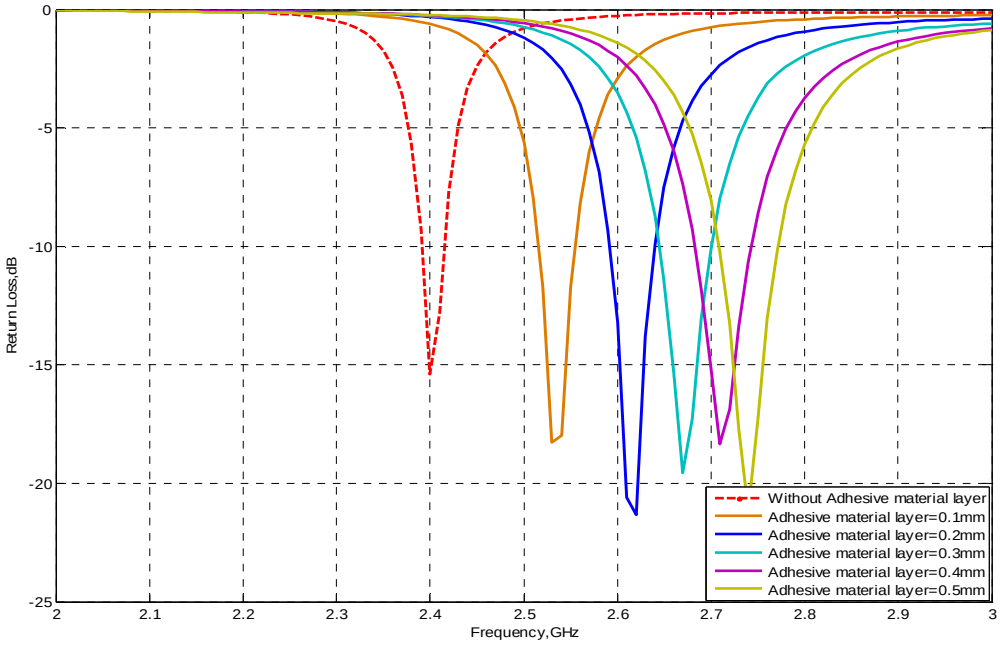

(a)

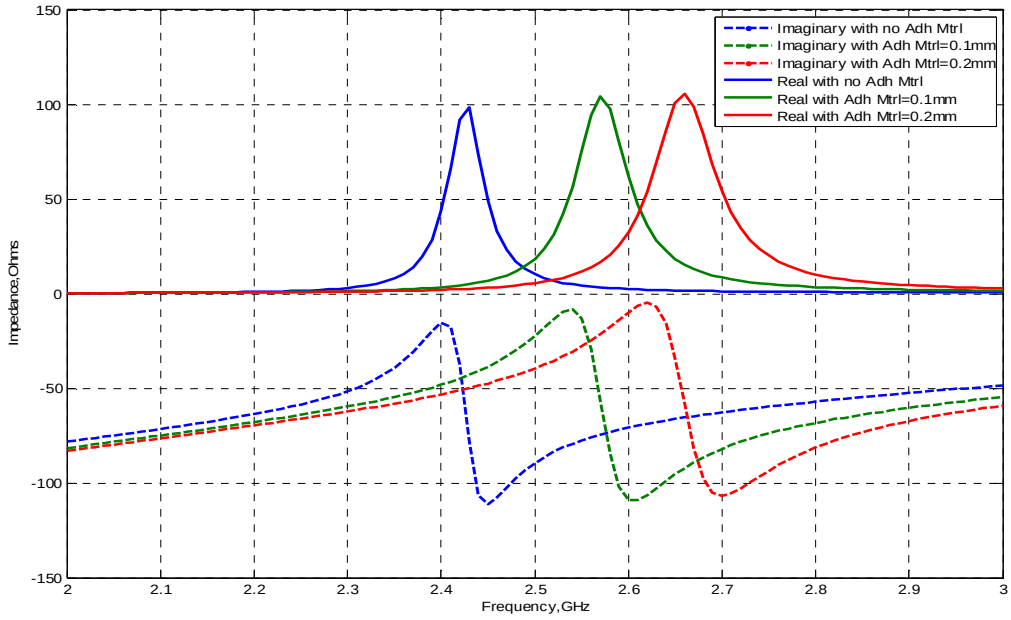

(b)

Figure 4.24: (a) & (b) Parametric set of results representing upward shift in resonance frequency corresponding to different adhesive material layers.

It can be observed from the results presented in 4.24 that corresponding to different adhesive material layers there is upward shift in the resonance frequency. The results available from appendix A predict that 0.2mm layer is suitable to be used in bonding the DRA body to the ground plane due to which it is expected to shift from 2.4GHz to 2.6GHz. It means the DRA design to resonant at 2.4 GHz is expected to resonate at 2.6GHz after the fabrication is realized. This suggests a design around 2.2GHz so that after including bonding material's effect at the time of fabrication, antenna be made to resonate around 2.4GHz.

4.3.1 Evaluation for adhesive material effect:

To make the DRA resonate at around 2.2 GHz the design parameters are given in Table4.7 while its simulation result is presented in Figure 4.25.

Table4.7: Monopole fed DRA design parameters to resonate at around 2.2GHz

Structure element	Radius / Height	Location
DRA	15mm / 18mm	Centre of slot loop
Embedded monopole	0.5mm /8mm	Centre of DRA

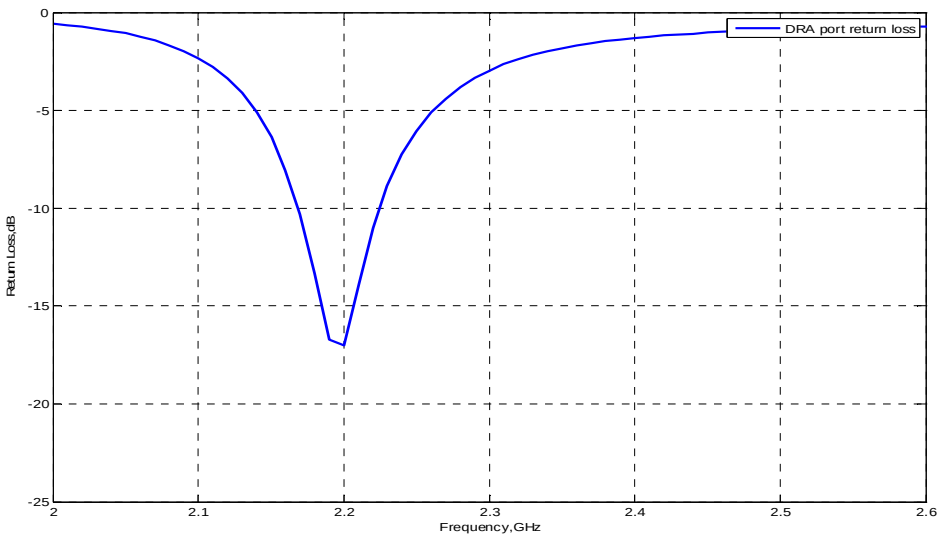

Figure 4.25: DRA return loss curve representing resonance at 2.2GHz

An expected result can be observed from Figure 4.25 where the design is resonating at 2.2GHz without considering the bonding material's effect.

As has already been analysed that upward frequency shift is imminent so assuming the real situation after the fabrication is made, a parametric analysis is performed for which the results are depicted in Figure4.26.

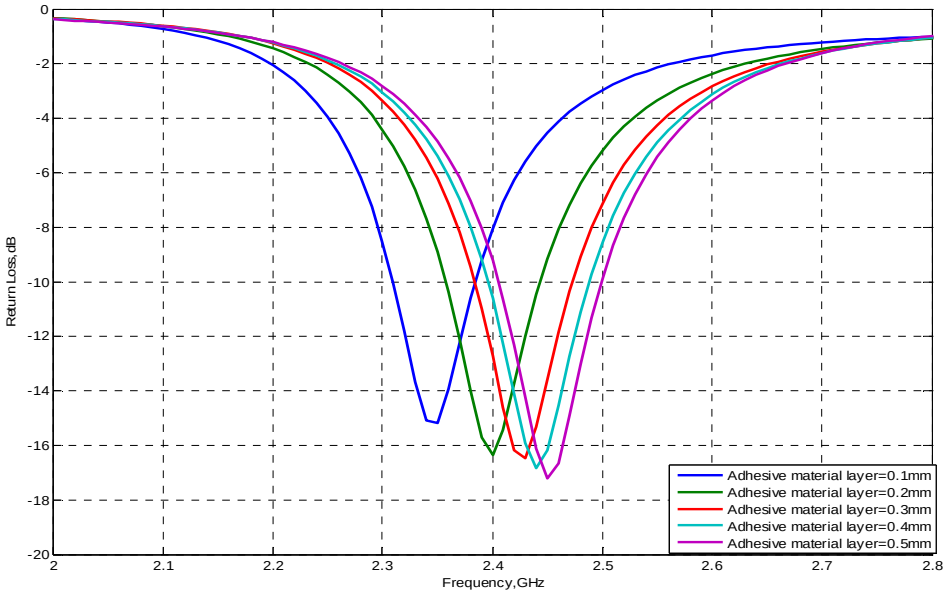

Figure 4.26: A family of curves representing return loss values corresponding to different adhesive material layers.

The results are expected and corresponding to different layers thickness an upward shift in resonance frequency is observed. The results are summarized in Table4.8

Table4.8: Upward shift in resonance frequency corresponding to different adhesive material layers.

No.	Adhesive material thickness	Upward shift in resonance frequency
1	0.1mm	2.35 GHz
2	0.2mm	2.40 GHz
3	0.3mm	2.43 GHz
4	0.4mm	2.44 GHz
5	0.5mm	2.45 GHz

From the results presented in Table 4.8 one can note the precise assumption of 0.2mm layer thickness that yields the desired results.

4.4 Vertical monopole fed DRA final design:

The aforementioned analysis suggests an error free design for which the values are given in Table4.9. This includes the effect of adhesive material so that after fabrication process one is sure of resonance to take place at 2.4GHz.

Table 4.9: DRA final design parameters.

Structure elements	Radius / Height	Location
DRA	15mm / 18mm	Centre of slot loop
Embedded monopole	0.5mm /8mm	Centre of DRA
Adhesive material layer	15mm /0.2mm	Between ground plane & DRA

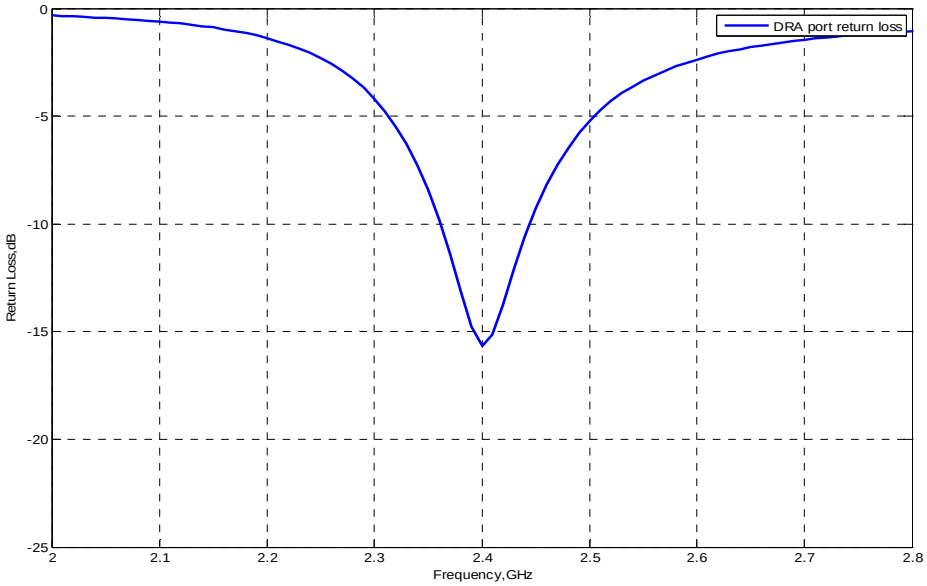

Figure 4.27: DRA return loss curve representing -10dB impedance bandwidth of 3.3%

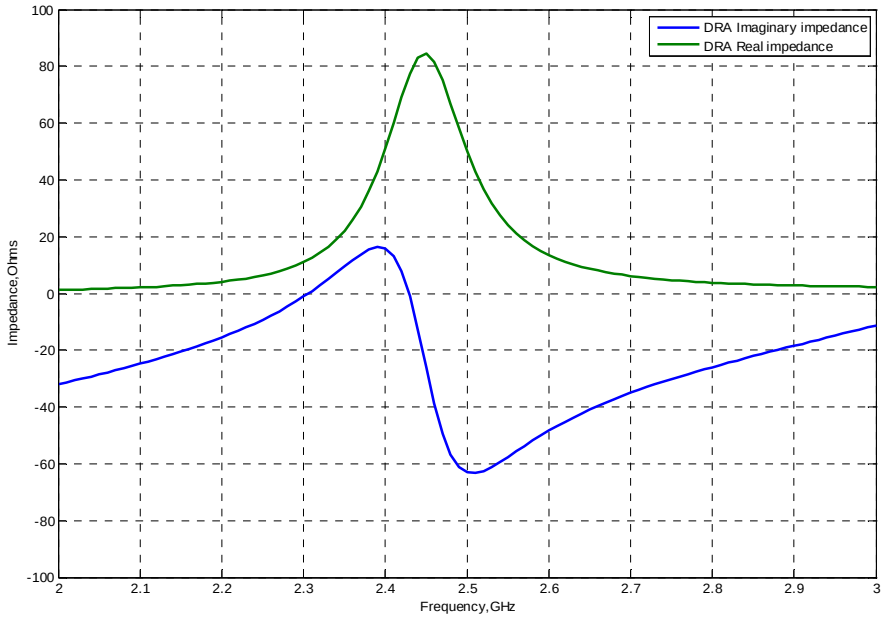

Figure 4.28: DRA impedance curves representing parallel resonance around 2.42GHz

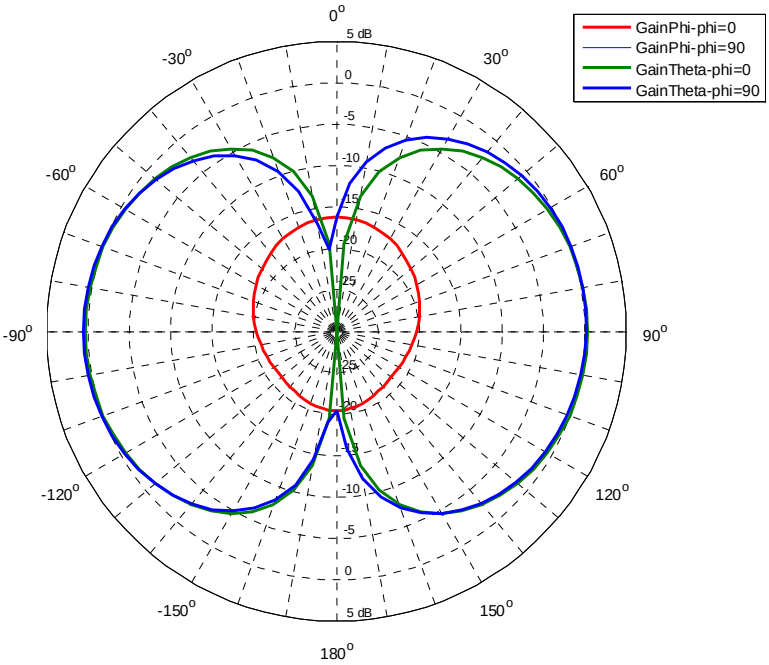

(a)

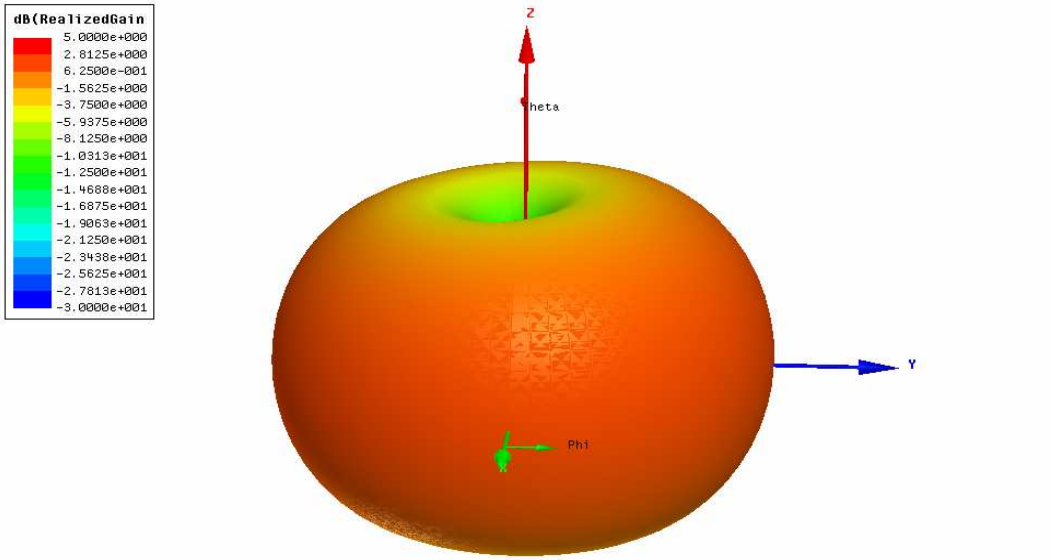

(b)

Figure 4.29: DRA end-fire type radiation patterns (a) (yoz & xoz) elevation plane patterns **5.** ┌ 3D polar plot.

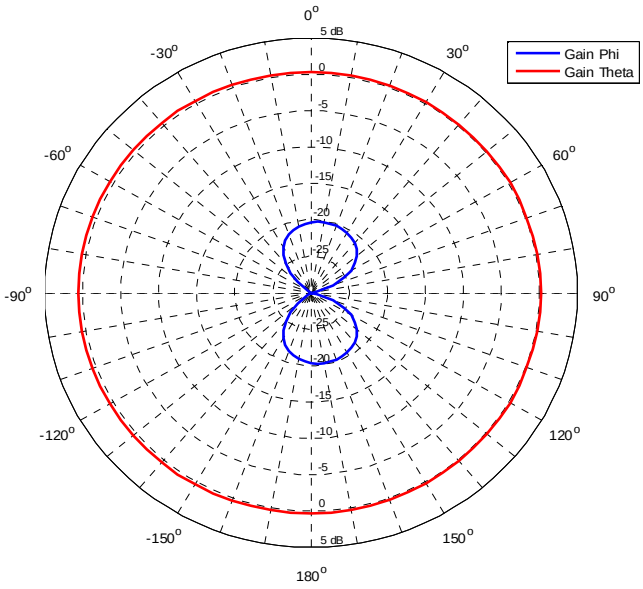

Figure 4.30: DRA azimuthal plane radiation pattern representing large value of Gain theta.

4.4.1 Final design analysis:

The DRA design results are depicted in Figure 4.27 through 4.30. The return loss curve presented in 4.27 represents an impedance bandwidth of 3.3% and that has been observed to be widened due to the effect of low permittivity adhesive material. The impedance curves presented in Figure 4.28 speaks of parallel resonance at 2.42GHz. The end-fire type radiation pattern in the (yoz & xoz) elevation plane is depicted in Figure 4.29(a) and (b).Both plane patterns are found to be purely symmetric with cross-polarizations of -12dB or better. The azimuthal plane radiation pattern is given in Figure 4.30 where it can be observed that Gain phi is -20dB smaller than that of Gain theta. The omni-directional gain of the DRA is observed around 0dBi while its radiation efficiency is found to be 96%.
To observe the effect of enlarging the ground plane, different ground plane sizes are subject to analysis as was done in the case of with slot loop structure. The results are summarized in Table4.10 that speaks of slight increase in impedance bandwidth while no considerable change in radiation patterns or antenna efficiency is observed.

Table4.10: Effects of ground plane size upon bandwidth, radiation pattern and efficiency.

Ground plane size(mm×mm)	Impedance bandwidth	Elevation plane radiation patterns	Azimuthal plane Gain phi /Gain theta	Antenna efficiency
50×50	3.3%	End-fire	-20dB/0dB	96%
60×60	4.2%	End-fire	-17dB/1dB	98%
70×70	4.6%	End-fire	-18dB/1dB	96%

4.4.2 Planar feed tests:

The antenna under investigation needs to have a planar feed structure to be tested on the body surface. Therefore, the DRA coaxial feeding is replaced by a microstrip line etched on the bottom side of the substrate to feed to the monopole embedded inside the DRA. As the microtrip line goes below the slot loop and might couple to it, a minimum current must be maintained at the interception point. To observe this minimum, the feed line is made to pass below that interception where E-field distribution in the slot seem negligible. The design structure is presented in Figure 4.31 while its results are depicted in Figure 4.32 through 4.34

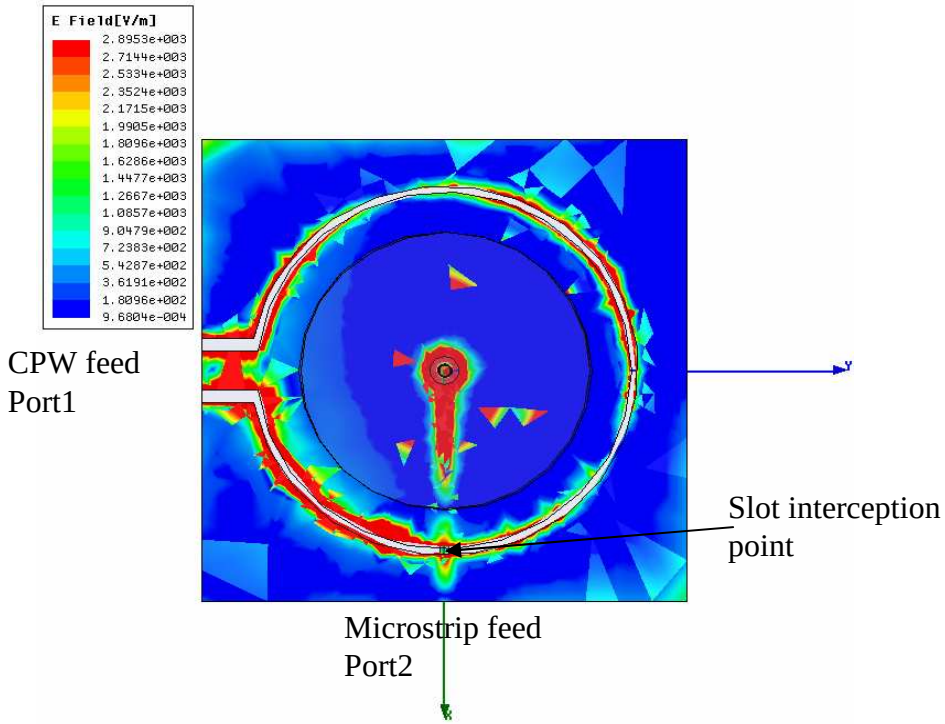

Figure 4.31: DRA fed by planar microstrip line passing below the slot loop where E-field distribution seems negligible

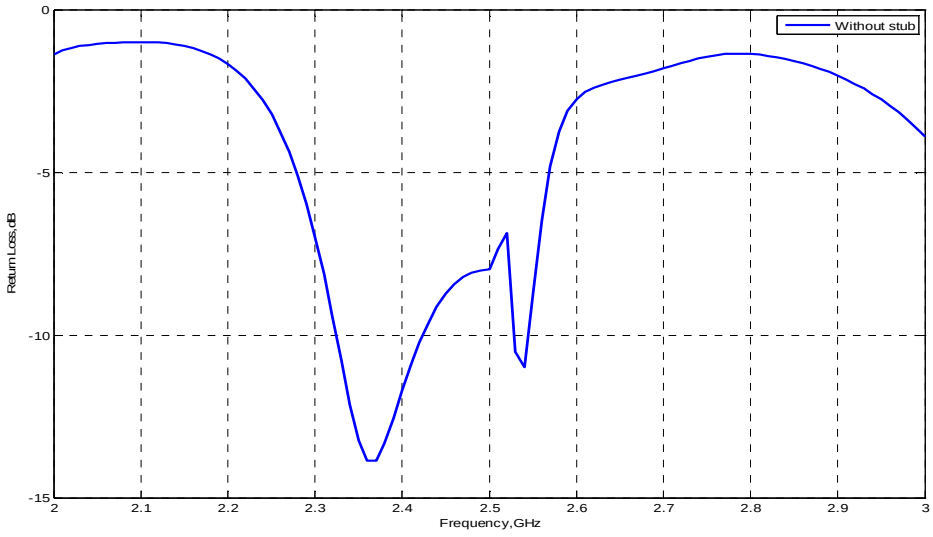

Figure 4.32: DRA return loss curve got affected by the presence of slot loop interruption

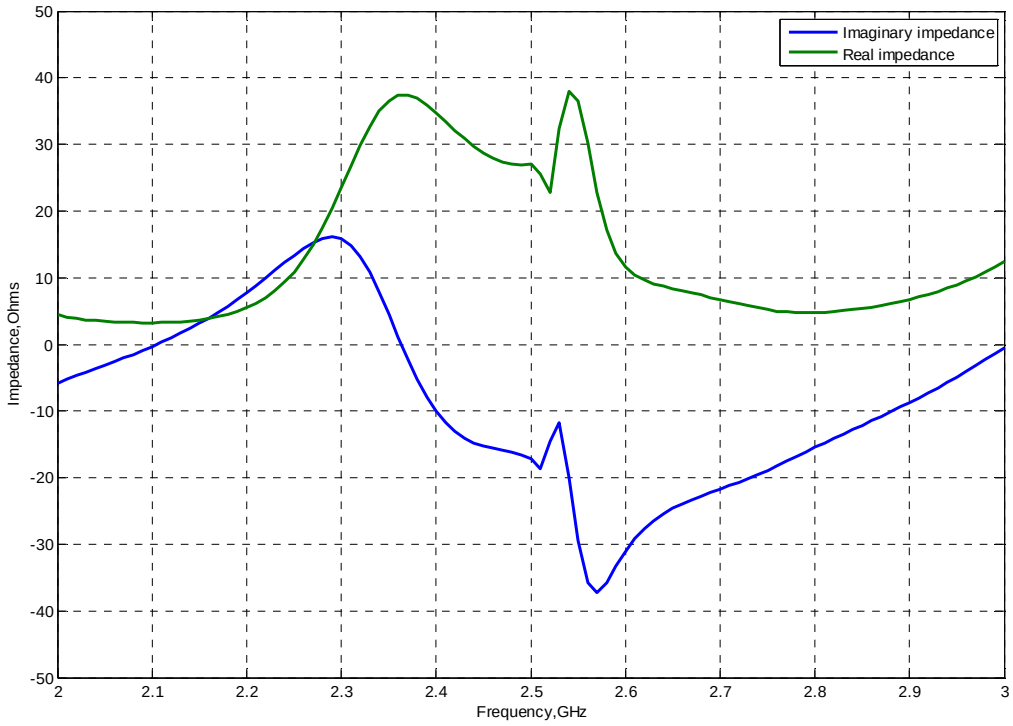

Figure 4.33: DRA impedance curves representing disturbed parallel resonance

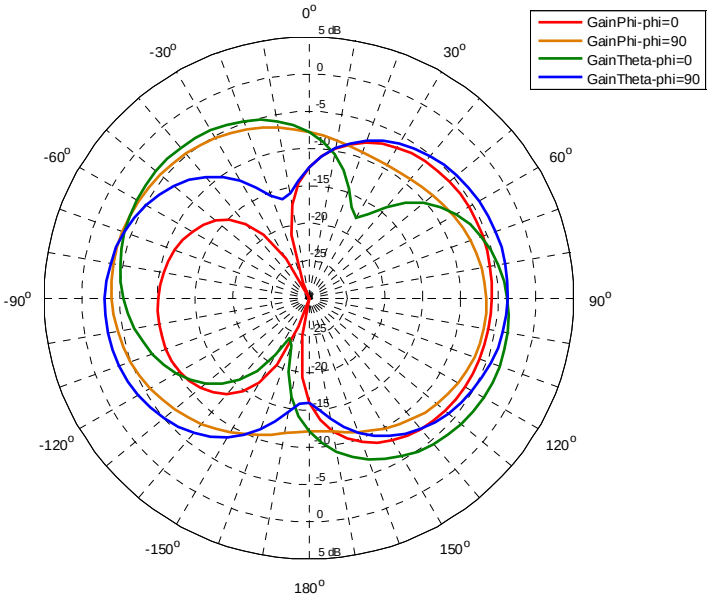

(a)

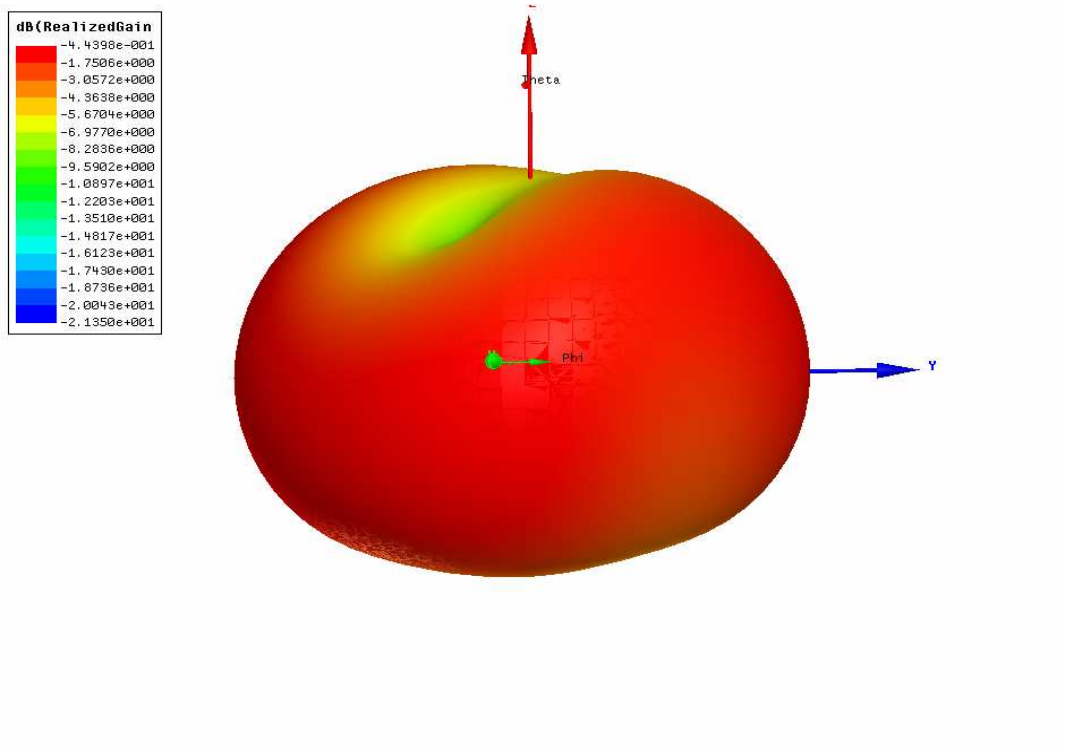

(b)

Figure 4.34: Radiation patterns (a) yoz & xoz plane (b) 3D polar plot

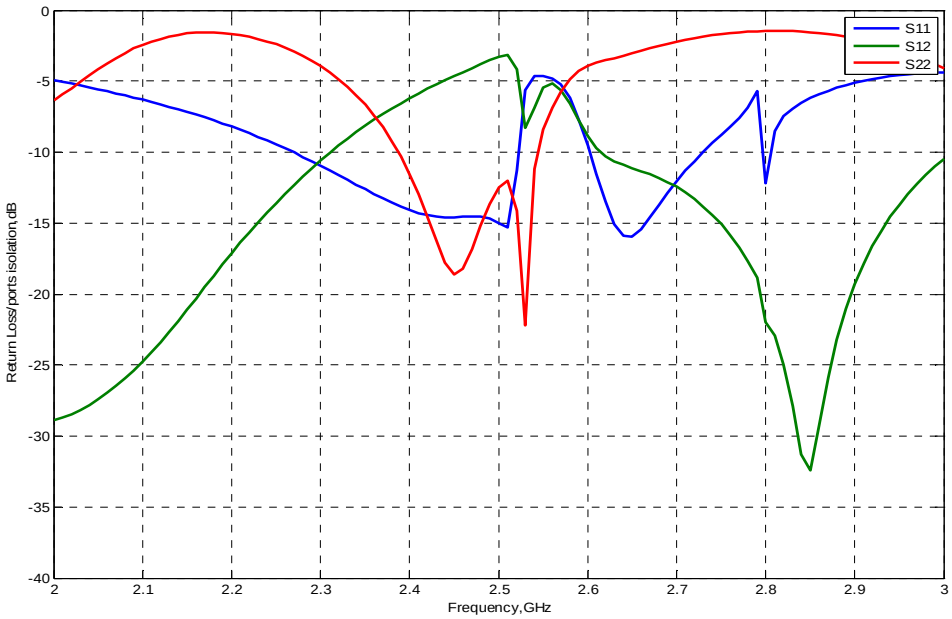

Figure4.35: Both ports return loss curves present high level of coupling

The return loss and impedance curves presented in 4.32 and 4.33 illustrate that due to the interception of slot loop the impedance bandwidth and resonance frequency of the DRA is affected. The DRA (S22) expected to resonate at 2.42GHz undergoes a shift to 2.35GHz while another resonance is observed around 2.54GHz. Due to disturbance in DRA resonance, the end-fire type radiation pattern in the elevation plain (yoz & xoz) presented in 4.34 (a) and (b) is observed to be de-shaped. In the radiation pattern no clear null is observed in the

broadside direction while omni-directional gain has dropped to -5dBi.This is attributed to high level of ports coupling as is presented in 4.35. The coupling level as large as of -5dB is obviously expected to badly influence the expected results.

A close observation of the E-field distribution in the slot loop reveals that they might have stronger effect at the observed point. So there is need to seek another point that may offer really negligible fields to observe better coupling between the two ports. One such situation is presented in 4.36 where the DRA feed line is made to pass below the slot where fields are seen totally null.

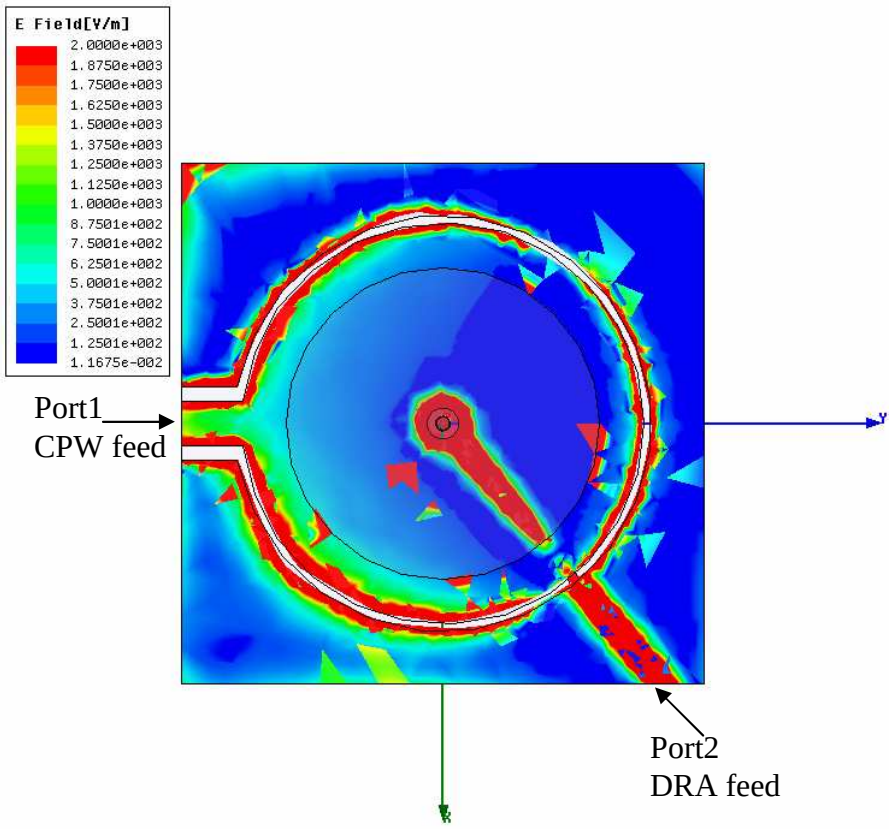

Figure 4.36: DRA fed by planar microstrip line passing below the slot loop where E-field distribution is totally null

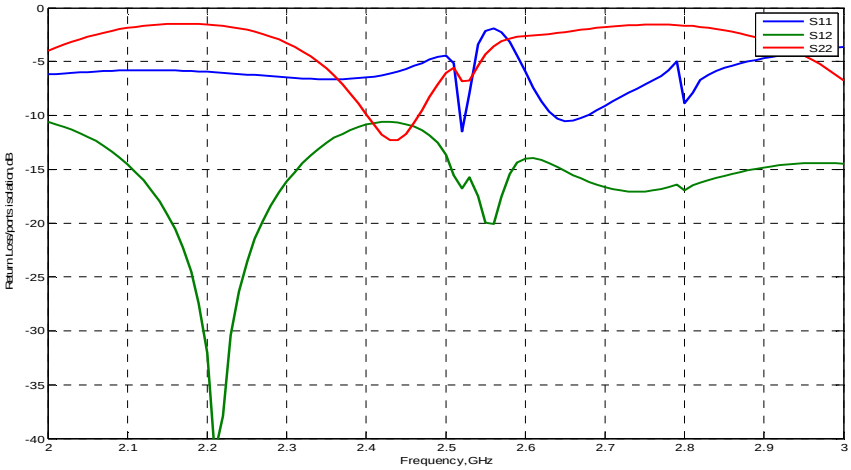

Figure4.37: Both ports return loss curves representing better level of de-coupling

As observed from 4.37 that though ports de-coupling (S12) improved (-10dB), yet slot loop (S11) performance disturbs. It is therefore inferred finally that slot loop and microstrip feed line can not be completely shielded from each other.

- So for this structure, the effort for planar feeding to DRA is curtailed and vertical feed is maintained.

4.4.3 On-body performance:

On the similar pattern of slot loop antenna, the DRA is also subject to on the body tests. The lossy nature of the skin characterized by dielectric constant of (εr=53) and loss tangent of .002 may influence the performance of DRA. The simulations tests are performed while placing the antenna at a height of 15mm above the cylindrical shaped phantom representing real human body' trunk with radius of 20cm and height of 40cm.

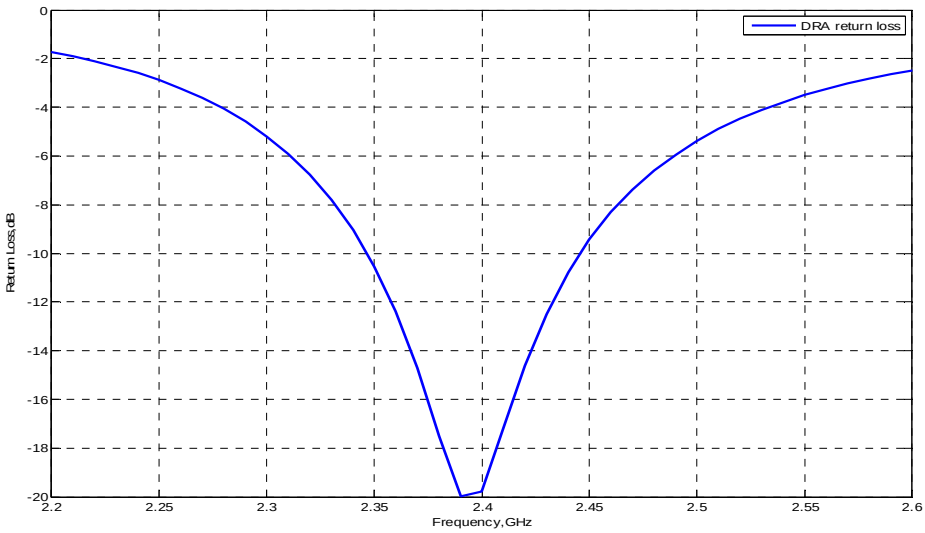

4.38: DRA return loss when placed on the phantom body at a height of 15mm.

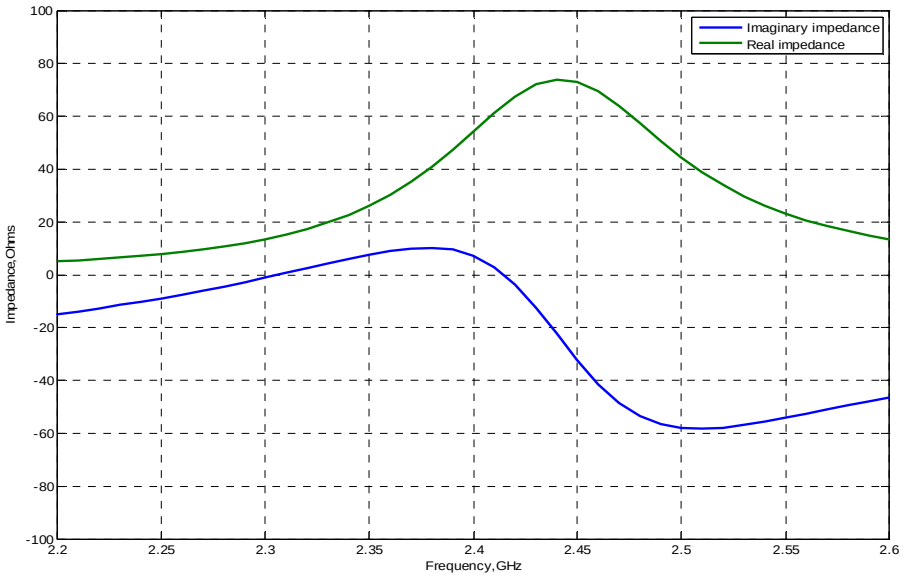

4.39: DRA impedance curve when placed on phantom body showing resonance around 2.42GHz

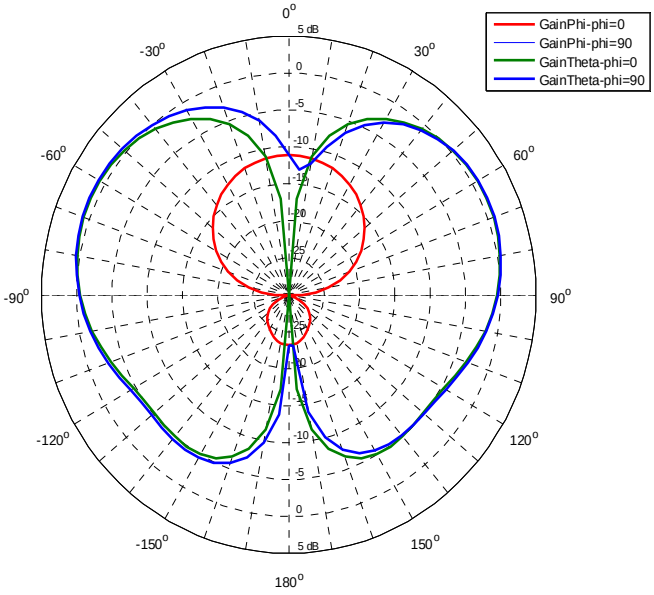

(a)

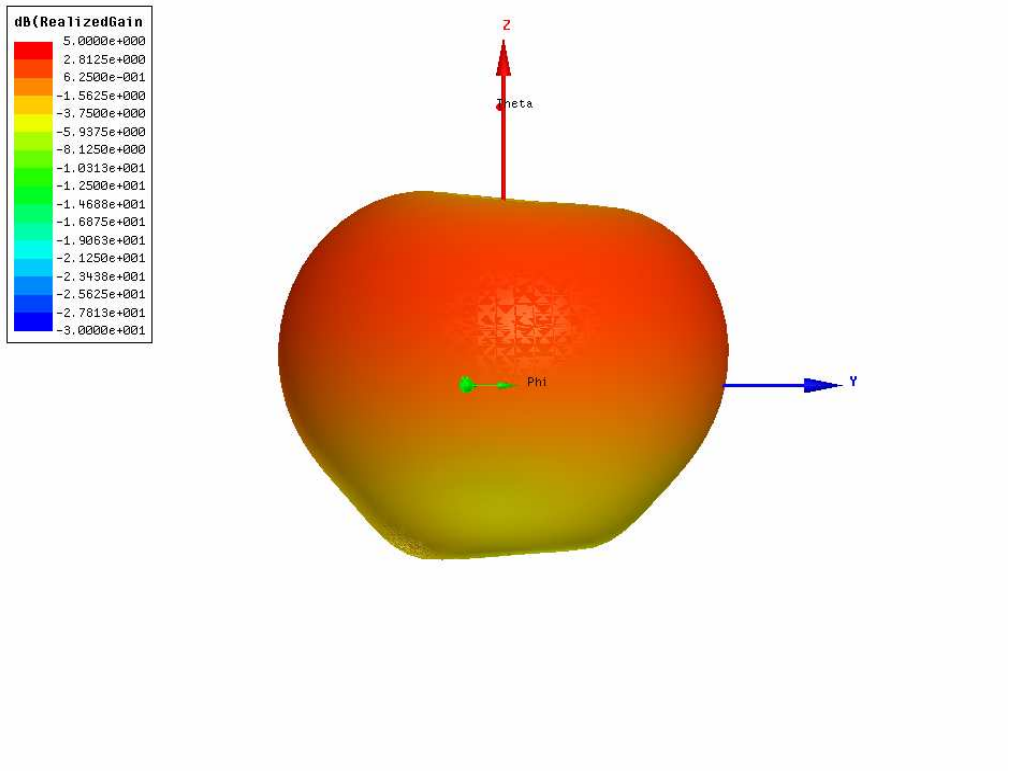

(b)

4.40: Radiation patterns on the body surface (a) yoz & xoz plane (b) 3D polar plot

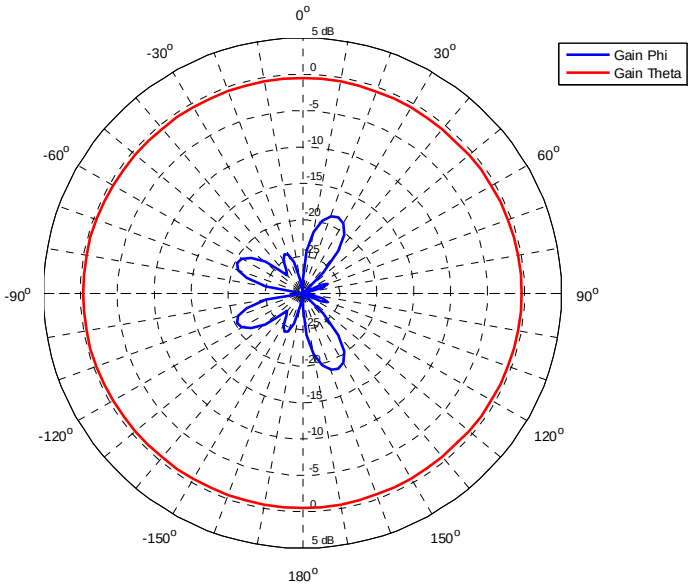

4.41: Azmuthal plane radiation patterns representing larger Gain theta.

The results of on the body are depicted in Figure 4.38 through 4.41. The return loss and impedance curves presented in 4.38 and 4.39 respectively show that DRA -10dB impedance bandwidth is nearly un-effected by the lossy nature of the phantom body and that yields

nearly the same results as without its presence. The yoz plane and xoz plane radiation patterns are depicted in Figure 4.40(a) and (b) and as expected no significant change in the end-fire pattern is observed. The radiation efficiency on the other hand is found to drop from 99% to 85% mostly because the back radiation is absorbed by the body tissues. The azimuthal plane radiation patterns that are presented in Figure 4.41 speak of much higher value of Gain theta as compare to Gain phi and it presents nearly the same situation as in body free case.
It can be concluded that when placed upon the body surface, the DRA undergoes very small changes as compared to the slot loop antenna.

4.5 Coupling performance:

Free space performance:

So far slot loop and DRA antennas have been analysed independently and are found to yield the desired results not only in free space but also upon the body surface for which it is particularly designed. Generally, it is expected that when both ports are excited, depending upon the level of mutual coupling between them, the return loss, resonance frequency and radiation pattern may undergo a slight change. Thus it is important to evaluate such behaviour before the design is finalised. Keeping all the design parameters intact, the two ports simulation results are presented in 4.42.

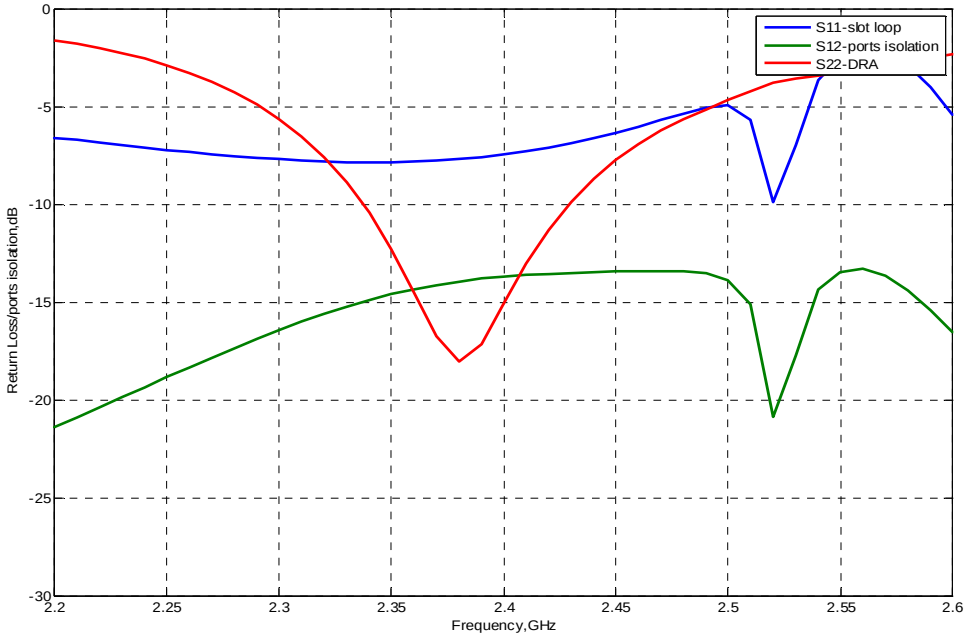

4.42: Two ports slot loop and DRA return loss and ports isolation curves

As can be observed from Figure 4.42 that both antennas perform well around approximately the same frequency of 2.4GHz thus yielding -10dB common bandwidth of 3.3%.The slot loop return loss remains at -7dB level and it could be attributed to the presence of adhesive material with which DRA is glued to the ground plane. The simulation results without it show the return loss deeper than -10dB level and it will be confirmed by the measured results that to what extant gluing can influence the -10 level. The ports isolation is around -13dB, though it

is not so ideal however it is found not to influence greatly the overall performance of the antenna.

On body performance:

It has been observed in individual cases for slot loop and DRA that the presence of the body influences their performance, though it is stronger for the former and slighter for the latter. So it is important to observe their combined behaviour in the presence of the body. Keeping all the factors same as in individual antenna (slot loop and DRA) cases, the phantom body tests are evaluated to observe dual ports antenna performance. The lossy nature of cylindrical phantom depicting human body trunk, is characterized by dielectric constant of (εr=53) and loss tangent of .002 and is expected to introduce some changes in the results. The simulations tests are performed while placing the dual ports antenna at a height of 15mm above the phantom formed by radius of 20cm and height of 40cm. The simulated results are presented in 4.43.

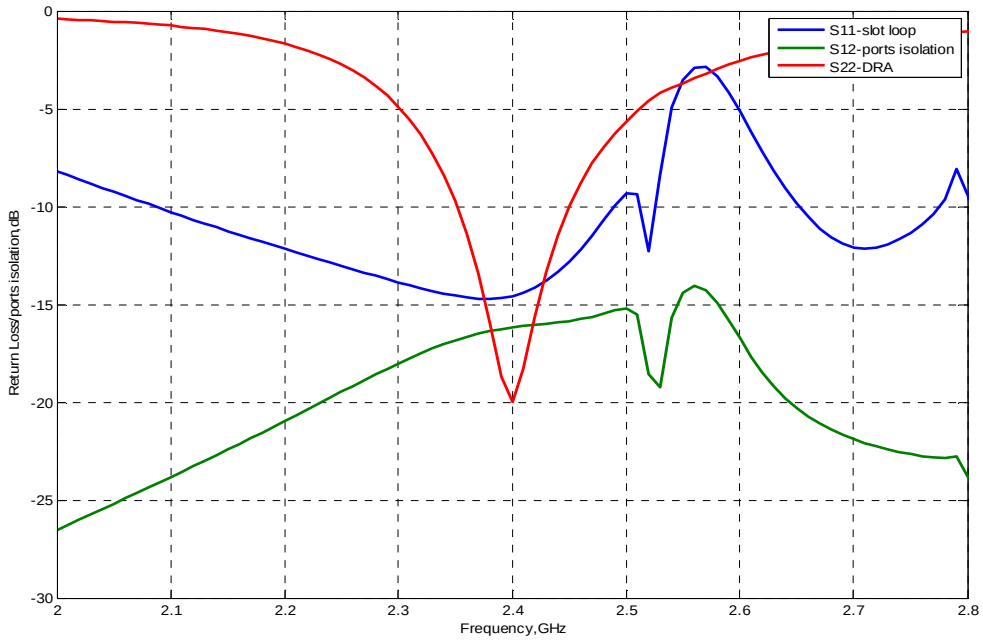

4.43: Two ports slot loop and DRA return loss and ports isolation curves upon the body surface

Figure 4.43 narrates that both slot loop and DRA perform well around 2.4GHz frequency and yield impedance bandwidths of 17% and 4% respectively. The slot loop return loss that has been observed to be more sensitive, remains lower than -10dB level and it could be attributed to the presence of lossy nature of the body with (εr=53 and loss tangent of 0.002). The ports isolation is now found to be -15dB or better. This concludes that dual pattern antenna works well upon the body surface.

- The proposed dual pattern antenna is expected to perform well and fulfil nearly all the requirements, except planar feeds to DRA so as to be used for on the body applications to seek certain Diversity Gain (DG). The measured results of this antenna are presented in section 5.3.

4.6 Two ports planar feed structure:

The antenna proposed in the previous section lacks planar feed to DRA though it can still be planted upon the body surface using L-shaped connector however, it would be more appropriate to replace it with planar feed to enhance its utility.
So following the same techniques, an alternative design is proposed that offers purely planar feeds to both antennas. The slot loop is fed by under-laid microstrip feed line instead of CPW line while DRA is fed too by microstrip line that runs below the interrupted section of the slot loop. Thus both feeding lines are etched on opposite side of the ground plane upon which DRA is residing encircled by the slot loop hence yielding end-fire and broadside types radiation patterns. This manipulation gives more compactness to the antenna structure.

4.6.1 Microstrip fed slot loop design:

A microstirp feed line of 1.4mm width with characteristics impedance of 50 Ω and fed by port1 is used to excite the slot loop antenna. The slot is etched on the square shaped ground plane supported by equivalent sized substrate of 50mm×50mm with dielectric constant of (εr=2.2) and of height h=0.508mm.The schematic diagram of the design is depicted in 4.44.

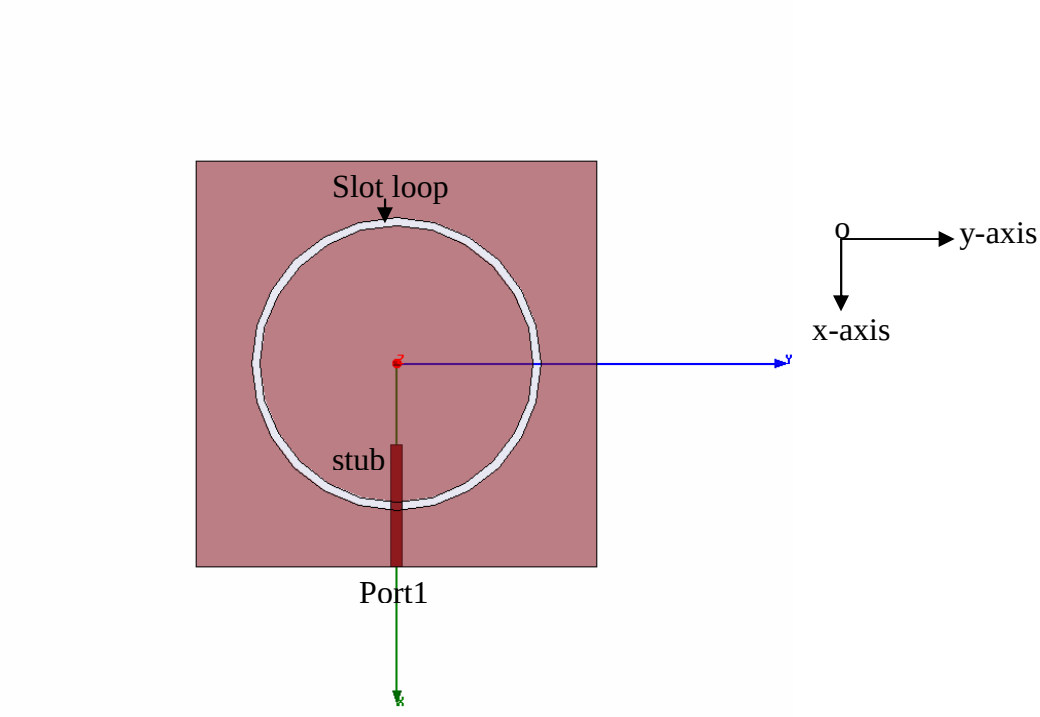

4.44: Slot loop etched on the ground plane is fed by microstrip line

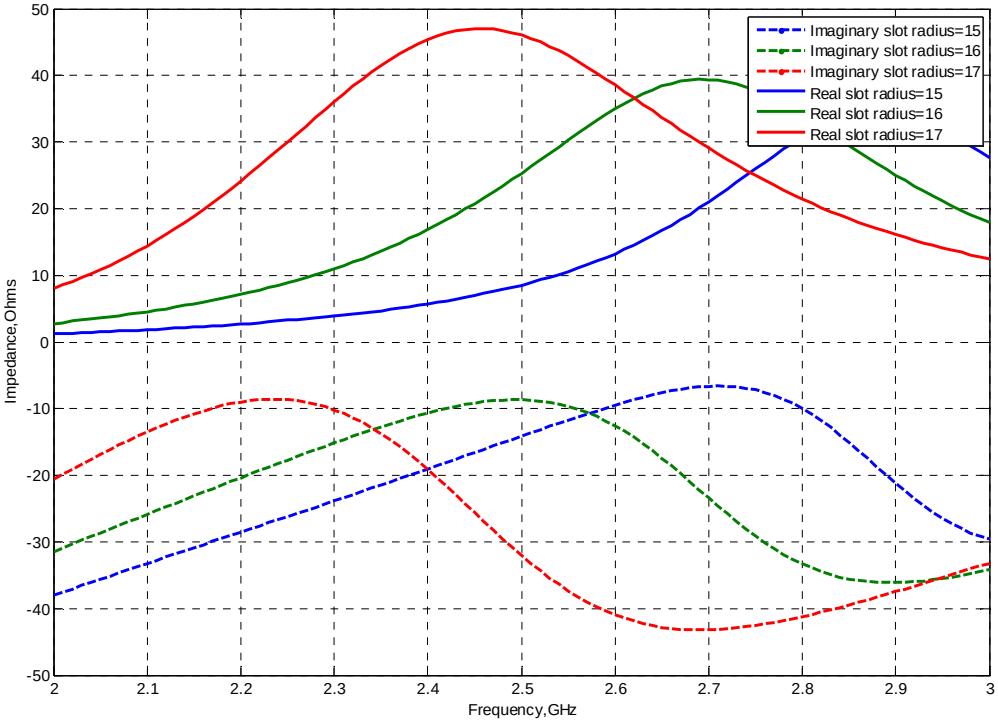

(a)

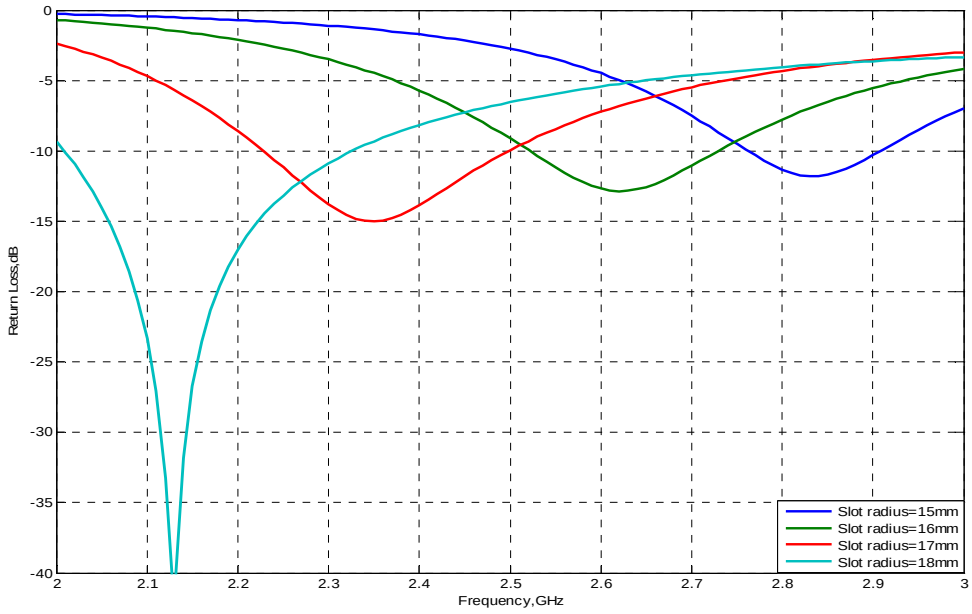

(b)

4.45: slot loop (a) impedance and (b) return loss curves corresponding to different loop radii.

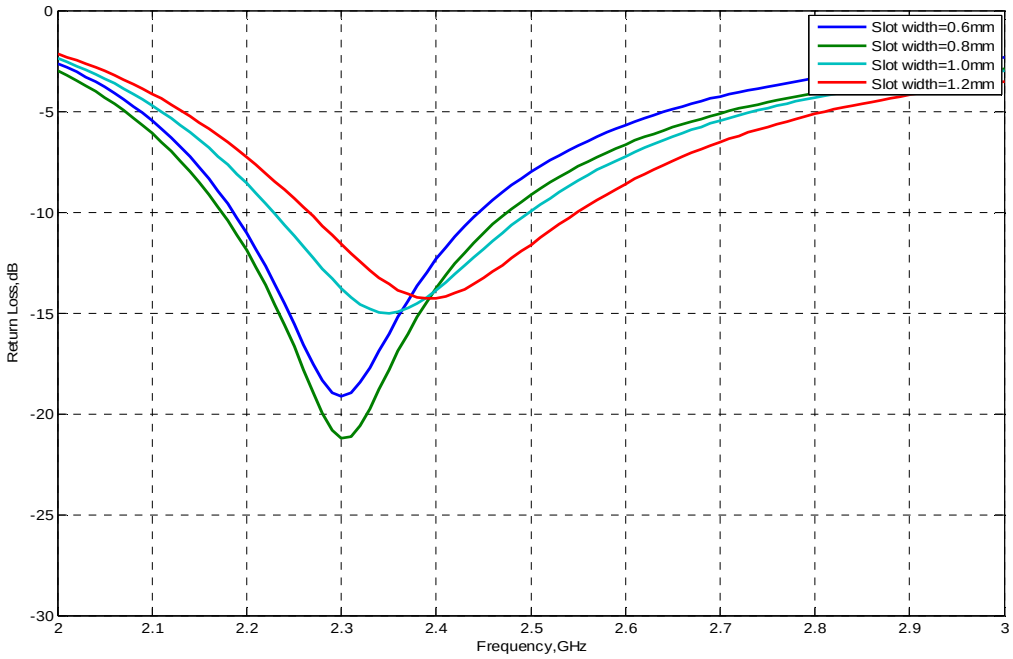

4.46: Slot loop return loss values corresponding to different loop widths.

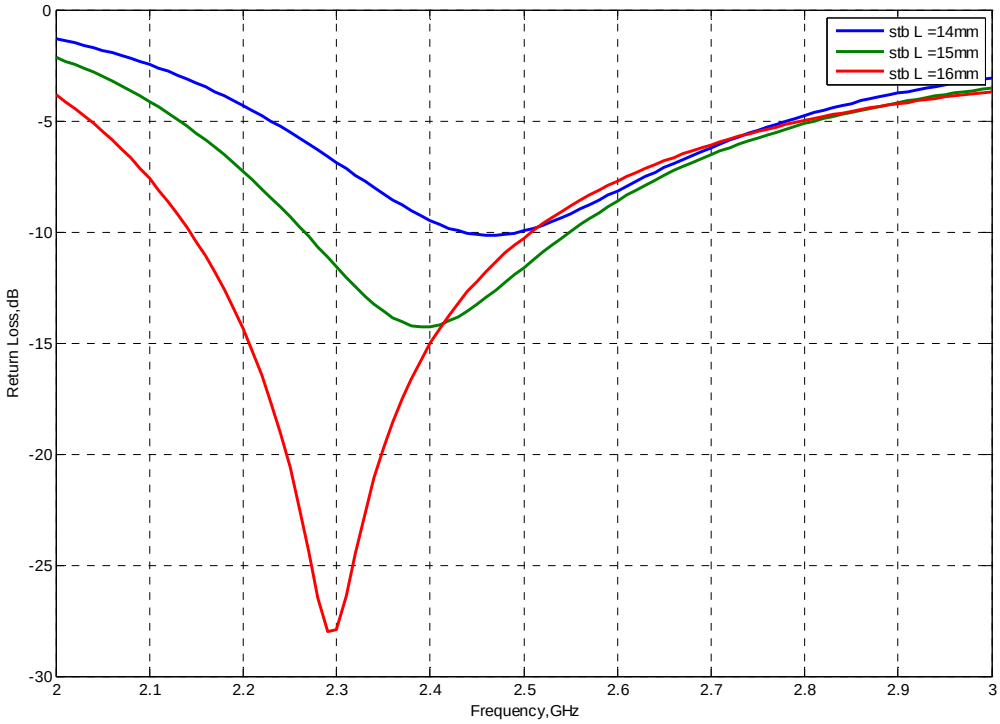

(a)

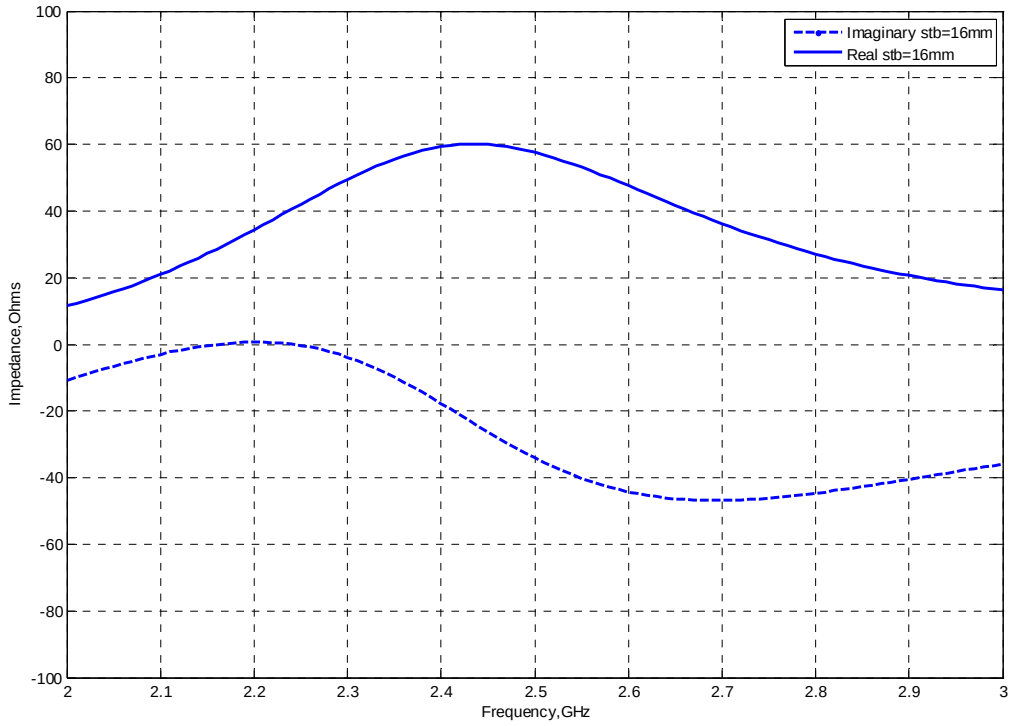

(b)

4.47: slot loop(a) return loss and (b) impedance curves corresponding to different stub lengths.

The results presented in 4.45 through 4.47 illustrate the antenna matching. The results depicted in Figure 4.45 present a family of impedance and return loss curves corresponding to various slot loop radii. The slot loop radius of 17mm and width of 1mm is found to yield resonance around 2.4GHz. Figure 4.46 depicts the effect of slot widths which is observed not to be so significant though width of 1.2mm seems more suitable to make loop resonate around 2.4GHz however, practically any suitable width available from the results can be chosen that fits to desired frequency. The stub lengths response is presented in the results of 4.47, where it can be observed that a stub of 16mm length improves coupling to the slot.

4.6.2 DRA loading effect:

As has been observed that DRA residing within the slot loop is expected to affect the slot loop resonance, hence slot loop return loss and impedance curves in the presence of DRA are presented in 4.49 and 4.50 respectively.

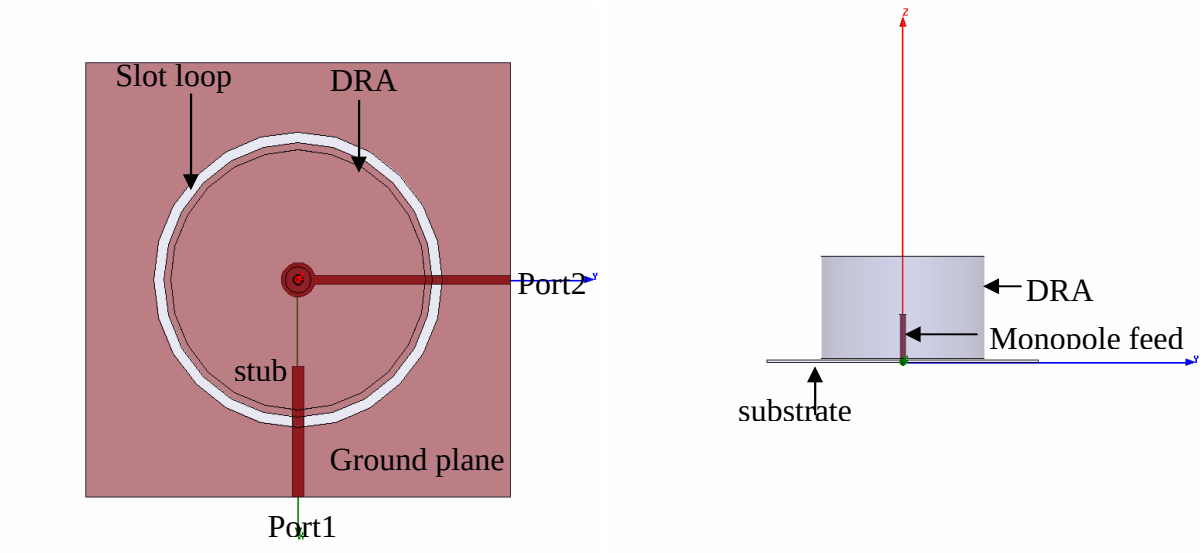

4.48: DRA encircled by the slot loop

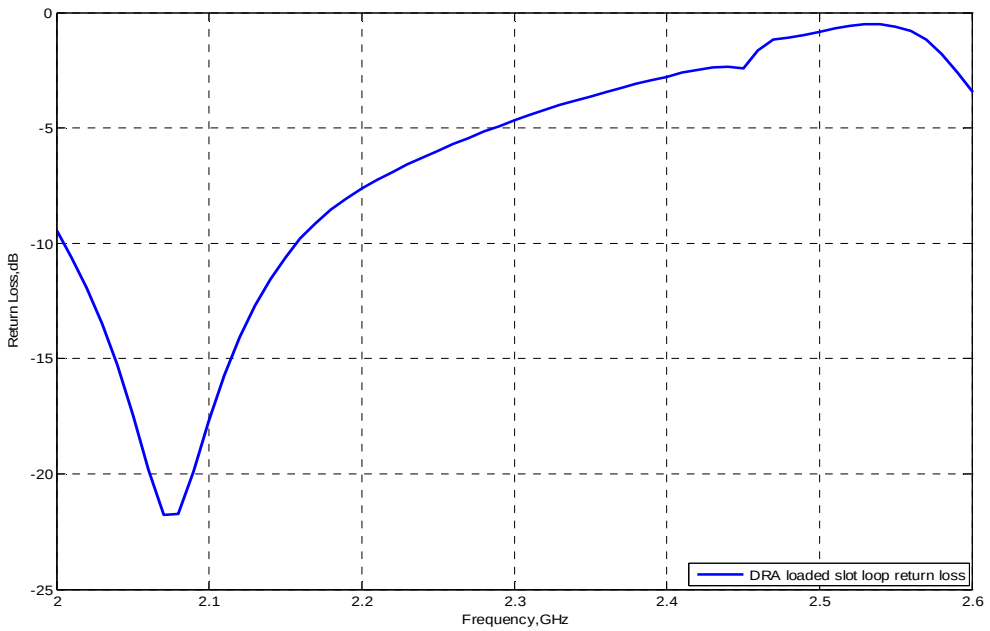

4.49: DRA loaded slot loop return loss depicting change in its resonance frequency

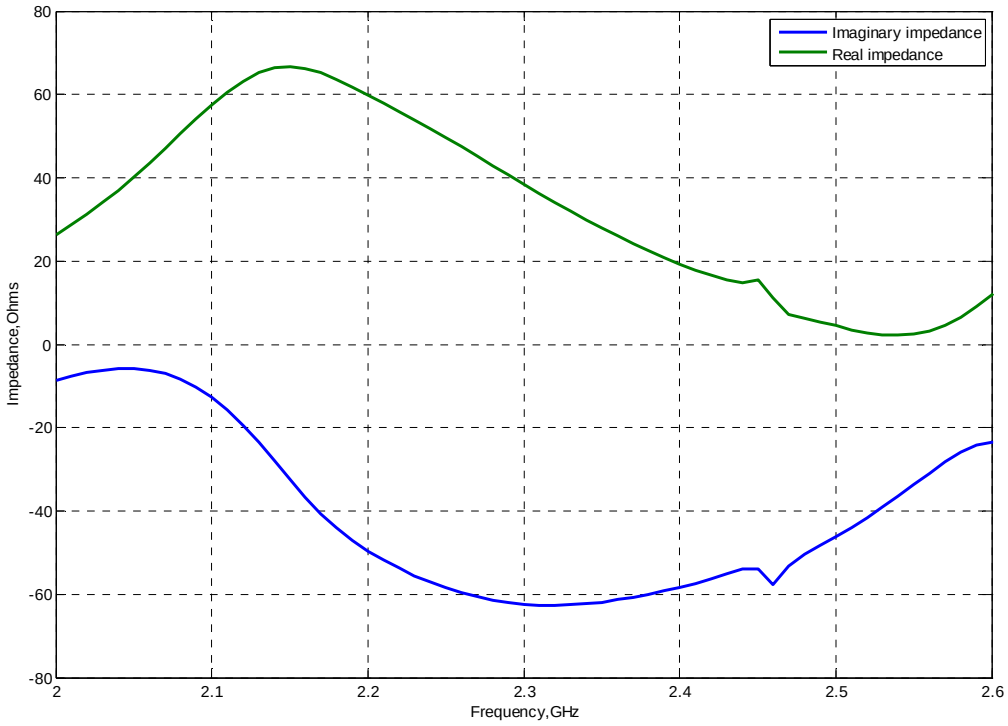

4.50: slot loop impedance curves in the presence of DRA

The DRA loaded slot loop is presented in 4.48. It is interesting to observe from 4.49 and 4.50 that the resonance frequency seems shifted down around to 2.05GHz. So in order to shift this frequency to 2.4GHz one is required to reduce its size and that ultimately reduces the antenna structure. As a result the design becomes more compact and hence introduces more usability for on the body applications.

4.6.3 Interrupted slot loop design performance:

To assign planar structure to the DRA feed, the feeding microstirp line of 1.4mm width is made to pass below the interruption point introduced in the slot loop where E-fields are found to be negligibly weak. This situation is narrated in 4.51. Owing to the need of miniaturization of the antenna structure the ground plane and substrate sizes are now reduced to 36mm×36mm.The slot loop design values in the DRA loading context are reviewed with slot loop radius of 15.5mm, width of 0.4mm and interruption gap of 11mm.On the same footings the stub length is optimised at 4.5mm. The slot loop performance is depicted in Figures 4.52 through 4.55.

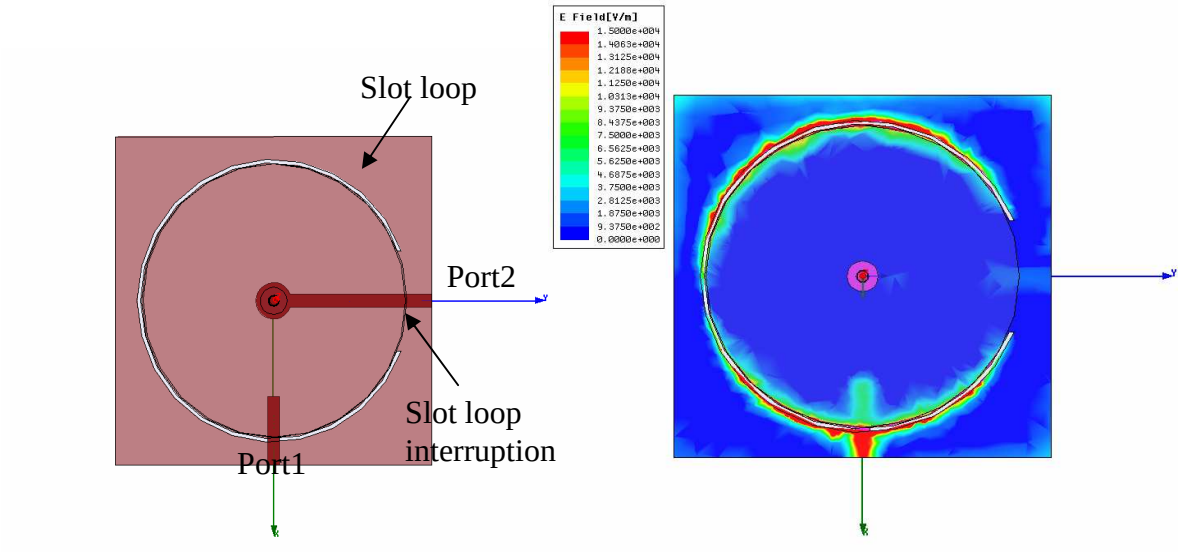

(a) (b)

4.51: DRA encircled by the slot loop with interruption to pass below microstrip line to feed to DRA

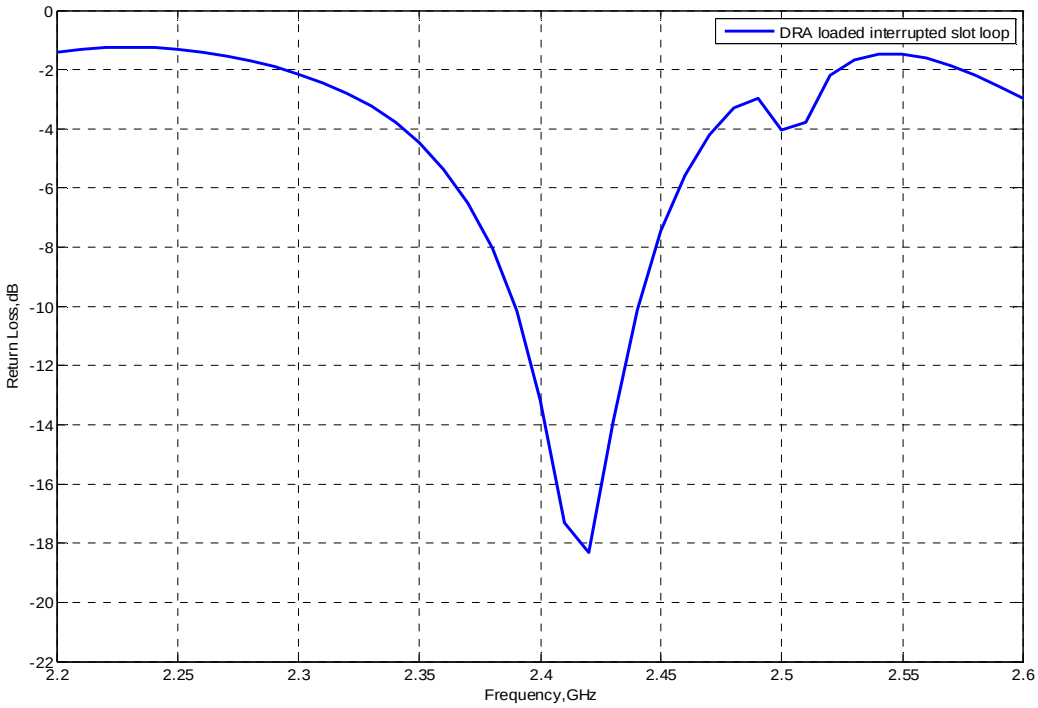

4.52: Slot loop return loss curve with interruption in it

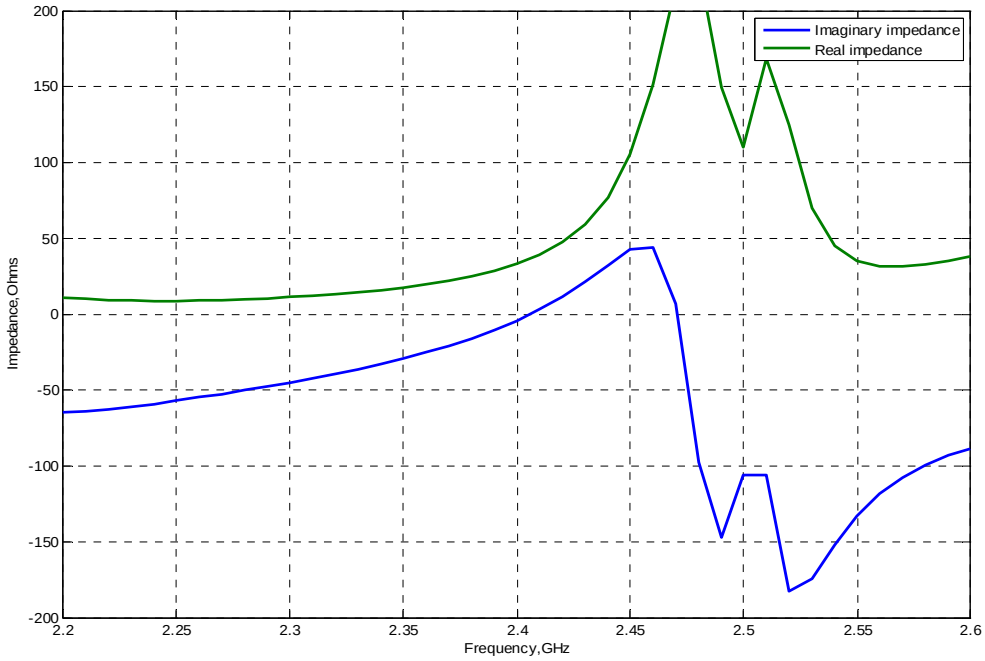

4.53: Slot loop impedance curves representing resonance at 2.47GHz

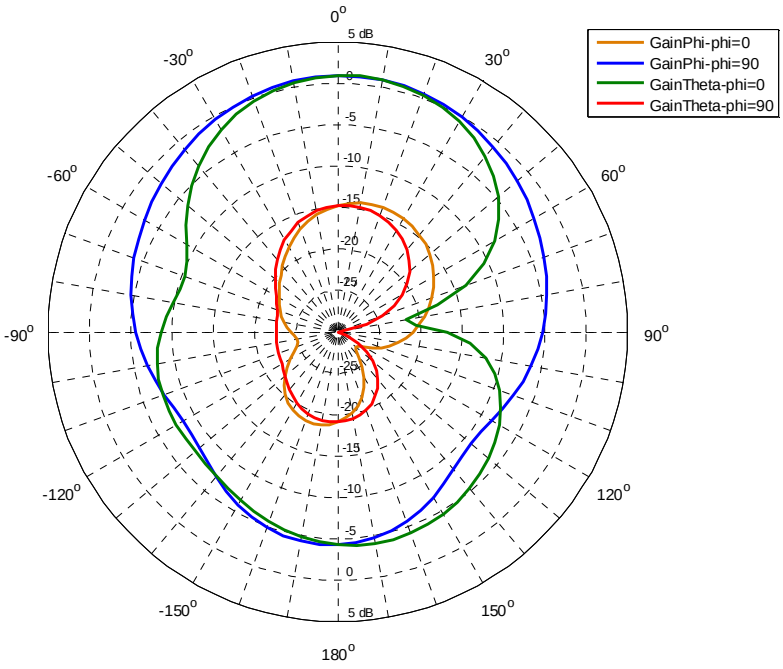

(a)

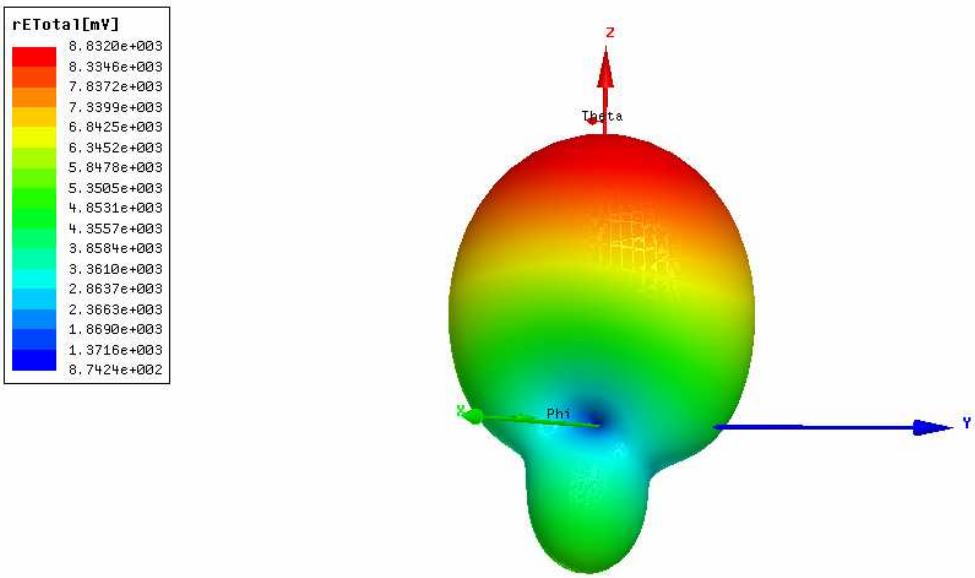

(b)

4.54: Slot loop broadside radiation patterns (a) xoz & yoz planes (b) 3D polar plot

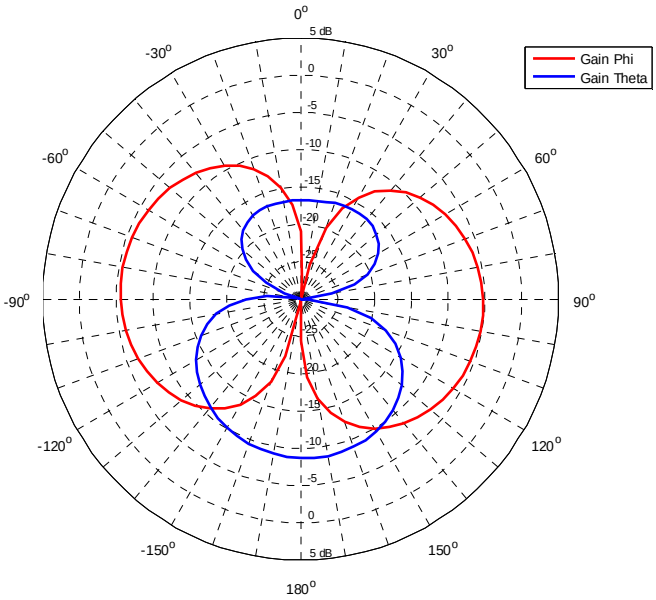

4.55: Azmuthal plane radiation pattern with larger Gain phi

The return loss and impedance curves given in 4.52 and 4.53 speak of -10dB impedance bandwidth as around 2% while antenna undergoes a parallel resonance to 2.47GHz. The xoz plane and yoz plane radiation patterns are depicted in Figure 4.54(a) and (b) that present symmetry in their shapes with gain of 0.8dBi however, xoz plane radiation pattern is found to be narrow as compared to the yoz plane. The cross-polarizations in the broadside direction are -15dB or better. The radiation patterns are found to be stable with in the frequency band from 2.39GHz to 2.44GHz. The radiation efficiency of the antenna is estimated to be 94%. The azimuthal plane radiation patterns that are presented in Figure 4.55 present slightly higher Gain phi value than that of Gain theta.
It has been estimated that a larger interruption gap directly influences the impedance bandwidth. There is an obligation to keep this gap large enough to keep slot size smaller to make it offer -10dB impedance bandwidth around 2.4GHz.

4.6.4 On-body analysis:

The antenna is placed at a height of 10mm above the cylindrical phantom body comprising of radius of 20cm and height of 40cm hence depicting a human corps trunk characterised by effective permittivity of 53 and loss tangent of 0.002. The estimated results are presented in Figure 4.56 through 4.59.

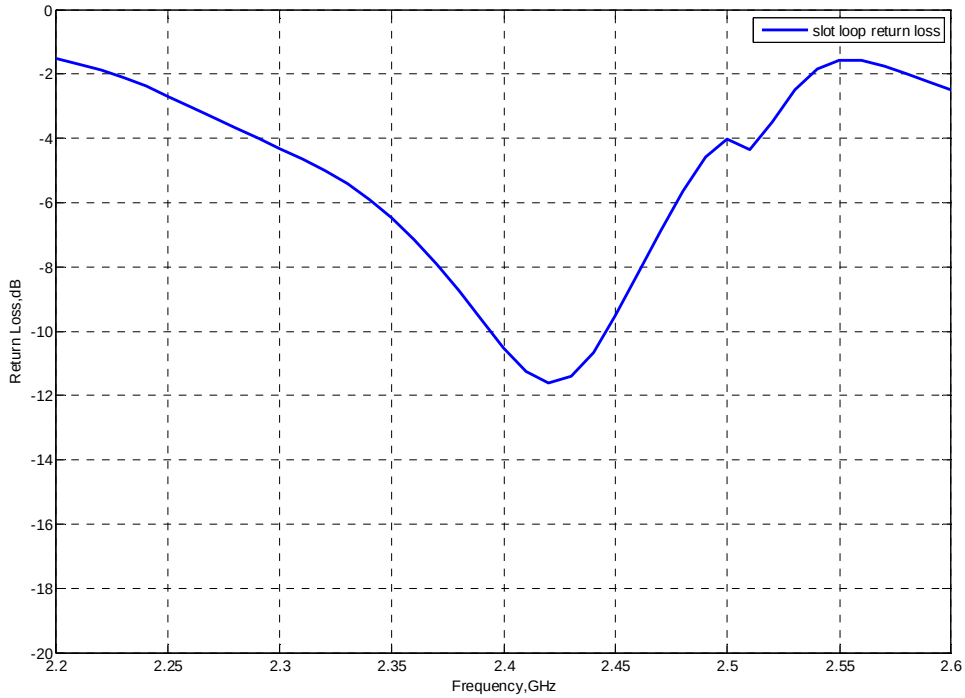

4.56: Slot loop on body return loss curve

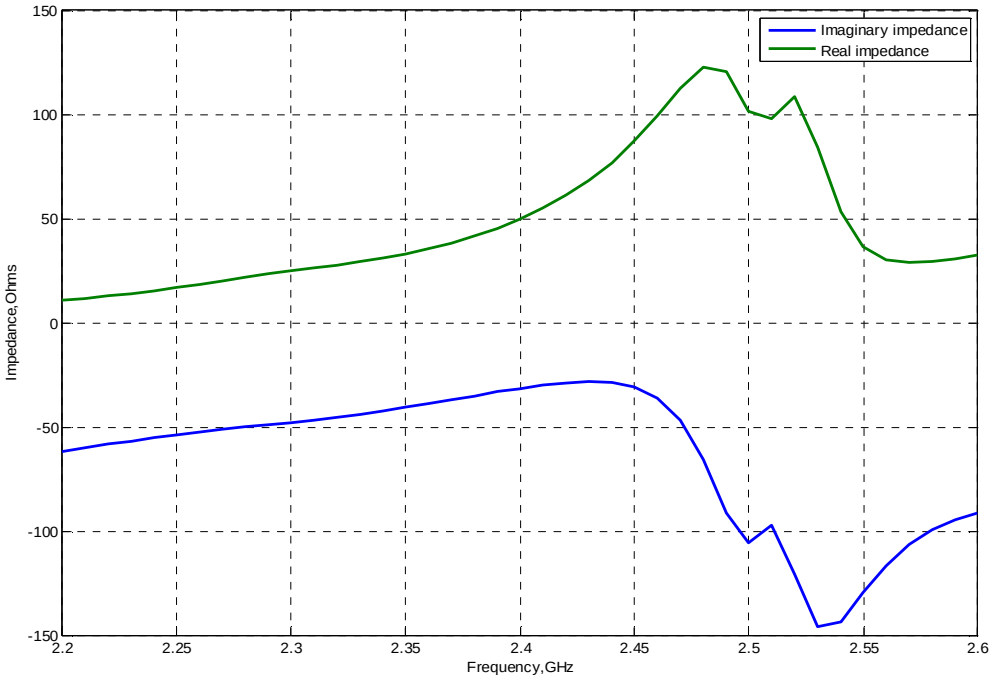

4.57: Slot loop on body impedance curves

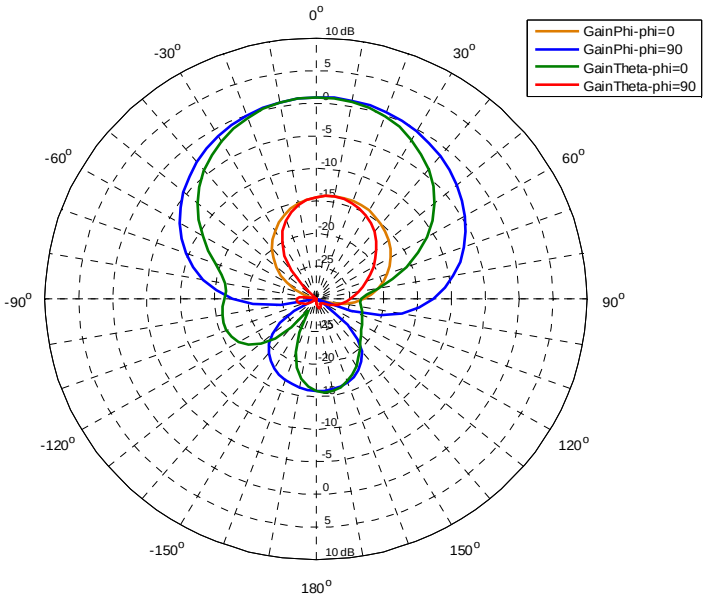

(a)

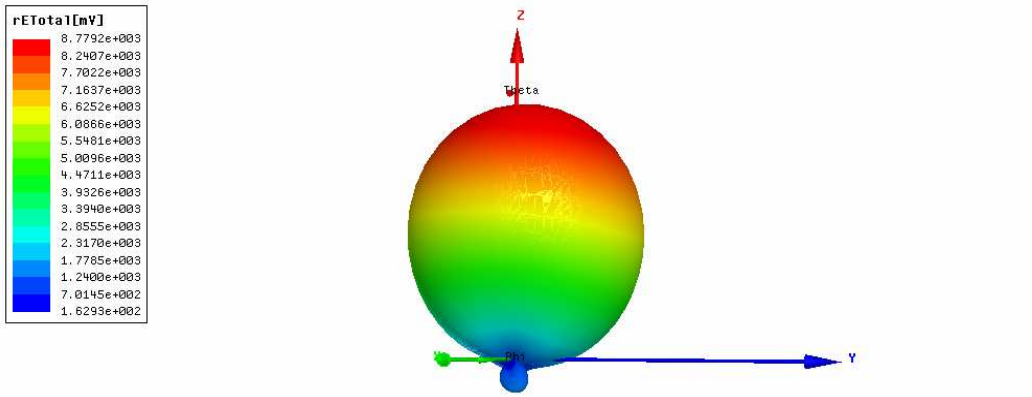

(b)

4.58: Slot loop on body radiation patterns (a) xoy & yoz planes (b) 3D polar plot

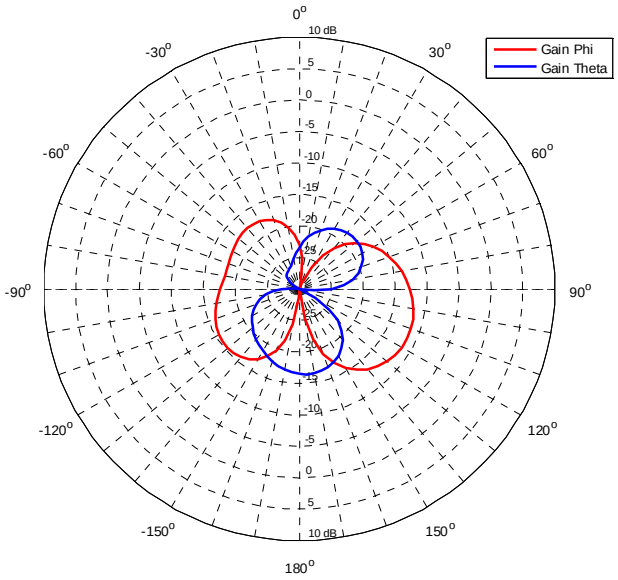

4.59: Azimuthal plane radiation patterns with nearly same Gain phi and Gain theta values

With reference to free space case certain changes are observed. The return loss and impedance curves given in 4.57 and 4.58 respectively yield -10dB impedance bandwidth that remains same around 2% while antenna resonance takes place around 2.45GHz frequency. The xoz

plane and yoz plane radiation patterns are depicted in Figure 4.59(a) and (b) that represent elevation plane to be more directional with gain of 0.8dBi.The backward radiation is found to be reduced significantly and this could be attributed to the lossy nature of the phantom model upon which the antenna is planted and that absorbs the radiations. The xoz plane radiation pattern is still narrow as compared to the yoz plane. The cross-polarizations in the broadside direction are -15dB or better. The radiation efficiency of the antenna is estimated to drop from 94% to 65%. The azimuthal plane radiation patterns that are presented in Figure 4.59 speak of nearly same Gain phi and Gain theta values that is -15dBi.

4.6.5 Microstrip fed DRA design performance:

The DRA design values do not undergo any wide change while planar feed in the form of microstrip line has yielded the desired results that are given in 4.60 through 4.63

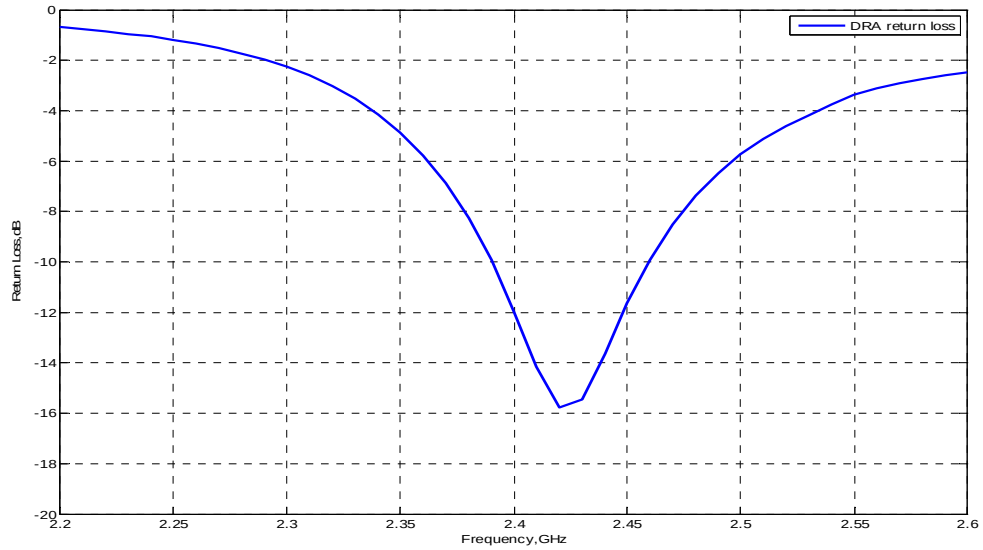

4.60: DRA return loss curve

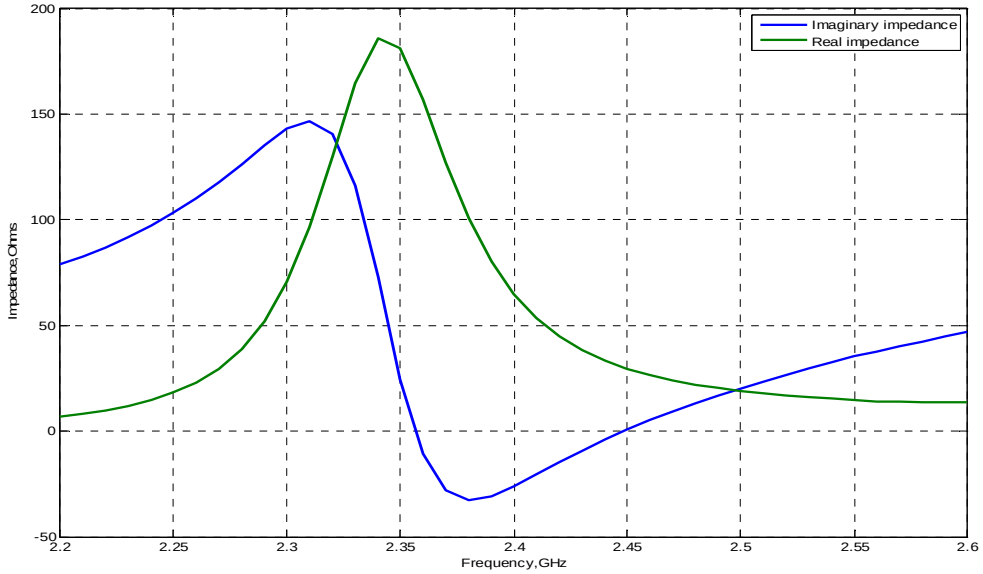

4.61: DRA impedance curve representing parallel and series resonance around 2.4 GHz

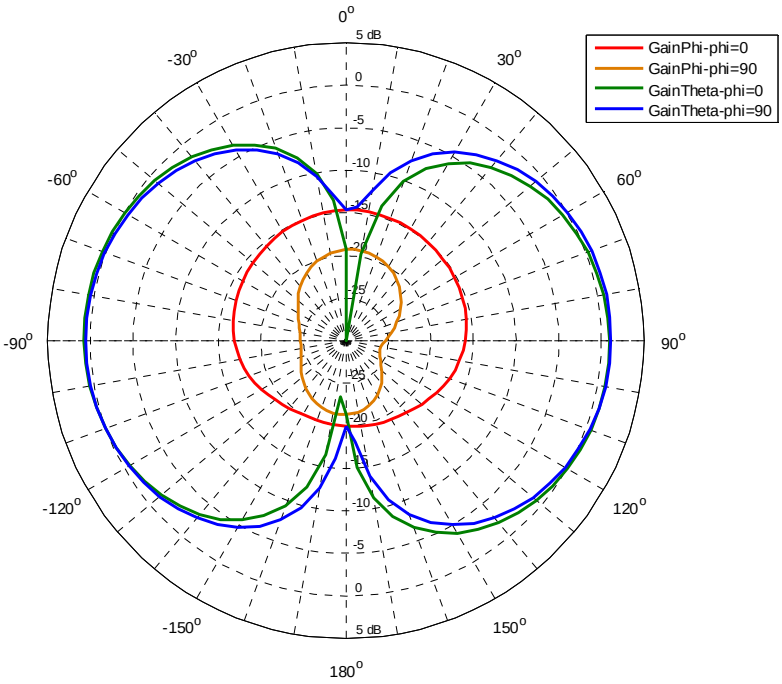

(a)

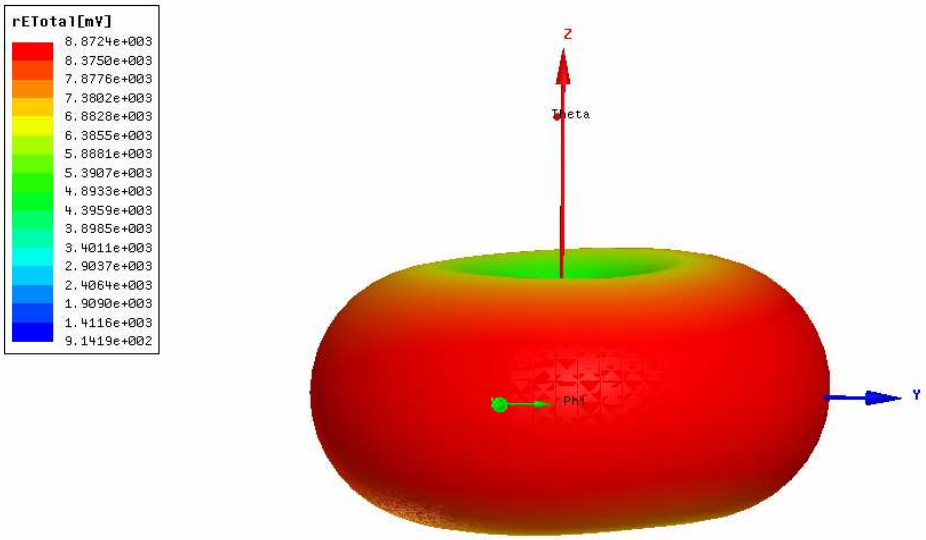

(b)

4.62 : DRA radiation patterns (a) xoz & yoz planes (b) 3D polar plot

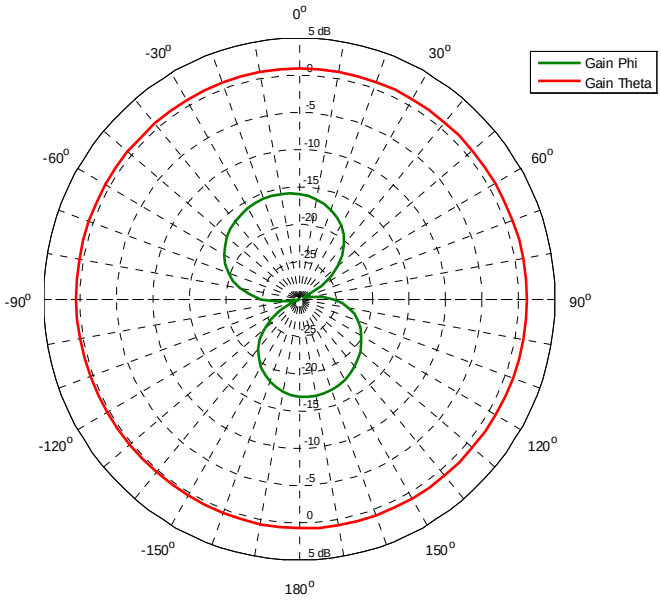

4.63: Azmuthal plane radiation patterns with larger value of Gain theta.

The DRA return loss curve presented in 4.60 while its impedance curves plotted in 4.61 speak of its impedance bandwidth of 3.3% at around 2.42GHz frequency. The end-fire type radiation pattern in the (xoz & yoz) elevation planes is depicted in Figure 4.62(a) and (b).Both plane patterns are found to be purely symmetric with cross-polarizations of -12dB or better. The azimuthal plane radiation pattern given in Figure 4.63 presents that Gain phi is -15dB smaller than that of Gain theta. The omni-directional gain is found to be around 0.5dBi with radiation efficiency of 98%.

4.6.6 On-body analysis:

In line with slot loop the DRA is also placed at a height of 10mm above the surface of phantom. The estimated results are presented in 4.64 through 4.67.

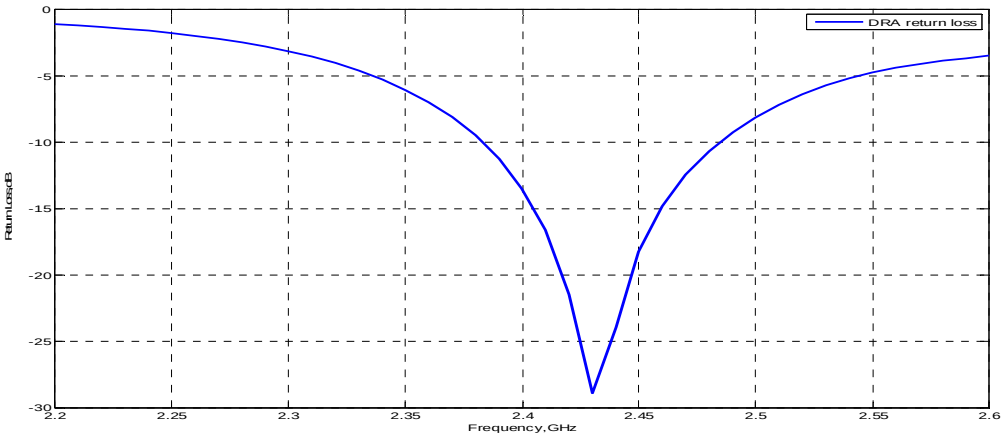

4.64: On body DRA return loss curve

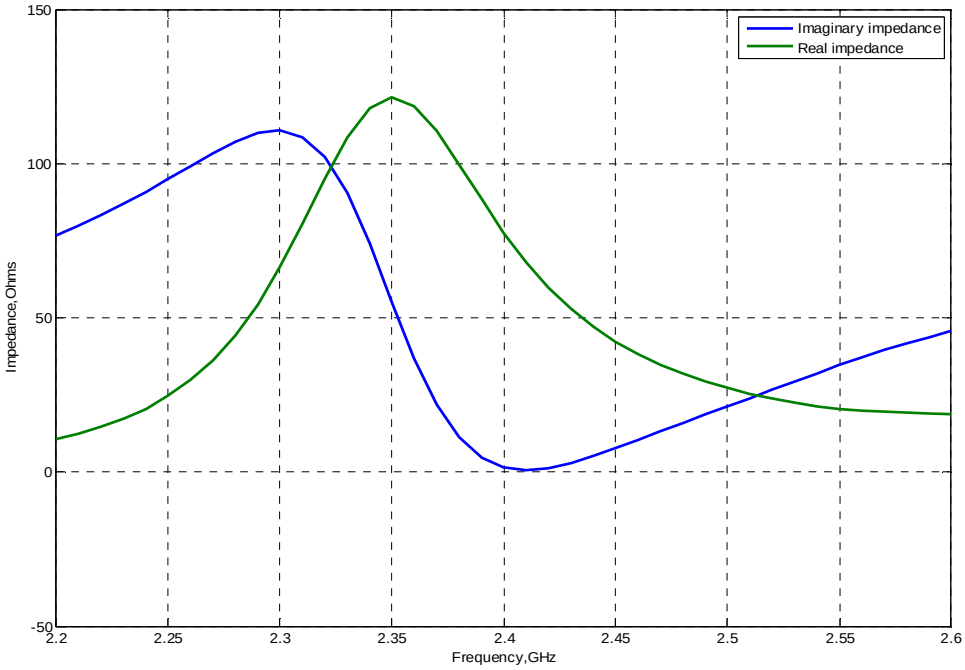

4.65: On body DRA impedance curves

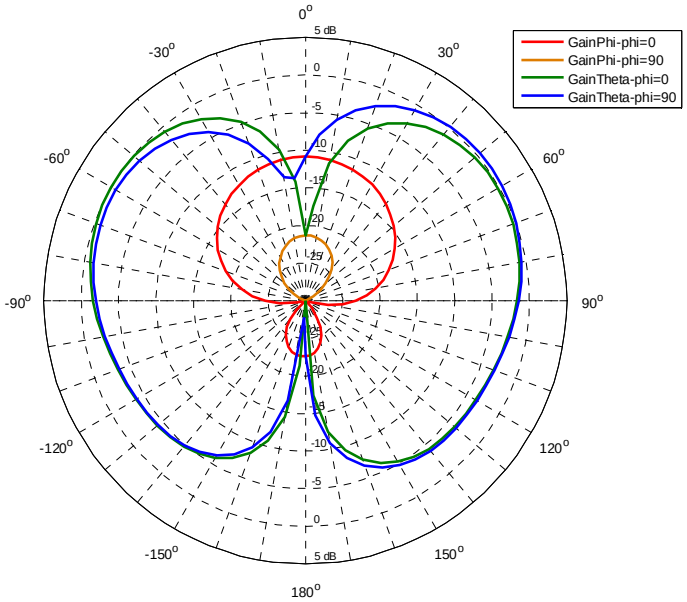

(a)

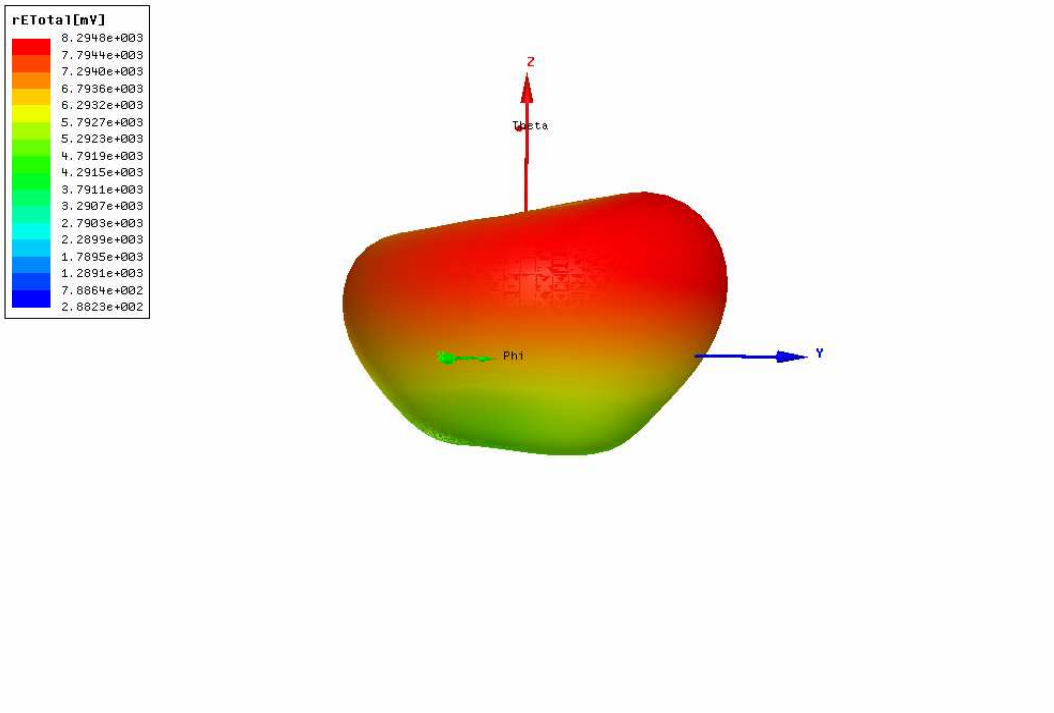

(b)

4.66: On body DRA radiation patterns (a) xoz & yoz planes (b) 3D polar plot

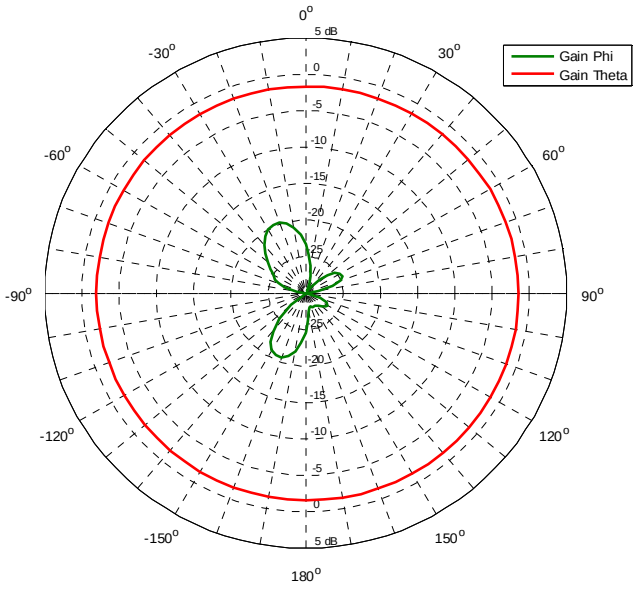

4.67: Azimuthal plane radiation patterns with larger value of Gain theta

The on body return loss curve is presented in 4.64 while impedance curves are plotted in 4.65. The -10dB impedance bandwidth is found around 4%. The end-fire type radiation pattern in the (xoz & yoz) elevation planes is depicted in Figure 4.66(a) and (b). Both plane patterns are found to be purely symmetric in the elevation plane while certain reduction in the backward direction can be attributed to the lossy nature of phantom model. The azimuthal plane radiation pattern is given in Figure 4.67 where it can be observed that Gain phi is -18dB smaller than that of Gain theta in any direction that means gain phi undergoes larger attenuation compared to gain theta. The radiation efficiency of the antenna is found to drop from 98% to 85% while gain drops to 0dBi.

4.7 Coupling performance

Free space performance:

As both antennas are found to perform well at same 2.42GHz frequency so it is important to evaluate coupling between their ports for which the overall design values are given in Table4.11 and result in Figure 4.68.

Table4.11: Slot loop and DRA optimal design with associated feed values

Antenna Type	Design Values	Feed Line size	Stub Length Ls	Resonance Frequency
Port1 (Slot Loop)	Loop radius=15.5mm Loop width=0.4mm	Length(L)=7.5mm Width(w)=1mm	4.5mm	2.4 GHz
Port2 (DRA)	DRA Diameter=30mm DRA Height=18mm	Length(L)=18mm Width(w)=1mm	0	2.4 GHz

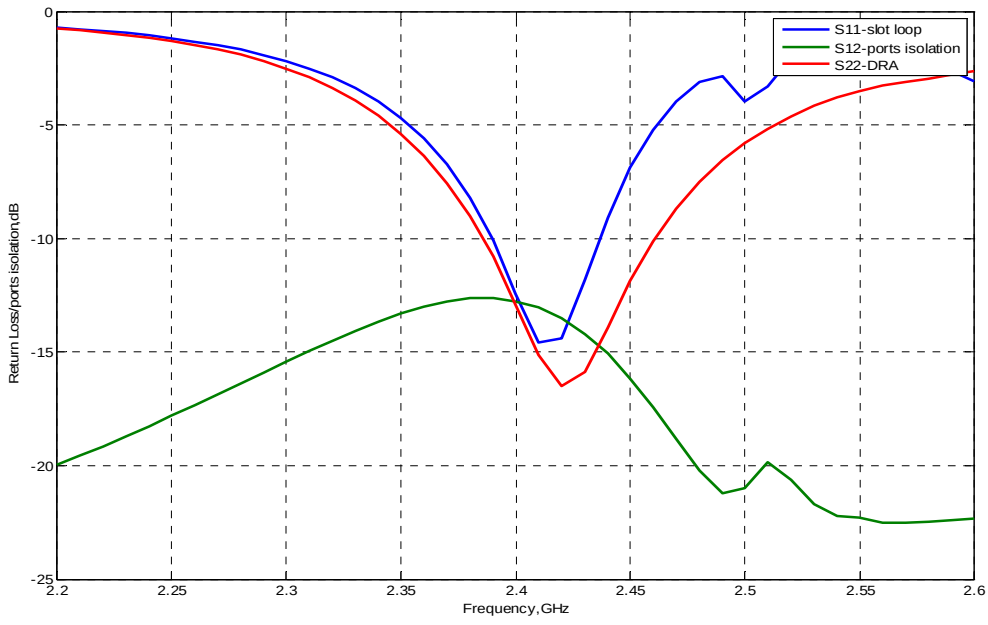

4.68: Slot loop and DRA return loss curves with ports isolation of -12dB

The results presented in 4.68 illustrate that slot loop -10dB impedance bandwidth is around 1.8% while for DRA it is 3.2%. Thus the common bandwidth is found to be 1.8% with ports isolation of -12dB.

On body performance:

The same dual ports antenna is planted upon the phantom body at the height of 10mm so as to evaluate its performance in the presence of lossy material with (ε_r=53 & loss tangent=0.002) The simulations tests are performed upon phantom formed by radius of 20cm and height of 40cm.

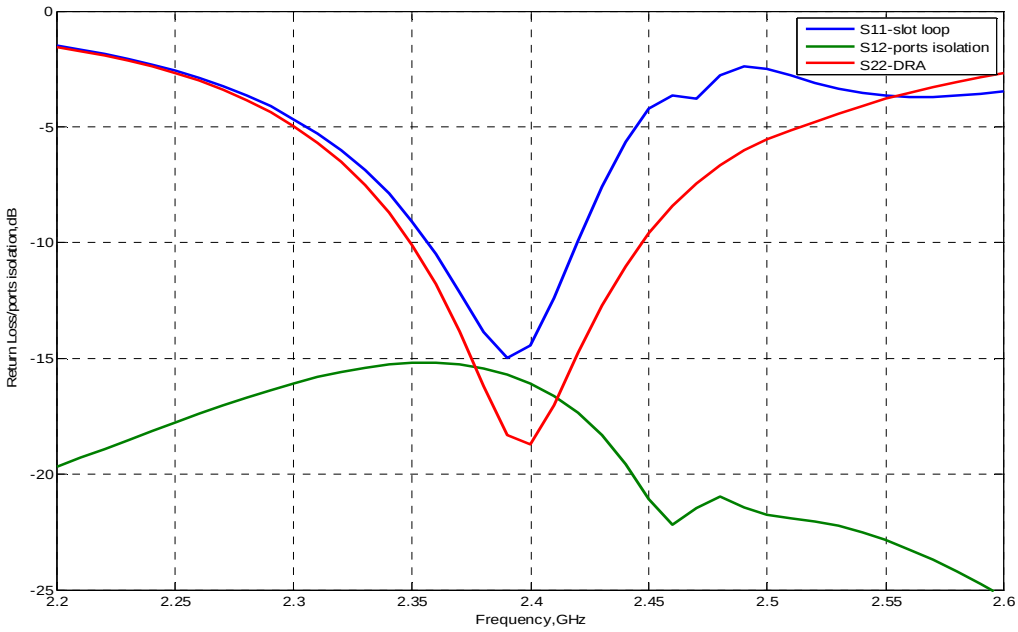

4.69: Slot loop and DRA on the body return loss and ports isolation curves

It can be observed from Figure 4.69 that due to the body influence both slot loop and DRA resonance has slightly shifted downward and yield larger impedance bandwidths of 2.5% and 4% respectively. The ports isolation is found to improve to -15dB.This slight change in results can be attributed to the presence of lossy nature of the phantom body, however the proposed antenna withstands such constraints meted out to its performance and exhibits fidelity to yield the desired results.

- The proposed antenna is more compact and conformal with both feeds exhibiting planar structure ideally suitable for on the body applications to yield Diversity Gain (DG) performance. The measured results of this antenna are given in section5.4

4.8 Conclusion:

Two types of dual patterns body wearable antennas have been presented one with non planar feeds while other with planar feeds. The antenna with non planar feed structure is though restricted to limited applications upon the body positions but it offers larger impedance bandwidth. While on the other hand, the planar feed antenna is easy to integrate upon the body but at the cost of reduced impedance bandwidth. Both antennas present endfire and broadside ports showing high isolation in a compact space and are expected to show good diversity gain performance in the next section.

References :

[1] Thierry Emmanuel Pires ALVES, PhD Thése " CONCEPTION D'ANTENNES POUR LE RESEAU BAN et MODELISATION DU CANAL DE PROPAGATION" Université Paris Est Marne La Vallée France.

[2] A.A.Serra,I.Khan,P,Nepa, G.Manara and P.S Hall " Dual-polarization and dual-pattern planar antenna for diversity in body-centric communications" Antenna and Propagation Society International Symposium,2008 AP-S 2008,IEEE Pages 1-4

[3] Imdad Khan, Peter S.Hall Andrea A.Serra, Anda R Guraliuc and Paolo Nepa " Diversity Performance Analysis for On-Body Communication Channels at 2.45GHz" IEEE TRANSACTIONS ON ANTENNAS AND PROPOGATION.VOL,57,NO.4,APRIL 2009, Pages 956-963

[4] A.A Serra, P.Nepa, G.Manara, and P.S Hall "Diversity Measurement for On-Body Communication Systems" IEEE ANTENNAS AND WIRELESS PROPAGATION LETTERS,VOL.6,2007, Pages 361-363

[5] S.V.Shynu M.J.Ammann "A printed CPW-fed slot-loop antenna with narrowband omnidirectional features" IET Microw.Antennas Propag.2009,Vol.3, Iss.4,pp.673-680

[6] Aldo Petosa "Dielectric Resonator Antenna Handbook" ARTECH HOUSE, INC. 685 Canton Street Norwood, MA 02062.

Chapter 5

Antennas Measurements and Diversity Gain Analysis

Contents

Diversity schemes are usually divided into space, polarization and pattern diversities. The space diversity scheme is used when replica of the signals, are received at two or more antennas. For an efficient combination, the signals at the antennas must be uncorrelated which requires a minimum distance between the antennas, typically a half-wavelength. This mostly happens at the mobile communication base stations. On the other hand, the polarization and pattern diversity schemes are used when a limited space is available for instance as in BAN context. The performance of BAN antennas is evaluated when employed into different channel configurations upon the body surface typically Line Of Sight (LOS) and Non Line Of Sight (NLOS) communication links. This chapter uses the two-port body wearable antenna described in chapter 4 which is specifically design for pattern diversity. This antenna provides radiation patterns complementing each other in a compact size for integration purposes. The performance of such an antenna is evaluated in terms of diversity gain (DG) for different channel configurations, i.e. different positions of the receiving and transmitting antennas on the body surface.

As many aspects of the radio communication are actively involved in the evaluation of diversity performance, a brief overview is presented here.

5.1 Overview of mobile radio channel:

In the indoor environment, the fading predominates and exhibits different behaviours that can be categorised into three main classes:

Very slow fading: It accounts for different body positions such as lying, standing and sitting postures. It can also be attributed to the changing of the body surroundings and is expected to last for several minutes to even hours.
Slow fading: It is associated to the proximity of slow moving objects such as arms movement or the types of antennas and is expected to last for few to several seconds.
Fast fading: It is assumed to be as fast as the process of transmission and reception between the respective antennas, its rapidity can be estimated as the time elapsed for the travelling of half wave lengths in the free space. Static channel's impulse response is given as [1]-[2]-[3]:

$$h(t) = \sum_{k=0}^{N-1} a_k \delta(t - t_k) e^{j\theta_k} \qquad 5.1$$

For each impulse h(t), the amplitude a_k depends upon the reflection coefficient of each scatterer and the distance traversed by each ray k. The phase θ_k is related to the complex value of the reflection coefficient while time of arrival t_k depends upon the total distance covered by each ray.
The model described by equation 5.1 represents the Ultra Wide Band(UWB) channel in which time difference "$t_k - t_0$" between the "direct ray and the k^{th} echo" is called *delay excess* while collective duration delivered to echoes by the scatterer is called *delay spread.* In general sense to traverse a distance of 30cm, a delay excess is assumed to be 1ns, however in BAN context the impulse response measurement is a complex task that requires additional set ups.
The time dispersion phenomenon leads to the signals fading in frequency band thus introducing distortion in terms of *Inter Symbol Interference* (ISI). The *Coherence Band* (Bc) that defines channel selectivity is a frequency band for which the channel is considered to be constant. If the band occupied by the transmitted signal is very large compared to it, the signal distorts and the channel is called selective.
It can be illustrated by a simple case of the interference of two rays for which equation 5.1 is subject to Fourier Transformation as [4];

$$H(f) = \sum_{k=0}^{N-1} a_k e^{-j\omega t_n} \qquad 5.2$$

considering N=2 represents two identical amplitudes of the rays, so

$$H(f) \approx a(e^{-j\omega t_0} + e^{-j\omega t_1}) \qquad 5.3$$

or

$$H(f) \approx 2ae^{-j\omega\frac{t_0+t_1}{2}} \cos[\omega(\frac{t_1 - t_0}{2})] \qquad 5.4$$

Coherence time "Tc" of the channel accounts for rapid changes taking place in the spreading environment or displacement of the mobile unit. If *Symbol time* "Ts" of the digital transmission is larger than "Tc" the communication distorts.

The equation 5.5 describes that in multi-path environment, the channel gets selective and Transfer function is observed to change from 0 to 2a (Band stop or Notch filter).This relates Bc with the delay time (τ) difference between two paths and that is given as:

$$B_C = \frac{1}{\tau_1 - \tau_0} \qquad 5.5$$

5.2 BAN channel in indoor environment:

In indoor environments, the propagation of the electromagnetic waves give rise to stationary waves owing to the interference of direct and indirect waves (reflected by wall etc). Corresponding to this phenomenon, maxima and minima are expected to be observed. For instance, if a receiving antenna is made to move with velocity v, the time between each maxima and minima is of the order of t= λ/2v. This time is very short that is around 100ms at 2.4GHz and represents fast fading.
The physical modelling of moving BAN channel in the indoor environment depicts that at receiver the signal is received directly (by body surface waves) and indirectly (by walls reflected waves). It is found similar to the model COST-207 that is used for GSM where impulse response of the Finite Impulse Response (FIR) filter represents a multi-path scenario. The analysis also reveals that more receiving antenna is close to the reflectors, highly dynamic is the received signal. Similarly smaller indoor size is observed to offer immense reflections thus dominating NLOS communication and yielding Rayleigh type Cumulative Distribution Function (CDF) curves while larger size is found to exhibit LOS communication that is confirmed by Rice type CDFs.

Due to Doppler's effect the channel modulation is found to distort the carrier signal when two carriers are 2fd distance away. It is found that in NLOS case the number of reflected waves form a continuous spectrum that spreads to several Hz. It is composed of leading stronger direct wave that is flanked by nearly equivalent reflected rays as is depicted in Figure5.1 however, Doppler effect influences these carrier signals and normal walking speed (0.8m/s) introduces a frequency shift up to 5/6 Hz.

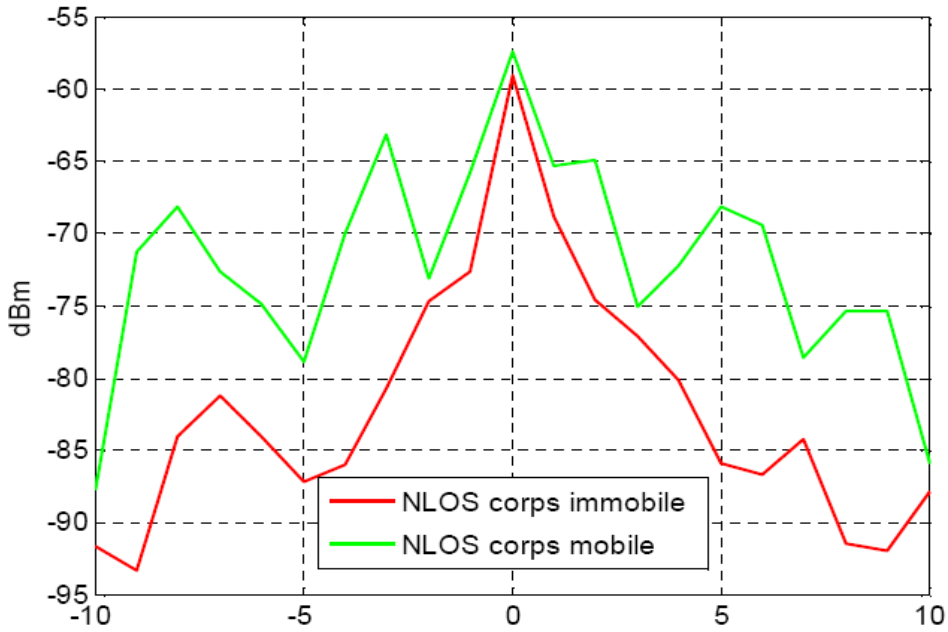

Figure5.1: Frequency in Hz surrounding 2.4GHz

5.2.1 Main channel parameters [4]

Cumulative Distribution Function (CDF):
It helps to know the probability of the received signal strength not to cross certain limit and to stay below it.

Time Autocorrelation:
This function helps to identify the coherence time used and to extract slow and fast fading of the received signal. Generally correlation of 0.5 or less is recommended to ascertain the better autonomy among signals. A coherence time of 100ms is observed for fast fading and 4s for slow fading.

Level Crossing Rate (LCR):
It allows to recognise the frequency of passing of the amplitude of the signal that is estimated to be around -3dBc with reference to the RMS value of the signal and equal to fd. One finds that the passages are few for weak and strong amplitudes but frequent for amplitudes that rest around RMS value of the signal that is with Doppler of 7.2 Hz at 2.4GHz, LCR is found to be maximum at 7.8 Hz that is very close to fd(7.2 Hz).

Average Fading Duration (AFD):
It represents the average fading duration for a given threshold, generally with reference to RMS value of the signal and it helps to fix the sampling time to correctly analyse the signals in BAN.

$$AFD.LCR=Prob(x<R)$$

Where Prob(x<R) correspond to CDF of the signal.

AFD and LCR allow to evaluate the performance of digital modulation in the form of channel characterization and bear great importance in designing BAN and mobile channel links.

5.2.2 Statistical channel modelling:

This type of modelling envisages the use of statistical laws which narrate the behaviour of the combination of direct and reflected signals carrying different amplitudes and phases in the static or dynamic environments. These include [4];

Rayleigh:

It takes into account the incidence of uniformly distributed NLOS rays being reflected with similar intensities. This is evaluated in terms of Probability Distribution Function (PDF) and Cumulative Distribution Function (CDF) which are given as:

$$\text{PDF:} \quad f(x) = \frac{x}{\sigma^2} e^{\frac{x^2}{2\sigma^2}} \qquad 5.6$$

$$\text{CDF:} \quad F(x) = 1 - e^{\frac{x^2}{2\sigma^2}} \qquad 5.7$$

Where $2\sigma^2$ is the average power of the signal with σ in volts.

Rice:

It assumes direct links between the antennas and accounts stronger signals as compare to the reflected ones. Its PDF and CDF are given as:

$$\text{PDF:} \quad f(x) = \frac{x}{\sigma^2} e^{\frac{x^2+r_0^2}{2\sigma^2}} I_0\left(x\frac{r_0}{\sigma^2}\right) \qquad 5.8$$

$$\text{CDF:} \quad F(x) = 1 - Q\left(\frac{r_0}{\sigma}, \frac{x}{\sigma}\right) \qquad 5.9$$

Where I_0 is the zero order Bessel function and Q is Marcum function.

The CDFs based upon Rayleigh and Rice models are extensively used in analysing and comparing the diversity gains in rich fading environments.

5.3 Antenna measurements (non planar feeds):

Based upon the simulated results presented in section 4.1 through section 4.5, the antenna is fabricated for which the design structures are photographed in Figure5.2 and measured results are presented in Figure 5.3 through Figure 5.6

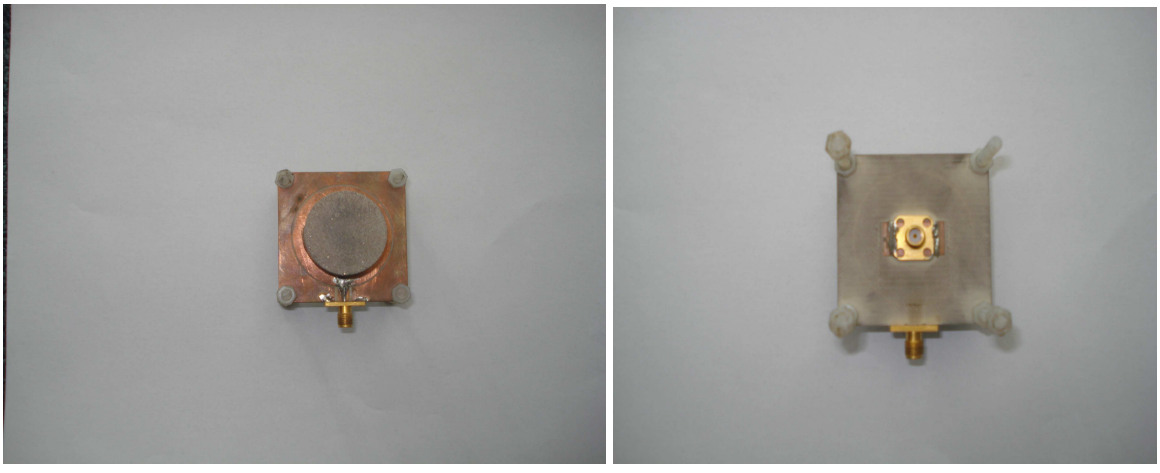

(a) (b)

Figure5.2: Fabricated antenna with non-planar DRA feed (a) top side (b) bottom side

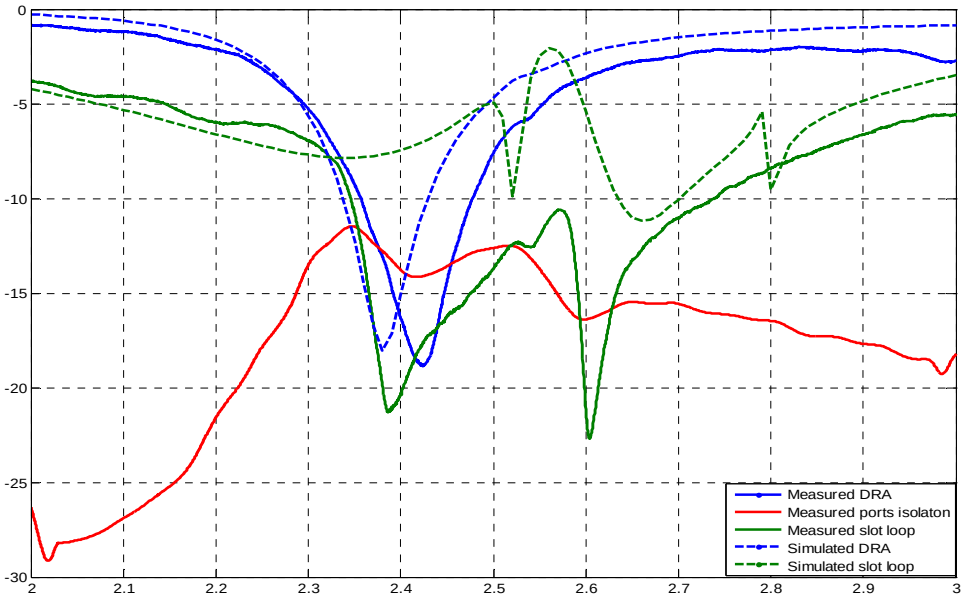

Figure5.3: Slot loop and DRA measured and simulated return loss and ports isolation curves

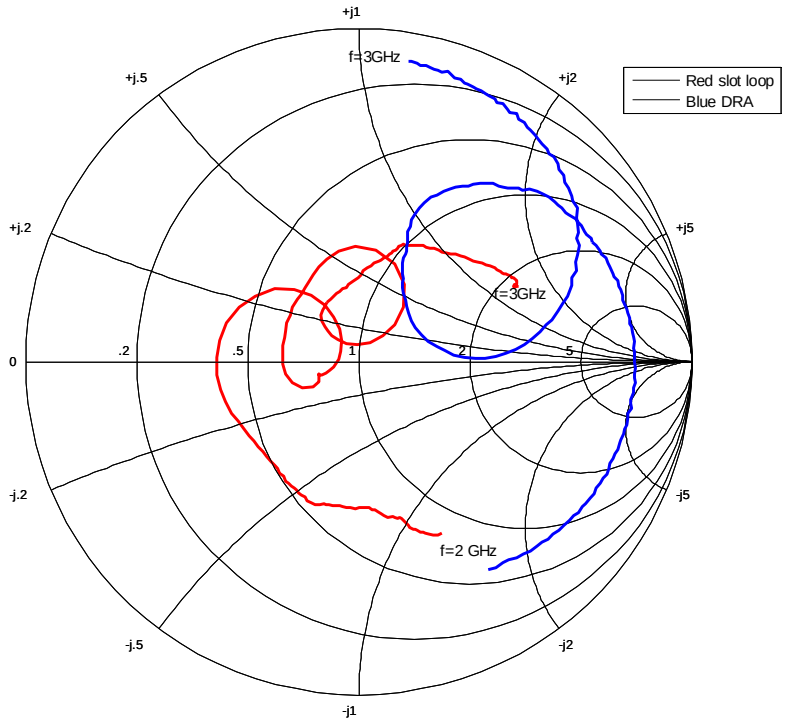

Figure5.4: Slot loop and DRA measured smith chart curves

The two ports return loss and isolation curves are presented in Figure5.3. The -10dB return loss for slot loop ranges from 2.34 GHz to 2.73 GHz while for DRA from 2.36 GHz to 2.48 GHz thus yielding impedance bandwidths of 15% and 4.95% respectively. This offers a common bandwidth of 4.95% centred around the working frequency of 2.4GHz with ports isolation of -13dB. Compared to the simulated results, the widening of the bandwidths can be

attributed to the exact DRA loading and bonding effects. As is observed from Figure5.3 that slot loop undergoes two close resonances and same can be noted from the simulated results.

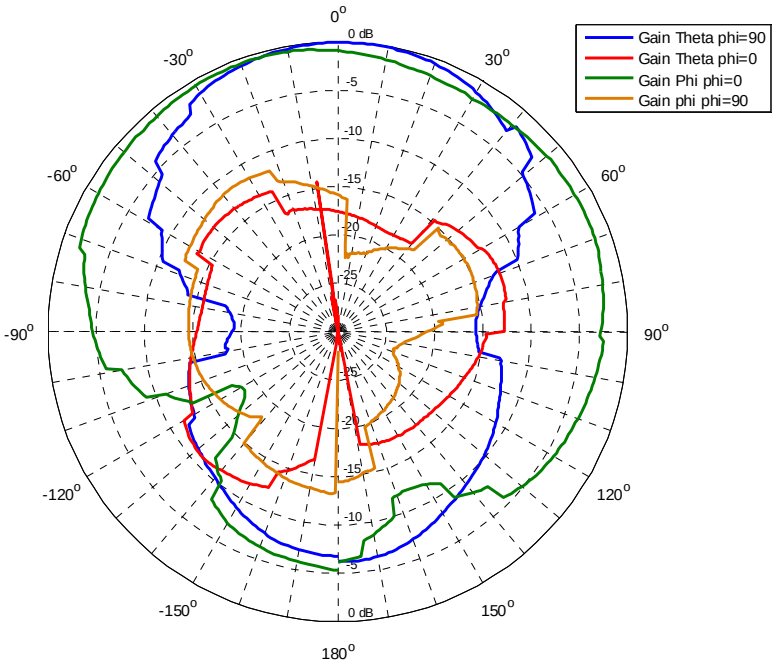

Figure5.5: Slot loop measured broadside radiation patterns in yoz (phi=90°) and xoz (phi=0°) planes.

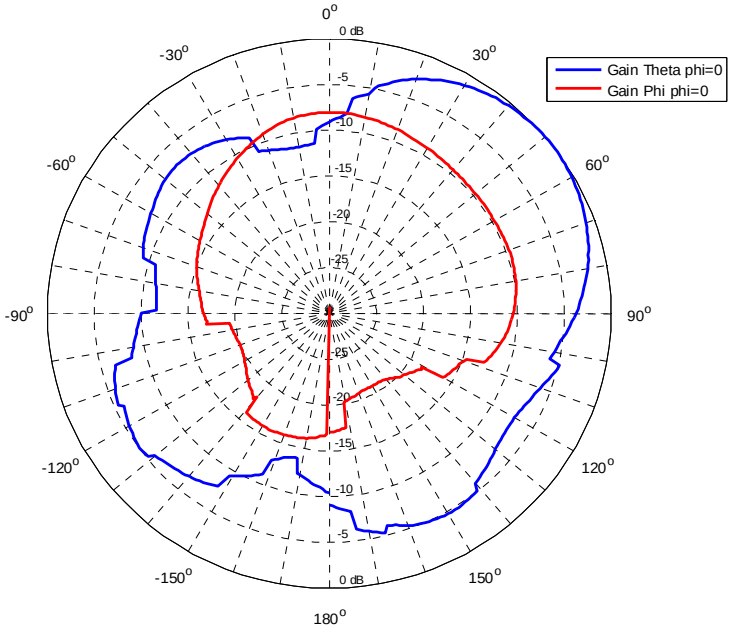

Figure5.6: DRA measured end-fire type radiation patterns in elevation plane.

The slot loop's broadside radiation patterns measured in free space are presented in Figure 5.5. It is observed that yoz-plane radiation patterns are narrow while xoz-plane exhibits wider radiation patterns and it is exactly what is observed in the simulated results (section4.2). The cross polarization, on the other hand in the broadside direction are found to be -15dB less than the co-polarization levels.
The DRA's end-fire type measured radiation patterns in the free space are presented in Figure 5.6. The xoz-plane co-polarization pattern is nearly symmetric, though a small distortion is observed towards left horizon and possibly it could be due to the presence of connector or CPW line etched on the ground plane. However, the patterns offer important realization that it bears a clear null towards its broadside direction.
Thus both antennas are found to establish dual radiation patterns one with estimated gain of 2.3dBi in the broadside direction while the other with a gain of 0dBi in the omni-direction with null towards broadside. These patterns are to be exploited to observe certain value of DG.

5.3.1 Diversity Gain Analysis:

The diversity gain test is pictured in Figure5.7 where a person wearing both the transmitting (top loaded monopole) and receiving diversity antenna (slot loop and DRA) is made to perform random walking motion so as to depict real type situation. The rich fading environment is assured inside the laboratory with randomly placed scattering objects such as chairs, desks, variety of instruments and computers etc.

Figure5.7: A person is walking in the laboratory by wearing diversity antenna in receiving mode at chest while top loaded monopole in transmitting mode at belly.

The diversity antenna is planted on the body at three different locations that is at chest, hip and at back to evaluate its DG performance. The elastic belts worn at belly and chest positions hold both the transmitting and diversity receiving antennas and help to slide them around easily. As this antenna is object to be mounted on the body and integrated into specially designed wearable kits or uniforms or in backpacks or chest packs. Assuming this type of

usage and avoiding slot loop's sensitivity to the proximity of skin, the antenna is planted at a height of 10mm under which a clothing pad was used. The measurement campaign was launched by placing a transmitting monopole antenna operating at 2.4GHz with 0dBm power held at belly position. The Agilent's VNA was calibrated in the power receive mode for a sample time period of 60 seconds and connected to the diversity antenna. This scheme then forms three on the body channels which are referred to as (1) *Belly to chest position (0°)* (2) *Belly to hip position (90°)*(3) *Belly to back position (180°).* Angles presented in parenthesis help to quickly understand angular position between the transmitting and receiving antennas.

(1)Belly to chest position (0°):
The diversity analysis tests for this situation are presented in Figure5.8 through Figure 5.10.

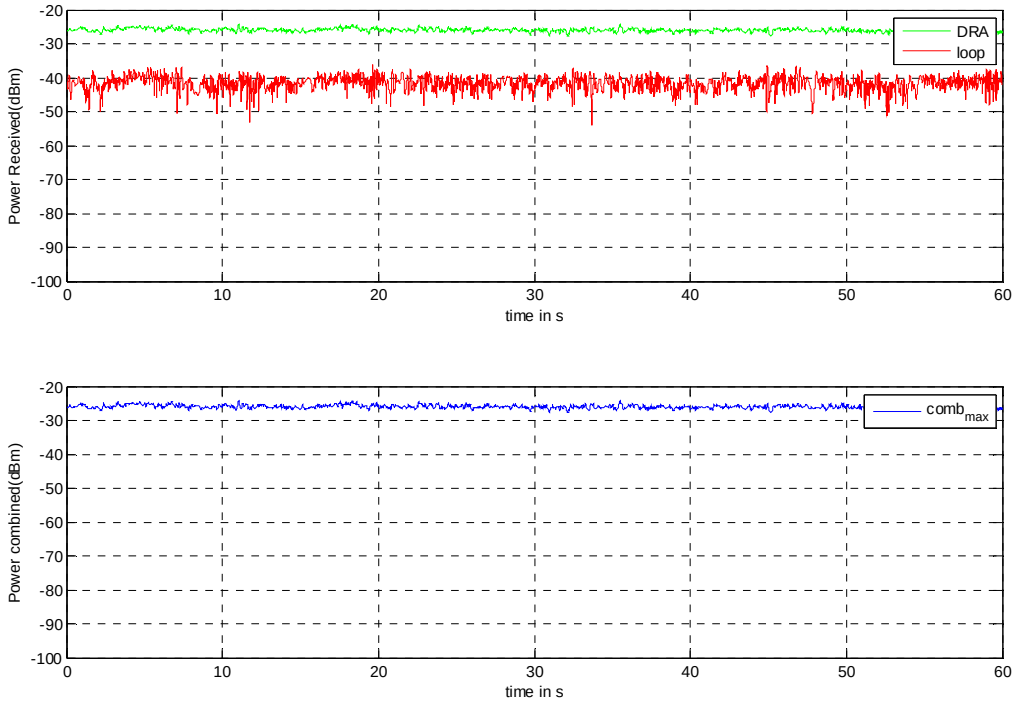

Figure5.8: Slot loop, DRA and their combined power reception patterns representing clear power imbalance between the two receiving branches.

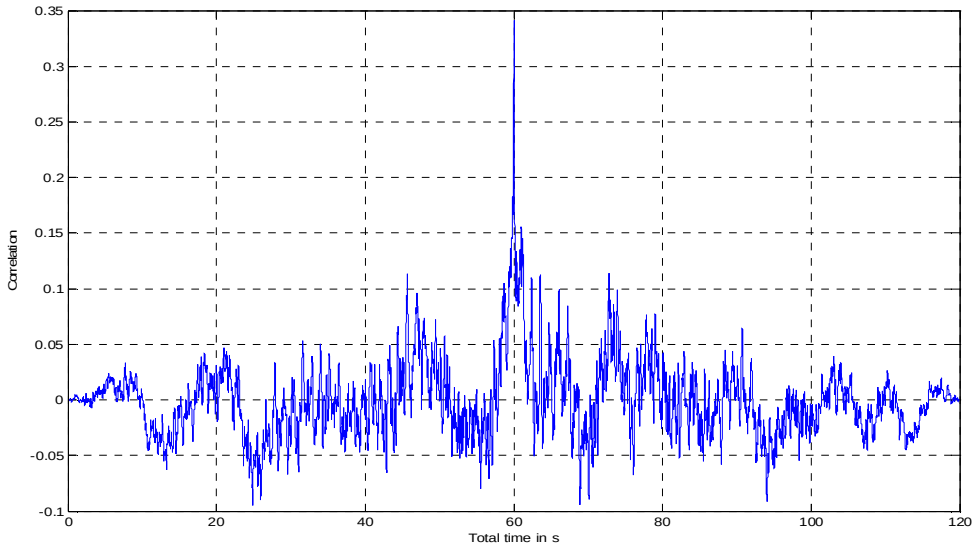

Figure5.9: Slot loop and DRA branches representing a maximum correlation of 0.35 between them.

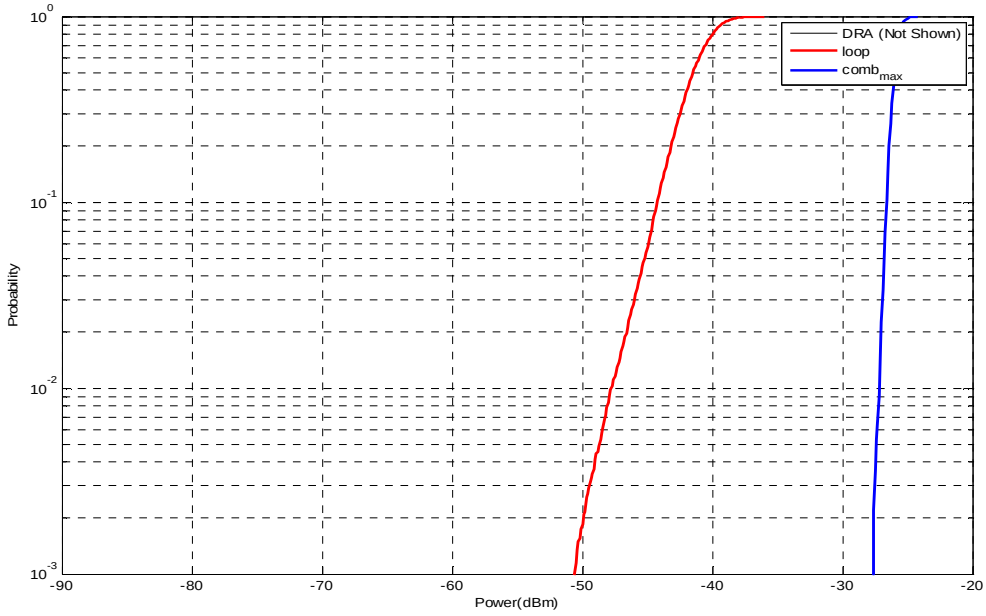

Figure5.10: CDF plots for slot loop and DRA representing no DG.

(2)Belly to hip position (90°):
The diversity analysis tests for this situation are presented in Figure5.11 through Figure 5.13

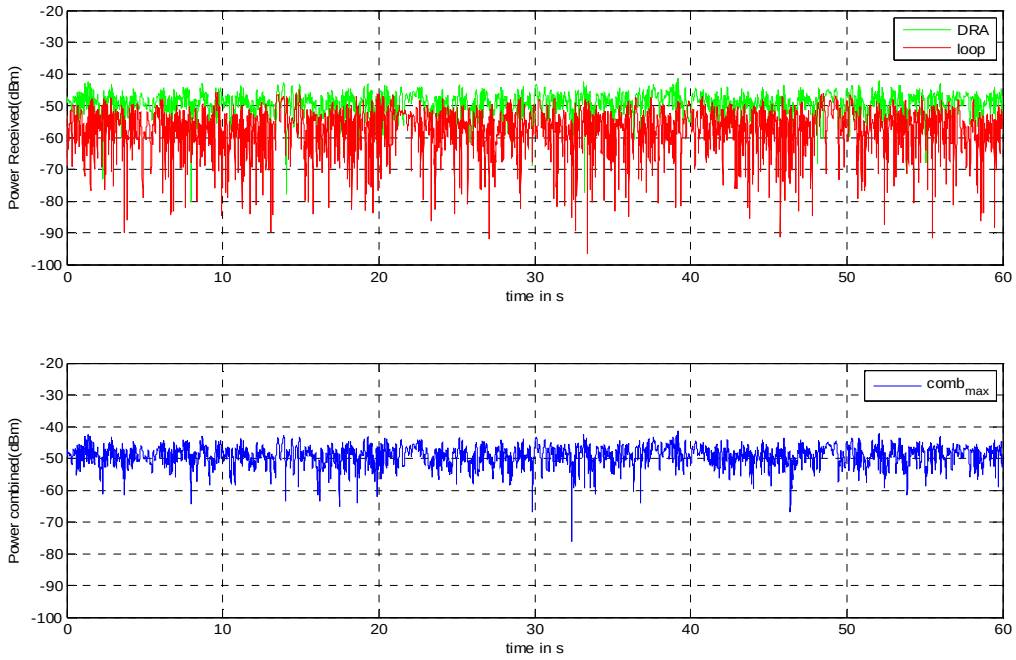

Figure5.11: Slot loop, DRA and their combined power reception patterns representing minor power imbalance between the two receiving branches.

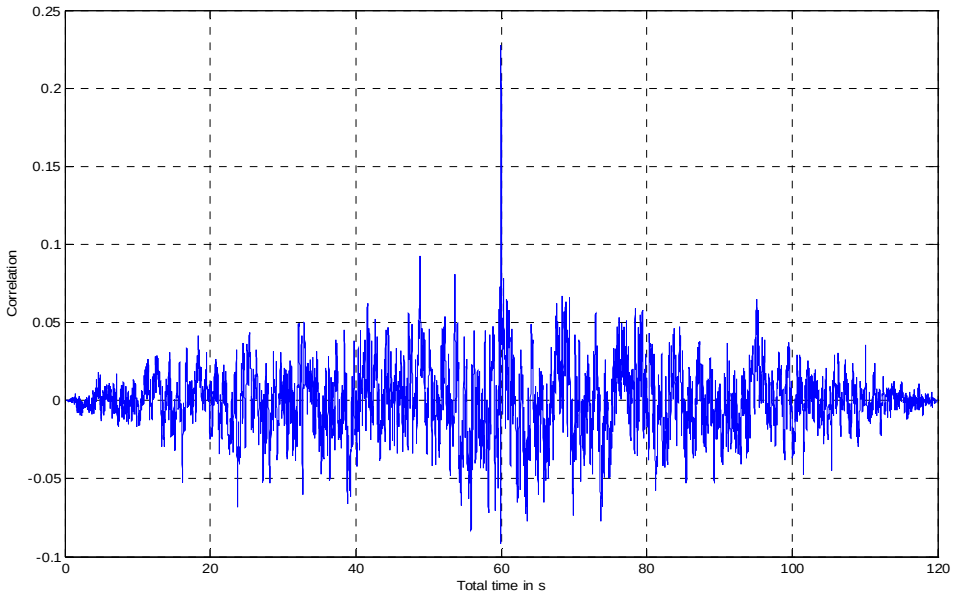

Figure5.12: Slot loop and DRA branches representing a maximum correlation of 0.23 between them.

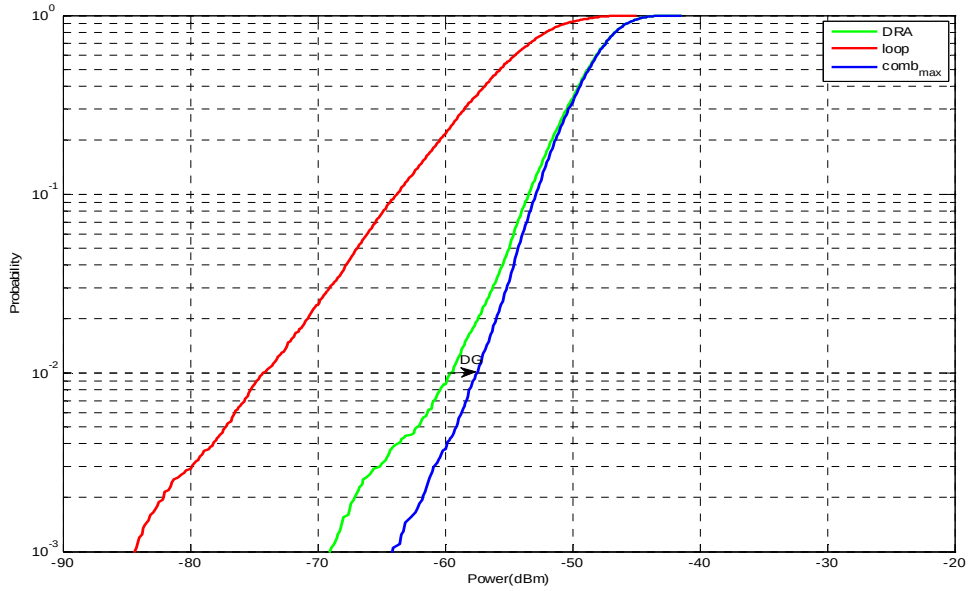

Figure5.13: CDF plots for slot loop and DRA representing about 3dB DG.

(3)Belly to back position (180°):

The diversity analysis tests for this situation are presented in Figure5.14 through Figure 5.16

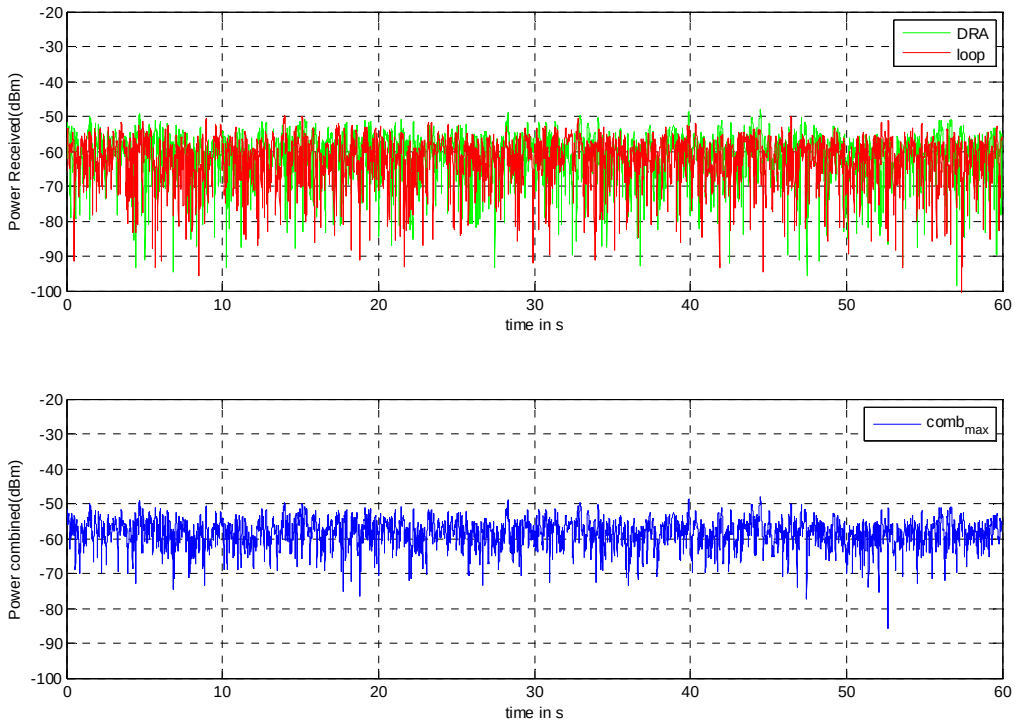

Figure5.14: Slot loop, DRA and their combined power reception patterns representing no power imbalance between the two receiving branches.

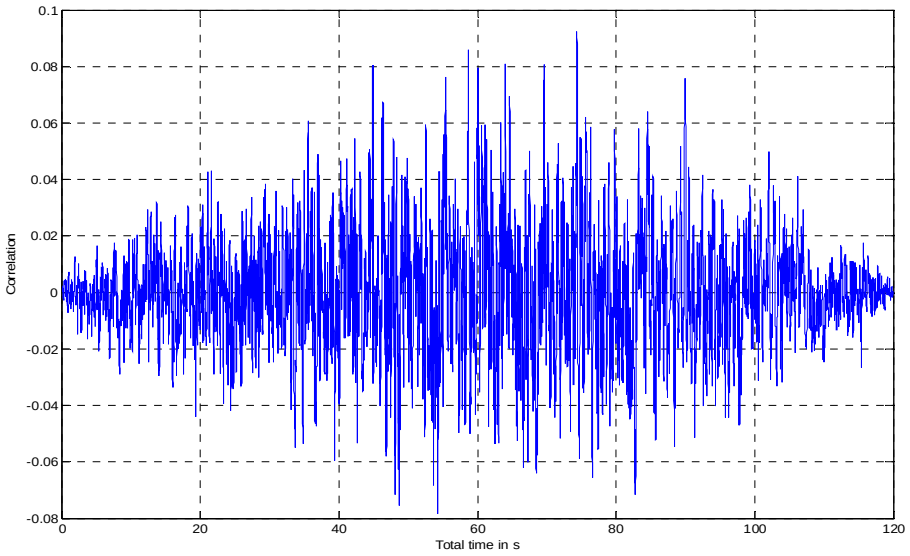

Figure5.15: Slot loop and DRA branches representing a maximum correlation of 0.08 between them.

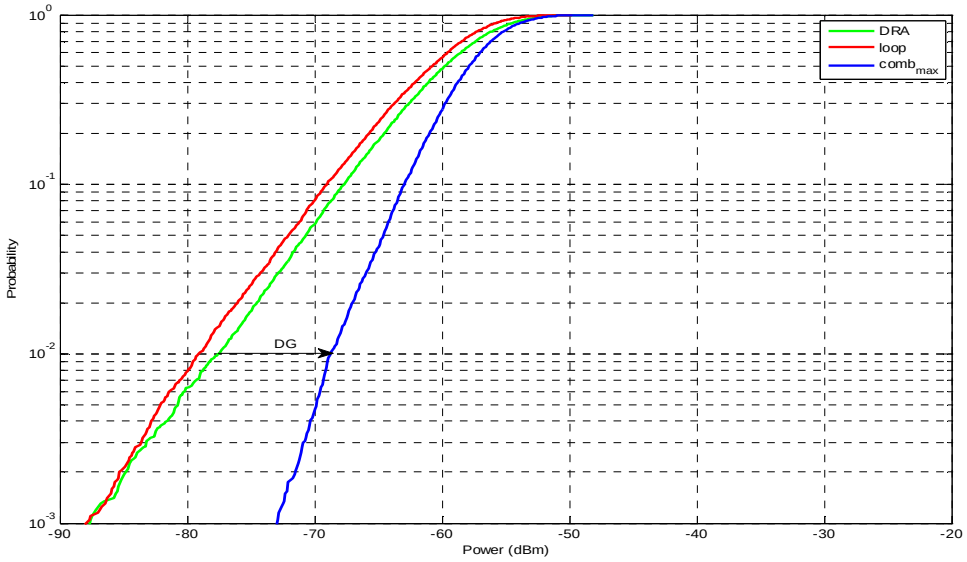

Figure5.16: CDF plots for slot loop and DRA representing about 9dB DG.

In all cases such as depicted in Figures5.9, 5.12, 5.15 the Envelop Correlation Factor (ECF) factor, that is considered to be a common yardstick to measure un-correlation or independence among replica of signals, is found to remain less than 0.4. The power samples of these replica collected at two different branches of the diversity antenna are combined together by Selection Combining (SC) method which are given in Figures5.8, 5.11,5.14 and then CDF curves are plotted at an outage probability of 1% which are depicted in Figures5.10, 5.13 and 5.16 for DG calculations.

For channel (1) *Belly to chest position (0°),* the DG is observed to be null, partly because of Line Of Sight (LOS) link between transmitting and receiving antennas but :mainly because it offers a clear power imbalance (in favor of DRA) that in turn is not able to realize the diversity performance. This is elaborated in graph curves presented in Figure5.10 where it can be noted that DRA's received replica are much stronger than slot loop's so that is favored by SC to yield no DG at all.

For channel (2) *Belly to hip position (90°),* a DG of 2dB is reported as now link is partially LOS and partially Non-LOS (NLOS), so owing to the contribution of faded signals impinging upon the antenna, though still exists a lower power imbalance favors a smaller improvement in DG value. This is presented in Fig 5.13 where an arrow marked shift from comparatively stronger DRA signal to CDF curve of combined signal is referred to as DG.

For channel (3) *Belly to back position (180°),* a DG of 9.5dB is observed as now both antennas are in the NLOS condition and both branches of the diversity antenna freely collect only pure replica of signals faded from the surrounding objects randomly placed in the laboratory environment .This mechanism totally eliminates the power imbalance factor in which SC gives nearly equal weight to both branch signals thus introducing a larger DG value. This is narrated in Fig 5.16 where an arrow marked shift from relatively stronger DRA curve to combined signal curve represents a maximum DG.

- Though overall performance of the antenna is found to be fine but its non planar feed structure (Port2-DRA) restricts its body wearable applications so an antenna with both planar feeds is presented.

5.4 Antenna measurements (planar feeds):

Based upon the simulated results presented in section 4.6 to section 4.7, dual pattern diversity antenna with purely planar feed structures is fabricated for which the design structures are photographed in Figure5.17 and measured results are presented in Figure 5.18 through Figure 5.21

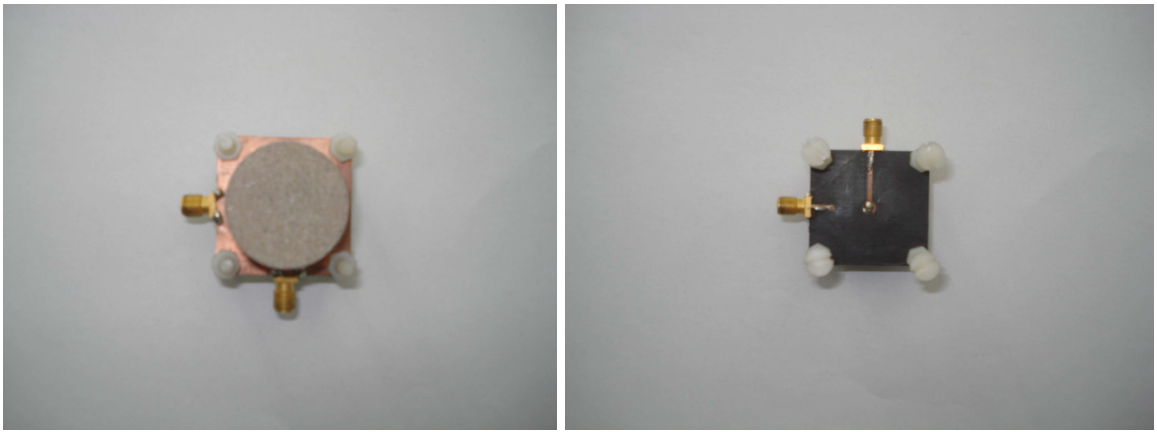

(a) (b)

Figure 5.17: Fabricated antenna with both planar feed (a) top side (b) bottom side

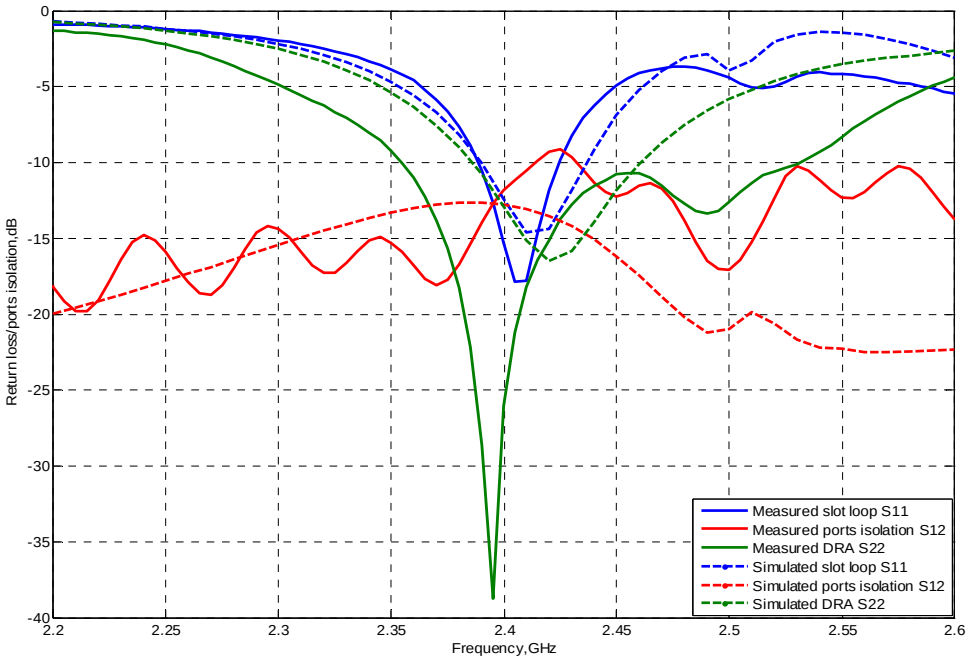

Figure5.18: Slot loop and DRA measured and simulated return loss and ports isolation curves

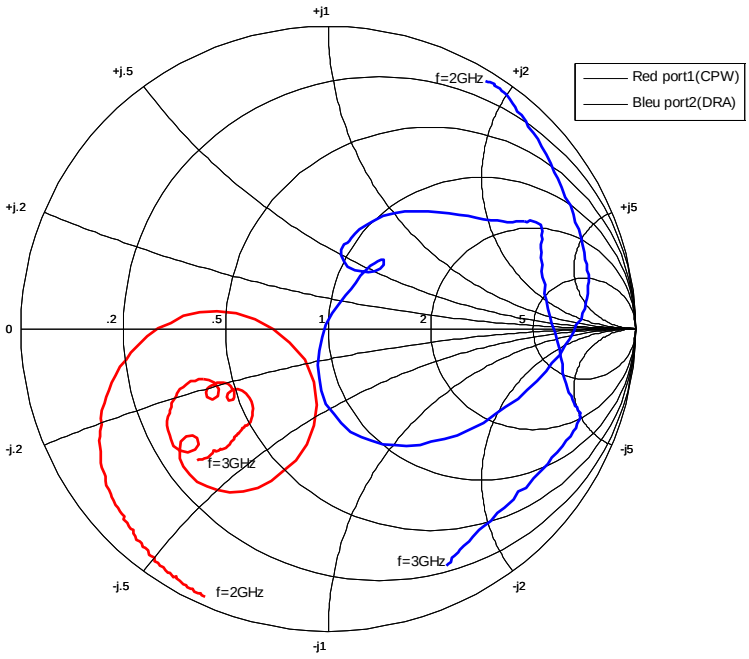

Figure5.19: Slot loop and DRA measured smith chart curves

The measured return loss and isolation curves are presented in Figure5.18. The return loss bandwidths (≤ -10dB) for port 1 (Slot Loop) and port 2 (DRA) are observed to be in the range of (2.387GHz-2.425GHz) and (2.35GHz-2.45GHz) respectively thus yielding a common bandwidth of 1.5%. The ports isolation is found to be -12dB at 2.4 GHz which is sufficient for an efficient diversity recombination of the signals. For both ports the smith chart is presented in Figure 5.19 that illustrates respective antenna's impedance response.

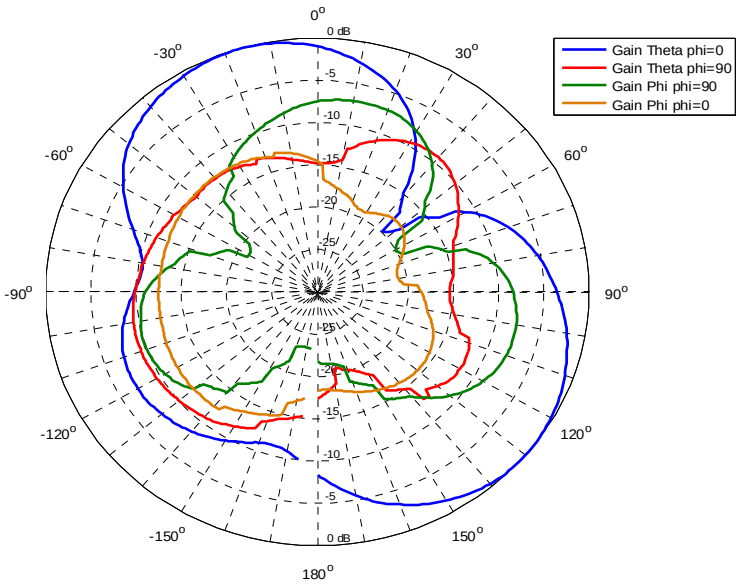

Figure5.20: Slot loop measured broadside radiation patterns in xoz and yoz planes.

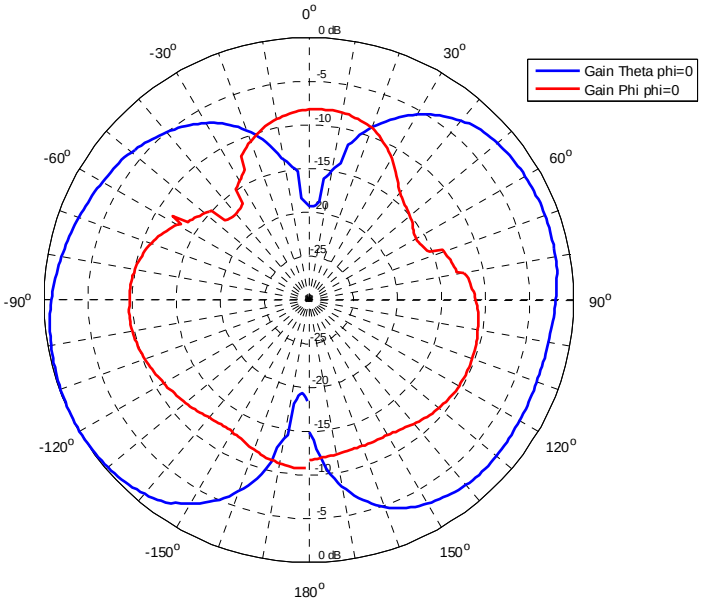

Figure5.21: DRA measured end-fire type radiation patterns in elevation plane.

The Slot Loop's broadside radiation patterns in free-space are presented in Figure5.20. An asymmetry is observed in the xoz(E) and yoz(H) planes while cross polarizations are found to be comparatively small. A large back radiation nearly of the same size as of broadside is attributed to the use of a small ground plane and the lack of slot loop's backing plate. The DRA's end-fire radiation pattern presented in Figure5.21 shows a purely symmetric shape in the xoz(E)-plane (elevation). It leads to the conclusion that the DRA's radiation pattern is less affected by the ground plane size compared to the slot loop.

5.4.1 Diversity Gain Analysis:

The experimental setup is nearly same as employed in the case of non-planar feed structure antenna. The transmitting monopole antenna mounted on a small ground plane (30×30 mm) is placed 10 mm above the body and fixed on a large elastic strip around the belt that can slide along it. The receiving diversity antenna is fixed on another strip at the centre of the chest. Foam spacers of 10 mm mounted on each antenna backside ensure a fixed antenna height above the body and strongly limit the antenna detuning due to the body.
Three links are studied: Link1: chest-to-belly (0°). Link2: chest-to-hip (90°). Link3: chest-to-back (180°), where the angle indicates the corresponding rotation of the transmitter with respect to the belly position. For the signal acquisition, an Agilent network analyzer E8361C PNA is used as a two-port narrowband receiver with an IF bandwidth set to 10 kHz. The PNA is synchronized to the transmitter whose power level is set to 0 dBm. For a given link, a measurement campaign was composed of three runs repeated three times. For each run, a set of 20 001 samples is recorded during 60 s (one sample each 3 ms). The person under test simulates a slow walk with large arms movements in a lab room that is a rich scattering environment with desks, shelves, chairs, etc…

The diversity gain test results for these links are presented in Figure5.22 through 5.30.

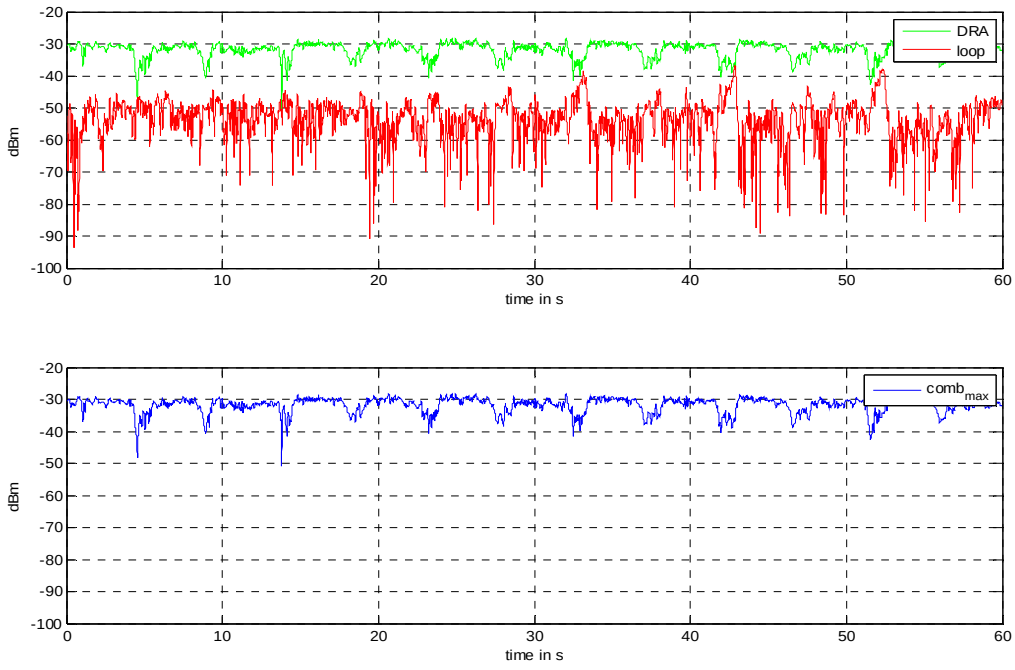

Figure5.22: Slot loop, DRA and their combined power reception patterns representing clear power imbalance between the two receiving branches.

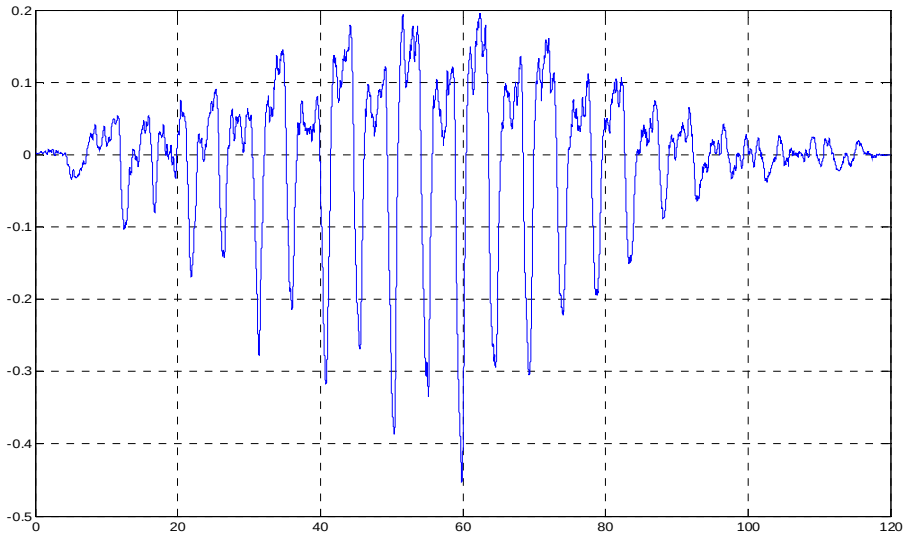

Figure5.23: Slot loop and DRA branches representing a maximum correlation of 0.2 between them.

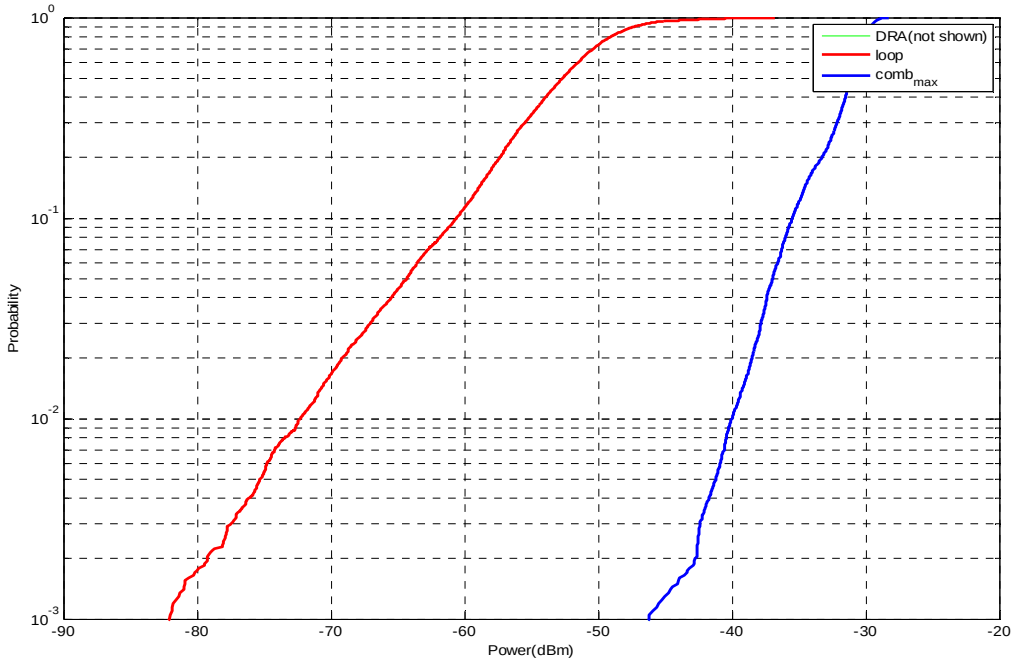

Figure5.24: CDF plots for slot loop and DRA representing no DG.

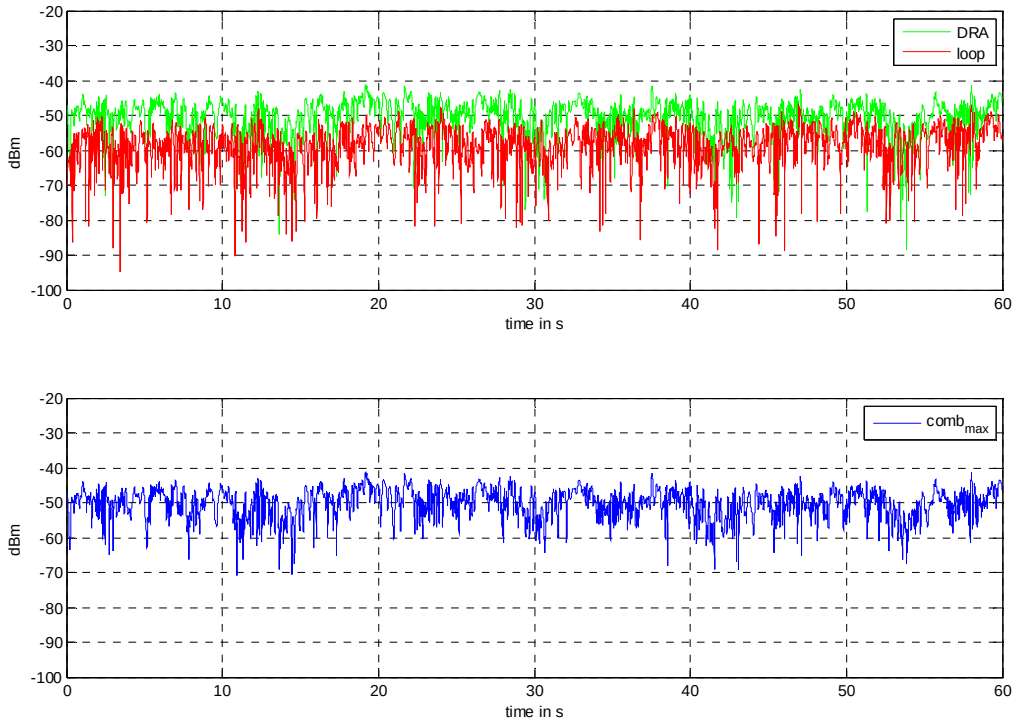

Figure5.25: Slot loop, DRA and their combined power reception patterns representing minor power imbalance between the two receiving branches.

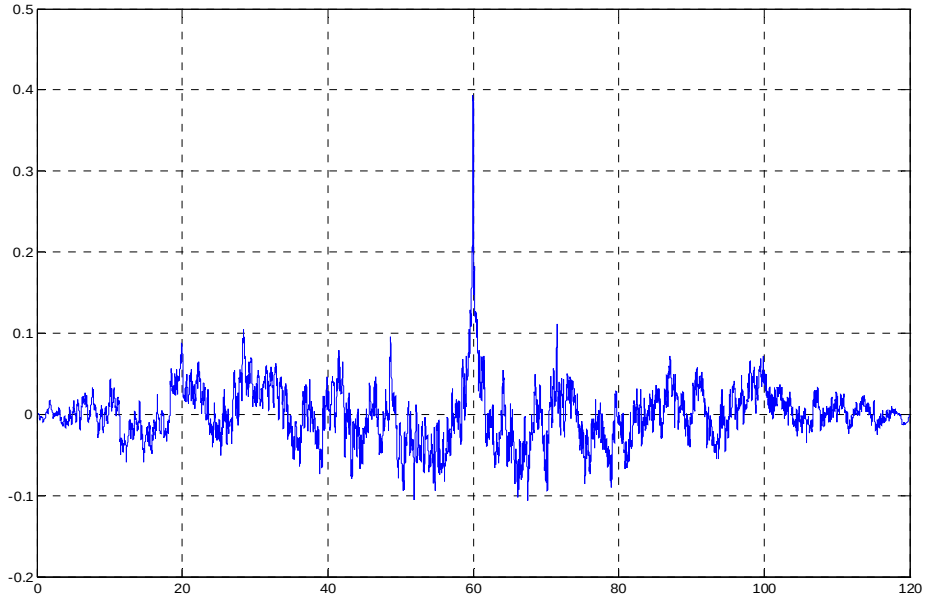

Figure5.26: Slot loop and DRA branches representing a maximum correlation of 0.4 between them.

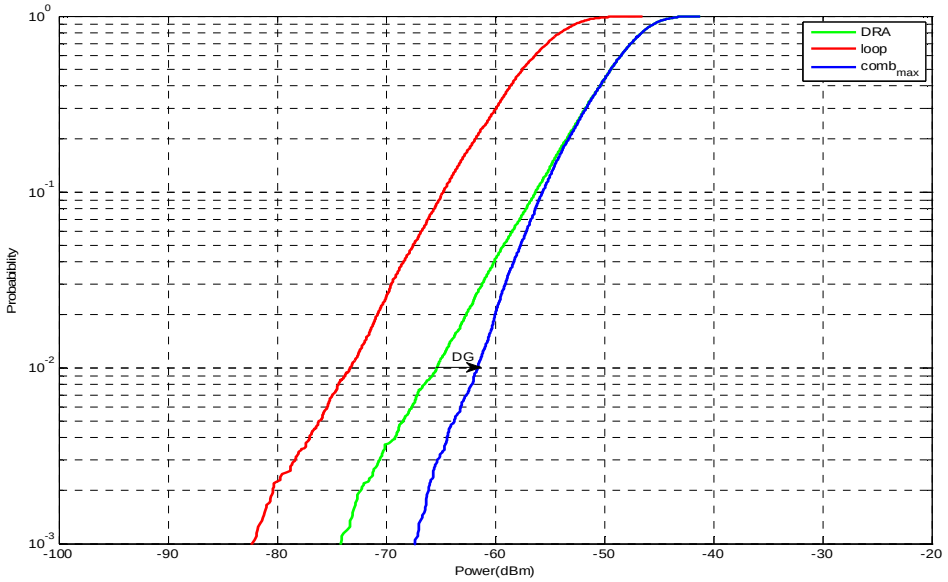

Figure5.27: CDF plots for slot loop and DRA representing about 4dB DG.

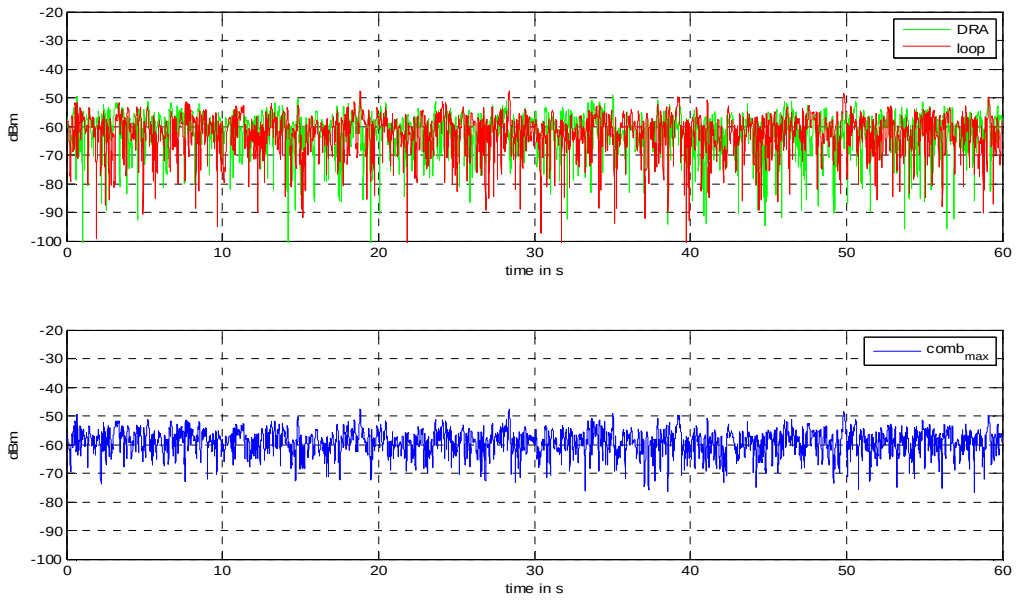

Figure5.28: Slot loop, DRA and their combined power reception patterns representing no power imbalance between the two receiving branches.

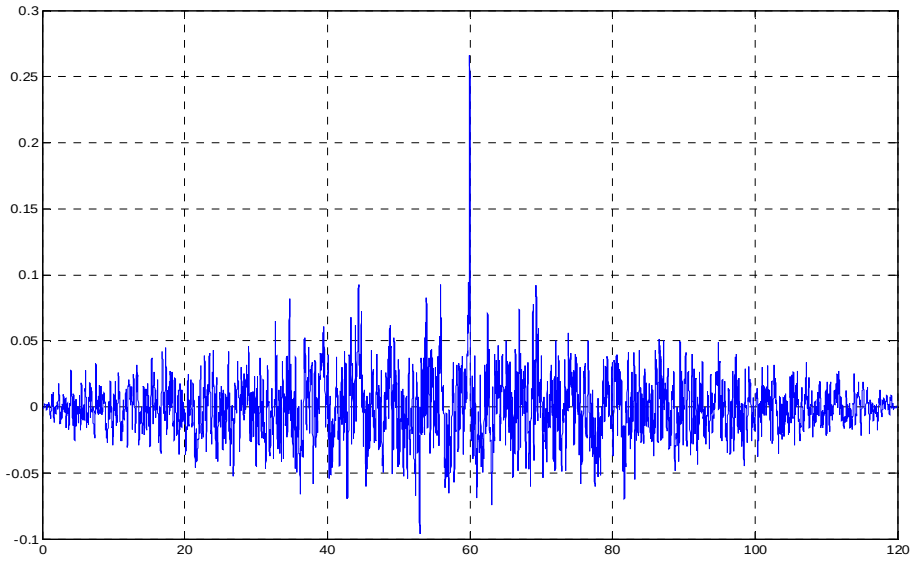

Figure5.29: Slot loop and DRA branches representing a maximum correlation of 0.27 between them.

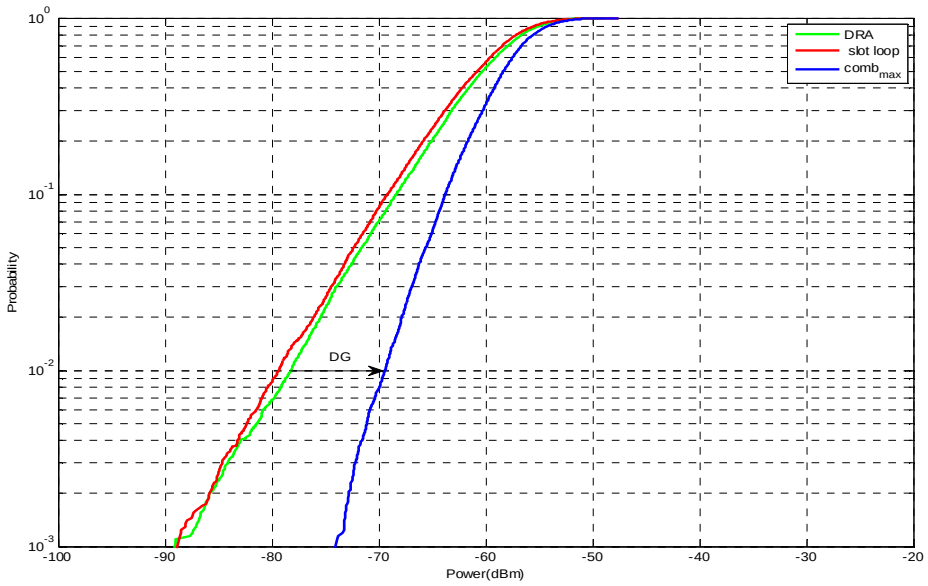

Figure5.30: CDF plots for slot loop and DRA representing about 9.5dB DG.

In all cases, the Envelop Correlation Factor (ECF) factor between the signals received at both ports remained less than 0.4 which are presented in Figures 5.23, 5.26 and 5.29. The power samples are combined together by the selection combining method and then CDF curves are plotted. For DG calculations, the outage probability of 1% is used. For channel (1) chest-to-belly, no DG was observed, possibly because of Line Of Sight (LOS) link between transmitting and receiving antennas with a clear power imbalance that in turn nullifies the

diversity performance. This situation is elaborated in Figure5.24. For channel (2) chest-to-hip, a 4dB DG was reported as now the link is partially LOS and partially non-LOS (NLOS) with a lower power imbalance. The resultant graph is depicted in Figure5.27. For channel (3) chest-to-back, a 9.5 DG was observed as now both antennas are in NLOS conditions and both branches of the diversity antenna collect only pure replica of signals faded from the surrounding objects present in the laboratory thus eliminating the power imbalance factor. This can be viewed from the results depicted in Figure5.30.

5.5 Conclusion:

Both antennas, one with non-planar feeds (slot loop is excited by CPW that is planar but DRA is excited by vertical monopole) and other with planar feeds exhibiting dual radiation pattern antenna are successfully measured and tested on the body and then analyzed into different channels schemes. The non-planar feeds antenna yields wider (4.95%) and the planar feeds antenna offers narrower (1.5%) common impedance bandwidths respectively. In both cases, a maximum value of DG=9.5dB is achieved when diversity performance tests are carried out in rich fading environments. This value is close to the one (10 dB) theoretically reached in a pure Rayleigh environment and is obtained with efficiencies of 70%/65% and 85% for the slot loop and the DRA respectively. Therefore, we conclude that this antenna could be used on the shoulders or the chest of professional clothes (firemen, policemen, soldier) where full planar integration is not a key issue but where the communication must be efficient in harsh environments and for various gestures, positions and scenarios.

References:

[1] F.Perez and P.Marino Espineira “Modeling the Wireless Propagation channel A Simulation Approach with MATLAB” University of Vigo, Spain.

[2] A.A Serra, P.Nepa, G.Manara, and P.S Hall “Diversity Measurement for On-Body Communication Systems” IEEE ANTENNAS AND WIRELESS PROPAGATION LETTERS,VOL. 6, 2007.

[3] Imdad Khan, Peter S.Hall Andrea A.Serra, Anda R Guraliuc and Paolo Nepa “Diversity Performance Analysis for On-Body Communication Channels at 2.45GHz” IEEE TRANSACTIONS ON ANTENNAS AND PROPOGATION.VOL, 57, NO.4, APRIL 2009.

[4] Thierry Emmanuel Pires ALVES, PhD Thesis “ CONCEPTION D’ANTENNES POUR LE RESEAU BAN et MODELISATION DU CANAL DE PROPAGATION“ Université Paris Est Marne La Vallée France.

[5] T.Alves, B.Poussot and J.M.Laheurte “PIFA-Top loaded Monopole Antenna with Diversity Features for WBAN Applications” IEEE ANTENNAS AND WIRELESS PROPAGATION LETTERS, Volume 10, 2011, Pages 693-696.

Chapter 6

Conclusion and Prospects

Contents

6.1 Overall conclusion

For tracking applications in the satellite and radar areas, DRA present several advantages over printed antennas: larger elevation coverage, higher efficiency in the X-band and above, high polarization purity. The first part of the thesis was dedicated to DRA designs for this purpose, i.e., high polarization purity, two ports dual linearly polarized X-band antennas. In reported literature, there is a lack of symmetry in the dual port radiation patterns that is very important for dual linear or circularly polarized applications. This was observed that due to improper excitation methods inefficient and uneven energy coupling mechanisms might have excited some parts of unwanted modes thus disturbing the symmetry of the desired radiation patterns. To avoid this problem, it is very important to employ such a feeding mechanism that precisely excites the required mode and suppresses the unwanted one. To accomplish it, two orthogonal H-shaped aperture slots were successful fitted within the prescribed bottom area of the cylindrical DRA to excite TM110 mode that yields broadside radiation pattern. H-shaped slots were found flexible in adjusting to the confined area below the DRA. This technique also improved level of coupling owing to smooth distribution of E-fields within the slot. One such

DRA with improved performance in terms of better ports isolation and symmetric radiation patterns has been successfully designed. The common impedance bandwidth (5.9%) though wider enough for a number of applications yet it needs to be improved. Due to high temperature tolerance and frequency stability features, this antenna with the exhibition of excellent radiation efficiency (98%) has promising applications in the satellite and radar communication systems.

The other aspect of the work was to design a dual radiation pattern, compact diversity antennas to be worn on the body to seek Diversity Gain (DG). Though two such autonomous antennas, one with broadside and the other with end-fire types of radiation patterns is not difficult to realize. The main issue was to integrate both of them with each other such that both operate at same 2.4GHz frequency while maintaining good level of ports de-coupling and thus assuring pure broadside and end-fire types of radiation patterns. Slot loop and DRA branches have been successfully integrated to yield broadside and end-fire types of radiation patterns. This diversity antenna is composed of two design structures.

As for first design, to feed these branches, Coplanar wave guide (CPW) was assigned to the slot loop and vertically embedded monopole from below the ground plane to the DRA. It could be termed as compact diversity antenna but with non-planar feed to DRA. The second design comprises of purely planar feeds in which both branches are fed by microstrip lines etched on the opposite side of the ground plane that contains the slot loop encircling the DRA. Both of these diversity antennas offer good level of ports de-coupling (-14dB) and exhibit dual radiation patterns. The first antenna is found to yield wider common impedance bandwidth (4.95%) with both radiation patterns symmetric in the elevation plane. The second diversity antenna offers narrower common impedance bandwidth (1.5%) with broadside radiation pattern slightly asymmetric and end-fire radiation pattern purely symmetric. Both antennas offer different types of advantages, the first one though not purely planar but yields wider impedance bandwidth while the second though lacks in common bandwidth but its pure planar structure enhances its usability upon the body surface.

After successful measurements, these diversity antennas were tested on the body to evaluate their DG performance in a rich fading environment inside the laboratory. Assuming slot loop's sensitivity to the proximity of skin, the antenna was planted at a height of 10mm under which foam spacer was used. The measurement campaign was launched by placing a transmitting monopole antenna operating at 2.4GHz with 0dBm power held at belly position while receiving diversity antenna at 3 distinctive body positions that is at chest, hip and at back. This scheme forms three on the body channels which are referred to as (1) Belly to chest position (0°) (2) Belly to hip position (90°) and (3) Belly to back position (180°). A maximum value of DG=9.5dB was achieved in channel3 while other channels exhibiting expected performance due to full or partial Line Of Sight (LOS) communication between them. Nearly same results were obtained from both diversity antennas. Therefore, it can be conclude that these antennas can be used successfully, for instance on the shoulders or the chest of professional clothes. These can also be integrated to special wearable kits to make the user to always remain connected to the distortion free communications while handling hostile or emergency situations.

6.2 Future prospects

This work has shown that DRAs offer promising applications at high frequencies due to high radiation efficiency and negligible dielectric losses. They have met successfully nearly all the requirements targeted in our research work. Though the size of the DRA in many applications such as in X band does not matter and can easily be integrated or incorporated to the desired

space. However, as a future course of works its common impedance will be improved. On the other hand diversity antenna needs further miniaturization so as to enhance its usage for on-body applications. The size of the DRA as part of the diversity antenna has a great potential to be reduced. With the commercial availability of high permittivity dielectric material these are expected to reduce in sizes. Similarly there is need to explore new range of miniaturized antennas which require simple integration techniques with DRAs and both been cohabited to each other. This strategy is expected to introduce more compactness to the overall structure and assure significant improvement in the overall performance of the diversity antenna

List of Journal publications:

1 A.M Faiz, T.Alves, B.Poussot and J.M Laheurte " Diversity antenna combining slot-loop DRA for BAN applications" ELECTRONICS LETTERS 5th January 2012 Vol.48 No.1 Pages 7-8.

2 A.M Faiz, T.Alves, B.Poussot and J.M Laheurte "Dual Linearly Polarized X-band Dielectric Resonator Antenna Yielding Symmetric Radiation Patterns" MICROWAVE AND OPTICS TECHNOLOGY LETTERS April 2012 Vol.54, No.4 Pages 999-1001.

Appendix A

Evaluation of Adhesive Material's Role in DRA Fabrications

As the DRA bonded to the feed structure and the ground plane has been estimated to be influenced by the adhesive material thus causing a change in its resonance frequency, impedance bandwidth and radiation patterns. Obviously, until this effect is duly accounted for and compensated with, the antenna can not be expected to yield the desired results [4]. Though some highly sophisticated technologies equipped with state of the art micromachining tools, are commercially available to fully exploit the fabrication tolerance in minimizing the possibility of errors but they are either too expensive or just confined to bulk productions.
Before the prototype fabrication of x band antenna takes place, first of all bonding issues are resolved while using an ordinary inexpensive adhesive material and thus tracing out a comparative shift in resonance frequency, consequent change in its impedance bandwidth and the radiation patterns.
As the DRA TM110(HEM11) mode has already been analyzed, so to seek solid conclusions the other frequently used mode TM01 is also subject to investigation and that is too employing different feed excitations that is monopole and aperture slot. For this purpose two frequencies that is 2.4GHz and 8.9GHz are chosen because of ready availability of DRAs thus composed of dielectric materials of (ε_r=30) and (ε_r=6) respectively.

A1: Antenna Designs

Two sets of DR antennas radiating in TM_{01} modes, fed by monopole and aperture slot are presented in Fig 3.35(a) & (b) while their design parameters are enlisted in Table3.

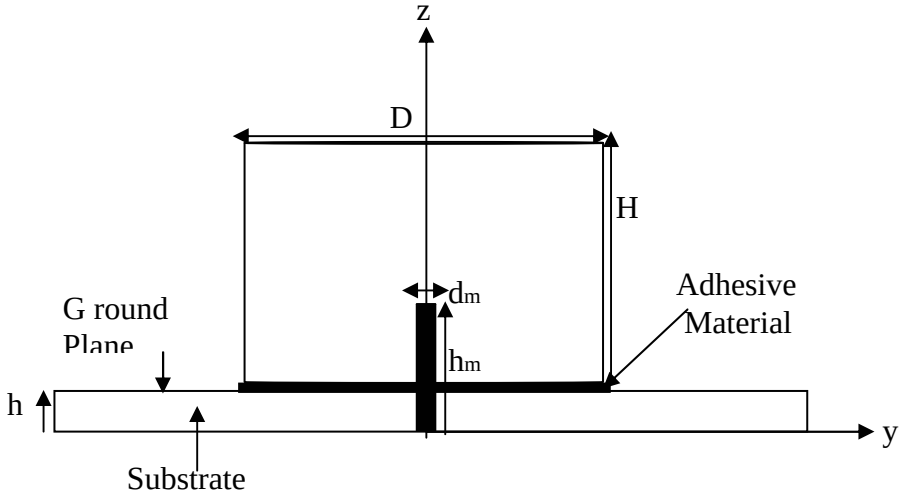

(a)

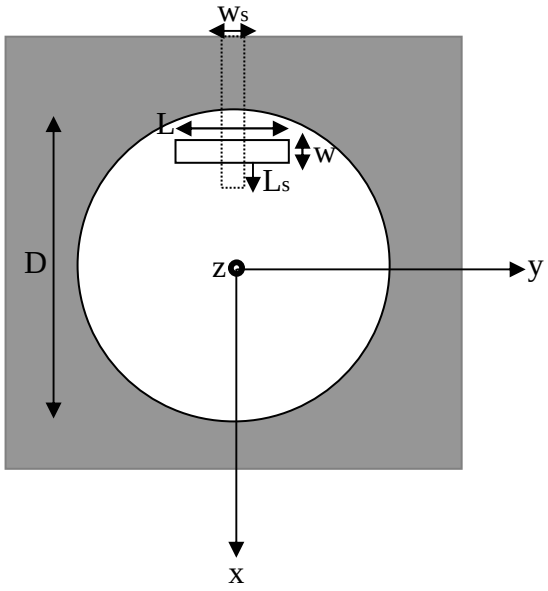

(b)

Figure 3.35: DRA's TM01 Design geometry fed by (a) monopole top view (b) aperture slot top view

Table3: Design parameters of the DRAs fed by monopole and aperture slot operating at 2.4GHz and at 8.9GHz.

DRA	*Ground Plane Size*	*DRA Cylinder Dimensions*	*Feed type Dimensions*	*Band width*
2.4 GHz with $\varepsilon_r=30$	50mm×50mm	Diameter(D)=30mm Height(H)=12mm	Monopole Diameter(d_m)=1.2mm Height(h_m)=6.508mm	1.6%
	50mm×50mm	Diameter(D)=38mm Height(H)=7.5mm	Aperture slot Length(L)=10mm Width(W)=1.2mm	1.4%
8.9 GHz with $\varepsilon_r=6$	30mm×30mm	Diameter(D)=18mm Height(H)=5mm	Monopole Diameter(d_m)=1mm Height(h_m)=4.8mm	17%
	30mm×30mm	Diameter(D)=18mm Height(H)=5mm	Aperture slot Length(L)=6mm Width(W)=0.5mm	13.7%

To reside various DRA sizes upon, a square ground plane supported by under-laid substrate of ε_r=3.38 and height h=0.508 mm is used. The monopole and the aperture slot are made to couple the energy to the DRA fed by 50Ω characteristics impedance microstrip line of width ws=1mm and that is etched on the substrate opposite to the ground plane side.

A2*: Monopole Feed*

To excite TM_{01} mode, a monopole of an appropriate height with an arbitrary diameter is supposed to be embedded exactly at the DRA centre. In the case of the 2.4GHz antenna, a monopole of diameter d_m=1.2mm and height h_m=6.508mm while in the case of 8.9 GHz antenna, a monopole of diameter d_g=1.0mm and height h_g=4.8mm are fitted into the equivalent sized holes drilled inside the DRA. The monopole penetrates the DRA vertically from below the substrate through the ground plane. So to avoid its shortening with the ground, isolations of diameters 3mm and 2mm with thickness of 17μm are introduced by removing metallic patches at the centre to correspond to the monopole diameters of 1.2mm @ 2.4 GHz antenna and 1mm @ 8.9 GHz antenna.

A3: *Aperture Feed*

The same TM_{01} mode excitation is accomplished by an aperture slot located at the periphery of the boundary area [3]. The exact size and location of the aperture is determined by the simulation process. The aperture is offset at 13.6mm for the 2.4 GHz antenna and 6mm for the 8.9 GHz antenna from the centre of the DRA. The aperture slot etched on the ground plane include an equivalent gap due to the removed metallic layer of 17 μm thickness and that is expected to be filled with adhesive material when the DRA is bonded to the ground plane. The energy coupling through the slot is maximized by using an open stub. The stubs lengths of $L_s(1)$=4.4mm @2.4 GHz antenna and $L_s(2)$=1mm @ 8.9GHz antennas are added by extending the corresponding microstrip feed lines.

A4: *Adhesive Material's Estimation*

To bond the DRA to the ground plane, an ordinary transparent adhesive material of supposed permittivity of (ε_r=2.2) is used but due to uncertainty in its applied thickness, various parametric simulations ranging from 0.05mm to 1.0mm are performed to latter compare with the measured results.

A5: Measured Results

For 2.4 GHz DRA, for which the fabricated designs are depicted in Figure3.36 the return loss (S11) results are presented in Fig3.37 while its monopole fed radiation patterns in Fig3.38(a) and aperture fed patterns in Fig3.38(b)respectively.

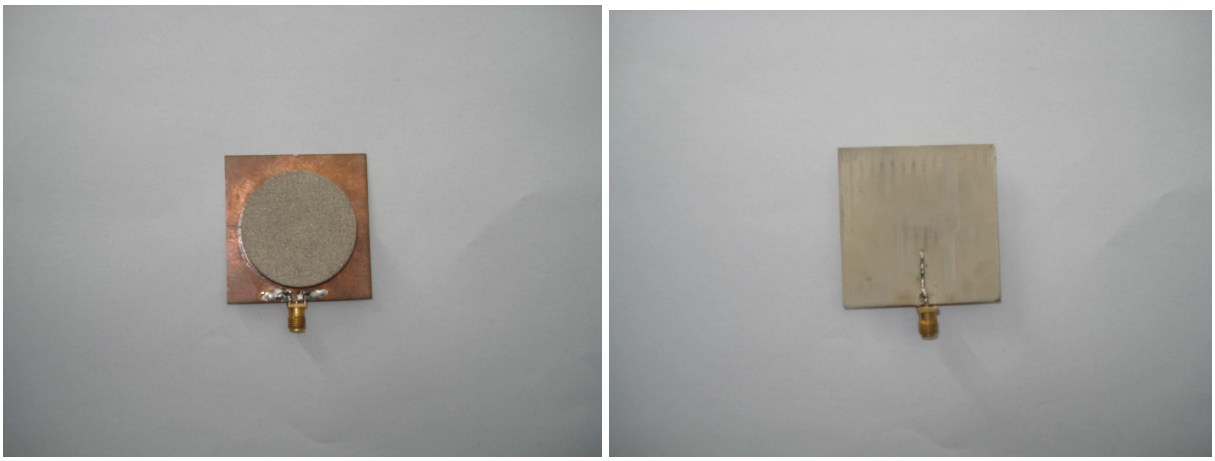

(a) (b)

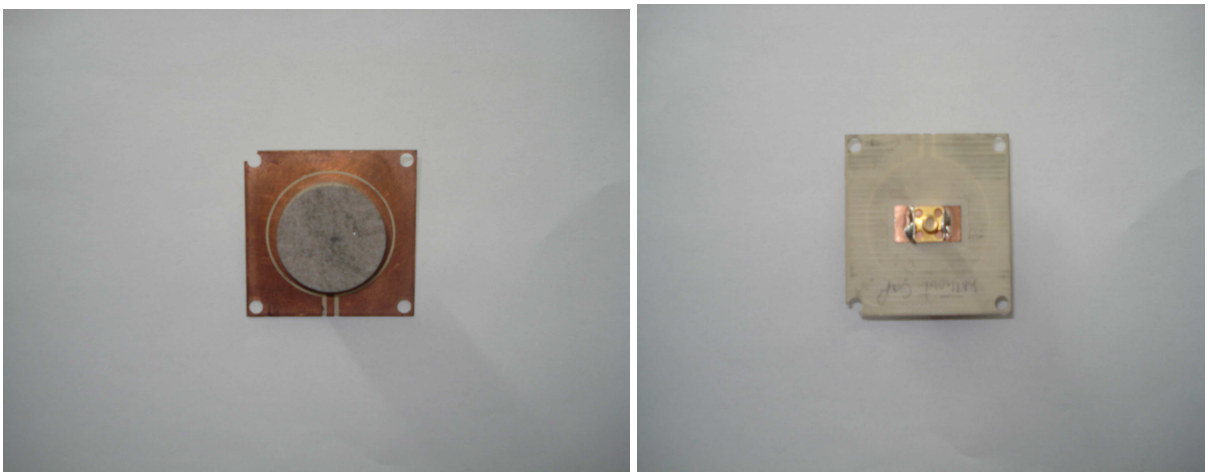

(c) (d)

Fig3.36: DRAs fabricated designs at 2.4GHz;
aperture slot fed: (a) top view (b) bottom view & monopole fed: (c) top view (d) bottom view

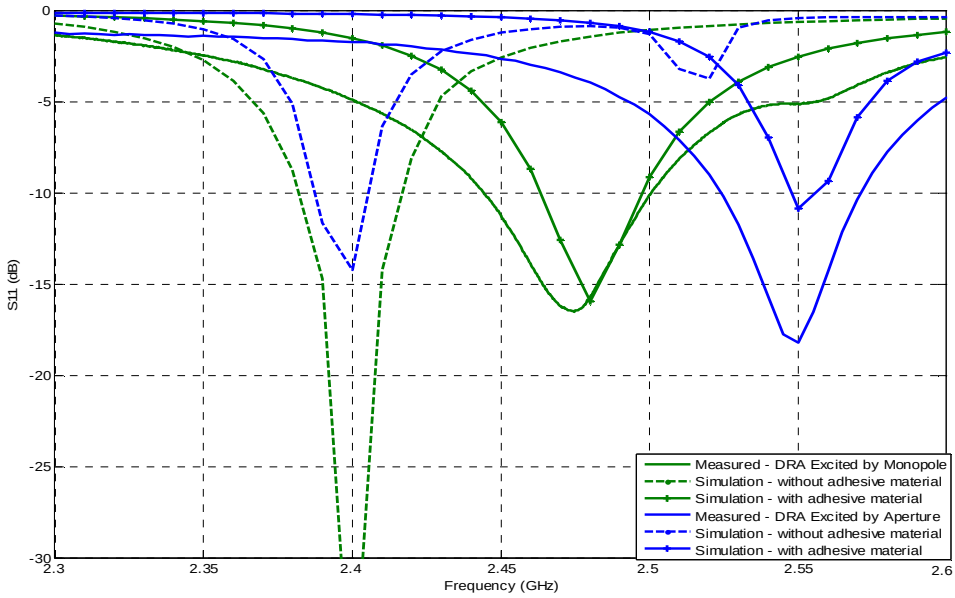

Fig3.37: DRA@2.4GHz measured and simulated return loss curves

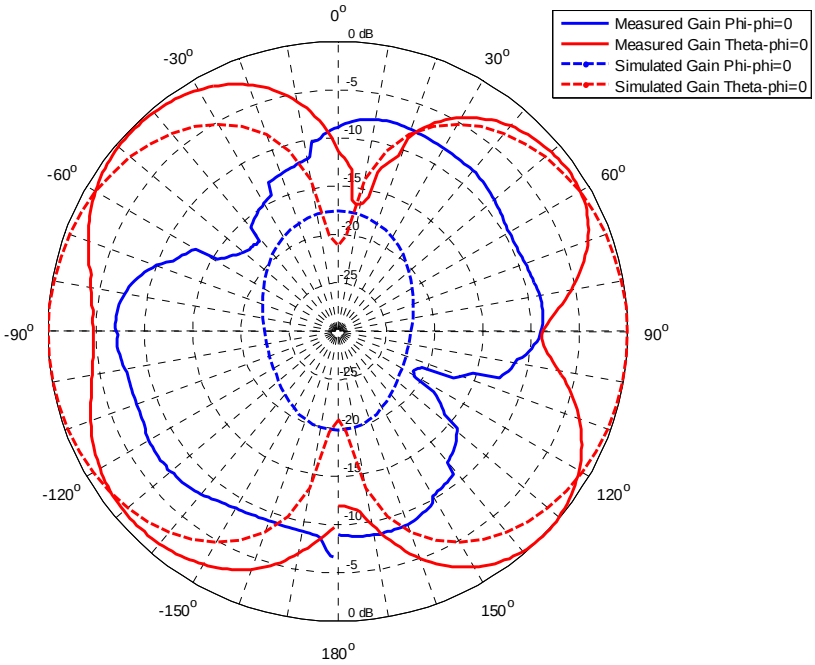

(a)

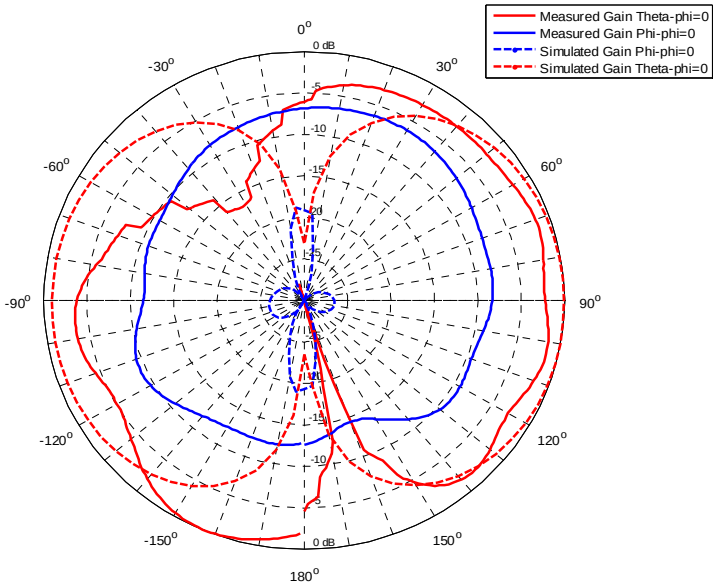

(b)

Fig3.38: DRA@2.4GHz measured and simulated radiation patterns
(a) monopole@2.48GHz (b) aperture slot@2.55GHz

Similarly for 8.9 GHz antenna, for which the fabricated designs are depicted in Figure3.39 the return loss (S11) results are presented in Fig3.40 while its monopole fed radiation patterns in Fig3.41(a) and aperture fed in Fig3.41(b) respectively.

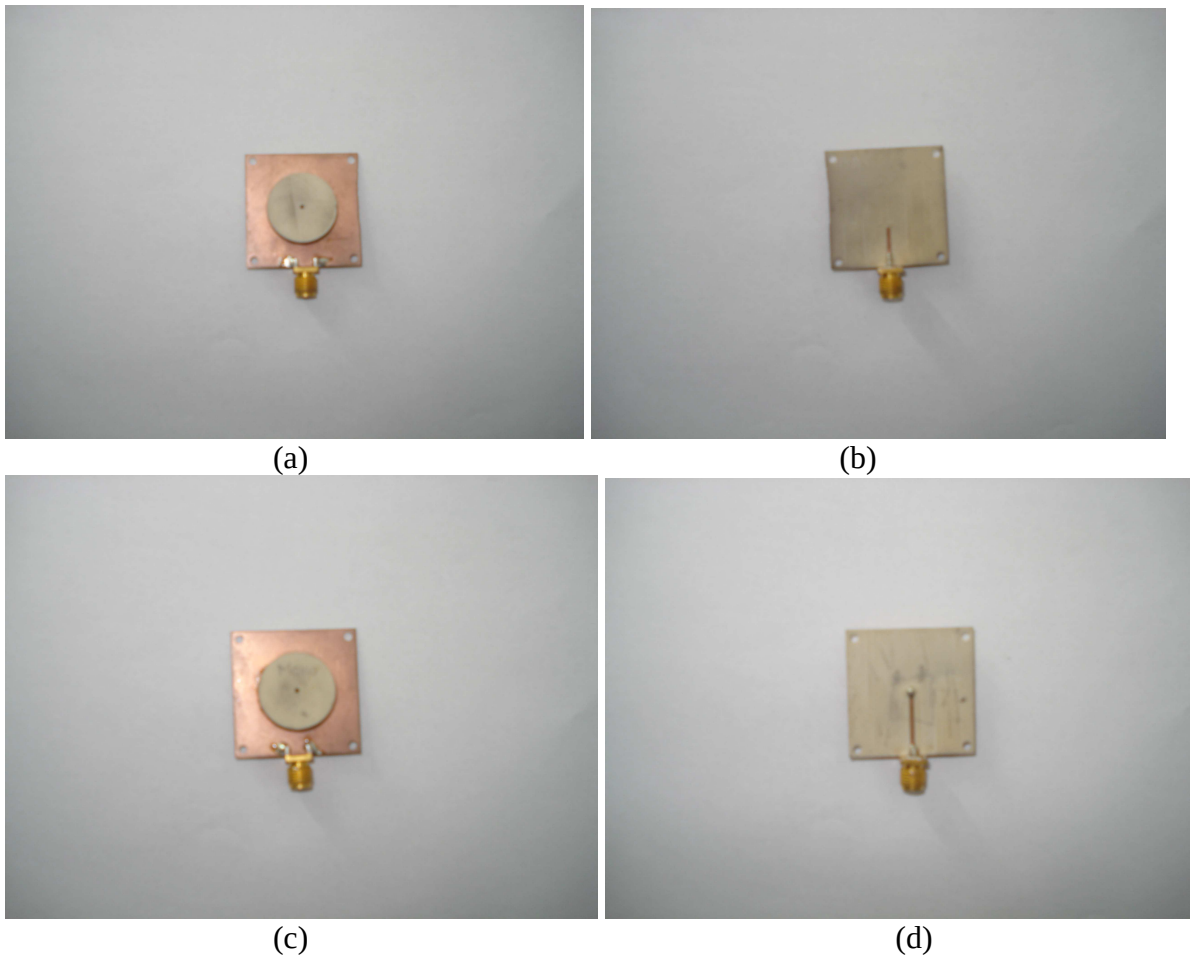

(a) (b)

(c) (d)

Fig3.39: DRAs fabricated designs at 8.9GHz;
aperture slot fed: (a) top view (b) bottom view & monopole fed: (c) top view (d) bottom view

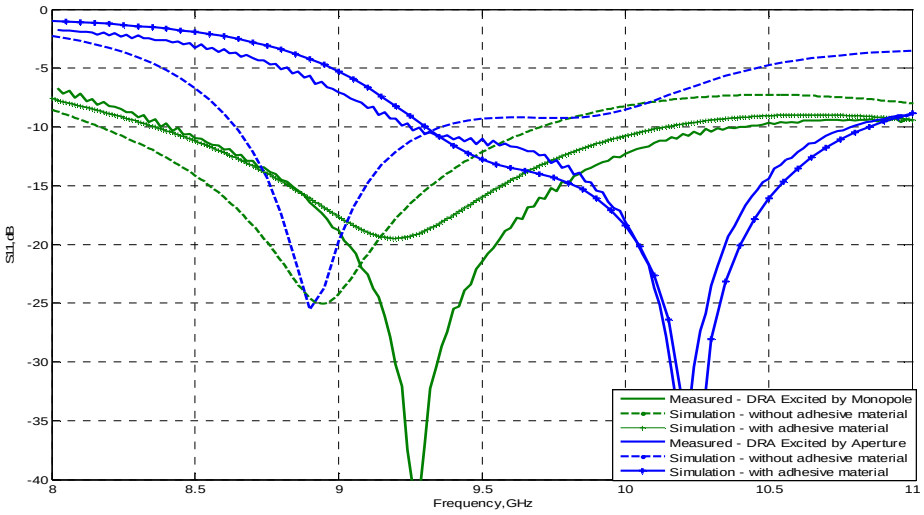

Fig3.40: DRA@ 8.9GHz measured and simulated return loss curves

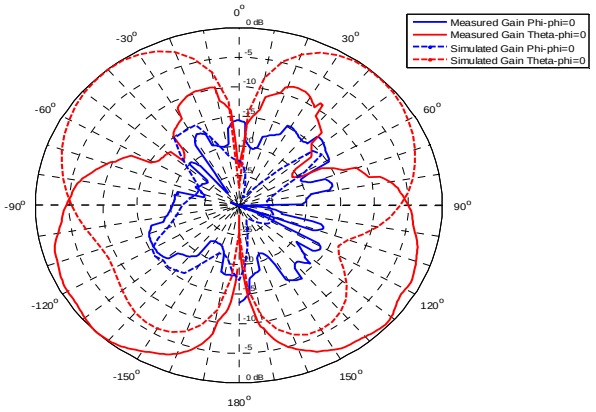

(a)

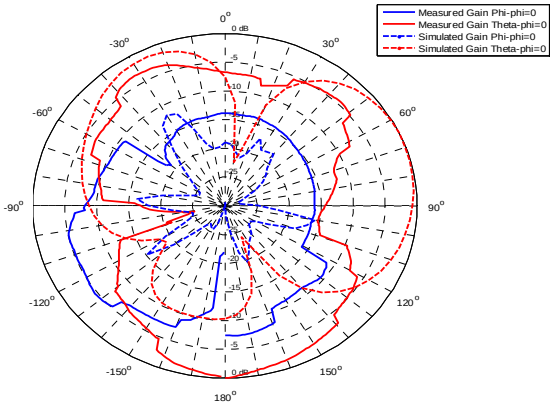

(b)

Fig3.41: DRA@8.9GHz measured and simulated radiation patterns
(a) monopole@9.25GHz (b) aperture slot@10.2GHz

A6: Performance analysis

With reference to 2.4 GHz antenna, in the case of the monopole's fitting inside the DRA, the measured resonance frequency has shifted to 2.47 GHz position, instead of the predicted one at 2.4 GHz. Corresponding to this effect, the measured impedance bandwidth has also increased to 2.4% in comparison with a 1.6% estimation. Similarly in the case of the aperture slot's DRA excitation, the measured resonance frequency has an upward shift at 2.55 GHz compared to the prediction at 2.4 GHz while the measured impedance bandwidth is found to be 2% in contrast with 1.4% of predicted one. The radiation patterns measured at new frequency positions that is for monopole at 2.47 GHz and for aperture at 2.55 speak of the same resonating mode in action thus yielding end-fire type pattern in which the measured Gain Theta(co-polarization) is found to be larger than the Gain Phi(cross-polarization).

For the 8.9 GHz antenna, in the case of the monopole excitation the measured resonance frequency has shifted upward to 9.25 GHz instead of calculated one at 8.9 GHz along with an increase in its impedance bandwidth from 17% to 20%. A similar pattern was observed in the case of the aperture excitation that has shifted to 10.2 GHz along with an increase in its impedance bandwidth from 13.7% to 15.5%.To observe if the same mode is working, the radiation patterns are measured for monopole at 9.25 GHz and for aperture at 10.2 GHz . Though a slight variation in patterns is noted but that can be attributed to the influence of connectors at high frequency or any imperfection in the measurement process. However, the overall shapes patterns resemble to the theoretically predicted results that justify the expected mode to resonate.

The results obtained are expected and justifiable on the basis of experimental evidences. In the 2.4 GHz antenna, the aperture feeding effect has been found to be more robust (6.2%) than the monopole's fed (2%). Similar pattern is observed in the 8.9 GHz antenna, the aperture fed undergoes a shift of 12% as compared to monopole's 4%.This upward shift can be attributed to the low permittivity adhesive material applied at the DRA bottom to glue it to the ground plane. A comparison of measured and simulated results suggests a more precise consideration of material's thickness that is of 0.1mm to 0.2mm. The robustness of aperture feeding compared to the monopole is due to the aperture's energy coupling mechanism in the presence of adhesive material's layer concentrated with near fields. The widening of the impedance bandwidth in all cases is obviously attributable to lower Q values of the adhesive material. This two pronged strategy not only resolves the outstanding DRA bonding issues but also additionally aids in increasing the impedance bandwidths.

The impact of an ordinary adhesive material bonding a Dielectric Resonator Antenna (DRA) to the ground plane is evaluated to precisely define its role in bringing about possible change in the resonance frequency, impedance bandwidth and radiation patterns. In terms of aperture slot feed, an upward resonance frequency shift of 6.2% along with an increase in impedance bandwidth from 1.4% to 2% @ 2.4 GHz while a shift of 12% with an increase in bandwidth from 13.7% to 15.5% @ 8.9 GHz have been observed. Similarly, in the case of monopole fed DRA, an upward shift of 2% with an increased bandwidth from 1.6% to 2.4% @2.4 GHz while an upward shift of 4% with an increased bandwidth from 17% to 20% @8.9 GHz were obtained. In all cases, the excited resonating mode TM01 is found to be stable and harmonious to its resonance frequency thus always yielding end-fire type radiation patterns. Thus it can be concluded that:

Appendix B

MatLab code to evaluate Diversity Gain performance of the antenna.

```
% ON-BODY DIVERSITY ANALYSIS
%
close all;
clear all;
%
fid=fopen('DRA ceinture 180 poitrine.prn','r');
a=fscanf(fid,'%e',[1 inf]);
a=a';
fclose(fid);
%
fid=fopen('LOOP ceinture 180 poitrine.prn','r');
b=fscanf(fid,'%e',[1 inf]);
b=b';
fclose(fid);
%
% % % % % % % % % % % % % fid=fopen('ref.prn','r');
% % % % % % % % % % % % % c=fscanf(fid,'%e',[1 inf]);
% % % % % % % % % % % % % c=c';
% % % % % % % % % % % % % fclose(fid);
%
L_pertes=6.5; % Pertes câble coaxial TX
a=a+L_pertes;
b=b+L_pertes;
% % % % % % % % % % % % c=c+L_pertes;
%
npi=length(a);
T=60;           % Temps d'analyse
R=50;           % Resistance de référence (50 ohms)
Te=T/npi;       % Temps d'échantillonnage
t=[0:Te:(npi-1)*Te];
tc=[0:Te:2*(npi-1)*Te];

%
% MAXIMUM COMBINING
%
for i=1:npi
    if a(i)>b(i)
```

```
        comb_max(i)=a(i);
    else
        comb_max(i)=b(i);
    end
end

%
% LINEARIZATION
%
s_a=sqrt(((2*R)/1000)*10.^(a/10)); %vecteur tension sur 50 ohms.
s_b=sqrt(((2*R)/1000)*10.^(b/10)); %vecteur tension sur 50 ohms.
% % % % % % % % % % % % % s_c=sqrt(((2*R)/1000)*10.^(c/10)); %vecteur
tension sur 50 ohms.
s_comb_max=sqrt(((2*R)/1000)*10.^(comb_max/10)); %vecteur tension sur 50
ohms.

%
% DIVERSITY CORRELATION
%
corr_s_channel=(xcorr(s_a-mean(s_a),s_b-mean(s_b),'coeff'));

%
% ECDF
%
[cdf_s_a  x_s_a] = ecdf(s_a);
[cdf_s_b  x_s_b] = ecdf(s_b);
% % % % % % % % % % % % % % % % % % % % [cdf_s_c  x_s_c] = ecdf(s_c);
[cdf_s_comb_max  x_s_comb_max] = ecdf(s_comb_max);
%
x_s_a_dBm=10*log10((x_s_a.^2/(2*R))*1000);
x_s_b_dBm=10*log10((x_s_b.^2/(2*R))*1000);
% % % % % % % % % % % % % % % % % %
x_s_c_dBm=10*log10((x_s_c.^2/(2*R))*1000);
x_s_comb_max_dBm=10*log10((x_s_comb_max.^2/(2*R))*1000);
%

%
% AFFICHAGE
%
figure(1)
subplot(2,1,1)
plot(t,a,'g');
axis([0 60 -100 -20]);
hold on;
plot(t,b,'r');
axis([0 60 -100 -20]);
legend('DRA','loop');
xlabel('time in s');
ylabel('dBm');
grid on;

subplot(2,1,2)
% % % % % % % % % % % % plot(t,c,'m');
% % % % % % % % % % % % hold on;
% % % % % % % % % % % % axis([0 60 -100 -20]);
plot(t,comb_max,'b');
axis([0 60 -100 -20]);
% % % % % % % % % % % % legend('reference','comb_m_a_x');
legend('comb_m_a_x');
xlabel('time in s');
```

```
ylabel('dBm');
grid on;

%
figure(2)
plot(tc,corr_s_channel,'b');
grid on;
%
figure(3)
semilogy(x_s_a_dBm,cdf_s_a,'g');
hold on;
grid on;
semilogy(x_s_b_dBm,cdf_s_b,'r');
% % % % % % % % % % % % % % % % % % % semilogy(x_s_c_dBm,cdf_s_c,'m');
semilogy(x_s_comb_max_dBm,cdf_s_comb_max,'b');
min_s=min(x_s_b_dBm);
max_s=max(x_s_comb_max_dBm);
axis([-100 -20 0.001 1]);
xlabel('Power(dBm)');
ylabel('Probability');
% % % % % % % % % % % % % % % % % % %
legend('monopole','PIFA','reference','comb_m_a_x');
legend('DRA','loop','comb_m_a_x');
```

Résumé en Français

Que l'on considère les domaines des télécommunications, de la navigation ou de la localisation, un niveau élevé de performance de l'antenne permet de relâcher l'effort sur les niveaux de sensibilité des récepteurs ou les performances en linéarité et en gain des émetteurs. Il est donc utile de poursuivre des recherches sur de nouveaux types d'antennes en particulier pour des applications émergentes.

Sujet de thèse :

Dans cette thèse, deux types d'applications de l'antenne DRA correspondant à ces 2 propriétés sont recherchés

1) La réalisation d'un élément rayonnant pour un réseau phasé embarqué sur un véhicule terrestre ou un avion. Cet élément de base requiert une couverture en élévation supérieure à celle des éléments imprimés pour permettre une poursuite typique comprise entre ±70°. Cette couverture dans un cône large est assurée avec une bonne pureté de polarisation circulaire en utilisant deux ouvertures à fente en H orthogonales parfaitement découplées en bande X.

2) La deuxième structure est destinée à la diversité d'antennes dans le contexte des réseaux corporels embarqués ou Body Area Network (BAN). L'antenne à diversité combine une antenne fente en boucle avec un DRA ce qui permet dans un espace compact de réaliser des diagrammes de type "broadside" et "endfire" respectivement. Les alimentations considérées sont de 2 types; Soit purement planaire (microruban et coplanaire) soit mixte en combinant une alimentation coaxiale et une alimentation coplanaire.

Caractéristiques principales des antennes à résonateur diélectrique (DRA):

Pour répondre aux attentes des utilisateurs en termes de débit, les systèmes de communication sans fils se tournent vers des fréquences de plus en plus élevée. La conséquence de cette montée en fréquence est notamment l'augmentation des pertes au niveau des éléments conducteurs et donc une diminution de l'efficacité globale des systèmes de communication. Dans ces circonstances, les antennes à résonateur diélectrique (DRA) offre de meilleurs résultats par rapport à d'autres familles d'antennes à base d'éléments métalliques. De plus, les antennes DRA offrent des pertes diélectriques négligeables, elles sont peu sensibles aux variations de température et s'intègrent facilement sur des technologies de fabrication planaires.

R1.0: Conception d'une antenne DRA en bande X

Afin de générer un diagramme de rayonnement de type « broadside », le mode TM110 (HEM11) de l'antenne DRA est excité. Pour obtenir une double polarisation linéaire au niveau de l'antenne, deux accès d'alimentation sont nécessaires. Ces accès sont réalisés en technologie microruban. L'énergie électromagnétique véhiculée par les lignes d'alimentation est transmise à l'antenne DRA via des fentes de couplage gravées dans le plan de masse. Pour un bon fonctionnement du mode TM110, ces fentes doivent être confinées au niveau de la zone centrale de l'antenne DRA de forme cylindrique. D'autre part, pour éviter tout décalage de la fréquence de résonnance de l'antenne et toute distorsion du diagramme de rayonnement la topologie des fentes doit garantir un fort niveau de découplage entre les ports d'alimentation. Pour satisfaire ces conditions, des fentes en forme de H positionnées de manière orthogonale sous l'antenne DRA ont été retenues.

R1.1: Performances simulées de l'antenne DRA en bande X :

L'analyse de l'antenne DRA en bande X indique des performances similaires sur les deux accès (dénommés port 1 et port 2). Au niveau de la réponse en fréquence de l'antenne, la bande passante à -10dB sur le port 1 est de 22% couvrant les fréquences de 6.7GHz à 8.3GHz. Pour le port 2, l'antenne est adaptée entre 6.75GHz et 8.25GHz soit 20% de bande passante. L'isolation entre les accès est élevée, égale à 42 dB. Les diagrammes de rayonnement sont symétriques et de forme quasi identique pour les deux l'accès. Pour chaque port le gain maximum est égal à 5.7 dBi. L'angle d'ouverture à -3dB est de l'ordre de 95°. Le rapport avant arrière est estimé à 12dB. L'efficacité de l'antenne est élevée avec un rendement proche de 98%.

R1.2: Effet du matériau adhésif sur performances simulées de l'antenne DRA en bande X:

Pour réaliser l'antenne DRA, un matériau adhésif est nécessaire pour fixer le résonateur diélectrique sur son plan de masse. L'estimation des caractéristiques électriques de ce matériau et de l'épaisseur requise est essentielle pour prédire avec exactitude les performances de l'élément rayonnant. Cette partie présente les performances simulées du DRA après optimisation en incluant le matériau adhésif. Au niveau de l'adaptation, la bande passante à -10dB simulée commune sur les deux accès couvre les fréquences de 7GHz et 8.6GHz soit 20%. L'isolation reste satisfaisante avec un niveau minimum de 42 dB. Les diagrammes de rayonnement restent symétriques dans les plans xoz et yoz. Dans ces deux plans les angles d'ouvertures à -3dB sont de 70° pour un gain maximum de 5.7dBi à la fréquence centrale. L'efficacité de l'antenne est de 98% et le rapport avant arrière est de 12 dB. Les diagrammes de rayonnement restent stables sur toute la bande passante de l'antenne.

R1.3 : Résultats de mesure de l'antenne DRA en bande X

Cette partie présente les mesures de l'antenne DRA à double polarisation linéaire orthogonale. En termes de fréquence, par rapport à la simulation on observe sur les deux accès un décalage positif de la fréquence de résonance et une diminution de la bande passante. La bande passante à -10dB sur le port 1 varie de 8GHz à 8.6GHz alors que pour le port 2, elle se situe entre 8.15GHz et 8.6GHz. Dans ces conditions, la bande passante commune aux deux accès est de 5,9%, valeur inférieure à celle attendue. Ce changement pourrait être imputé à l'impact réel du matériau adhésif notamment au niveau de son inhomogénéité en termes d'épaisseur et plus globalement aux tolérances de fabrication de l'antenne. L'isolation entre les ports est de 35 dB. Le gain maximum mesuré est de 2.5dBi à la fréquence de 8,4 GHz. Au niveau du rayonnement, la polarisation croisée est de 20dB sur l'accès 1 avec un diagramme de rayonnement de type « broadside ». Sur l'accès 2, on observe une dégradation de la polarisation croisée avec une valeur minimale de 15 dB. Sur les deux accès les diagrammes de rayonnement sont symétriques. La taille finie du plan de masse génère un rayonnement arrière non négligeable, ce dernier pouvant être réduit en augmentant les dimensions du plan de masse. Nous avons observé lors des mesures un fort impact des connecteurs sur la distorsion des diagrammes de rayonnement, distorsion négligeable si ces connecteurs sont correctement protégés avec des matériaux absorbants.

Bien que la bande passante commune en impédance reste insuffisante, l'antenne proposée présente une forte isolation entre les ports d'excitation conduisant à des diagrammes de rayonnement de qualité. Il serait possible d'utiliser l'antenne réalisée dans la bande X, plus précisément pour les liaisons montantes couvrant des fréquences de 7.9GHz à 8.4Ghz pour les systèmes satellitaires et radar.

R2.0: Antenne à diversité pour application BAN (Body Area Network)

R2.1: Antenne boucle alimentée par ligne coplanaire couplée à un résonateur diélectrique excité par une sonde coaxiale.

L'antenne boucle et l'antenne DRA sont dans un premier temps dimensionnées indépendamment. L'optimisation des antennes est menée en espace libre puis à la surface d'un modèle équivalent matérialisant le corps humain. Lorsque que les deux antennes sont co-localisées, pour former une structure compacte, les effets de couplages mutuels entrainent la modification des paramètres de chaque antenne (adaptation, fréquence de résonnance et diagramme de rayonnement). Il est important de quantifier ces effets pour l'optimisation globale de la structure antennaire.

Performance en espace libre

Pour les deux antennes, les résultats de simulation en espace libre présentent une fréquence de résonance située autour de 2.4 GHz, la bande passante commune étant de 3.3%. L'isolation entre les accès reste acceptable avec un niveau minimum de -13dB.

Performance sur le corps humain

L'interaction avec le corps humain entraine l'altération des performances des antennes. La présence du plan de masse au niveau de l'antenne DRA, limite cet effet, en revanche la boucle est fortement perturbée. La modélisation du corps humain est réalisée par un cylindre équivalent caractérisé par une permittivité relative égale à 53 ($\varepsilon_r = 53$) et une tangente de perte de .002. Ce cylindre a un rayon de 20 cm et une hauteur de 40 cm. L'optimisation de l'antenne à deux accès est menée à une hauteur de 15 mm au dessus du corps.

Résultats de mesure :

Les résultats de mesure montrent une bande passante comprise entre 2.34 GHz et 2.73 GHz pour l'antenne boucle soit 15%. Pour l'antenne DRA la bande passante se situe entre 2.36 GHz et 2.48 GHz soit 4.95%. La bande passante commune aux deux accès est donc limitée autour de 2.4 GHz par la bande passante de l'antenne DRA. L'isolation entre les accès est de 13 dB. Les diagrammes de rayonnement mesurés correspondent aux attentes, en espace libre, l'antenne boucle présente un diagramme de rayonnement de type « broadside » et l'antenne DRA de type « endfire ».

R2.2: Antenne boucle et antenne DRA alimentée par uns structure planaire

L'antenne proposée dans la section précédente présente une alimentation de type coaxial au niveau du DRA. Ce type d'alimentation est difficilement compatible avec les contraintes d'intégration d'une antenne sur le corps. Cette partie aborde la conception d'une antenne à deux accès, composé d'une boucle gravée dans un plan de masse, couplée à un résonateur diélectrique. Chacune de ces structures rayonnantes est alimentée par une structure planaire (ligne microruban) facilitant l'intégration de l'antenne pour des applications de type BAN.

Performance de l'antenne.

L'antenne fonctionne autour de 2.42Ghz. Les bandes passantes relatives sont de 1.8% et de 3.2% respectivement pour l'antenne boucle et l'antenne DRA. L'isolation entre les accès est de 12 dB.

Performance sur le corps
L'antenne est optimisée pour fonctionner à 10 mm du corps humain dont le modèle à été présenté dans la section précédente. A cette distance on remarque une légère diminution de la fréquence de résonnance des antennes. Au niveau des bandes passantes, nous observons une augmentation (2.5% pour l'antenne boucle et 4% pour l'antenne DRA), cette augmentation est attribuée à la présence du milieu à pertes. L'isolation entre les accès reste satisfaisante avec un niveau de 15dB.

Résultats de mesure :

Les mesures montrent des performances légèrement inférieures à celles obtenues en simulation. Au niveau de l'antenne boucle, la bande passante se situe entre 2.387GHz et 2.425GHz, pour l'antenne DRA la bande passante est comprise entre 2.35GHz et 2.45GHz. Dans ces conditions la bande passante commune sur les deux accès est de 1.5%. L'isolation mesurée entre les accès est de 12dB à la fréquence de 2.4Ghz, isolation suffisante pour obtenir de bonnes performances en diversité. Le diagramme de rayonnement de l'antenne boucle présente une asymétrie dans le plan yoz, cependant le niveau de polarisation croisée reste faible. L'antenne boucle présente également un rayonnement arrière important, rayonnement qui pourrait être limité en ajoutant un plan métallique supplémentaire. Le DRA présente un diagramme de rayonnement « endfire » peu affecté par la présence du plan de masse limité.

R2.3: Analyse du gain en diversité

Pour évaluer les performances de l'antenne, des campagnes de mesure pour estimer le gain en diversité ont été menées en conditions réelles. Une personne est équipée d'un réseau BAN, l'antenne d'émission est un monopôle chargé, le récepteur se compose de l'antenne sous test (l'antenne boucle combinée à l'antenne DRA). Pendant la mesure le sujet effectue des mouvements simulant les conditions de la marche dans un environnement propice aux phénomènes de multi trajets. Les performances de l'antenne sont mesurées pour 3 scénarios différents correspondant à 3 positions de l'antenne sous test respectivement au niveau du torse, de l'épaule et du dos. Pour l'ensemble des configurations, l'antenne d'émission reste fixée au niveau de la ceinture. L'instrumentation est composée d'un VNA Agilent calibré en mode récepteur connecté à l'antenne sous test. Un générateur alimente l'antenne d'émission, la puissance est fixée à 0dBm à la fréquence de 2.4Ghz. Pendant les campagnes de mesures l'ensemble des antennes sont maintenues à une distance de 10 mm du corps humain.
Pour les deux antennes à diversité présentées dans cette thèse les mesures montrent un gain en diversité de 9.5 dB dans des conditions favorables (pas de trajet prépodérant). Cette valeur approche la valeur théorique de 10 dB, obtenue dans un environnement de type Rayleigh.
Dans ces conditions, les antennes développées peuvent être utilisée et intégrée directement dans des vêtements pour des applications liées à la surveillance des personnes. (pompiers, pêcheurs…)

R3.0: Conclusion:
Ces travaux de recherche montrent les possibilités offertes par les antennes DRA. Grâce à une efficacité élevée et des pertes diélectriques négligeables, les antennes DRA sont bien adaptées aux applications hautes fréquences. Les prototypes antennaires développés en bande X présentent de bonnes performances et peuvent facilement s'intégrer aux systèmes standards. Cependant, des améliorations pourront être apportées, notamment au niveau la bande passante des antennes. Pour les applications BAN, l'antenne à diversité de diagramme développée

pourrait-être miniaturisée pour une meilleure intégration, notamment au niveau de la taille du DRA. Pour atteindre cet objectif, une possibilité serait l'utilisation de matériaux à constante diélectrique élevée. De plus, il semble nécessaire d'explorer d'autres pistes de recherche sur les antennes électriquement petites capables de s'intégrer facilement avec les antennes DRA.